RÉPUBLIQUE FRANÇAISE
Liberté Égalité Fraternité

Université de Toulouse

Doctorat de l'Université de Toulouse

préparé à l'ISAE-SUPAERO

Optimisation d'un problème de conception d'avion pour des configurations hybride-électriques sous contraintes de fabrication et de certification

---

Thèse présentée et soutenue, le 26 juin 2026 par

Florent LUTZ

École doctorale
MEGEP - Mécanique, Energétique, Génie civil, Procédés

Spécialité
Energétique et transferts

Unité de recherche
ISAE-ONERA EDyF Energétique et Dynamique des Fluides

Thèse dirigée par
Marc BUDINGER

Composition du jury
M. Fabrizio NICOLOSI, Rapporteur, Università degli Studi di Napoli Federico II
M. Andreas STROHMAYER, Rapporteur, Universität Stuttgart
M. Xavier ROBOAM, Président, CNRS Occitanie Ouest
Mme Rhea LIEM, Examinatrice, Imperial College of London
M. Dominique ALEJO, Examinateur, SAFRAN
M. Marc BUDINGER, Directeur de thèse, INSA Toulouse

Membres invités
M. Joel JEZEGOU, ISAE-SUPAERO
M. Aurélien REYSSET, Co-encadrant de thèse, INSA Toulouse

"Life is like walking along a long road shouldering a heavy load; there is no need to hurry. One who treats difficulties as the normal state of affairs will never be discontented."

Lord Tokugawa Ieyasu, *Testament of Ieyasu*

Remerciements

«Bon, qu'est-ce que je vais bien pouvoir écrire ?» Telle est la question à laquelle je suis confronté quelques jours après la présentation des travaux qui ont occupé plus de quatre ans de ma vie. Et en un sens, résumer la contribution de tous ceux qui m'ont aidé et soutenu durant cette période est presque plus compliqué que de mettre en forme ma modeste contribution au monde de la recherche. Alors voilà, sans vouloir, ni pouvoir, être exhaustif, ces quelques paragraphes sont l'occasion de remercier des personnes exceptionnelles à qui je dois d'être aujourd'hui Dr Lutz 3eme du nom (j'ai oublié de faire la blague le jour de la soutenance avec le stress).

Commençons par le plus sérieux: je veux (et non je dois) remercier les membres du jury pour leur expertise technique ainsi que les retours précieux qu'ils m'ont faits et qui ont contribué à amener ce manuscrit à son acmé. Au-delà de ça, d'une manière ou d'une autre, ils ont tous inspiré certains des modèles, des méthodes ou des cas d'étude présentés dans ce document. Recevoir cette "approbation par les pairs" est donc un honneur et une forme de validation pour moi qui me fait espérer que le travail que j'ai produit contribuera, d'une manière ou d'une autre, à faire progresser la Science (en toute modestie, bien sûr).

Je remercie bien évidemment aussi Marc et Aurélien qui m'ont permis d'évoluer d'un ingénieur toujours le nez dans son code à quelqu'un capable de prendre du recul et de prendre des décisions avisées sur la bonne conduite à adopter, quelles pistes explorer et quels cas présenter (et comment surtout!). Et un remerciement particulier à Joël qui m'a recruté en sortie d'école et grâce à qui j'ai pu me lancer dans ce projet et qui a été un vrai mentor au cours des 6 dernières années.

Un grand merci à tous mes collègues aussi. Celles et ceux de l'équipe CADV pour leurs savoirs et les discussions techniques (et pas que) toujours enrichissantes. Aux membres originels du "bureau des légendes": Aurélien (encore lui), Antoine, Félix, Giulia, Louis, Martin, Sofiane et Valérian; ainsi qu'à tous ceux qui ont rejoint les héritiers de ce bureau mythique: Abdoulaye, Alice, Antonio, Bastien, Chung-Huan, Gabriele, Ian, Jason, Juilana, Lea, Luca, Ousmane, Paco, Pierre, Roberto, Romain, Thomas, Valentine, Yohan et Younes. Un grand merci à Scott et Thomas aussi qui m'ont permis de surmonter, avec le sourire, certaines situations beaucoup trop absurdes et pour le soutien sur les tâches qui dépassaient la recherche pure. Merci aussi à l'équipe des admissions et de la prospection qui a aidé à rendre supportable (et même agréable pour certaines) une partie des tâches administratives

que j'ai dû assumer en parallèle de cette thèse. Bien évidemment, un grand merci à l'équipe des inspectrices des études pour leur bonne humeur permanente avec une mention spéciale à MC pour tout le travail qu'elle produit et pour son franc-parler toujours rafraîchissant. Une pensée aussi pour tous les autres collègues avec qui j'ai le plaisir de partager des sourires et des plaisanteries dans les couloirs. De grands merci enfin à la team #FAST-OAD, pour leur support sur ce qui est incontestablement le meilleur outil d'OAD au monde: Christophe, Enrico, Eric, Sébastien et Jean à qui je dois en plus une expérience en stage qui a, à elle seule, orienté ma carrière vers la recherche et les nouvelles configurations avion.

Comment ne pas mentionner aussi tous les amis qui m'accompagnent et me supportent, certains depuis longtemps et d'autres depuis moins longtemps. En particulier, un grand merci à tous ces amis que je me suis faits lors de mes premières classes en Alsace, la plus belle région du monde (il fallait que je le rappelle), je parle bien sûr de la team des Bretzels (je n'ai malheureusement pas la place de tous les nommer mais je les remercie tous). Et je voudrais remercier plus spécifiquement le Big Five: Aurélien, Simon, Simon et enfin Sami qui est probablement responsable de mon rêve de travailler dans l'aéronautique. J'ai bien sûr une pensée aussi pour tous ces camarades que je me suis faits lors de mes classes à SUPAERO. Je pense plus spécifiquement à Pierre-Louis et à ces soirées du vendredi, en pleine période de confinement, qui ont rendu cette période moins infernale. Et enfin un grand merci tout particulier à Pierre-Louis à la fois parce que je lui avais promis de l'inclure dans mes remerciements il y a quatre ans, mais aussi et surtout pour tous les bons moments qu'on passe ensemble à chaque fois qu'on se voit (on se refait un Kami quand tu veux).

Je voudrais finir en remerciant ma famille proche et étendue. Mes parents, d'abord, pour leur soutien constant, leurs conseils précieux et pour avoir traversé la France en pleine canicule pour m'apporter un soutien inestimable et nécessaire le jour de la soutenance. Un grand merci à ma petite sœur aussi, à laquelle je ne dis jamais assez à quel point je l'admire et l'apprécie. J'ai aussi une pensée pour mes grands-parents, maternels, qui pensent toujours à moi quand ils voient un article sur les avions électriques et à hydrogène, et paternels aussi, qui, je l'espère, seraient fiers de ce que je suis devenu. Un grand merci aussi à tous les cousins et cousines, à mes tantes, à mon parrain et à ma marraine, aux amis de la famille et bien évidemment aux derniers venus, les petits neveux et nièce.

Florent

Résumé

Dans le cadre de la transition écologique du secteur aéronautique, des objectifs ambitieux pour réduire l'impact environnemental de l'aviation sont visés. Si le CO2 est souvent mentionné, les avions rejettent d'autres polluants qui contribuent également à l'impact du secteur. Malgré leur faible contribution aux émissions du secteur, les avions de l'aviation générale ont un rôle majeur dans cette transition. Bien qu'ils ne représentent qu'une infime partie de la consommation de carburant du secteur, ils sont responsables de 10% des émissions d'imbrûlés, de 40% des émissions de CO et de la totalité des émissions de plomb. En outre, ils sont utilisés différemment et moins intensément que leurs homologues commerciaux, indiquant une voie différente vers la soutenabilité. Par ailleurs, en raison de leur faible puissance et de leur faible autonomie, ils constituent des candidats idéaux pour dérisquer les nouvelles technologies avant leur adoption sur les avions commerciaux. Une solution potentielle pour répondre à la question de la transition est l'introduction de la propulsion électrifiée. Bien que cette technologie en soit encore à ses débuts, soulevant des questions de certifiabilité, elle offre des avantages allant d'une réduction à une élimination des émissions pendant le vol. Elle offre également la perspective de synergies multidisciplinaires et de permettre d'alléger les contraintes de conception. Parmi les nombreux projets proposés pour explorer cette solution, diverses approches, allant de la conception "feuille blanche" à la réutilisation de cellules existantes, ont été explorées. Il est donc nécessaire de créer des méthodologies de dimensionnement capables de tirer parti de ces synergies et d'évaluer les impacts, au niveau de l'avion, des groupes propulseurs électrifiés. Compte tenu de la diversité des architectures et de la nécessité de pouvoir modéliser différentes approches de conception, une formulation dynamique est nécessaire.

Cette thèse répond à ce besoin en présentant de nouvelles méthodes et modèles permettant d'évaluer, au niveau de l'avion, les effets de la chaîne de propulsion électrifiée. Tout d'abord, une revue des méthodes de dimensionnement existantes est proposée, soulignant la nécessité d'un cadre capable de saisir les synergies multidisciplinaires introduites par la propulsion électrique. Cette thèse contribue en proposant l'intégration, dans le code FAST-OAD, d'un nouveau module capable de modéliser n'importe quelle architecture de propulsion. L'intégration de modèles capables de capturer les gains issus de plusieurs disciplines ainsi que les degrés de liberté supplémentaires dans la conception est ensuite abordée. Des modèles de fidélité moyenne sont choisis comme compromis idéal entre les méthodes de densités et

rendements constants et les simulations coûteuses de haute fidélité. L'application de cette méthode à divers scénarios d'hybridation pour les avions dans la catégorie de certification CS-23 est ensuite discutée. Les résultats montrent que, même si une électrification permettant d'atteindre les mêmes niveaux de performances que les avions conventionnels n'est pas réalisable, elle peut être mise en œuvre et s'avérer avantageuse pour les missions plus courtes et pour de petits aéronefs, même avec les technologies actuelles. Un point de bascule en termes de maturité technologique est également mis en évidence, montrant que certaines chaînes hybrides ne seront compétitives que temporairement. Enfin, il est montré que, pour certaines configurations, la réduction des émissions ne peut être obtenue qu'en tirant parti du soulagement des contraintes de conception, et non grâce à la faible intensité carbone de l'électricité. Ces comparaisons sont ensuite approfondies en utilisant une ACV dans le processus de conception. Cela permet d'obtenir des pistes cruciales sur les impacts de la propulsion électrique et de nuancer les gains découlant des nouvelles compositions chimiques des cellules de batterie.

Abstract

As part of the ecological transition of the aeronautics sector, many national and international agencies have set very ambitious targets to reduce the environmental footprint of aviation. While scrutiny is usually on CO_2, aircraft release a wider range of pollutants that also contribute to the sector's impact on the environment. Although they contribute only marginally to the emissions of the sector as a whole, General Aviation aircraft pose themselves as an essential step of this transition. Firstly, although they represent only a minute fraction of the total fuel burn in the sector, they account for 10% of unburnt hydrocarbons, 40% of CO emissions, and the entirety of lead emissions. Additionally, they are used in different ways and with a different intensity when compared to their commercial counterpart thereby indicating a different path to sustainability. Secondly, on account of their lower required power and lower ranges, they are ideal candidates to de-risk and gain knowledge about newer technologies before adoption on commercial aircraft. A popular potential solution to the question of the sustainability of the aeronautics sector is the introduction of electrified propulsion. Although the technology is still in its infancy, raising questions about its certifiability, it offers gains ranging from reduced to zero emissions during flight. It also offers the prospect of multidisciplinary synergies and relieving design constraints on the aircraft. Out of the numerous projects proposed to explore this solution, numerous approaches, ranging from blank sheet design to retrofit, have been adopted to address those novel designs. This thus creates a need for new sizing methodologies capable of capturing those synergies and capable of assessing the impacts, at aircraft level, of electrified powertrains. Given the variety of propulsive architectures and the need to be able to model both retrofit aircraft and new designs from scratch, dynamic formulation is necessary.

This thesis addresses the need for such a methodology by presenting new methods and models enabling the assessment, at aircraft level, of the effects of electrified propulsion chain. First, a review of existing methods for the sizing of aircraft is proposed, highlighting the need for an integrated framework capable of capturing multidisciplinary synergies introduced by electric propulsion. This thesis contributes by proposing the integration, into the existing modular framework FAST-OAD, of a new module capable of dynamic reconfiguration of the MDAO problem to model any propulsive architecture. The integration of models capable of capturing gains stemming from multiple disciplines, as well as the added degrees of freedom in the design, is then discussed. Medium fidelity models are chosen as an ideal compromise

between top-down kW/kg and efficiency methods and expensive high fidelity simulations. The application of this method to various hybridization scenarios for CS-23 certification category aircraft is then discussed. This reveals that while electrification achieving the same levels of performances as conventional design is unfeasible, it can be achieved and beneficial for shorter missions and small aircraft, even with current technologies. A tipping point in terms of electric technology maturity is also highlighted, showing that, for some aircraft, hybrid designs will only be competitive temporarily. Finally, it is shown that, for certain configurations, reductions of emissions can only be achieved by leveraging the relief of aircraft design constraints enabled by electric propulsion and not thanks to its low carbon intensity. Lastly, the comparison between conventional and electrified designs is further investigated by using Life Cycle Assessment inside the aircraft design process. It enables critical insights into the impacts of electric propulsion and nuances the gains stemming from new battery cell chemistries.

Contents

List of Figures **xiii**

List of Tables **xviii**

Nomenclature **xxi**

1 State of the art and thesis objectives **1**
1.1 Sustainability of the aeronautics sector 1
1.2 Technical Context of electrification of propulsive architecture 3
1.2.1 Terminology and nomenclature electrified aircraft propulsion 3
1.2.2 Benefits of electrified propulsive architectures 3
1.2.3 Challenges and limitations to the introduction of electric powertrains 6
1.2.4 Barriers to the applicability of conventional design methodologies . . 7
1.3 Problem statement 8
1.4 Identification of research questions 10
1.5 Manuscript overview 10

I Design of Hybrid-Electric General Aviation aircraft **13**

2 Sizing methodologies for electrified propulsive architectures **15**
2.1 Introduction 15
2.2 State of the art of methodologies for the sizing of aircraft 16
2.2.1 Multidisciplinary Analysis and Optimization (MDAO) 16
2.2.2 Review of existing approach for the modeling of electrified aircraft . 20
2.2.3 Review of existing Overall Aircraft Design integrated framework . . . 26
2.2.4 Identification of modeling gaps in major OAD frameworks 28
2.3 Development of an integrated framework for the sizing of electric and hybrid aircraft 32
2.3.1 The FAST-OAD framework 32
2.3.2 Extension to hybrid and all-electric configurations 34
2.4 Conclusions and perspectives 41

3 Modeling of General Aviation aircraft propulsive architectures 45
3.1 Introduction . . . 46
3.2 Propulsive architecture components . . . 46
3.3 Modeling techniques . . . 48
3.4 Propulsive elements . . . 50
3.4.1 Propeller . . . 50
3.5 Electric loads . . . 52
3.5.1 Electric motor . . . 52
3.6 Sources . . . 54
3.6.1 Battery packs . . . 54
3.6.2 Generators . . . 57
3.6.3 Piston Internal Combustion Engines (ICEs) . . . 58
3.6.4 Gas turbines . . . 59
3.7 Connectors . . . 62
3.7.1 Inverters and Rectifiers . . . 62
3.7.2 DC/DC Converters . . . 63
3.7.3 Cables . . . 64
3.7.4 Buses and Splitters . . . 66
3.7.5 Circuit breakers . . . 68
3.7.6 Gearboxes . . . 68
3.7.7 Tanks and fuel system . . . 69
3.8 Summary . . . 69
3.9 Conclusion and perspectives . . . 69

II Emission optimized hybrid- and full-electric alternatives for General Aviation aircraft 75

4 Electrification scenarios for CS-23 certification category aircraft 77
4.1 Introduction . . . 77
4.2 Selection of electrification scheme for the propulsive architecture . . . 79
4.2.1 Aircraft use phase emissions estimation . . . 79
4.2.2 Limitations of electric components technology maturity . . . 80
4.2.3 Pre-selection of electrification scenario for the different applications 82
4.3 Level 1 aircraft . . . 85
4.3.1 Velis Electro . . . 85
4.3.2 Comparison with the Pipistrel SW 121 . . . 88
4.4 Level 2 aircraft . . . 90
4.4.1 Electric version . . . 92

4.4.2 Hybrid version . . . 96
4.5 Level 3 aircraft . . . 104
4.5.1 Selection of the reference aircraft . . . 104
4.5.2 Hybrid TBM 900 . . . 107
4.5.3 Hybrid DAHER Kodiak . . . 115
4.6 Level 4 aircraft . . . 119
4.6.1 Identification of representative aircraft . . . 119
4.6.2 Hybrid Cessna 208B . . . 122
4.7 Conclusion and perspectives . . . 125

III Design under environmental life cycle considerations 129

5 Life Cycle Analysis 131
5.1 Introduction and context . . . 131
5.2 LCA . . . 133
5.3 Review of LCA use cases in the aviation sector . . . 135
5.3.1 Review of representative products in LCA applications . . . 135
5.3.2 Integration into the design process . . . 138
5.4 Application to the LCA of electrified General Aviation aircraft . . . 140
5.5 Application of the LCA methodology for the design of electrified aircraft . . . 147
5.5.1 From CO2 emissions to Life Cycle impacts . . . 147
5.5.2 Influence of cell chemistry choice on environmental impacts . . . 159
5.5.3 Effect of change in airframe materials . . . 165
5.5.4 Effect of battery aging . . . 171
5.6 Application of the LCA for the assessment of future aircraft configurations . . . 183
5.7 Conclusion and perspectives . . . 191

IV Conclusions and perspectives 195

6 Conclusion 197
6.1 Summary . . . 197
6.2 Answer to the research questions . . . 198
6.3 Perspectives for future work . . . 203

Contributions 205

References 206

Appendix A Reproducibility and accessibility 239

A.1 Organization of powertrain component model directories 239
A.1.1 Model implementation directories 240
A.2 Organization of test cases directories 242

Appendix B Appendix to the Part I **245**
B.1 Establishment of the propeller performances surrogate model 245
B.1.1 Identification of dimensionless parameters 245
B.1.2 Training and validation dataset generation 246
B.1.3 Creation of the surrogate 246
B.2 Establishment of the turboshaft performances surrogate model 248
B.3 Inverters and Rectifiers losses model 250

Appendix C Appendix to the Part II **253**
C.1 Virus SW 121 253
C.2 Reference Cirrus SR22 255
C.3 Reference DAHER TBM 900 257
C.4 Reference Quest/DAHER Kodiak 257
C.5 Reference Cessna 208B 258
C.6 Summary of battery cells used for prospective electrification scenarios . . . 260

Appendix D Appendix to the Part III **263**
D.1 LCA in the context of the aeronautics sector 263
D.1.1 Goal and Scope definition 263
D.1.2 Extraction and Emissions inventory 265
D.1.3 Impact assessment 267
D.1.4 Interpretation 269
D.2 Background processes used for the LCI of General Aviation aircraft 270

List of Figures

1.1 Summary of the main hybrid-electric and electric aircraft configurations [15]. 4
1.2 Typical on-board conversion chains with typical component efficiencies and total chain efficiency [23]. 5

2.1 An N2 diagram representation of an aircraft design problem, generated with the FAST-OAD package [69]. 17
2.2 Most common optimization problem formulation, represented as XDSM diagram. Adapted from [73]. 19
2.3 Application of the constraint analysis method to the sizing of a hybrid electric aircraft [77]. 21
2.4 Powertrain representation based on the generic description and variation of H_P and H_E [64]. 22
2.5 Illustration of the Initiator process flow for the design of a distributed hybrid-electric propulsion aircraft [99]. 28
2.6 FAST-OAD disciplines interrelationship, adapted from [69]. Problem inputs and their classification are further discussed in Table 2.2. 33
2.7 Schematic drawing of the working principle of the FAST-OAD-CS23-HE framework. 38
2.8 Description of the powertrain preconditioning for the computation of the mission. 39
2.9 Example of model classification and aggregation for components in the FAST-OAD-CS23-HE library. The N2 is generated using FAST-OAD's built-in post-processing capabilities applied to the models used for the electric motor. 40
2.10 Schematic representation of the disciplines and couplings in the FAST-OAD-CS23-HE framework. 43

3.1 Correlation between the uninstalled weight of turboprops and their rated power [58]. 50
3.2 Statistical analysis on the characteristics of the PT6A turboshaft family. . . 61

3.3 Distribution of the relative error between data and the statistical trends implemented in the framework. 61
3.4 Architecture considered for the DC/DC converter, adapted from [189]. . . 64
3.5 Schematized drawing of the cable. 66
3.6 Operating principle of the splitter. 67
3.7 Influence of the operating principle of the splitter on the power repartition. 67

4.1 Excerpt from a marketing brochure from the TBM850. 78
4.2 Cape Air commuter flight distribution as a function of distance, adapted from Cape Air's *Commuter Airline Perspective* 81
4.3 Evolution of MTOM with respect to design range for different CS-23 level electric aircraft. 83
4.4 Classification of concepts identified in the literature review based on the powertrain type. 84
4.5 Pipistrel aircraft under consideration. Source: Pipistrel. 85
4.6 Propulsive system architecture for the Pipistrel Velis Electro, the components highlighted in red are the ones modeled in this study. 86
4.7 Comparison of the flight performances computed by the code with those published in the POH for the Velis Electro. 88
4.8 Cumulative number of piston aircraft of each type produced since 1994. 91
4.9 Distribution of flights for aircraft in the Cirrus SR22 Series. 92
4.10 Propulsive system architecture considered for eSR22. 93
4.11 Sensitivity of the Electric Cirrus SR22 masses to the design range. 95
4.12 Modified Tecnam P2010T for the needs of the H3PS project. Source: https://h3ps.eu/. 96
4.13 Optimization of the hybridization ratio to minimize the emission of the Cirrus SR22. 97
4.14 Optimization of the hybridization ratio to minimize the emission of the Cirrus SR22 with a higher energy density cell. The results with the original cell are presented as a comparison point. 98
4.15 Comparison of emissions of the hSR22 on off-design missions. 100
4.16 Feasibility study for a 200 nm eSR22 based on battery energy density. . . . 102
4.17 Results of the emission minimization for various battery energy densities. . 103
4.18 Cumulative number of turboprop aircraft of each type produced since 2006. 105
4.19 Distribution of the countries of registration of the TBM 900 and the Kodiak 100/900 [226]. 106
4.20 Distribution of flights for aircraft in the TBM900 Series. 107

4.21 Powertrain considered for the study of EcoPulse as a retrofit. 108
4.22 Powertrain considered for the study of EcoPulse with a design from scratch. 109
4.23 Uncertainties on the main outputs of the sizing process. 113
4.24 Distribution of flights for aircraft in the DAHER Kodiak Series. 115
4.25 Powertrain considered for the hybridization of the DAHER Kodiak. 116
4.26 Propeller shaft power profile with each contributing source. 117
4.27 Evolution of the masses of the components of the powertrain between the Kodiak 100 and its hybrid retrofit. 119
4.28 Variation of SFC and power demand for the turboshaft of the reference Kodiak 100 and its hybrid retrofit. 120
4.29 Distribution of flights for aircraft in the Cessna 208 Series. 121
4.30 Influence of the hybridization threshold power on the emissions per kg of payload per km. 124
4.31 Power profile with each contributing source. 125
4.32 Summary of all the validation and prospective cases investigated in this Chapter. 126

5.1 Flowchart providing an overview of the life cycle of the two-seater all-electric aircraft [227]. 133
5.2 Phases of LCA, adapted from [246]. 135
5.3 Framework of parametric life cycle assessment (PLCA) based ecodesign process for power electronic. [275]. 139
5.4 Boundaries for the LCA study of electrified General Aviation Aircraft, adapted from the initial draft of the PEFCR for aircraft. 142
5.5 Average age of the fleet per category reported in the GA survey from the BTS. 144
5.6 Average yearly usage of the fleet per category reported in the GA survey from the BTS. 144
5.7 Example process tree associated with the retrofit EcoPulse presented in Section 4.5.2. 148
5.8 Relative contributions to each impact category for the reference Cirrus SR22. 149
5.9 Relative contributions to each impact category for the electric Cirrus SR22. 150
5.10 Evolution of impacts in the Climate Change category for the hybrid Cirrus SR22. 152
5.11 Minimization of the environmental single score for the hybrid Cirrus SR22. 154

5.12 Evolution of the single score with life expectancy of the aircraft. 156
5.13 Normalised and weighted impacts for the reference Kodiak 100, expressed per pax.km. 156
5.14 Relative comparison of the environmental impacts for the reference Kodiak 100 and the hybrid variant. 157
5.15 Sensitivity of the Pipistrel Velis Electro masses to the battery energy density. 161
5.16 Process tree for the Skeleton Technologies SuperBattery production proxy. 162
5.17 Normalized and weighted impact score for the Pipistrel Velis Electro with different battery cells. 163
5.18 Comparison of impact magnitude in select categories for the Pipistrel Velis Electro with different battery cells. 165
5.19 Relative comparison of the environmental impacts for the reference Velis Electro and its metallic variant. 167
5.20 Relative contributions to each impact category for the reference Pipistrel SW121. 169
5.21 Relative comparison of the environmental impacts for the reference SW121 and its metallic variant. 170
5.22 Variation of battery lifespan, battery mass per FU, and single score for decreasing SoC at the start of the mission. 173
5.23 Derivative, with respect to DoD, of the function representing the effect of DoD on the cyclic aging. 175
5.24 Variation of battery lifespan, battery mass per FU, and single score for decreasing SoC at the start of the mission for the Velis Electro+. . 177
5.25 Approach adopted to evaluate the effect of SoH on the performances of the Velis Electro. Adapted from Figure 2.1 in Pollet et al. [276]. 180
5.26 Effect of battery aging on flight performances. The main x-axis represents the number of cycles since renewal, the secondary axis shows the corresponding SoH. 180
5.27 Effect of battery aging on average energy required for one FU. 181
5.28 Effect of battery aging on score in EF V3.1 impact categories. 182
5.29 Normalized and weighted impact score for an electric commuter aircraft with various technological assumptions. 188
5.30 Relative contributions to each impact category for the electric commuter aircraft with Li-S battery. 190
5.31 Relative contributions to each impact category for the electric commuter aircraft with Sodium-Ion battery. 190

B.1 Results of the surrogate modeling for the propeller performances. 247
B.2 Comparison, on the validation set, of the values computed by the surrogate (gray dots) and the ones computed with the original method (dashed line). 248
B.3 Results of the surrogate modeling for the turboshaft fuel consumption. . . 249
B.4 Typical turn-on/-off energy for the SEMiX453GB12M7p semiconductor from *the manufacturer's website*. 251

C.1 Comparison of the flight performances computed by the code with those published in the POH for the Virus SW121. 255
C.2 Comparison of Kodiak 100 design mission and operational mission. 259
C.3 Position of the cells used for the case studies on a Ragone plot. 261

D.1 Schematic view of the integration of an environmental module in an aircraft design framework in support of eco-design [276]. 264
D.2 Data collection challenges in a typical process tree in life cycle assessment (LCA) [312]. 266
D.3 Framework of the ReCiPe method: Relationship between LCI results, midpoint impact category, and endpoint impact categories. Source: https://pre-sustainability.com/articles/recipe/, Accessed 2025-09-22. 268

List of Tables

2.1 Functional comparison of integrated OAD frameworks. 30
2.2 Description of input types and examples in the FAST-OAD framework. 35

3.1 Value for the emissions indices considered for the operation of piston ICE. 59
3.2 Value for the emissions indices considered for the operation of turboshafts. . 62
3.3 Physical properties of the materials considered for the cable core. 65
3.4 Summary of the models implemented. 70

4.1 Carbon intensity of all considered energy carriers. 80
4.2 Main input parameters for the validation study on the Pipistrel Velis Electro. 87
4.3 Main outputs for the FAST-OAD sizing process of the Pipistrel Velis Electro. . 87
4.4 Performances and emission metrics of the Level 1 designs. 89
4.5 Main input parameters for the prospective study on the eSR22. 94
4.6 Main outputs for the FAST-OAD sizing process of the eSR22. 94
4.7 Specification for the hSR22 optimization problem. 97
4.8 Main outputs for the FAST-OAD optimization process of the hSR22. 99
4.9 Average emission reduction and weight for each segment. Average emissions reductions are obtained based on the average reduction of emissions for the mission at both ends of the segment. 101
4.10 Main input parameters for the sizing process of the EcoPulse. 109
4.11 Main outputs for the FAST-OAD sizing process of the retrofit version of the EcoPulse. 109
4.12 Main outputs for the FAST-OAD sizing process of the EcoPulse with a design from scratch. 110
4.13 Uncertain parameters. 112
4.14 Rescaled total Sobol' indices. 113
4.15 Main input parameters for the sizing process of the hybrid Kodiak 100. . . . 116
4.16 Main outputs for the FAST-OAD sizing process of the different versions of the Kodiak. 118

4.17 Summary of the main modeling assumptions for the design investigation of the Cessna 208B. 123
4.18 Active battery pack constraints for the hybrid C208. 123

5.1 Main outputs for the LCA of the reference SR22 and the eSR22. 151
5.2 Specification for the hSR22 optimization problem using the LCA methodology. 153
5.3 Environmental single score for the two Kodiak 100 variants. 156
5.4 Variation of contributing factors to the single score, for the mission of interest. 158
5.5 Characteristics of the cells considered for the Pipistrel study. 161
5.6 Main outputs for the sizing and LCA of the Pipistrel Velis Electro with different battery cells. 162
5.7 Impact intensity of the battery manufacturing process for the different battery cells. 164
5.8 Main outputs for sizing of the reference Velis Electro and its metallic variant. 166
5.9 Evolution of endpoint impacts for the reference Velis Electro and its metallic variant. 167
5.10 Main outputs for the sizing process and LCA of the reference SW121 and its metallic variant. 169
5.11 Main input parameters for the battery aging model. 172
5.12 Added assumptions for the sizing of the Pipistrel Velis Electro+. 175
5.13 Main outputs for sizing of the Velis Electro+. 176
5.14 Main outputs for sizing of the Velis Electro++. 178
5.15 Predicted evolutions of characteristics in power electronics. 184
5.16 Predicted evolutions of characteristics in electric motors [53]. 184
5.17 Predicted evolutions of characteristics in battery cells. 185
5.18 Main TLARs for the sizing process and LCA of the electric commuter aircraft. 186
5.19 Main outputs for the sizing of the electric commuter aircraft. 186
5.20 Environmental single score of the electric commuter aircraft. 187
5.21 Evolution of the factors contributing to the environmental score of the battery manufacturing process. 188

B.1 Range of values for the similarity parameters covered in the surrogate. . . . 246
B.2 Range of values for the input parameters covered in the dataset. 248

C.1 Main input parameters for the validation study on the Pipistrel Virus SW 121. 253

C.2 Main outputs for the FAST-OAD sizing process of the Pipistrel Virus SW 121. 254
C.3 Main input parameters for the validation study on the Cirrus SR22. 256
C.4 Main outputs for the FAST-OAD sizing process of the Cirrus SR22. 256
C.5 Main outputs for the Daher TBM 900 run compared with original results [91]. 257
C.6 Main outputs for the FAST-OAD sizing process of the Kodiak 100. 258
C.7 Main input parameters for the validation study on the Cessna 208B. 259
C.8 Main outputs for the FAST-OAD sizing process of the Cessna 208B. 260
C.9 Summary of cells used for the case studies and their characteristics. 262

D.1 Ecoinvent 3.9.1 processes for the LCI of the GA aircraft. 271

Nomenclature

Abbreviations

AC	Alternating current
ADT	Actuator Disk Theory
AF	Activity Factor (-)
AFPMSM	Axial Flux Permanent Magnet Synchronous Machine
AvGas	Aviation Gasoline
BEMT	Blade Element Momentum Theory
BLI	Boundary Layer Ingestion
BMS	Battery Management System
BTS	Bureau of Transportation Statistics
BWB	Blended Wing Body
CFRP	Carbon Fiber Reinforced Plastics
CG	Center of Gravity
CH_4	Methane
CO	Carbon monoxide
CO_2	Carbon dioxide
CS	Certification Specifications
DAB	Dual Active Bridge
DALY	Disability-Adjusted Life Year
DC	Direct Current
DCAS	Département Conception et conduite des véhicules Aéronautiques et Spatiaux (Department of Aerospace Vehicles Design and Control)
DEP	Distributed Electric Propulsion
DOD	Depth Of Discharge (%)
EAP	Electrified Aircraft Propulsion
EAS	Equivalent AirSpeed or Essential Air Service
EASA	European Union Aviation Safety Agency

ECM	Equivalent Circuit Model
EF	Emission Factor (gCO2/kgPAX/km) or Environmental Footprint
EI	Emission index (g/kg)
EIS	Entry-Into-Service
ESAR	Energy Specific Air Range (NM/kWh)
ESC	Electronic Speed Controller
ESE	Energy Specific Endurance (h/kWh)
EWIS	Electrical Wiring Interconnection System
FAR	Federal Aviation Regulations
FAST	Future Aircraft Sizing Tool
FU	Functional Unit
GA	General Aviation
GAMA	General Aviation Manufacturers Association
GHG	Green House Gases
H_2O	Water
HC	Unburnt hydrocarbons
HTP	Horizontal Tail Plane
IAM	Integrated Assessment Models
ICAO	International Civil Aviation Organization
ICE	Internal Combustion Engine
IDF	Individual Discipline Feasible
IGBT	Insulated-Gate Bipolar Transistor
ISA	International Standard Atmosphere
ISAE	Institut Supérieur de l'Aéronautique et de l'Espace
ISO	International Organization for Standardization
ITT	Inter Turbine Temperature (°K)
KEAS	Knots Equivalent AirSpeed
KIAS	Knots Indicated AirSpeed
KTAS	Knots True AirSpeed
LCA	Life Cycle Assessment or Life Cycle Analysis
LCC	Life Cycle Cost
LCI	Life Cycle Inventory
LCIA	Life Cycle Impact Assessment
LCSA	Life Cycle Sustainability Assessment

LLT	Lifting Line Theory
LTO	Landing and TakeOff
MCP	Maximum Continuous Power (kW)
MDA	MultiDisciplinary Analysis
MDAO	MultiDisciplinary Analysis and Optimization
MDF	Multidisciplinary Design Feasible
MEP	Mean Effective Pressure (Pa or bar)
MK	MegaJoule
MLM	Maximum Landing Mass (kg)
MTOM	Maximum TakeOff Mass (kg)
MTOW	Maximum TakeOff Weight (N)
MW	MegaWatt
MZFW	Maximum Zero Fuel Weight (N)
NA	Not Applicable
NEC	National Electrical Code
NM	Nautical miles
NMC	Nickel Manganese Cobalt
NO_X	Nitrous Oxide
OAD	Overall Aircraft Design
OCV	Open Circuit Voltage (V)
OME	Operating Mass Empty (kg)
OPR	Overall Pressure Ratio (-)
OWE	Operating Weight Empty (N)
PAX	Passengers
PEFCR	Product Environmental Footprint Category Rules
PLCA	Parametric Life Cycle Assessment
PMAD	Power Management and Distribution
PMSM	Permanent Magnet Synchronous electric Motor or Machine
POH	Pilot Operating Handbook
PWM	Pulse Width Modulation
RMS	Root Mean Squared
RPK	Revenue Passenger Kilometers
RPM	Revolutions Per Minute
SAF	Sustainable Aviation Fuel

SAR	Specific Air Range (NM/kg)
SFC	Specific Fuel Consumption (g/kW/h)
SM	Surface-Mounted
SMR	Short Medium Range
SO_X	Sulfur Oxide
SOC	State Of Charge (%)
SOH	State Of Health (%)
SSPC	Solid State Power Controller
SSSD	Solid State Switching Device
STOL	Short TakeOff and Landing
TBO	Time Between Overhaul
TCDS	Type Certificate DataSheet
TLAR	Top Level Aircraft Requirements
TLARs	Top-Level Aircraft Requirements
TMS	Thermal Management System
TOM	TakeOff Mass (kg)
TRL	Technological Readiness Level
TSPC	Thrust Specific Power Consumption (g/N/h)
TTW	Tank to Wake
UAV	Unmanned Aerial Vehicle
VLM	Vortex Lattice Method
VOC	Volatile Organic Compounds
VPLM	Variable Power Law Meta-model
VTP	Vertical Tail Plane
WTT	Well to Tank
WTW	Well to Wake
XDSM	eXtended Design Structure Matrix

Nomenclature for Part I

α	Angle of attack (°or rad), or scaling factor
Δ	Variation in
$\dot{m}$	Mass flow (kg/s)
$\mathcal{C}$	Length specific heat capacity (J/°K/m)
$\mathcal{R}$	Length specific resistance (Ω/m)
m	Length specific mass (kg/m)

ν	Kinematic viscosity (m^2/s)
ω	Rotation speed (rad/s)
ρ	density (kg/m^3)
ρ_{elec}	Resistivity (Ωm)
σ	Density ratio (-)
σ	Solidity (-)
Θ	Temperature (degK)
θ	Twist (rad)
A	Cross section (m^2)
a	Speed of sound (m/s)
C	Aerodynamic coefficient (-) or capacity (Ah)
cp	Specific heat (J/°K/kg)
D, d	Diameter (m)
FF	Fuel flow (kg/h)
I	Current (A)
k	Constant
l	Length (m)
m	Mass (kg)
N	Number of (-)
n	Revolution frequency (s^{-1})
P	Power (W)
Q	Heat (J)
Q	Torque (N.m)
R	Radius (m)
R	Resistance (Ω)
R_{th}	Thermal resistance (°K/W)
Re	Reynolds number (-)
T	Thrust (N)
t	Time (s)
U	Voltage (V)
V	Velocity (m/s)

Nomenclature for Part II

H_P	Hybridization ratio (%)
PL	Payload mass (kg)

Nomenclature for Part III

E	Energy stored (W.h)
ESS	Environmental Single Score (pts)
IF	Impact factor (unit depend on the impact category)
IS	Impact score (unit depend on the impact category)

Superscripts

$.^*$	denotes the scaling of a physical quantity x, $x^* = x/x_{ref}$

Subscripts

$\cdot_{(h-s)}$	case to heatsink
$\cdot_{(j-c)}$	junction to case
$\cdot_{(s-a)}$	heatsink to ambient
$\cdot_0$	relative to the inlet of the turboshaft
$\cdot_9$	relative to the exhaust of the turboshaft
$\cdot_\infty$	relative to freestream air
$\cdot_{\text{airframe}}$	relative to the airframe
$\cdot_{\text{battery}}$	relative to the battery
$\cdot_{\text{climate change}}$	relative to the climate change impact category
$\cdot_{\text{combustion}}$	relative to the fuel combustion
$\cdot_{\text{cycles}}$	relative to charge/discharge cycles
$\cdot_{\text{fuel}}$	relative to the fuel
$\cdot_{\text{production}}$	relative to the fuel production
$\cdot_{air}$	relative to the air
$\cdot_b$	relative to the blade
$\cdot_{cable}$	relative to the cable
$\cdot_{cell}$	relative to the battery cell
$\cdot_{clean}$	relative to aircraft in clean configuration
$\cdot_{core}$	relative to the core
$\cdot_{cu}$	relative to copper losses
$\cdot_C$	relative to the capacity
$\cdot_{des}$	relative to design conditions
$\cdot_{diode}$	relative to the diode
$\cdot_D$	relative to the diameter
$\cdot_D$	relative to the drag
$\cdot_{ec}$	relative to eddy current losses

$\cdot_{em}$	electric motor
$\cdot_{ex}$	relative to excitation losses
$\cdot_{fr}$	relative to friction losses
$\cdot_{hub}$	relative to the blade hub
$\cdot_{h}$	relative to hysteresis losses
$\cdot_{IGBT}$	relative to the IGBT
$\cdot_{ins}$	relative to the insulation
$\cdot_{iron}$	relative to iron losses
$\cdot_{i}$	relative to i-th step of the flight
$\cdot_{loss,calendar}$	relative to calendar aging
$\cdot_{loss,cyclic}$	relative to cyclic aging
$\cdot_{losses}$	relative to the losses
$\cdot_{L}$	relative to the lift
$\cdot_{max}$	relative to the limit value
$\cdot_{max}$	relative to the maximum value
$\cdot_{mech}$	relative to mechanical losses/power
$\cdot_{mission}$	relative to the aircraft mission
$\cdot_{m}$	relative to the pitching moment
$\cdot_{nom}$	relative to nominal conditions
$\cdot_{oc}$	internal
$\cdot_{oc}$	open circuit
$\cdot_{ref}$	relative to reference conditions
$\cdot_{req}$	relative to a requirement
$\cdot_{R}$	relative to the resistance
$\cdot_{sheath}$	relative to the protective sheath
$\cdot_{storage}$	relative to storage conditions
$\cdot_{tape}$	relative to the shielding tape
$\cdot_{tip}$	relative to the blade tip
$\cdot_{U}$	relative to the voltage
$\cdot_{wdg}$	relative to windage losses
$\cdot_{w}$	relative to the wing

Chapter 1

State of the art and thesis objectives

Contents

1.1 Sustainability of the aeronautics sector **1**
1.2 Technical Context of electrification of propulsive architecture **3**
1.2.1 Terminology and nomenclature electrified aircraft propulsion . . 3
1.2.2 Benefits of electrified propulsive architectures 3
1.2.3 Challenges and limitations to the introduction of electric powertrains 6
1.2.4 Barriers to the applicability of conventional design methodologies 7
1.3 Problem statement **8**
1.4 Identification of research questions **10**
1.5 Manuscript overview **10**

1.1 Sustainability of the aeronautics sector

Within the context of the Paris Agreement, governments have set long-term goals to limit the increase in global temperature to below 2°C [1]. Among the Green House Gases (GHG) that drive this elevation in the global temperature, CO_2 has been recognized as the most important contributor from anthropogenic origin [2]. One of the biggest sources of CO_2, accounting for up to 23 % of global emissions in 2014 [3], is the combustion of fossil fuels by the transportation sector. Aviation, as for itself, represents 2.1% of global human-induced CO_2 emissions. In addition to that, aviation also contributes to global warming through other physical phenomena such as the creation of condensation trails and the emission of NO_x [4], which are the results of the combustion of aviation fuels inside the engines. All in all, by integrating all of the aforementioned effects, the global contribution of aviation amounted in 2011 to 3.5% of the effective radiative forcing [5], a number which is likely to increase because of a forecasted annual growth of 3-5% [6]. The impact of the aeronautics sector on the environment, however, is not limited to its contribution to the elevation in temperature.

Indeed, in addition to GHG, the combustion of aviation fuel releases other harmful pollutants that can impact the health of ecosystems as well as that of humans. Light aircraft, in particular, although only marginal contributors to the emissions of the sector as a whole, account for more than 40% of carbon monoxide emissions and the entirety of lead emissions [7, 8]. The reason for these emissions is that, because of lighter certification requirements on the release of harmful pollutants, propulsive architectures have barely evolved since the 1960s [7]. Therefore, a vast majority of General Aviation designs still rely on outdated piston engines and leaded energy vectors for simplicity, robustness, and cost reasons.

For those reasons and because the sector is undergoing heavy scrutiny, many national and international agencies have set very ambitious targets for the reduction of emissions [9]. Among those, the European Commission aims to reduce the emission CO_2 per passenger kilometer by 75%, the NO_x emission by 90 % and the perceived noise of flying aircraft by 65% [10]. Likewise, NASA plans on a reduction of fuel burn by 50%, a reduction of NO_x of 75% during take-off and landing phases, as well as a great reduction in the cumulative noise [11].

Among the levers of action investigated by the aeronautics community, four main avenues of improvement have been identified: the improvement of known technology, the optimization of trajectories and infrastructures, as well as the introduction of new energy vectors [12]. Outside of the use of Sustainable Aviation Fuel (SAF), disruptive technologies for the powertrain, such as electric propulsion and innovative aircraft configuration (the utilization of Distributed (Electric) Propulsion, for instance), would also enable the reduction of emissions. Full-electric aircraft even offer the prospects of no in-flight emissions. These changes, however, come with new challenges and opportunities at aircraft level and need to be considered early in the design stage in order to make the best possible use of them [13]. A more gradual approach to the introduction of electric technologies in the fleet is also envisioned by some aircraft manufacturers as demonstrators[1] to increase the technological readiness level of electric propulsion. Small-scale standalone products [14] could also be used for that purpose. These disruptive technology choices will, however, drastically change the performance of the aircraft with gains far exceeding the yearly 2% promised by continuous improvement. It is thus paramount to develop sizing tools capable of assessing the feasibility of hybrid and all-electric aircraft as well as the viability of retrofitting new powertrains on existing aircraft.

All things considered, the General Aviation segment will play a pivotal role in the adoption of electrified propulsive architectures in the aeronautics sector. Although it is only a minute contributor to the overall fuel consumption of the sector, its specifics in terms of propulsion technologies leave considerable room for improvement in terms of environmental impacts. Moreover, General Aviation (GA) aircraft routinely serve as test beds for emerging aeronautical

[1] Such as the EcoPulse demonstrator, Rolls-Royce's Spirit of Innovation, or the H3PS project

innovations, offering a low-risk, low-cost, and adaptable platform for technology maturation. Additionally, the orders of magnitude of power requirements for GA aircraft place the sector at a unique crossroads: it can leverage maturing technologies developed for road transportation while simultaneously aligning with the emerging needs of the urban air mobility market. For these reasons, GA aircraft pose as credible test cases for the electrification of propulsive functions.

1.2 Technical Context of electrification of propulsive architecture

1.2.1 Terminology and nomenclature electrified aircraft propulsion

The use of electricity for the generation of part or the totality of the propulsive force on the aircraft is referred to in literature as Electrified Aircraft Propulsion (EAP). The terms electric and hybrid-electric propulsion are also commonly used to refer to that principle. More than one power source can be used jointly for the generation of electric power and to produce thrust. The possible combinations of power consumers and power generators dictate the taxonomy of the chain [15–17]. The term hybrid electric is used to describe power architectures where there is more than one power source, which can include: electro-chemical energy storage (e.g., batteries or super-capacitors), electro-chemical cell that transforms the chemical energy of a fuel into electricity (e.g., Fuel Cells), or fuel-burning devices (e.g., turbo-machinery or Internal Combustion Engine (ICE)). On the other side of the spectrum, all- or full-electric configurations only have a single electricity-generating source type. Likewise, turbo-electric configurations use generators to transform the mechanical energy of a fuel-burning device into electric power. A summary of some of those architectures is shown in Figure 1.1.

1.2.2 Benefits of electrified propulsive architectures

One of the main advantages of battery-generated electricity is that it does not release any emissions during the flight [18], meaning that all-electric aircraft have the potential for zero-emission flights. Electric propulsion and electric-propulsion-enabled architectures can also pave the way to a sharp reduction in aircraft noise [19–21], and in the case of General Aviation (GA), it will even reduce the emission of lead particles. Indeed, the combustion of Avgas 100LL, which remains today the go-to fuel to power light aircraft, is responsible for lead emissions. In addition to those reduced emissions, directly linked to the technology itself, electric propulsion could also be used as a way to increase the efficiency of the energy conversion chain [22]. Indeed, while the thermodynamic performances of fuel burning engine limit the efficiency of fuel-based architecture to around 45% [23, 24], full electric chains have average efficiencies of nearly twice as much as turbo-machinery [23] and even three times higher than ICE [25] as illustrated in Figure 1.2. The main reason for this difference is

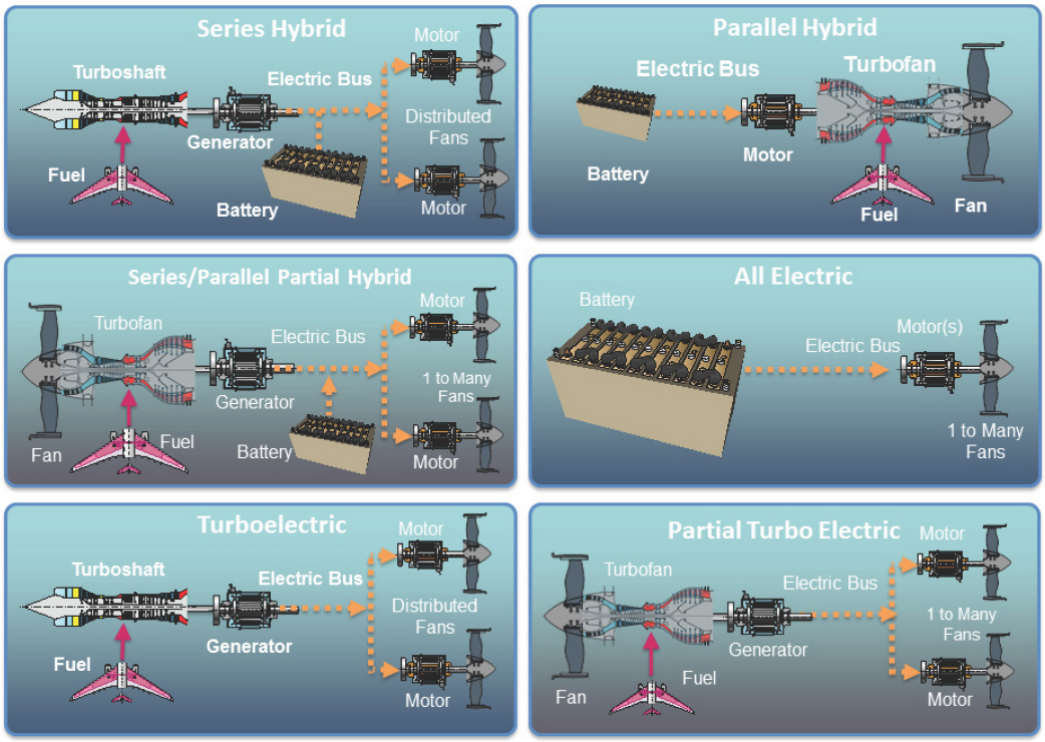

Figure 1.1 Summary of the main hybrid-electric and electric aircraft configurations [15].

that the component typically found in an electric power chain can reach efficiencies of above 90-95% with modern technologies and even higher in near-future technological scenarios [16, 18, 21, 26, 27]. Consequently, this enables a reduction in the need for primary energy for the same amount of required propulsive energy [22]. All in all, and including the intrinsic gain stemming from the use of de-carbonated in-flight power sources, the estimated reductions in CO_2 emissions are evaluated as between 40 and 80% for hybrid aircraft and up to 100% for all-electric aircraft [28].

In addition to that, electric propulsion is a scalable technology [13] which can allow for a gradual integration of its use in the aviation sector [28]. Furthermore, components in an electric powertrain have greater efficiencies on a wider range of power outputs contrarily to gas turbines [6, 29] which have irreversibilities linked to scale factors. This also means that technologies envisioned to reduce the emissions of fuel-based propulsion will have a greater impact on small to medium aircraft [30]. Another major advantage that the scalability of electric propulsion enables is a greater freedom in the placement of propulsive elements [31]. Easier distribution of the propulsion on the airframe, which is commonly known as Distributed (Electric) Propulsion (DEP), becomes possible thanks to that. In turns, strategic distribution of the propulsion elements allows for aero-structural [32] and aero-propulsive synergies, enabling smaller wings, shorter takeoffs and landings [33, 34], reduced drag [35, 36] and improved propulsive efficiency [26, 37–39].

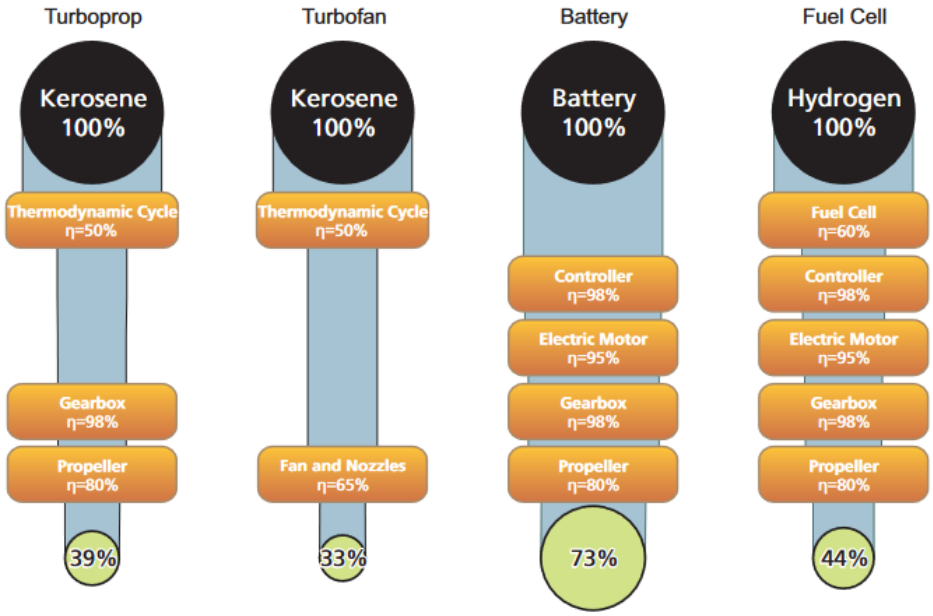

Figure 1.2 Typical on-board conversion chains with typical component efficiencies and total chain efficiency [23].

An additional freedom in the design of the aircraft granted by the usage of electric propulsion and its scalability is the relief of some of the design constraints imposed on conventional propulsion systems. The most striking example of such constraint is the fact that, although the engine spends most of its time operating in cruise conditions, it is sized for the significantly greater power demand experienced during takeoff and initial climb. Using electric propulsion in complement of a conventional engine would allow to optimize it for cruise conditions and provide the supplement of power through high-capacity batteries [6, 40]. In the same spirit, an aircraft whose propulsion would be distributed over a great number of small propulsive elements would suffer less from the loss of one of these — the one-engine inoperative case — both in terms of lost power and in terms of sizing of the Vertical Tail Plane (VTP). Because of the nature of electric power, it is also intrinsically easier to add secondary power paths to bypass the loss of a cable or of a component, which makes it very easy to build fail safe electric architecture with high redundancy. Pairing the propulsive elements symmetrically with respect to the fuselage could also ensure that if a bus bar or a power electronic were to fail, there would not be any thrust imbalance [27]. On the topic of operational considerations, it has also been suggested that, since the aircraft would not be relying on fuel burning machine for the production of propulsive power, the maintenance work to be done would be less expensive [21, 40]. Finally, some reductions in operating costs can also be hoped for based on the observation that, on a conventional architecture, the price of energy represents 30 to 50 % of the total operating costs [13, 41, 42].

1.2.3 Challenges and limitations to the introduction of electric powertrains

One of the main drawbacks and technological locks preventing the widespread feasibility of EAP in the aeronautics sector is the battery weight [43]. In terms of energy density, the unit energy stored in one unit of mass, batteries are several orders of magnitude below that of conventional fuel. Current state-of-the-art batteries, using Li-Ion chemistry, have densities of around 250 Wh/kg, compared with the 12.6 kWh/kg of Jet A-1 fuel. This has been identified as one of the bottlenecks for the creation of all-electric aircraft [44], with some pessimistic estimations even estimating that an all-electric aircraft will never be feasible [45]. Other, more optimistic sources judge that a sixfold increase in battery energy will still be required for on-par performances with conventional aircraft, even when taking into account the increased efficiencies of the powertrain [6]. This low energy density only worsens the impact on the aircraft of the snowball effect (the added weight increases the energy use, which increases the added weight), through which the weight dependency on the energy use is amplified. A side-effect of not burning fuel, albeit a second-order one, is that the aircraft's mass remains the same during the whole flight. This means the energy use stays constant, and the used battery becomes a dead mass that has to be carried, unlike fuel.

Another major issue with the use of electricity on board an aircraft is the need to evacuate all the heat the components produce, which, for a conventional fuel-based architecture, is generally done through the exhaust of hot gases. At the MW order of magnitude, even with the high efficiency of electric components, the amount of waste heat becomes significant. At this magnitude and even assuming near-future efficiencies of 97% [21], the heat induced by losses is equivalent to the propulsive power of a Pipistrel Velis Electro. This implies that components that do not directly contribute to the generation of thrust will need to be carried on the aircraft for cooling. This not only adds weight (up to 17% of the propulsion system weight [46] depending on the configuration) but also adds drag and power consumption [47]. This is all the more so important since the temperature at which the components are being used has a big impact on the performances of said component [48–50] as well as on its lifespan. Finally, safety aspects on the operability of the powertrain are strongly linked with thermal management aspects because an overheated battery can lead to a fire, with potentially catastrophic consequences for the aircraft.

Another crucial point to consider when designing an electric or hybrid-electric aircraft is to keep a global view of the aircraft and how/where it is going to be used. Indeed, while batteries and hydrogen offer the potential to remove any direct emissions, the way the electricity and the hydrogen are produced plays a significant role in the computation of the aircraft's life cycle environmental footprint [6, 48, 51]. In some countries where the electricity is primarily generated through the use of coal plants, the electric aircraft could actually be worse than a conventional jet engine aircraft [52]. Besides the operation phase, the production of the electric aircraft also has to be considered. The battery currently in use

relies on Lithium or a derivative as a cathode, which is a material whose demand is already strained and which has a great impact on the environment in terms of rare metal depletion [6]. The same could be said for a lot of the envisioned technologies for electric motor which rely on rare earth materials [53]. Finally, because CO_2 has a very long residency time, it is also paramount to take the date of Entry-Into-Service (EIS) of those future electric aircraft into account [54]. An earlier EIS with a smaller reduction in emissions might be better than a late EIS with far better reductions in terms of cumulative emissions.

Perhaps a more direct impact on the design of an electric or hybrid-electric aircraft is the fact that the added freedom for the design also comes at the cost of unfamiliar and unknown design constraints. These new power architectures indeed come with a lack of historical data, which makes proving that these aircraft are safe and worthy to fly all the more challenging [51]. This might add some very harsh constraints on the choice of architecture in terms of redundancy and alternative power path, which has the potential to considerably narrow the allowable design space [6, 55]. Along with the lack of feedback on electric and hybrid-electric architectures comes the lack of readiness and trust in this technology. Specialist estimates that, as of today, the Technological Readiness Level (TRL) of batteries, fuel cells, or hydrogen as an energy source does not go above 4 [6, 28].

The combined impact of these various points of focus makes it so that the market of commercial transport will likely not be the first adopter of this technology, even with a very mild hybridization level [18]. This is in part due to the highly disruptive nature of those new technologies. Rather, on those types of aircraft, gains might come from the electrification of non-propulsive functions [47] and the replacement of heavy hydraulic and pneumatic circuitry. On the other hand, gains on small GA aircraft and Unmanned Aerial Vehicle (UAV) seems to be rather promising, even considering today's technical level [56]. This makes all the more sense knowing that the predicted range of viability of all-electric aircraft is likely to be around 50-200 miles [57], which is particularly well suited for GA and trainer aircraft. It could also make sense for commuter aircraft, knowing that some airlines report that most of their flight have a range below 200 miles.

1.2.4 Barriers to the applicability of conventional design methodologies

The creation of a new aircraft, either innovative or conventional, starts with a conceptual design phase in which the preliminary assessment of a variety of possible configurations is studied. This phase, if conducted properly, allows to rule out unfeasible layouts, to identify key features, and to perform trade-offs between various design parameters spanning different aircraft design disciplines [58]. This step is thus key to ensuring the feasibility of innovative configurations. It is during this phase that a great number of parameters are frozen, like the main geometrical parameters or the choice of propulsion. A choice that usually relies on compromises between the different design disciplines. Because the goal of this phase is to

quickly iterate on design choices to freeze the aircraft's final configuration, models with a low-to-medium level of fidelity are preferred because the gain in terms of computation time largely compensates for the slight reduction in accuracy. Historic design methodologies have been covered in many aircraft design books [58–61] and are largely based on statistical formulas and regressions established thanks to a dataset of existing aircraft. While these methods tend to generally do well on conventional configurations, because of the way they were constructed, they inherently fail to capture new design trends, not to mention multidisciplinary synergies that could lead to significant gains on new, innovative configurations.

The introduction of electric propulsion thus shifts the focus traditionally done on the aerodynamics-mass-performances triptych. System designs and other disciplines that were not considered in the preliminary design stage, such as the development of the thermal management system, which now accounts for a significant part of the electric aircraft [46], must also be considered. Additionally, standard metrics like weight and fuel consumption are no longer relevant. These metrics are, however, proxies, historically used on conventional configuration [35], for other quantities such as emissions [31], total energy use, operating costs [13, 62], safety and reliability [13, 63], in which new configurations could be better [13]. Finally, the interactions between the structure and the propulsion system could also be the source of significant savings or a point of concern for hybrid and electric designs [32, 34, 35, 38, 64, 65]. Consequently, physics-based, components-based, or direct estimation methodologies [58, 66] seem better suited to capture those effects and are a good fit for preliminary design because the reduced complexity of the approach still allows to capture, at the first order, the main synergistic effects.

In this context, and with the recent progress made in the field of MultiDisciplinary Analysis and Optimization (MDAO), fast and reliable multidisciplinary optimizations have been identified as a key enabler for a new generation of innovative and highly efficient aircraft [6]. Indeed, since the biggest gain will come from the optimization of the trade-offs between the highly coupled aircraft design disciplines, there is a need for methodologies capable of capturing those couplings and optimizing them. The added freedom in the choice of the design of the aircraft highlights a strong necessity for highly flexible models and methodology, which would allow designers to quickly perform trade-offs between different choices of powertrain architecture and aircraft configurations.

1.3 Problem statement

For all those reasons, electrified propulsive architectures for aircraft in the General Aviation segment are seen as the next logical step due to the potential benefits they could offer in terms of reduction of environmental impacts, as well as the alignment of their expected capabilities with the operational requirements of aircraft in this segment. Thus, considering its importance, it largely justifies the development of detailed methodologies for the sizing

and the estimation of the performances and impacts of hybrid electric powertrains. This thesis aims to tackle this problem by developing a holistic methodology capable of accurately assessing the potential of electrified aircraft propulsion for the General Aviation segment. More specifically, this manuscript will be organized around three main research areas:

i the development of a methodology for sizing hybrid- and all-electric aircraft,

ii the identification of plausible electrification scenarios in the General Aviation segment and,

iii the integrated assessment of the environmental impacts of electrified configurations.

1.4 Identification of research questions

These three axes will then be formalized around various research questions:

RQ1. What disciplines and components linked with electrified propulsion should be considered for accurate assessment at aircraft level?

RQ2. Are traditional design methodologies suited for the sizing of electrified aircraft? What disciplines of coupling are present/missing?

RQ3. How can MDAO methods and integrated Overall Aircraft Design (OAD) frameworks be adapted to assess hybrid and all-electric aircraft ?

RQ4. How to enable the assessment of a great number of configurations and orders of magnitude of power?

RQ5. Given the wide variety of usage of aircraft in the General Aviation, what electrification scenario should be considered?

RQ6. How to conciliate the expected limitations of electrified propulsion with credible operational scenarios?

RQ7. How to integrate, in the sizing process, design constraints stemming from manufacturing considerations? What is the influence on the vehicle?

RQ8. Is the evaluation of the impacts on climate change emission during the use of General Aviation aircraft enough to assess its sustainability?

RQ9. How can the environmental footprint of aircraft be tightly integrated in the design process?

RQ10. What design drivers and aircraft specifications should be considered when minimizing the impacts?

1.5 Manuscript overview

In accordance with the three axes of research, the manuscript will be organized into three parts. Part I describes the creation of an Overall Aircraft Design framework capable of optimizing aircraft with an electrified propulsion chain at vehicle level. It includes, in Chapter 2, a review of existing methods and an identification of research gaps for the modeling of electrified propulsive architectures. It also presents the integrated framework developed to address this question. Chapter 3 describes the models adopted for the components of the

powertrain included inside the library, and based on which architectures can be modeled in the developed framework. It also tackles the question of synergistic interactions between disciplines and what level of fidelity to adopt to address them. Part II proposes scenarios for the reduction of emissions of aircraft in the General Aviation sector by leveraging the developed framework. More specifically, Chapter 4 offers a study of possible electrified propulsion chains for various types and usages among the wide variety covered by the CS-23. Part III then ponders whether focusing solely on emissions during the use phases of the aircraft is sufficient to assess the sustainability of these new configurations. In particular, Chapter 5 proposes the adoption and integration of a Life Cycle Assessment (LCA) into the design workflow. This implementation is then used to evaluate the environmental impacts of electrified propulsion and isolates the phenomenons who drives them.

Part I

Design of Hybrid-Electric General Aviation aircraft

Abstract

As shown in the introductory part of this thesis, the novelty of EAP and its potential at aircraft level highlights the need for methodologies capable of capturing multi-disciplinary synergies. This first part focuses on the development of an extension of an Overall Aircraft Design methodology to enable the sizing of hybrid- and full-electric aircraft with a focus on aircraft certified under the European Union Aviation Safety Agency's (EASA) CS-23. Chapter 2 proposes an overview of identified gaps in existing OAD methodologies and the proposed developments to enable the sizing of hybrid and electric configurations. Chapter 3 presents the model retained for the sizing and the estimation of electric and thermal components commonly found in electrified propulsion concepts.

Author's contribution

Journal paper

Lutz, F., Jezegou, J., Budinger, M. and Reysset, A., 2025. Open-Source Framework for Sizing Hybrid and Electric General Aviation Aircraft. Journal of Aircraft, 62(2), pp.381-395.

Conference paper

Lutz, Florent, et al. "FAST-OAD-GA: an open-source extension for Overall Aircraft Design of General Aviation aircraft." ICAS 2022. 2022.

Chapter 2

Sizing methodologies for electrified propulsive architectures

Contents

2.1 Introduction **15**
2.2 State of the art of methodologies for the sizing of aircraft **16**
2.2.1 Multidisciplinary Analysis and Optimization (MDAO) 16
2.2.2 Review of existing approach for the modeling of electrified aircraft 20
2.2.3 Review of existing Overall Aircraft Design integrated framework . 26
2.2.4 Identification of modeling gaps in major OAD frameworks 28
2.3 Development of an integrated framework for the sizing of electric and hybrid aircraft **32**
2.3.1 The FAST-OAD framework 32
2.3.2 Extension to hybrid and all-electric configurations 34
2.4 Conclusions and perspectives **41**

2.1 Introduction

THE analysis of the context revealed that, in addition to its potential in terms of zero in-flight emissions, electric propulsion, thanks to its scalability [31], allows for a greater variety of powertrain designs and more possibilities in the placement of propulsive components. These added degrees of freedom also allow to take profit of synergistic interactions between design disciplines for significant gain on the overall design of the aircraft. Yet, this added leeway comes at the cost of new constraints in the design process. Additionally, these new power architectures come with a lack of historical data, which makes proving that these aircraft are safe and worthy to fly all the more challenging [51]. Quickly ruling out unfeasible design as well as identifying key parameters for the assessment of new, electrified designs and their optimization, thus becomes paramount. Consequently, new methodologies to enable

quicker and more accurate modeling of new propulsive architectures in the early stages of the design will play a key role as an enabler of hybrid and electric aircraft. Therefore, there is a necessity for quick, easy-to-use tools that are capable of capturing the multidisciplinary synergies to better perform trade-off studies on the design of the aircraft.

The finality of this chapter is to identify and adopt, or adapt if necessary, a sizing methodology that would enable the assessment of the use of electric propulsion on General Aviation. In order to select accurate sizing criteria and because it has been identified as a key enabler to size future propulsive architectures, lessons to be learned from the field of Multidisciplinary Analysis and Optimization (MDAO) will first be reviewed. Existing methods proposed in literature will then be analyzed and classified to identify which type of approaches is best equipped to tackle the design problem. It will be shown that integrated frameworks capable of modeling all disciplines involved in the aircraft design problem and their interactions are likely the best candidates. A comparison of existing frameworks, with particular focus on open-source ones, will then allow us to identify a suitable software for the implementation of a load-flow analysis type method. The resulting framework, as well as the constraints that will need to be fulfilled for the modeling of the components in the powertrain, will finally be discussed.

2.2 State of the art of methodologies for the sizing of aircraft

2.2.1 Multidisciplinary Analysis and Optimization (MDAO)

This increased number of design variables and new constraints associated with the use of electric propulsion create the need for preliminary design tools capable of rapidly assessing the viability of new concepts. In this context, and with the recent progress made in the field of MDAO, these tools have been identified as a key enabler for new generations of innovative and highly efficient aircraft [6]. The term MDAO refers to the field of engineering that studies the design of systems involving multiple disciplines and/or subsystems that present strong interactions between each other or for which gains can be achieved through synergistic coupling [67]. This definition fits the field of aircraft design, meaning that many of the techniques used in this field will be applicable when trying to design a hybrid electric aircraft and, more generally speaking, an aircraft. Graphic representation can help with comprehending the interactions involved, which is the reason why N2 diagrams or eXtended Design Structure Matrix (XDSM) diagrams [68] are such precious tools. An example of the representation of an aircraft design problem in the form of an N2 diagram is given in Figure 2.1.

A generic design optimization problem will contain coupling between the disciplines or systems. Based on this observation, multiple types of variables can be identified. The first type of variable is design variables. They are entries of the problem representing the

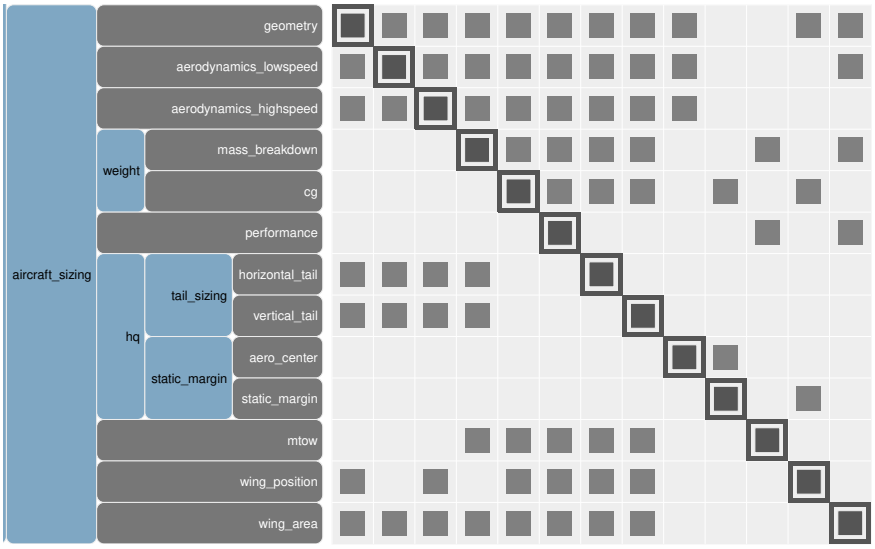

Figure 2.1 An N2 diagram representation of an aircraft design problem, generated with the FAST-OAD package [69].

designer's choices and the degrees of freedom for the design at their disposal. For instance, in the design problem illustrated in illustrated in Figure 2.1, the wing aspect ratio or the cruise speed are design variables. The second type of variable is state variables. These variables are shared between different subsystems and disciplines and thus represent the coupling between disciplines, which the field of MDAO deals with. In the context of an aircraft design problem, they would represent parameters such as the aerodynamic coefficient of the aircraft, which must then be used to estimate the fuel consumption, or, keeping the same example, the aircraft's Maximum TakeOff Weight (MTOW). Further breakdown based on the type of coupling can be made. When the results of one discipline are used in a subsequent discipline, it is called a feed-forward connection. When it is the other way around, it is called a feed-back loop. In Figure 2.1, feed-forward connections are above the diagonal while feed-back loops are represented by the light gray squares below the diagonal. The solving of those coupling is known as a MultiDisciplinary Analysis (MDA) [70] and consists in, for a set of design variables x, finding the value of the state variables u, for which the residuals $r(x,u)$ of the problem are equals to zero. It is worth noting that while the governing equations do depend on the design variables, they won't appear in the resolution of the residuals equation as the couplings are solved for one set of input variables [70].

Beyond solving the coupling between disciplines, techniques from the MDAO field can be used to find the best design satisfying the design specifications with significant speed up and increased robustness when compared to older practices. For instance, taking again the design problem illustrated in Figure 2.1, it could be of interest to find the value of the wing aspect ratio, a design variable, which gives the lowest fuel consumption, an objective, while keeping in mind that the resulting wing span should not be greater than what airports can

accommodate. This simple example illustrates the generic formulation of an optimization problem presented in Equation 2.1.

$$\begin{array}{lrl} \text{Minimize} & f(x,u) & \text{the objective function} \\ \text{With respect to} & x \in I & \text{the design variables} \\ \text{under} & c_i(x,u) = 0 & \text{the equality constraints} \\ & g_j(x,u) \leq 0 & \text{the inequality constraints} \end{array} \tag{2.1}$$

In practice, there is a wide variety of approaches to writing and orienting the models that can be used, depending on the complexity of the problem. The simplest one is called Multidisciplinary Design Feasible (MDF). It does not require any specific effort in organizing the disciplines and relies on solving the MDA for various design points chosen by the optimizer. Once the coupling between systems is solved, the objective functions and constraints that rely on the state variables, as well as the design variables, are computed and fed back to the optimizer to orient the next choice of design variables. The main advantage of that approach is that it provides, for each iteration of the optimizer, a feasible design which is useful in case of a premature stop to the process. The drawback, however, is that because the MDA is solved at each iteration, it can be significantly longer than other formulations [70]. A second type of approach found in literature is the Individual Discipline Feasible (IDF) approach [71], which breaks the explicit links between disciplines, thus removing the need for an intermediate solve of the MDA. Consistency between variables is instead taken care of by the optimizer, ensuring it has full control over the search. While it allows significant speed-up thanks to the potential parallelization of the discipline computation, IDF formulation requires more effort in the architecturing of the problem and translates into more constraints for the optimizer to handle. As opposed to MDF, it also doesn't ensure consistency of the solution in case of a failure of the convergence of the optimizer. Finally, hybrid formulations have also been proposed [72] as an in-between where some relations, like feed-forward connections, are handled by a solver instead of the optimizer as is done for the IDF formulation. The two formulations, MDF and IDF, are illustrated as XDSM diagram in Figure 2.2. Based on the choice of framework, which will be discussed in Section 2.3 and the implementation of the existing models, an MDF formulation will be adopted.

In addition to the question of the formulation, comes the question, common to all formulations, of the choice of the optimizer. Generally speaking, optimizers can be classified into one or two categories based on whether they use information contained in the derivatives [72]. Gradient-free approaches have the advantage of not requiring a computation of the discipline's derivatives, only needing the results of the function. This allows the use of black-box models (such as proprietary engine decks) and allows the interfacing with disciplinary software. Gradient-based method on the other hand, rely on the computation of the derivatives of residuals or optimization objectives with respect to the problem's design

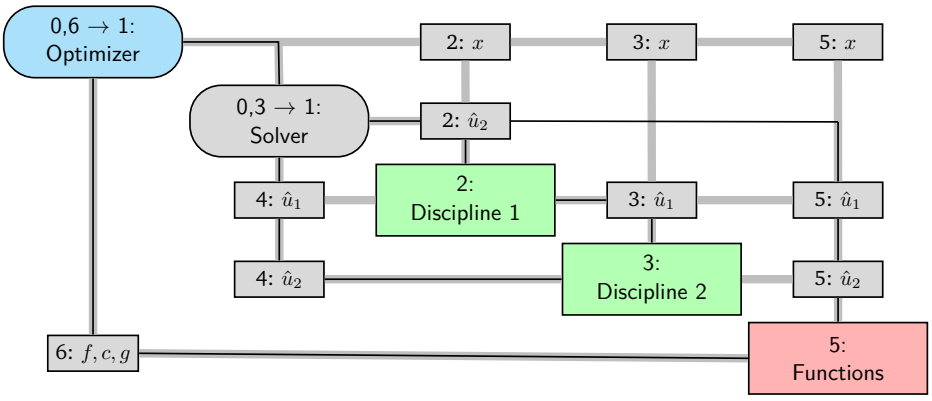

(a) MDF formulation.

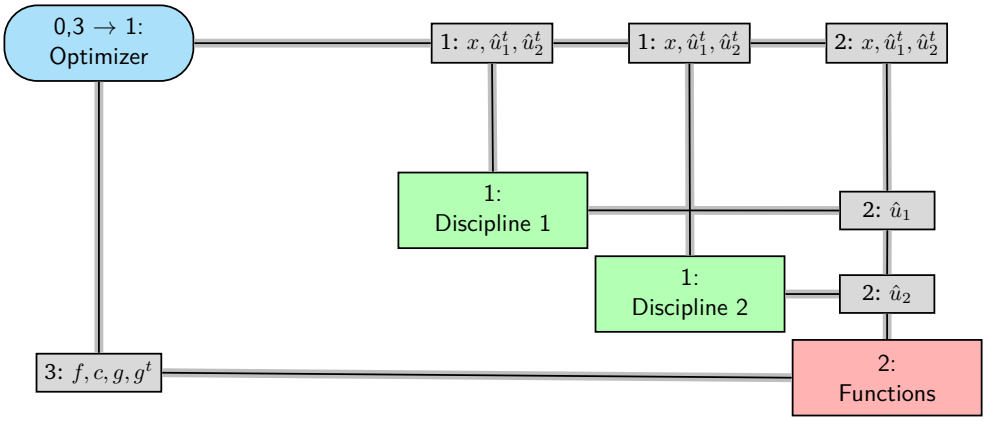

(b) IDF formulation.

Figure 2.2 Most common optimization problem formulation, represented as XDSM diagram. Adapted from [73].

variables. They are generally better suited and more efficient for problems containing large numbers of variables [6, 72–74], which is the case for aircraft design problems. Gradient-based optimizers, however, are known to sometimes get stuck in local minima as opposed to stochastic methods, which are ensured to find the global minimum, at the cost of significantly higher computational time [75]. Techniques can, however, be used to circumvent that issue, such as coupling the optimization with a multistart approach. As such, gradient-based approaches will be preferred in this work when usable. Unfortunately, the original FAST-OAD-CS23 framework, of which we reuse the aircraft design models, does not use analytical derivatives. Therefore, to avoid using finite differences, gradient-based optimizers will not systematically be used depending on the scope. Nonetheless, the simulation of the mission and the powertrain's state during the flight phases will leverage Newton-based solvers and partial derivatives.

The question of the computation of those derivatives thus becomes an important point. There are four main methods for the computation of partial derivatives: finite difference,

complex step, analytical differentiation, and algorithmic differentiation, each with its pros and cons [72, 73]. Finite difference is based on the computation of the variation of the value of the function over an arbitrarily small interval around the point of interest. There are various ways of computing this difference, depending on whether the scheme is backward differentiated, centered, or forward differentiated. This method is really easy to use and does not impose any constraints on the function that needs to be differentiated, making it well-suited for black-box disciplines or sub-disciplines. It does, however, require a lot of calls to the function, especially when there are a lot of inputs and outputs in the model. Additionally, the truncation error is directly linked with the size of the step, leading to potential errors when the step is too small. The complex step method relies on the approximation of the derivative as the imaginary part of the function evaluated over a small complex interval. The main advantage of this method, when compared to the finite difference one, is that it does not rely on a subtraction, allowing more freedom in the choice of the step. It does, however, require that the function to differentiate can take complex numbers as input, making it impractical for black box components. Analytical differentiation, sometimes referred to as symbolic differentiation, relies on the fact that the designer knows the function and can thus explicitly write formulas for the computation of the partials. This is a very efficient solution, but it does require a lot of effort upstream of the computation, and, like for complex step, it can't be applied to a black box component. Finally, algorithmic differentiation can be used to automatically generate the derivatives by systematically applying the chain rule to a computer program. It is also a very efficient solution and can largely be automated thanks to frameworks like Jax [76]. In this context, it can be advocated that models and their partials should be developed at the same time, because while it may take more time to implement, it pays off in the long run to keep in mind that the code is going to be differentiated [73]. The reason is that, if differentiated analytically, it can make solving the problem highly efficient. Finally, partials can be used for several other applications, such as uncertainty qualification or error analysis. This can play a key role, especially when considering that there is a huge uncertainty on the figure of merit of future electric technology, and thus, sensitivity studies on technological parameters should always be performed to enable fair comparison of future aircraft concepts [51].

2.2.2 Review of existing approach for the modeling of electrified aircraft

One of the main conclusions of Chapter 1 was that design methodologies capable of assessing the gains stemming from multidisciplinary synergies were a key enabler for the production of a new generation hybrid and all-electric aircraft. It was also highlighted, in the previous section, that efficient solving of MDAO problems, a lens through which aircraft design problems could be seen, depended a lot on the algorithm used for solving as well as the formulation of the models. As such, a procedure capable of the joint optimization of the aircraft, its powertrain, and the interactions between the two, and which also uses effective and accurate modeling

to represent the electric aircraft, should be sought. Thus, literature was reviewed to identify and categorize the main approaches to assessing the sizing and performance of hybrid and electric aircraft.

Constraints analysis

A first approach commonly used for the conceptual sizing of aircraft, conventional and hybrid-electric alike, is the constraint analysis. It consists in rewriting and adapting the aircraft flight equations for different sizing scenarios such that they all express constraints under the form $T/W = f(W/S)$, with T the sizing thrust of the aircraft, W the gross weight, and S the wing area [58]. This graph is also sometimes displayed in the form $W/P = f(W/S)$ for propeller aircraft, using the sizing power P of the aircraft instead of the thrust. An example of such a graph is given in Figure 2.3. The design point is then selected as one of the points inside the space designated by all the satisfied constraints, often called the design space. The constraints that can be considered include, but are not limited to: desired rate-of-climb, desired level rate-of-turn, desired level cruise speed, or one engine inoperative climb out, which, as was pointed out earlier, is a key issue to consider [65].

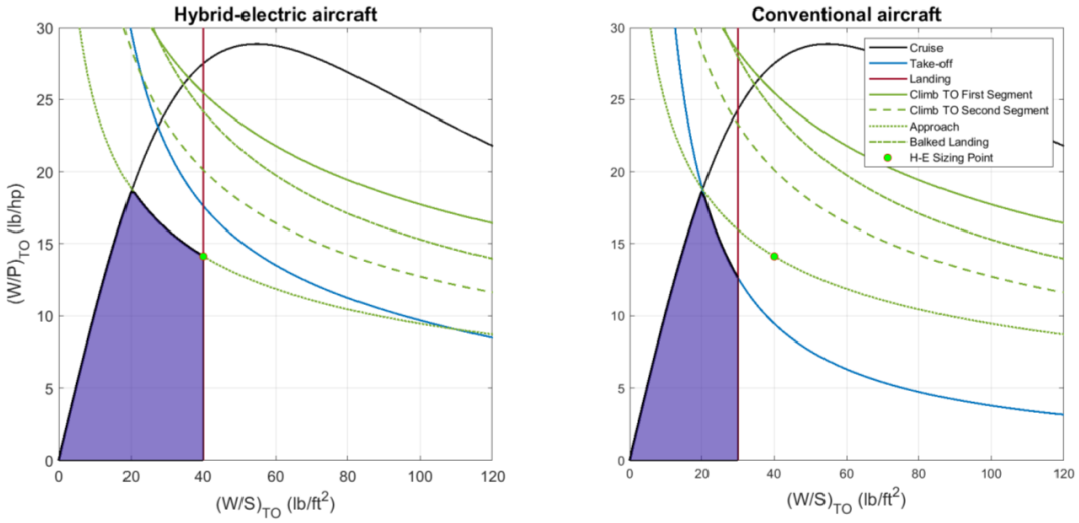

Figure 2.3 Application of the constraint analysis method to the sizing of a hybrid electric aircraft [77].

This method was adapted to take into account the effect on the sizing of the inclusion of slipstream effects by the addition, to the flight equations, of an increment in the lift and drag coefficient as prescribed by the method developed in [34]. This thus results in an enlarged design space [64, 77, 78], which translates well the gains that can be obtained with DEP, as illustrated in Figure 2.3 with an increased wing loading for the hybrid-electric configuration. This can then be used, with a choice on the Degree Of Hybridization of power H_P, to estimate the power rating of each of the components in the powertrain [44, 79].

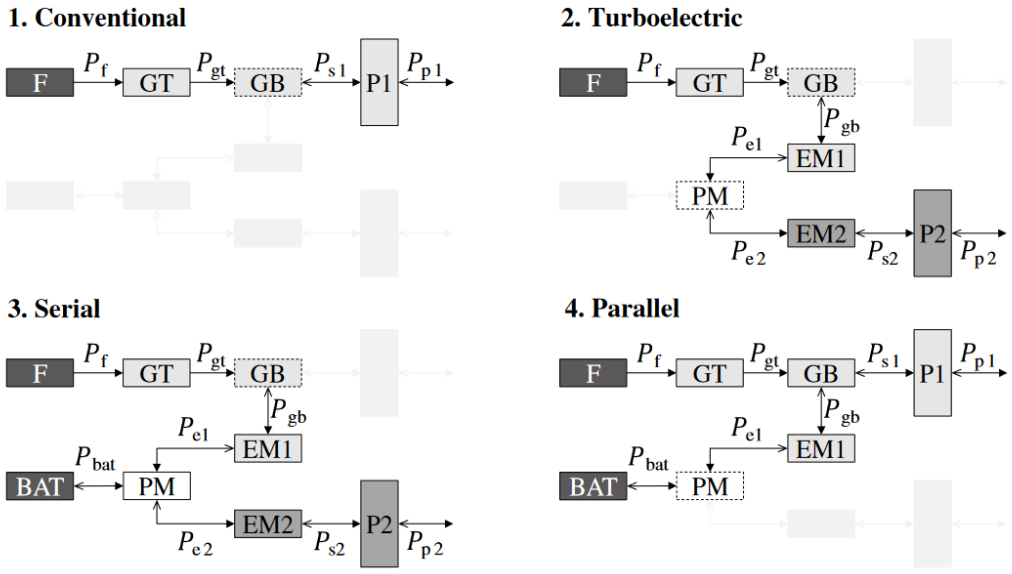

Figure 2.4 Powertrain representation based on the generic description and variation of H_P and H_E [64].

To determine the gross weight of the aircraft, an iterative process, which includes a computation of the energy consumed and a computation of the empty weight, is then conducted. For the computation of the energy consumed, be it as fuel or chemical storage, a generic powertrain is often assumed [64, 65, 77, 79–81]. This powertrain nonetheless uses some control parameters, mainly in the form of the H_P and its counterpart for the energy, the Degree of Hybridization of energy H_E. This allows to replicate a variety of powertrains by varying those values between zero and one, allowing, with the same method, the evaluation of many architectures. An example of the types of powertrains that can be modeled is represented in Figure 2.4. By writing the formula for the efficiency at the interface between components, the power at all stages of the powertrain can be computed. This allows to find the power rating for each of the components and subsequently their weight using classical power density values. It also allows very fast computation of energy consumed by formulating the equations of the components' efficiencies throughout the propulsive chain as a matrix. Further emphasis is often put on the computation of the propeller performance, which is typically computed using Actuator Disk Theory (ADT) or Blade Element Momentum Theory (BEMT). The reason behind this is that there is an important trade-off to consider between a large propeller with better efficiencies and smaller propellers, which are better for high lift generation because they have higher disk loading [34, 77]. The energy for the mission can then be computed using the aforementioned matrix formulation at each point of the flight [64].

Despite relying on statistical values for the establishment of the constraints diagram and despite the relatively low level of details provided by this methodology, it gives very good insight into key drivers for the design of electric aircraft. It is also often used in literature as an entry point for more detailed analysis using the classical aircraft design loop. For instance, in [78], a constraints diagram is coupled to a Vortex Lattice Method (VLM) code, which has been modified for better computation of the aerodynamics. Slipstream effects were also included in the form of corrective factors added to the clean wing aerodynamic coefficients, often referred to as deltas. Particular attention is also given in this paper to the sizing of tail surfaces, with the Horizontal Tail Plane (HTP) sized according to a target static margin and the Vertical Tail Plane (VTP) being sized with the volume coefficient method. Wing mass is also sized with an analytical methodology, but as opposed to [82], where only the bending moment is computed, the whole load distribution is considered. The sizing of the powertrain is usually based on power ratings and energy densities for the battery.

Overall, constraint analysis is well-suited as a tool for conceptual design and can capture some synergistic couplings enabled by the electrification of propulsion. However, it cannot typically use higher fidelity modeling of the powertrain, nor can it handle complex propulsive architectures.

Interaction with engineering knowledge-based software

Another possible choice is to put more focus on the evaluation of a single discipline or a couple of disciplines, leaving the OAD to be done with low-fidelity models [16]. This type of approach often relies on the use of proprietary software for detailed modeling of powertrain components [16, 83, 84] or aircraft disciplines [85]. It allows to include disciplinary engineering knowledge very early in the design process for a more accurate assessment of the feasibility of novel designs. In addition to that, some software can perform multi-physic and multi-fidelity analysis, allowing for better evaluation of synergistic interactions and associated gains. Furthermore, since the use of electric aircraft is predicted not to be widespread before 2035 [83], prospective studies on turbomachinery could allow for more accurate evaluation of hybrid electric aircraft with future entry into service. For those reasons, software like Gasturb or PROOSIS are often used. Their utility can also come from the calibration of a classical low-fidelity approach with higher fidelity data [83]. This, in addition to a prospective fixed efficiency model, gravimetric densities, as well as cost and environmental impact modeling, can help assess the environmental footprint and competitiveness of future aircraft configurations [83]. The use of GasTurb can also be more direct to have a higher level of fidelity for both the modeling of turbomachinery [84] and of electric architecture. Recent versions of the software have indeed begun including electric component models. Earlier papers, however, only make use of this software for the computation of the performances of fuel burning engine and complement the design methodology with electric component

modeling taken from literature [16, 84]. To match the level of detail provided by GasTurb, efficiency maps for a Permanent Magnet Synchronous electric Motor's (PMSM) operation are implemented. A cable model based on voltage and current requirement is also used, as well as a model based on semiconductor losses for power electronics [84]. The impact of the mass, drag, power, and size of the Thermal Management System (TMS) has also been modeled. For aircraft concepts utilizing powertrain which are not turbo-electric, a detailed model for battery operations, which reflects its dependency on the State-Of-Charge (SOC) and power drawn [86], can also be used in complement to GasTurb [87].

However, some issues are linked to the use of such methods in the preliminary design phase. Mainly, as one software is rarely enough to perform all the disciplinary analysis required for OAD, the interfacing between multiple tools is required. Unless automated, intervention of humans in the sizing loop would be required, which, in addition to the already long runtime of higher fidelity tools, would make the whole sizing process long for a preliminary design phase. Moreover, the high computational time can lead to numerical failures, which makes the sizing process less robust [88]. Finally, it can prevent the efficient assessment of synergistic interactions because these software often focus only on a single discipline, contradicting the shift towards a vehicle-focused paradigm [89].

While the use of disciplinary software is well-suited for the increase in model fidelity required to capture the effects and multidisciplinary couplings enabled by the use of electrified propulsion, some limitations excluded its use in this work. First, it induces specific focus on a limited number of disciplines, which contradicts the paradigm shifts towards vehicle-level optimization. Second, it cannot be easily automated, and the information on the derivatives is rarely available.

Integrated framework

The third type of method is the implementation in a common OAD framework of medium-fidelity and physics-based modeling of the aircraft and its components. Since this type of framework, which will be referred to as an integrated framework, is not focused on a limited number of disciplines, aircraft-level optimization is possible. Additionally, some frameworks have multi-fidelity capabilities, which allow for the automatic interfacing of disciplinary tools and their inclusion in a complete OAD process [69, 90, 91]. While these tools come from different developers (universities, manufacturers, ...), they will likely focus on different disciplines of aircraft design and have different levels of availability (open-source, open access, private). Some points of caution must thus be raised [31, 92]. The ability to easily customize the analysis for the needs of a specific study, be it the design of the powertrain or the switch between the study of a retrofit or a design from scratch, is key. Furthermore, because of the number of design variables and their complex interactions with the optimization objectives, gradient-based solvers should be preferred [72].

The final category, integrated framework, regroups all methods that allows vehicle level assessment considering multiple disciplines in the design of the aircraft. Its modularity, however, is both a boon — allowing for customization of the design process according to the needs of the studies as well as multi-fidelity modeling — and a bane — requiring a lot of upstream work —.

Key takeaways

This subsection reviewed the main methodologies that are leveraged in literature to perform the sizing and evaluate the performances of innovative aircraft configurations. It revealed that existing integrated frameworks, because they allow aircraft-level optimization in reasonable computational time, are better equipped to solve multidisciplinary problems like the design problem of hybrid and all-electric aircraft. They also have the advantage of centralizing all the information between disciplines, whether it is the value of design variables, objectives, and constraints, or their derivatives. This allows the solving of problems with a great number of design variables using a gradient-based approach. As such, they will be further investigated and compared in the next section to identify gaps in existing tools.

This review also revealed that multiple levels of fidelity can be adopted. On one end of the spectrum, low-fidelity methods that typically rely on top-down efficiencies and power density values remain very popular. They allow for rapid assessment of the potential of numerous new configurations thanks to inexpensive models, but the underlying over-simplifying assumptions mask off lots of effects. While they can be fairly accurate for some components for which losses do not strongly depend on operating or sizing conditions, it is far from being the norm. Losses in electric motor, for instance, have strong dependencies on torque and rotational frequency [53, 93, 94]. They also cannot capture the full range of impacts that the installation of these new power sources can have on aircraft. On the opposite end of the spectrum, some studies have been shown to use high-fidelity methods. These, although presenting strong capabilities to deliver insights into the impacts on the aircraft of those new propulsion chains, also show some significant drawbacks, making them unsuitable for the preliminary design phase. They are prohibitively expensive in terms of computational time and can often only be interacted with as black boxes, thus making them non-differentiable. Additionally, finite difference is impractical due to the cost of one function evaluation, thus making them non-differentiable. They also typically require a great deal of detail on the aircraft and powertrain, which are typically not known this early in the design stage. Finally, and from a more practical point-of-view, they are often proprietary, impeding the reproducibility of results. Consequently, medium-fidelity methods appear as a great compromise between speed of execution, ability to assess all impacts on the aircraft, and capability of identifying technological design drivers.

2.2.3 Review of existing Overall Aircraft Design integrated framework

One key capability for the preliminary design process is its ability to quickly test a great number of configurations and assess their feasibility in different sizing scenarios. In this context, software that provides at least a minimal user interface and that can aid the designer in making choices can be very useful. In particular, professional software often come with a comprehensive user interface and can be of great help early in the design process. JPAD is an example of such a software suite, which, in addition to a complete interface, can guide the user to correct Top Level Aircraft Requirements (TLAR) to achieve a feasible design. The JPAD Modeller software enables a detailed description of the aircraft geometry for use in high fidelity model [95]. The core software uses a simplified representation of the detailed geometry coupled to a modified version of Prandtl's Numerical Lifting-Line theory [95]. The estimation of weight and performance seems to rely on statistical values and user-provided engine tables, which — as has been mentioned earlier — can be very limiting when designing new configurations. Another example of such software is Pacelab APD, now called Desmo, a software built around its user interface. Pacelab APD originally provided a sizing of the aircraft based on some aircraft design books, but was extended with more sophisticated methodology, among which a physics-based model for the estimation of the wing weight [84]. The fact that the software had to be supplemented with the help of disciplinary software like GasTurb for the sizing of a partial turbo-electric commercial aircraft seems to indicate its limit regarding the sizing of a hybrid-electric powertrain [84]. Another software, developed by the same company and called Pacelab SysArc, now also part of the Desmo suite, allows for the sizing of electric subsystems and to evaluate their impact in an aircraft design environment. It allows a graphical-schematic definition of system architectures and the inclusion of failure modes in sizing scenarios. Pacelab SysArc was used for the sizing of an electrically propelled UAV [96], which describes the use of a simplified model under the form of specific power and energy for the estimation of system mass. As for its APD counterpart, its mass and aerodynamics models are part empirical, part physical, with no mention made of slipstream effects. While such tools for aircraft design can, through a comprehensive user interface and graphical schematic of systems, help the design process of unconventional aircraft, the fact that they are license-bound makes it hard to modify the existing tools to account for new technologies. It also adds a barrier to the comprehension of models, which are seldom accessible to the user, thus preventing critical hindsight about the validity of the design.

In addition to professional software, a great number of research institutes have developed their own research tools. This is the case for the DLR (Deutsches Zentrum für Luft- und Raumfahrt), which developed a conceptual design tool called VAMPZero. It is coded in Python, and is mostly based on handbook methods, such as the one already mentioned, both for mass and for aerodynamics estimation [97, 98]. A great deal of work has been done on the ease of interfacing of the software through the implementation of a CPACS format for

data exchange, but the simplicity of the models and the reduced number of design variables [97] severely limit the scope of what can be modeled with this tool. The Aircraft Design Initiator, a similar tool developed by TU Delft, has been adapted to provide a methodology for the conceptual design of distributed propulsion hybrid electric aircraft [99]. Its process flow is presented in Figure 2.5. It includes a physics-based methodology for the sizing of the fuselage mass and wing mass. For the latter, it takes into account the effect of distributed propulsion on the loading of the wing. For the aerodynamics part, a lifting-line model is used to study the effect of propeller blowing on the wing. These effects are also included in the computation of mission energy and in the constraints diagram according to the methodology presented in [64]. The study of the influence of Boundary Layer Ingestion (BLI) on the sizing is also included. Power densities are used for the estimation of powertrain mass, and penalties are included to account for the mass of the cooling and power distribution systems. The tool does not seem to be open-source, and the process workflow seems to be fixed, preventing the adaptation of the code for a retrofit approach. A final point of caution is the fact that this tool seems to be adapted for the sizing of CS-25 aircraft, for which the certification constraints are different from the CS-23 category that will be studied here. Developed by the Institute of Aerospace Systems at Aachen University, the UNICADO framework [100], a successor to the previously established MICADO software, was also investigated. Although the reference cases developed in the scope of this framework only concern CS-25 aircraft and apparently lack models for hybrid or electric aircraft, the advertised modularity of the code hints at the possibility to adapt it for an electrified powertrain.

NASA has worked on the development of FLOPS, a conceptual design software, for over 30 years [35]. The code is advertised as very versatile, with the ability to tune almost all of the models. It also provides models for very different configurations of aircraft, such as transport aircraft, Blended Wing Body (BWB) aircraft, fighters, or general aviation [101]. Several limitations of the code regarding the sizing of electric powertrains were however identified [102]. First of which was the fact that it relies on the assumption that fuel was consumed during the mission, an assumption which could be worked around by setting the Specific Fuel Consumption (SFC) at zero [102]. The second limitation, which is a direct consequence of the first one, was that only one type of propulsion could be used at the same time, either fuel where SFC is not nil or full-electric where SFC is nil. Finally, as the original code relied a lot on the calibration of models, it cannot be used for unconventional configurations because of the lack of data for recalibration [88]. This led to the development of a new tool, a spiritual successor to FLOPS, called Layered and Extensible Aircraft Performance System (LEAPS), which reuses a good part of the models, mainly the aerodynamic and weight estimation methods [92]. The main focus for the development of this code was to create a modular, multidisciplinary, multi-fidelity analysis tool capable of modeling a wide range of propulsion systems. Mission analysis is enabled on a variety of segments, climb, cruise, descent, or loiter, and allows the user to replace any model. On the topic of the modeling of electric propulsion

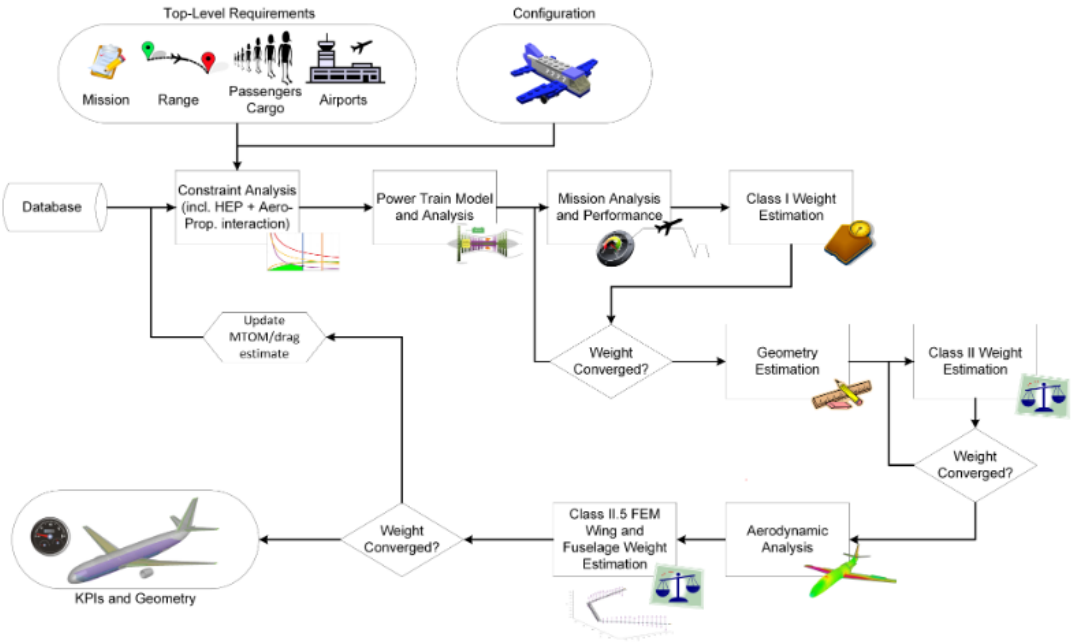

Figure 2.5 Illustration of the Initiator process flow for the design of a distributed hybrid-electric propulsion aircraft [99].

and DEP architectures, the first working version of LEAPS [92] enables the modeling of different types of propellers (BLI, high-lift propellers, and wingtip propellers at the same time) and the use of multiple power sources without complex workarounds. The modularity of the tool was used for the sizing of the PEGASUS concept [92] with the integration of several engine models for different types of propellers. Even though the modularity of the code looks very promising as the base for the integration of models for electric powertrains, this code doesn't appear to be open-source.

Out of the integrated frameworks reviewed so far, several promising candidates were identified. To identify the most promising solution, however, it was decided to study in more detail the major frameworks found in literature. This will be the subject of the next section.

2.2.4 Identification of modeling gaps in major OAD frameworks

A study comparing various sizing methodologies used for the evaluation of different hybrid electric concepts is presented in [31]. While this study compares how different electric aircraft design disciplines are assessed for different conceptual studies, most of the concepts were not evaluated in a single framework. Nonetheless, we propose to reuse similar criteria and augment them with the key disciplines identified in the introductory chapters to compare OAD frameworks. We will additionally consider the accessibility, ease of use, and the type of aircraft that can be modeled with those frameworks. The reason for that last point is that, as discussed and based on the limitations of current electric technologies, the General Aviation

segment will likely be the first adopter for that technology [13, 18]. Finally, based on the observation previously made regarding the capabilities of gradient-based solvers, we will also investigate the optimization capabilities of the frameworks.

The study conducted in [31] served as a base to identify the current gap in publicly available frameworks for the modeling of electric propulsion aircraft, which justified the development of a new framework named OpenConcept. This framework [31, 103] was developed as a toolkit for rapid optimization of electric aircraft concepts, considering thermal aspects as well as costs. It is built on the OpenMDAO framework [113] and inherits its MDAO capabilities, which OpenConcept makes full use of by providing analytic derivatives to use gradient-based algorithms. Other sizing codes have been built around the OpenMDAO framework: FAST-OAD, a modular framework for performing rapid OAD with model libraries for CS-25 aircraft [46, 69, 110], CS-23 aircraft [91, 108], blended wing bodies [112] and UAVs [107, 109]; or the Aviary code [104] which provides a flexible optimization platform that incorporates methods of legacy software such as FLOPS [114] and GASP [115]. Another tool widely used to assess the preliminary design of unconventional configurations is SUAVE [85, 105, 111, 116]. It is a Python-based open-source environment that enables multi-disciplinary and multi-fidelity analysis of advanced concepts. Finally, TASOPT is a code to evaluate conventionally-fueled aircraft. It has been developed using physical methodology for the computation of structural weight and turbomachinery performances [66, 106]. A separate version of the code has also been developed to enable the sizing of electric aircraft [18].

Table 2.1 summarizes the capabilities of the aforementioned frameworks regarding the modeling of electric and hybrid-electric aircraft. Regarding the level of fidelity for the modeling of electric components, frameworks still mostly use fixed efficiencies and top-down kW/kg coefficients, which, while adequate for a preliminary assessment of the impact of electrification of propulsion, do not provide enough details regarding the technological drivers of electric components. Additionally, this simplified modeling of the components does not allow to include aircraft level impacts such as volume allocation constraints or weight and balance. Besides, while some frameworks already offer the possibility to build a complex powertrain by assembling components, it has to be done inside scripts, which makes the tool harder to use and the interfacing with other software more complex. While the importance of including the sizing of TMS and safety aspects in the design has already been highlighted [31, 117], low-fidelity models are also mostly used. Finally, even though close integration of safety aspects will be crucial for assessing novel architecture, their interfacing with a preliminary OAD framework is not widely treated, although tools have been developed to bridge this gap [55].

Table 2.1 Functional comparison of integrated OAD frameworks.

	OpenConcept	**FAST-OAD**	**Aviary**	**SUAVE**	**TASOPT**
Aerodynamics	Drag polar, interface with OpenAeroStruct, which uses VLM [103]	Drag buildup, drag polar, interface with OpenVSP/Xfoil, built-in VLM [91]	Drag buildup, drag polar from FLOPS or GASP, interface with VSPAero, external polars [104]	Drag polar, Built-in VLM and LLT, interfacing with VSPAero, SU2 [105]	2D polar with MSES, slender body theory, double linear lift distribution with tip and fuselage connections
Weights	Textbook OWE correlations [31], kW/kg methods for propulsion	Textbook empirical formula and physics-based method [91]	Textbook empirical formula from FLOPS [104], kW/kg methods for propulsion	Textbook empirical formula and physics-based method, detailed propeller weight model [88]	Physics-based method for wing and fuselage and correlations [66]
Performances	Step by step residual driven resolution of the mission, takeoff analysis [31]	On- and Off-design step by step resolution of the mission, takeoff analysis	Step by step residual driven resolution of the mission via collocation and shooting methods, takeoff analysis	Step-by-step residual-driven resolution of the mission	On- and Off-design step by step residual driven resolution of the mission, takeoff analysis
Propulsion	Surrogate turbofan, constant SFC turboprop, efficiency map for propeller	Rubber engine turbofan, 1D thermo turboprop, scaled map ICE and BEMT for propeller [91]	Lookup in user-defined table, interface with pyCycle [104]	BEMT for propeller, thermo equations for turbomachinery components	2D thermo turbofan with variable c_P for fuel and air, BLI, compressor/turbine map [106], ducted fans [18]
Electrical	Efficiency parameter for motor, generator, and battery, power split for hybridization	Medium fidelity model for power electronics, battery, motor, and fuel cells for tailored studies [46, 107]	Medium fidelity model for battery, efficiency map for motor, lookup table for converter [104]	Medium/low fidelity models and equivalent circuit for the battery	Constant efficiencies for electric components, equivalent circuit model for battery [18]
Thermal	Medium fidelity model for ducts, coolant, pump, manifold	Medium fidelity model for fuel-cell based powertrain [108]	NA	Models for component cooling, limited for thermal management system	Weight to heat removal requirement coefficient [18]

Table 2.1 continued: Functional comparison of integrated OAD frameworks

	OpenConcept	**FAST-OAD**	**Aviary**	**SUAVE**	**TASOPT**
Operating Cost	Rudimentary components, airframe, energy, and depreciation costs	NA	Private interface with models from internal projects	Medium fidelity models for industrial and non-recurring costs	NA
Noise	NA	NA	Noise footprint computed during takeoff	Medium fidelity models	Sideline, flyover and cutback noise [66]
Climate impact	NA	LCA for tailored studies [109, 110]	Emission index for NO_x from FLOPS	Supplementary models for CO, CO_2 and NO_x emissions [111]	Emissions indices for fuel, electricity, and battery production [18]
Safety	NA	NA	NA	NA	NA
Accessibility	Open-source	Open-source	Open-source	Open-source	Open-source (conventional), available on request (electric)
Ease of use	No user interface	Plugin system, pseudo user-interface [69]	External subsystem can be added, minimal user interface depending on level	No user-interface, external analysis possible, powertrain building via scripts	No user-interface
Aircraft modeled	SMR, Light aircraft, Regional	SMR, Light aircraft, Regional, BWB, UAV [46, 91, 107, 112]	SMR, Light aircraft	SMR, Light aircraft, Regional, BWB, UAVs	SMR and long range, double bubble fuselage, strut-braced wing
MDAO capabilities	Inherited from OpenMDAO, extensive use of analytical derivatives	Inherited from OpenMDAO, limited use of analytical derivatives	Inherited from OpenMDAO, extensive use of analytical derivatives	Built-in optimizer, interfacing possible with external optimizer [85]	Built-in gradient-based optimizer with a fixed number of design variables

BEMT = Blade Element Momentum Theory, BLI = Boundary Layer Ingestion, BWB = Blended Wing Body, SMR = Short and Medium Range

2.3 Development of an integrated framework for the sizing of electric and hybrid aircraft

The observations carried out in Section 2.2.4 have prompted the selection of the FAST-OAD framework and its extension with a new plugin whose aim was to provide a convenient way to assess the performances and sizing of a hybrid electric powertrain. The reasons behind the choice of the FAST-OAD framework are multiple: the plugin, module and submodel system which allow for easy customization of the analysis process, the presence of models for the sizing of General Aviation (GA) aircraft, an existing pseudo user interface which makes it easier to customize the MDAO process, and a performance module designed to allow complex powertrain to be assessed and which extensively uses analytic derivatives. First, the features of the original framework will be discussed with a particular emphasis on the available disciplines and the data structure. Then, a discussion on the rationale behind the development of the extension and its implementation will be considered.

2.3.1 The FAST-OAD framework

FAST-OAD (Future Aircraft Sizing Tool - Overall Aircraft Design) is an open-source aircraft sizing and optimization tool co-developed by ISAE-SUPAERO and ONERA [69, 118]. It is based on the OpenMDAO framework and a previous sizing tool called FAST, developed since 2015. To fully use the MDAO capabilities of OpenMDAO, the aircraft sizing methodologies have been written as components. In the OpenMDAO framework, components are the base building blocks of the design problem. Each OpenMDAO component defines its inputs, outputs, and governing equations. These components are then assembled to form the design problem. As opposed to the previous tool, FAST-OAD uses a variable naming convention that makes clear what each variable refers to and allows for easier interfacing of the methodologies. This makes the handling of the multidisciplinary aspect of aircraft design easier for the end user. Moreover, thanks to the module system put into place, it is easy to add/remove models from the process. This is done with the help of a configuration file, which is where the management of the models is centralized. This all makes the FAST-OAD framework a very flexible tool for aircraft design and opens the way for the integration of custom models and the revision of existing ones to accommodate the analysis of new aircraft configurations.

FAST-OAD codes come by default with models adapted for CS-25 aircraft, which are grouped by aircraft design disciplines. It includes: Geometry, Aerodynamics, Weight, and Performances among others. Those disciplines and the way they are connected in a typical FAST-OAD run are illustrated in Figure 2.6.

Based on the observation that the models implemented were unsuitable for aircraft other than those in the CS-25 category and because only turbofan engines could be modeled, a plugin tailored to General Aviation aircraft, named FAST-OAD-GA, was developed. It

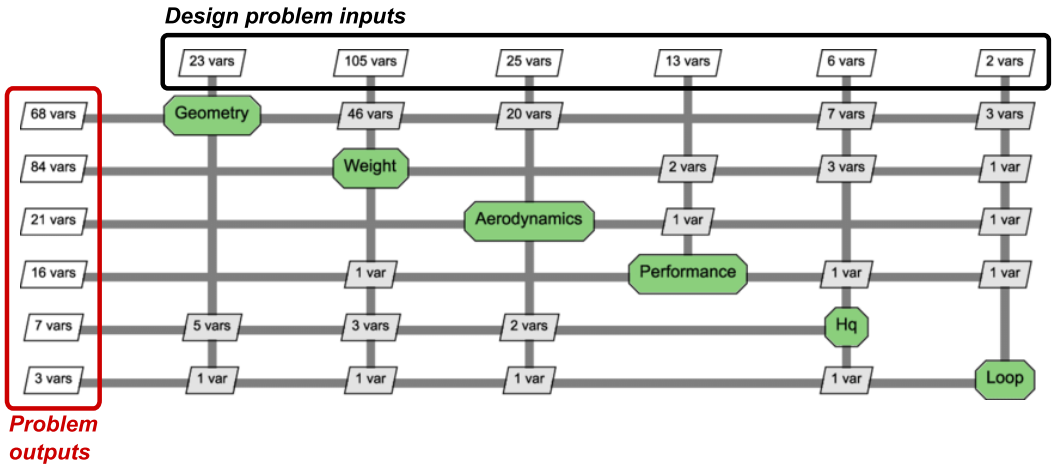

Figure 2.6 FAST-OAD disciplines interrelationship, adapted from [69]. Problem inputs and their classification are further discussed in Table 2.2.

introduced several changes in some key aircraft design disciplines [91]. The aerodynamics were augmented with a built-in VLM code, an interface with OpenVSP to compute the effect on lift repartition of propellers, the computation of trim drag based on the aircraft center of gravity (CG), and the computation of lateral and longitudinal derivatives. Regarding the computation of the masses, the semi-empirical formulas used for all mass items were changed to formulas tailored for CS-23 aircraft. Physics-based formulas were also added to compute the mass of the wing and fuselage based on the loads experienced by structural elements, thus enabling to account for the structural effect of distributed propulsion [32].

More interestingly, in this context, new models for the powertrain were also introduced. Propeller performances were modeled using Blade Element Momentum Theory (BEMT) and Actuator Disk Theory (ADT), and new methods to assess the fuel consumption of piston engines and turboprop were also added. Because of the requirement imposed by the interfacing with the performance module, their implementation, however, did not allow for easy extensibility, thus severely hindering the ability to quickly assess a wide variety of architectures. Moreover, this interface does not allow for the computation of partial derivatives, which, as discussed, is essential for the efficient solving of the tight coupling between the performances of the aircraft and of the powertrain. Finally, the lack of models for electric components prevented the simulation of hybrid and all-electric configurations, further reinforcing the need for a new extension of the framework that will be discussed in Section 2.3.2.

As previously mentioned, the FAST-OAD framework adopts a structured naming convention that clarifies to which discipline each variable belongs. Using OpenMDAO's capabilities, more specifically the name promotion mechanism, components that use variables with the same name are connected, thus ensuring consistency between the values used in each discipline. As discussed in Section 2.2.1, these variables, which connect multiple disciplines, can

be handled differently depending on the problem formulation. As the FAST-OAD plugins used here adopt the MDF formulation, consistency variables will be treated internally; therefore, there will be no need for explicit consistency constraints [68] to enforce coherence between disciplines. However, it is worth noting that although the consistency variables are handled internally, their initial value can be set to provide a fair first initial guess, as exemplified by the smart initialization of the problem, which will be discussed in the next section.

In the FAST-OAD framework, variables serving as problem inputs are processed in a so-called input file. The aforementioned naming convention also allows to identify the different types of inputs. Indeed, besides the aircraft's TLAR and other designer variables, data linked to model calibration and tuning parameters are also treated as inputs by the FAST-OAD framework. Consequently, because of the richness of the models in the FAST-OAD framework, there are hundreds of variables as inputs to the design problem. Additionally, thanks to the capabilities inherited from the OpenMDAO framework, any problem inputs can be selected as a design variable and any problem output as an objective function. Furthermore, any variables can be used as design constraints. Not all variables, however, are pertinent as design variables or objective functions, for instance, variables linked to the tailoring of models. This is the reason why, during the exploration of electrification scenarios presented in Chapter 4, only the relevant parameters will be discussed. Indeed, even excluding the calibration parameters and the data used for some models, not all the remaining ones can be selected as design variables. TLARs, for instance, are inherited results from market studies and are thus fixed specifications. Some variables describe choices on the aircraft architecture, like the shape of the empennage or the landing gear configuration. In the end, only a few tens of inputs are really worth investigating, such as the hybridization ratio or the wing geometry. When an optimization is conducted, the design variables, objective functions, and constraints will be specified. The different types of inputs, as well as examples taken from the framework discussed in the next section, are presented in Table 2.2.

2.3.2 Extension to hybrid and all-electric configurations

Based on the lessons learned from the investigation into the modeling gaps in the major frameworks discussed in Section 2.2.4, several guidelines were identified and followed for the development:

i The models used for sizing and evaluating the performances of the electric components should have a level of fidelity higher than simple efficiency and power densities considerations. This stems from the fact that such models don't provide enough details to study the effect of technological design drivers, and their influence at aircraft level.

ii The implementation of the models should make it possible to analytically differentiate the formulas. This will then allow the use of efficient gradient-based methods for both the solving and the optimization of the powertrain, enabling a reduction in computation

Table 2.2 Description of input types and examples in the FAST-OAD framework.

Type	**Description**	**Example**
Tuning variables	Variables that are used to recalibrate the results of a model to reflect the adaptation to a new technology, for instance,	0.85 factor on the airframe mass to account for the use of composite
Model assumptions	Variables that are used as inputs of the models	Characteristics of a reference engine in a family for scaling laws (more details on that in Section 3.3), turboshaft power offtakes
Architectural choices	Variables that define a choice on the aircraft or powertrain architecture that cannot be changed during the optimization	Position of the wing (high wing or low wing), position of the powertrain components (front, rear, on the wing, ...), type of landing gear (retractable or not)
Specifications	Variables that represent the requirements imposed on the design, mainly the TLARs, but also requirements from the certifications	Design range and payload, approach speed
Design variables	Variables which can actually be changed to optimize the design	Voltage of the network, wing aspect ratio, hybridization ratio

time and an increase in the number of concepts that can be evaluated in the preliminary design phase.

iii The impact of each electric component on the overall design of the aircraft should be considered. It means that models for the mass, additional drag, and power consumption should be implemented [119]. Additionally, the effect on the center of gravity and volume allocation should be considered. In addition to that, and in order to model slipstream effects, the influence of the components on the lift, drag, and pitching moment of the aircraft should also be included generically. Finally, the question of the emissions of the components and the computation of their impacts on the environment should also be addressed.

iv It should be possible to freeze the enforcing of design constraints for the components to allow for a simple verification that the user-provided sizing parameters are below the required maxima for the aircraft. This should be done in the spirit of allowing users to assess the use of "off-the-shelf" components, allowing the implementation of manufacturing constraints in the process. For example, the same process and models should allow to size an electric motor tailored to the needs of a specific mission and to evaluate an aircraft using an electric motor with the specifications of an existing model.

In accordance with these guidelines, a new plugin for the FAST-OAD ecosystem, called FAST-OAD-CS23-HE [1], was developed. This newly developed plugin adds to the existing models for the sizing of General Aviation aircraft, a methodology to estimate the performance of hybrid-electric powertrains and their impact at aircraft level. To do so, a load flow analysis method [120] was adapted and implemented. This method, and its original implementation,

[1]https://github.com/florentLutz/FAST-OAD-CS23-HE, Accessed: 2025-11-20

makes use of the OpenMDAO framework, which allows to represent the operating equation of the electric components either as explicit or implicit relations. This implementation also allows for the computation, for each component, of the flow and effort quantities (voltage/current, rotational speed/torque, ...), enabling a full characterization of the powertrain state and evaluation of the effect of a change in the architecture's technological design drivers. Thanks to OpenMDAO's object-oriented approach and the ability to connect variables at will, this type of methodology allows for automatically and dynamically generating a design problem based on a user-specified architecture description. In practice, notwithstanding the computational time, a near infinite number of different architectures can be represented with any number of physical components and connections. Instead of explicitly writing the physical components' state equations and their connection as is typically done, this method advocates for a different approach. Each physical component is represented as a set of equations with a defined interface to connect to other physical components, and which consists of the variables describing the type of power flowing at the output or input. Then, using OpenMDAO's features, the interfaces are connected to ensure coherent power flow from the loads to the sources. Additionally, OpenMDAO components using implicit equations are proposed for the case where multiple physical components need to be connected at the same interface. By driving the residuals of these OpenMDAO components to zero, the consistency of the power flow can be ensured. Additionally, this residual-driven approach supports easy extension of the framework for multi-physic simulation. The flexibility of the load flow analysis was also used to provide a pseudo-user interface for the description of the powertrain. This is done by describing the powertrain in the form of a graph, where components are nodes and their connections are edges, inside a so-called powertrain file. This file uses the same YML format as the configuration file in the FAST-OAD framework. The working principle of the framework is described in Figure 2.7.

Starting from a physical description of the powertrain to be evaluated and the available list of components in the framework, the user builds a modeled version of the architecture. This modeled architecture is then translated into the powertrain file, which, thanks to its format, can both be written and read by humans. Additionally, thanks to its relative simplicity, this powertrain file also serves as an interface with other tools that can read a graph-based description of the powertrain, such as Altarica [121], for future safety evaluation. Based on the OAD models inherited from the FAST-OAD ecosystem, the framework will then create an OpenMDAO problem for the sizing and evaluation of the aircraft. This problem is then dynamically adapted based on the description of the propulsive architecture in the powertrain file to include the sizing and the evaluation of the performances of the propulsion chain, which corresponds to the bold red arrows in Figure 2.7. According to the sizing parameters obtained in models from the pre-existing FAST-OAD frameworks, the effects at aircraft level are then included in the OAD models, which is illustrated by the green arrows. Specifically, effects on the aerodynamics (installation effects), on the weight and balance (components

mass and effect on the CG), on the performances (energy use of the powertrain), on the sizing of the wing (slipstream effects in low speed conditions) and on the assessment of the environmental impacts of the aircraft can be seen, thus validating the third guideline.

In addition to starting from an existing physical propulsive architecture, it is also possible to build an architecture from scratch. Except for a few compatibility checks that ensure, among other things, that at least one propeller and one power source are present in the powertrain file and that all connections are respected, any architecture can be modeled. More specifically, thanks to the modularity of the code and the load-flow analysis method, any architecture built from components in the model library can be evaluated regardless of the number of components and how they are connected. This makes the number of possible architectures virtually infinite.

To make this framework capable of representing different architectures with multiple technological drivers and power scales, its robustness to input parameters was also emphasized. For this reason, and to ensure efficient solving of the problem, smart initialization of the flow and effort quantities across the whole powertrain is performed. As in the original implementation of the load flow analysis [120], the voltages for all components are computed based on the values set by generators and power converters. Knowing the target value for those components thus allows to identify a good initial guess for the value of all the components' voltages . A check is also performed to prevent some hard-to-debug convergence errors in case multiple components that set the voltage are connected but provide different values. For the preconditioning of currents, an initial guess on the aircraft-level thrust required during all steps of the mission is first computed. In conjunction with an initial guess for the values of the aircraft airspeed, the propulsive power required at each time step can thus be computed. Using top-down efficiencies, this initial guess is then used to compute the power at the input and output of each component. Together with the initial guess on the components voltage, this allows a first guess for the components current. A graph summarizing the different steps of the powertrain preconditioning is presented in Figure 2.8. The white parallelograms on the top of the figure represent data that are either inputs or computed by other parts of the code, while the ones on the left represent values used for the preconditioning. The choice has been made to leave efficiencies used for the computation of the initial guess out of user accessible inputs to avoid confusion with the actual value of component efficiencies computed by the code.

To allow high modularity of the code, the choice was made to use one OpenMDAO component per model or equation. Furthermore, leveraging OpenMDAO's Group components, for each physical component of the powertrain, unitary models are aggregated depending on their types. For this purpose, three main model categories are identified:

I Estimation models: this category regroups all of the models that allow the assessment of the characteristics of the component, such as its mass, its center of gravity, its reference resistance, its heat capacity, or added profile drag, depending on their sizing conditions

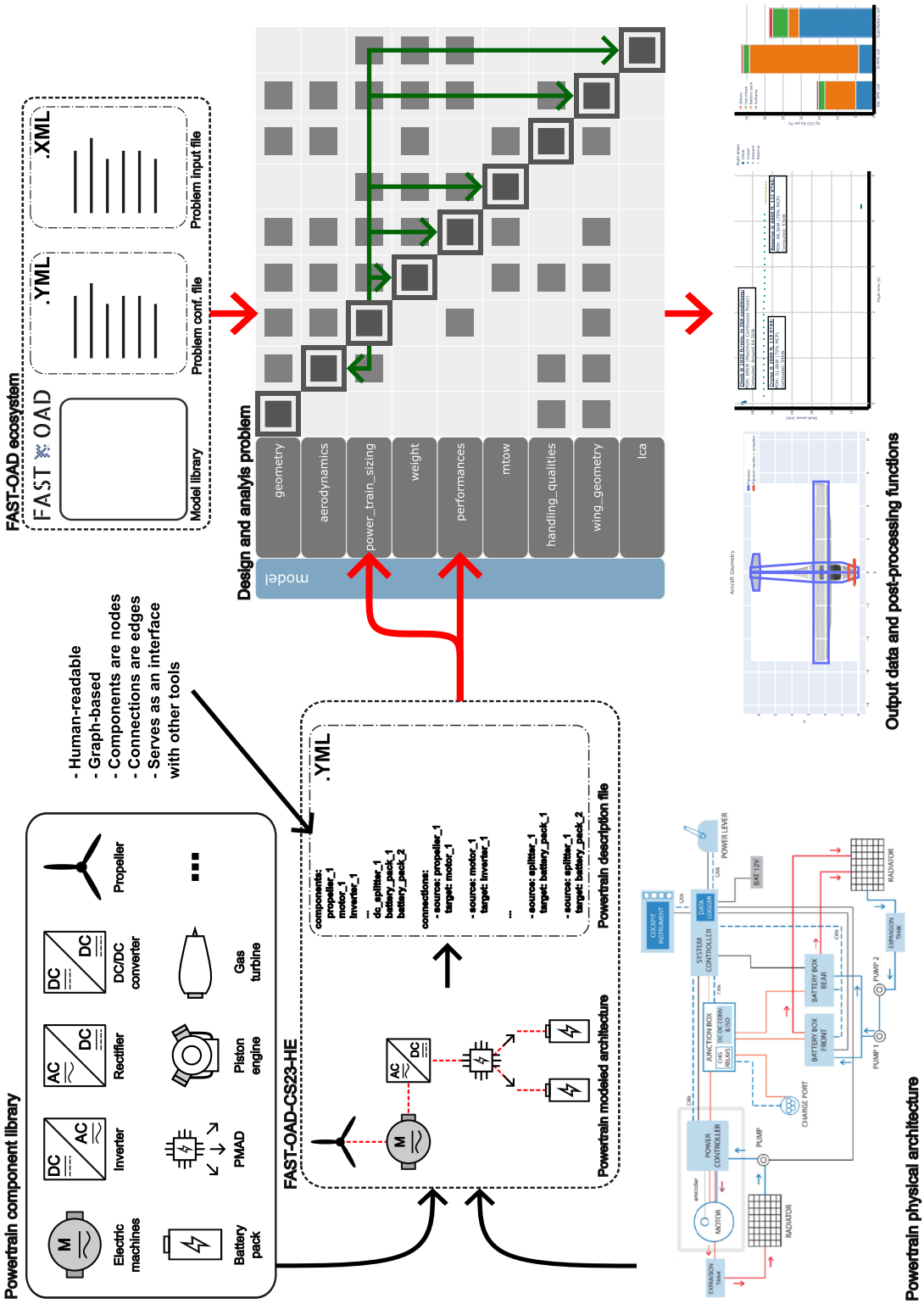

Figure 2.7 Schematic drawing of the working principle of the FAST-OAD-CS23-HE framework.

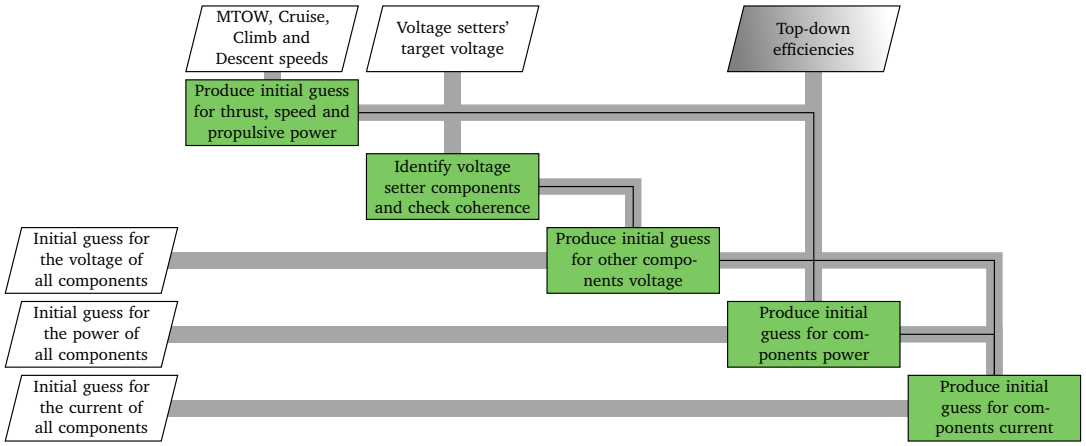

Figure 2.8 Description of the powertrain preconditioning for the computation of the mission.

(which vary depending on the component). The precise form these models will take will largely depend on the literature and data available and will be further discussed in Chapter 3. Regarding the implementation, to improve readability of the code, the choice was made to have all the scripts containing estimation models start with the same prefix `sizing`. Depending on the content of the powertrain file, these models are then added, possibly multiple times if multiple components of the same type are required, and regrouped under the `power_train_sizing` module in Figure 2.7.

II Simulation models: this category contains all the models that compute the flows of power during the simulated mission. In particular, they evaluate the energy used during the flight, e.g., the computation of efficiencies, the currents and voltages at each point of the flight for electric components, the torque and rotation speed for mechanical components, or the fuel flows. The names of the scripts that regroup this subset of simulation models all start with the `perf` prefix. This category also includes the models that compute the impact on the aerodynamics of the aircraft when these impacts vary according to flight conditions. The profile drag caused by an electric motor nacelle, for instance, is considered constant in FAST-OAD-CS23-HE and is thus treated by the estimation models. The impact of the slipstream effect of propellers, on the other hand, is included in this category. For this subset of the simulation models, the `slipstream` prefix is used. Similarly to the modules containing estimation models, they are added based on the contents of the powertrain description file, which is used to dynamically adapt the content of the `performances` module in Figure 2.7. Although in this case, the module also includes the computation of the aircraft's equilibrium during the mission.

III Evaluation models: this category represents all the models that allow the identification of the operational limitations that the components will be subjected to during the representative aircraft sizing mission. Depending on the needs of specific analysis

and following the fourth guidelines, these operational limitations are then either used as the sizing conditions for the components or as constraints when the sizing conditions are provided by the users. Those are located in scripts using the `cstr` (which stands for constraints) prefix. This category also regroups all the models that evaluate characteristics of the components that do not have a direct influence on the sizing of the aircraft, such as the component's lifespan.

An example of the organization of these models and the exchange of information between them is shown in Figure 2.9 for an electric motor. The detailed models used for each component available in the framework will be discussed in Chapter 3. It is worth noting that although each component of the powertrain will be evaluated with different models, thereby meaning that the number and names of each line in their N2 might differ from those presented in Figure 2.9, they will all be structured in the same way. The contribution of the component to the LCA module, which will be discussed in Chapter 5, is purposefully hidden in Figure 2.9 for clarity, as the methodology retained for that particular module required a different architecture. However, evaluation models are added to the code when quantities necessary for the evaluation of environmental impacts are required. These models follow the same rationale as the others, and the names of the scripts all start with the `pre_lca` prefix.

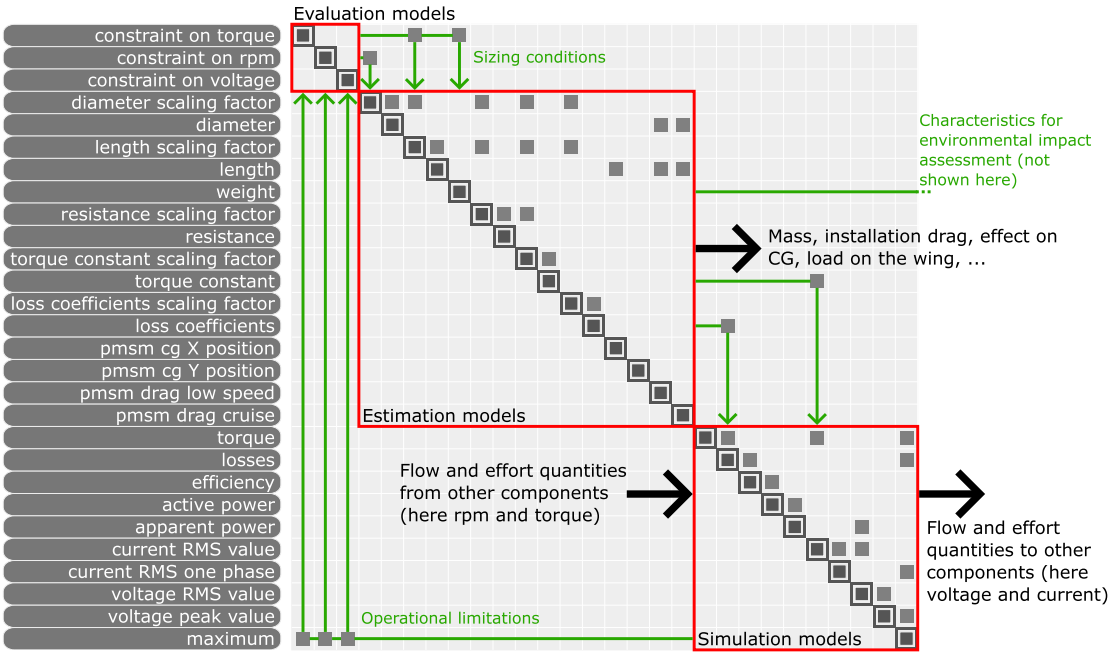

Figure 2.9 Example of model classification and aggregation for components in the FAST-OAD-CS23-HE library. The N2 is generated using FAST-OAD's built-in post-processing capabilities applied to the models used for the electric motor.

The choice of segregating each equation in a single OpenMDAO component and the ability of OpenMDAO to handle residual-based equations allow easy reconfiguration of each model.

Therefore, while the framework has been presented so far as a design tool (i.e., finding a design solution from a set of Top Level Aircraft Requirements), it can also be used as an analysis tool (estimating the performances of a candidate aircraft). It is worth stressing that both directions for the problem use the same model as enabled by the framework's modularity, thus showing consistent results regardless of the formulation of the problem. This modularity was also leveraged in the computation of the wing area, which was also reworked. Instead of the explicit formula previously used, the wing area is now computed using a nested optimization that minimizes the wing area so long as the aircraft can be at an equilibrium along the longitudinal axis. This approach allows to include the impact on the wing sizing of slipstream effects and ensures consistency with the formula used during the estimation of the aircraft's performances. A routine was also developed to interface the mass and position of the component with the physics-based method developed to compute the mass of the wings [32] and fuselage [91] based on connected loads.

2.4 Conclusions and perspectives

Chapter summary

This chapter proposed a review of the design methodologies used in literature for the sizing and assessment of the performance of aircraft with electrified propulsive architectures. Out of the methods surveyed, integrated frameworks leveraging MDAO techniques were identified as the best candidates thanks to their innate ability to deal with multidisciplinary problems and capture cross-disciplinary synergies, thereby allowing optimization at aircraft level. These capabilities make them especially well-suited for electrified aircraft design problems where the number of design variables is expected to increase very quickly and where big savings are predicted to come from vehicle-level optimizations. Existing integrated OAD frameworks were then reviewed on the basis of the challenges and opportunities brought by electrified propulsion and discussed in the introductory chapter. Particular emphasis was also put on the level of fidelity of the models adopted in each framework, as constant top-down kW/kg and efficiencies were recognized as too limiting to model some of the design constraints relieved by the scalability of electric powertrains. More specifically, open-source frameworks were investigated, and it was concluded that although most of them had strong advantages to make them suited for the preliminary design of electrified GA aircraft, a methodology capable of dynamically reconfiguring the design problem for the vast array of usage and envisioned electrified propulsive architecture was missing.

From these observations, a new methodology was developed and implemented as a plugin of the existing FAST-OAD framework, leveraging the existing OAD disciplines from its CS-23 extensions (airframe masses, geometry, aerodynamics, performance module, etc.). The implemented framework uses the flexibility of the load flow analysis method coupled with OpenMDAO capabilities of adjusting the models and connecting variables at will to

dynamically adapt the MDAO problem based on user-inputted powertrain architectures. As the architecture is described in an easily adjustable user input file, the proposed implementation proved capable of simulating a great number of propulsion chains on various aircraft configurations. Additionally, the framework was built on a generic description of the powertrain components, which enforces the evaluation of the impacts at aircraft level. This description not only allows to consider the impacts of the weight, energy use, and propeller slipstream effects, but also the impacts on profile drag, weight, and balance of the aircraft. Additionally, interface with physics-based methods for the estimation of airframe weight based on loading envelopes and estimation of the wing surface were added, thus enabling to accurately transcribe aircraft level impacts seldom considered. Furthermore, this implementation enables the use of medium-fidelity models to capture the complex design trends of electrified aircraft. This implementation also paves the way for the implementation of a module for the assessment of the environmental impacts of electric aircraft. This implementation, however, will be further discussed in Chapter 5. All in all, the new connections brought forth by the proposed methodologies are showcased in Figure 2.10.

Perspectives

While the implemented framework does not currently support the evaluation of the other disciplines of interest, the residuals-based approach allows easy extension to additional disciplines. In particular, because of the importance in terms of weight and drag, extension to the co-design of thermal management systems is envisioned. While work in the FAST-OAD ecosystem has already been presented [108], it has been developed for a fixed architecture; therefore, work on adapting it to the new formalism is required. Additionally, while the position of the components is considered through its impacts on the weight and balance, the question of the volume of the components and their ability to fit inside the zones of the aircraft is currently not considered. Similarly, the question of the zonal allocation of components could give rise to the assessment of zonal risk [122] and add to the framework the evaluation of safety issues that must be considered, given the lack of historical knowledge on those technologies. In addition to the assessment of environmental impacts, which will be discussed in Chapter 5, the question of the assessment of cost should also be integrated as a simultaneous assessment of the two disciplines is recommended in literature [123, 124]. Finally, the question of the evaluation of noise should also be addressed, as it has been identified as a possible advantage electric configuration could have. These avenues of improvement for the framework are shown in Figure 2.10 with the red connections and shaded disciplines.

Despite these limitations and perspectives, the framework proposes a generic description of models for the physical components of the propulsive architecture that allows to assess their impacts at aircraft level. The specific models used for each physical component inside

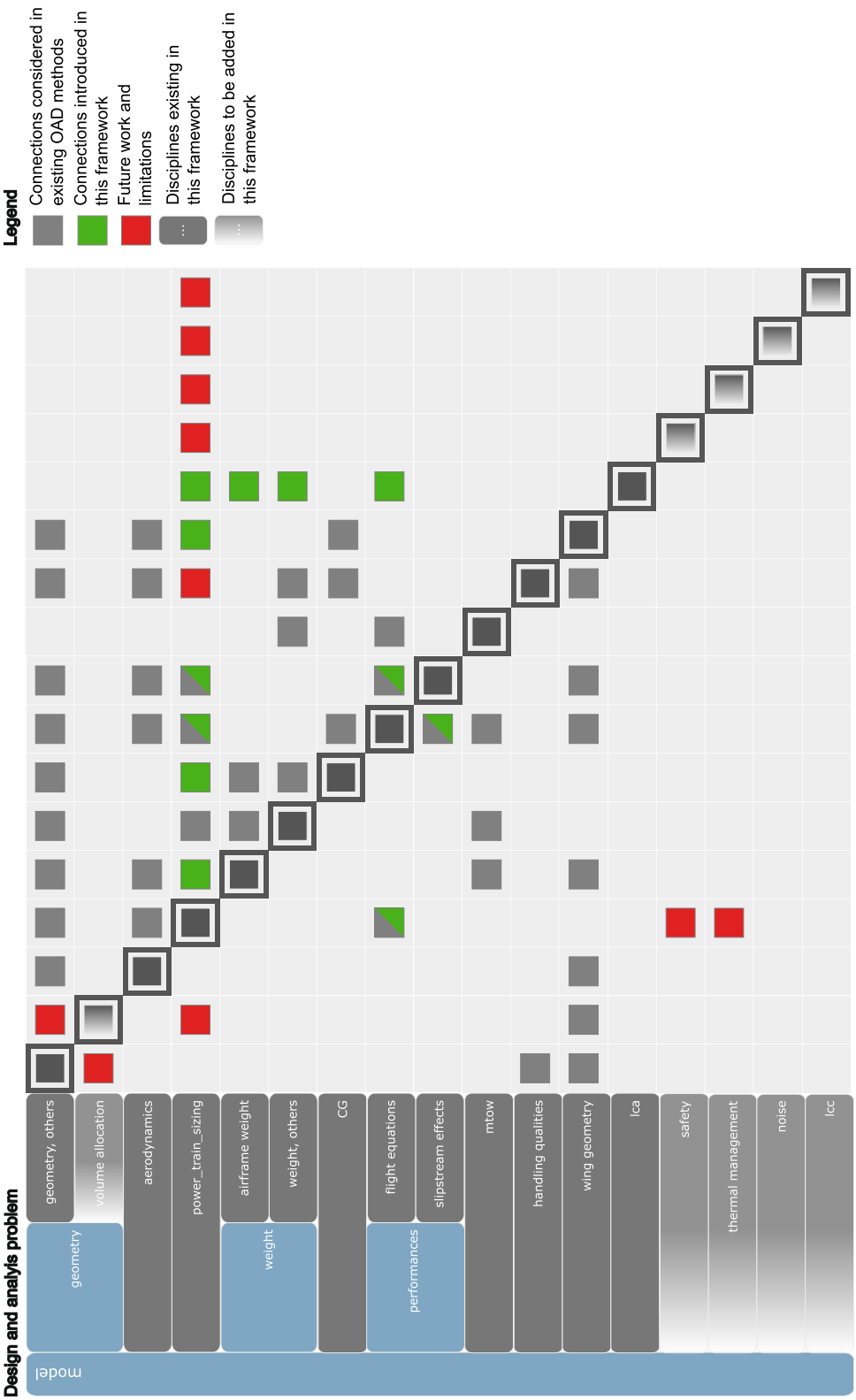

Figure 2.10 Schematic representation of the disciplines and couplings in the FAST-OAD-CS23-HE framework.

the model library delivered by default with the open-source code will be discussed in the next chapter.

Chapter 3

Modeling of General Aviation aircraft propulsive architectures

Contents

3.1 Introduction **46**
3.2 Propulsive architecture components **46**
3.3 Modeling techniques **48**
3.4 Propulsive elements **50**
3.4.1 Propeller 50
3.5 Electric loads **52**
3.5.1 Electric motor 52
3.6 Sources **54**
3.6.1 Battery packs 54
3.6.2 Generators 57
3.6.3 Piston Internal Combustion Engines (ICEs) 58
3.6.4 Gas turbines 59
3.7 Connectors **62**
3.7.1 Inverters and Rectifiers 62
3.7.2 DC/DC Converters 63
3.7.3 Cables 64
3.7.4 Buses and Splitters 66
3.7.5 Circuit breakers 68
3.7.6 Gearboxes 68
3.7.7 Tanks and fuel system 69
3.8 Summary **69**
3.9 Conclusion and perspectives **69**

3.1 Introduction

INTRODUCTORY chapters highlighted the need to assess the impacts, at aircraft level, of the components in the propulsive architecture as well as the need for models capable of capturing multi-disciplinary synergies to truly evaluate the benefits of hybrid- and full-electric aircraft. For this reason, Chapter 2 introduced the load flow analysis method, which enables the characterization of the complete state (flow and effort quantities) of the power network. The original model, and the implementation that was proposed for it, are relatively simple and do not highlight the dependencies of the components on either the operating conditions or technological drivers. The need for analytically differentiable models was also established to ensure robust convergence using derivatives. Finally, as discussed, this methodology will be implemented in the FAST-OAD framework, and more specifically in the existing FAST-OAD-CS23 plugin [91], thus inheriting its OAD models. Consequently, particular emphasis will be put on the modeling of the powertrain.

This chapter begins with a non-exhaustive review of the components of the propulsion chain that were modeled due to their significant impact at aircraft level, along with a brief description of the functions of said components. Models for those components, as well as the ability provided by the framework to define the architecture, suffice to replicate most of the electric powertrains envisioned for light and regional aircraft. The models used to improve the fidelity of the original load flow analysis method and enable the sizing and estimation of the performance of electrified propulsion architectures are then introduced.

3.2 Propulsive architecture components

A review of concepts presented in literature, existing aircraft, and demonstrators led to the identification of several key components common to multiple propulsive architectures. In the framework and in this thesis, the components of the powertrain will be organized based on their role in the architecture of the propulsion chain.

The first role identified is the conversion of mechanical power into useful thrust for the aircraft. This category of components, which was dubbed propulsive elements or propulsors, contains, as of now, only propellers, even though ducted fans have been identified in several configurations presented in literature [26, 27]. Propellers are the most common way of generating thrust for subsonic applications because of their high efficiency and relatively low cost [58]. They are also used in unconventional configurations to generate induced speed on the wing and create extra lift [34].

The second type of components is power loads. Following the terminology presented in the original implementation of the load flow analysis method, the term load will be used to describe any components that demand power from the rest of the network [120]. As such, electric motors will be considered as loads. Their role is to turn the electric power it

receives into mechanical power on their shaft. There are many categories of electric motor: Alternating Current (AC) or Direct Current (DC), brushed or brushless, ... Currently, electric motors are the only loads implemented, but the definition of power loads is wide enough that it could include other actuators.

On the other side of the electrical network lies the third type of components identified: the sources. The term sources is used here to refer to components that provide power to the network. For this reason, along with batteries and Internal Combustion Engine (ICE), generators are also presented as sources. Out of the possible sources identified in literature, this work will focus on the following:

- **Batteries:** Batteries are one of the components that can provide power on board an electric aircraft. They generate DC power thanks to chemical reactions between their terminals. Batteries are built by assembling arrays of individual cells to match the required electrical characteristics of the network.

- **Generators:** The role of the generator is to transform mechanical power into electrical power. Generators are a key component of hybrid-electric aircraft because they are the ones that allow conventional engines to supply power to a distributed electric network.

- **Piston Internal Combustion Engine (ICE):** They are also found in conventional architecture, and are very common on light aircraft because of their price when compared to turbomachinery. Combined with a generator, they are often used on hybrid aircraft either as range extenders or to provide power during extended flight phases where a battery alone can't provide enough energy.

- **Gas turbines:** Very much like piston ICE, gas turbines provide mechanical power by burning fuel. The fundamental difference comes from the fact that the flow is continuous and not in cycles.

The final category of components identified for this work is connectors. The term connectors is used here to designate components that are designed to connect power sources to power loads, but also fuel-burning machines to tanks. Regarding the latter, two components were modeled: fuel tanks and fuel systems. Tanks are responsible for storing the fuel used to supply the thermal machines. As for fuel systems (which include pumps, valves, sensors, ...), they make the connection between the tanks and the thermal machines. Gearboxes were also included in this work. They are a purely mechanical component, but can be conceptually compared to a DC/DC converter as they do not change the type of power, merely how it is delivered, in that case, with a change in rotational speed.

The remaining components in the connector category can be described as being part of the electrical network or electrical distribution system. The role of this network can be formulated as: "supplying, with the appropriate level of reliability, electrical power to the aircraft systems" [125]. This main function is then usually further broken down into sub-functions, the first of

which is "adapting voltage levels". This role is fulfilled by power electronics, three of which are available in the library of components offered by this framework:

- **Inverter:** The role of inverters is to transform DC power into AC power. It can also play the role of a controller for the electric motor, in which case it is often referred to as an Electronic Speed Controller (ESC).
- **Rectifier:** Rectifiers are also a type of power electronics, and they perform the opposite duty of inverters, turning AC power into DC power. They are often used after devices that generate AC power as a connection to the rest of the grid, for which DC current is often preferred.
- **DC/DC converter:** as the name indicates, they transform DC power into DC power, although with a different voltage. When the voltage decreases significantly across the converter, it is called a buck; when it increases significantly, it is called a boost, and when the voltage is only slightly adjusted, it is called a buck-boost [126].

Among the other sub-functions fulfilled by the electrical network, two can be attributed to the distribution system, sometimes referred to as the Electrical Wiring Interconnection System (EWIS). These functions are: "distributing the electrical power" and "managing the electrical loads". Among the components covered by the acronym EWIS [127], three are of particular interest to fulfill those functions and will be further detailed in the rest of this section:

- **Cables:** The role of cables is to transport the power from one component to the others. It usually consists of a core which carries the current and insulation layers (mechanical protection, Electromagnetic compatibility protection, ...)
- **Bus Bar:** Fairly similar to the cables, the role of the bus bar is to connect power loads and power sources. In this framework, we will also consider a specific type of bus bar that we will call splitters [31], which will be used to simulate power management strategies. In real-world architectures, this is dictated by the difference in voltage of the power electronics, but for ease of use, a separate component was created.
- **Circuit breakers:** Circuit breakers play a crucial role in the protection of the circuit. They prevent damage from overcurrent by disconnecting and isolating faulty components. They are also used to switch between primary buses and backup buses in case the former were to fail, and allow reconfiguration of the electrical network architecture.

3.3 Modeling techniques

A wide variety of approaches can be used to model powertrain components, ranging from fully analytical methods like high-fidelity finite element simulations to top-down efficiencies

and kW/kg methods. The medium-fidelity methods favored for this framework will be briefly described here.

A popular sizing approach for electric motors and power electronics is the use of scaling laws [125, 128–130]. These laws, also called similarity laws or allometric models, are based on the assumption that, among a family of components with the same technology, a certain number of dimensionless parameters and material properties will be identical. This then allows to establish formulas comparing the value of the parameters of a reference component to those of a derivative component. This provides a quick way to estimate a wide number of designs by only requiring detailed knowledge of a single component. They also allow to reduce the number of required inputs by expressing all useful relations (dimension parameters, simulation parameters, ...) according to a few key design parameters. For instance, assuming the same stress limit in all components of a family (the same material used implies the same strength), the following can be written:

$$\frac{F_{\text{ref}}}{S_{\text{ref}}} = \sigma_{\text{ref}} = \sigma_{\text{new}} = \frac{F_{\text{new}}}{S_{\text{new}}} \tag{3.1}$$

By denoting $x^* = x_{\text{new}}/x_{\text{ref}}$ the scaling ratio of a quantity, we then have:

$$\sigma^* = \frac{F^*}{S^*} = 1 \implies F^* = S^* \tag{3.2}$$

Uniform scaling of all dimensions is commonly assumed, which then allows to write:

$$F^* = l^{*2} \tag{3.3}$$

which allows to compute component size based on the required load. Another common approach is the use of regressions. This type of approach can allow, when a sufficient amount of manufacturer's data are known, to estimate the characteristics of a fictitious component inside a family. It also has the merit of estimating performances close to those of real-life components. This approach has been widely used for the estimation of conventional aircraft masses [58–61]. Figure 3.1 shows a regression between engine weight and rated power at sea level for turboprop engines established based on published manufacturer's data [58].

The downside of using regression models is that, because of their statistical natures, the accuracy of their results cannot be guaranteed outside of the bounds of the data used to establish them. In particular, the relations presented in the classical aircraft design book to estimate the Operating Weight Empty (OWE) based on the MTOW [58–61] likely won't hold for electric architectures.

Surrogate models are also frequently used. It allows to replace computationally expensive simulations with lightweight functions [131], thus reducing overall computational time and improving robustness of the simulation. In addition to that, explicit functions can be chosen for the approximation, allowing for the analytical differentiation of a complex model.

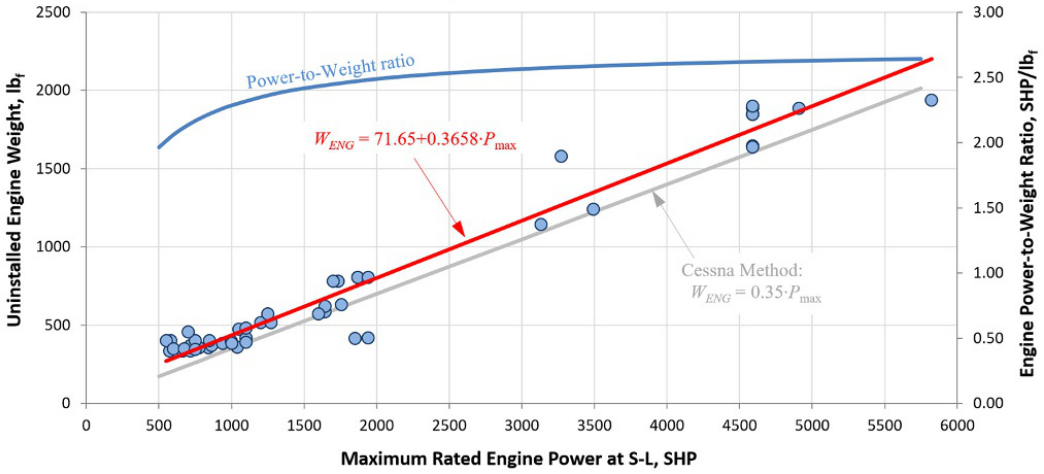

Figure 3.1 Correlation between the uninstalled weight of turboprops and their rated power [58].

Finally, analytical models can also be used when the physical phenomena at stake are well known. Typical examples include the flight equations of an aircraft or the thrust resulting from the acceleration of hot gases in the exhaust of a gas turbine. Quasi-analytical model, which results from the simplification of complex systems of equations, thanks to a few key simplifying modeling assumptions are also used. A Vortex Lattice Method (VLM), for instance, is the preferred way of estimating the wing aerodynamics in the original framework [91].

3.4 Propulsive elements

3.4.1 Propeller

Conceptually, propeller blades can be seen as rotating airfoils that produce aerodynamic forces, like a wing would. These forces are called thrust T and torque Q. Their performances are traditionally estimated using dimensionless parameters. These parameters are the thrust coefficient C_T, the power coefficient C_P and the advance ratio J and are computed using:

$$C_T = \frac{T}{\rho_{air} n^2 D^4} \tag{3.4a}$$

$$C_P = \frac{P}{\rho_{air} n^3 D^5} = \frac{2\pi n Q}{\rho_{air} n^3 D^5} \tag{3.4b}$$

$$J = \frac{V_\infty}{nD} \tag{3.4c}$$

where ρ is the density of the air in kg/m^3, n is the propeller revolution speed in rotation-per-second or rps, D is the propeller diameter in m, P is the shaft power in W and V_∞ is the freestream air velocity in m/s.

While the original FAST-OAD-CS23 plugin [91] already provides an estimation model for the performances of the propeller based on a BEMT code, a surrogate model was preferred to allow for analytical differentiation. The original model was, however, augmented beforehand with corrections to account for Reynolds effects [132], compressibility [133], and rotational effects [134] and used to generate the training dataset for the surrogate. The resulting model allows the power coefficient to be expressed as a function of the thrust coefficient and other dimensionless parameters:

$$C_P = f\left(C_T, J, M_{\text{tip}}, Re_D, \sigma, AF, \theta_{\text{blade}}\right) \tag{3.5}$$

More information on the model, its full expression, and the definition of the dimensionless parameters is available in Appendix B.1.

For the estimation of the propeller mass, a literature review revealed a variety of approaches. Although a detailed physics-based formula exists [88], it was decided to opt for a statistical formula. While semi-empirical formulas tailored for turboprop and piston engines alike exist [59], they were not retained because they were established based on old aircraft data. Consequently, it was decided to establish a new formula based on data publicly available on the EASA's website, which contains the Type Certificate DataSheet of propellers certified under CS-P [135]. A coefficient was added to allow a consideration of the choice of materials for the propeller, based on the observation that composite propellers were lighter for the same ratings. This led to the formula presented in Equation 3.6.

$$m_{\text{prop}} = N_{\text{blade}} \frac{9.03 + 1.074 \times 10^{-3} \times Q_{\text{nom}} + 2.841 \times 10^{-3} \times D^3}{k_{\text{materials}}} \tag{3.6}$$

Where m_{prop} is the propeller mass in kg, Q_{nom} is the nominal torque rating of the propeller in Nm, and $k_{materials}$ is equal to 1.0 for aluminum blades and 1.66 for composite blades.

As briefly mentioned in Section 3.2, and while propellers are mostly used to generate thrust on conventional designs, they can also be leveraged to enable aero-propulsive synergies. The generation of thrust indeed increases the velocity of the air going through the propulsor. This, in turn, makes it so any lifting surface downstream of the propulsive element sees a greater speed compared to that of the aircraft, thus creating more lift than an isolated wing. The induced tangential velocity also creates a variation of the local Angle-of-Attack (AoA) [136]. Distributing the propulsion on the wing with the use of electric propulsion would then allow to reduce the size of the aircraft wing and the thrust required during takeoff [33, 34], thereby reducing wet area and consequently drag but also wing mass and thus widening the design space [65, 77].

In literature, these effects are commonly considered using a model established based on the results of a 2-D aerodynamic analysis to account for the effect of propeller performances, installation, and location with respect to the wing [34]. This led to a modeling of the lift and drag coefficient of the wing+propeller system, which is commonly expressed as an increase

in the clean aerodynamic coefficient [79, 99]. Models for the change in the wing pitching moment [137] were also included as the pitching moment induced by slipstream effects can have a significant impact on the aircraft's equilibrium [138]. This yields the generic expressions found in Equations 3.7 [64].

$$C_L = C_{L,clean} + \Delta C_L(T, C_{L,clean}, S_w, ...) \tag{3.7a}$$
$$C_D = C_{D,clean} + \Delta C_D(T, C_{D,clean}, C_{L,clean}, S_w, ...) \tag{3.7b}$$
$$C_m = C_{m,clean} + \Delta C_m(T, C_{L,clean}, S_w, ...) \tag{3.7c}$$

3.5 Electric loads

3.5.1 Electric motor

Many technologies exist for electric machines, each with its own design principles and corresponding sizing methodologies. They can depend on the type of input current (AC/DC), the type of movement in output — linear or rotating —, and the electromagnetic to mechanical conversion principle (synchronous/asynchronous) [139]. A high-level breakdown of the various electric motor technologies can be found in literature [140]. Because they can realistically be used on GA aircraft and because they present high torque densities and efficiencies [141, 142], the choice was made to focus on Axial Flux Permanent Magnet Synchronous Machine (AFPMSM). Among existing AFPMSM, the EMRAX family[1] has been extensively used in airborne electric powertrains. Electric motors from this family are used on the Pipistrel Electric Taurus and on various other electric gliders. A derivative of the EMRAX is also used on the Pipistrel Velis Electro. They advertise power densities of up to 10 kW/kg and efficiencies of up to 98%. Additionally, engine manuals are available on the manufacturer's website, which allows to create regression or validate formulas.

For the modeling of electric motors, scaling laws are favored because they offer a good compromise between computational time and fidelity [53, 128, 129]. This approach [143] will be retained to obtain the external dimensions of the motor, length and diameter, based on the sizing torque and maximum rotational speed.

$$d^*_{em} = {\omega^*_{max}}^{-1} \tag{3.8a}$$
$$l^*_{em} = T^*_{em,nom} \times {d^*_{em}}^{-2.5} \tag{3.8b}$$

While scaling laws are also commonly found for estimating the electric motor's mass [128, 144], it was decided to derive a regression. The reason behind this choice is that the scaling laws commonly used only represent preponderant sizing criteria, which, in this case, were

[1] https://emrax.com/e-motors/

not sufficient. Instead of a classical polynomial regression, which was found to be suitable for the EMRAX family, a regression guided by the main influencing terms found in literature was created. Three main terms were identified: a constant term to account for accessories, a linear term to account for mechanical stress [128], and a term that has an exponent of 3/3.5 to account for the sizing of the magnetic core of the engine [128]. The resulting formula is given in Equation 3.9

$$m_{em} = 2.8 + 9.54 \times 10^{-3} \times Q_{\text{em,nom}} + 0.1632 \times Q_{\text{em,nom}}^{3/3.5} \tag{3.9}$$

For the estimation of the engine performances under operating conditions, various approaches have been found in literature. It is possible to estimate the performances of an electric motor during the mission through the use of a map that gives the value of the efficiency as a function of the torque and the rpm [145–147]. This approach is very well suited when studying the performances of a motor for which no resizing is done and for which available maps can be found, which would be particularly well suited for off-the-shelf use of an engine in the EMRAX family. The process of digitizing the map, however, can be tedious, and it does not translate well to new designs. A different approach based on the predicted operating performances of an electric motor and a parametric performance map can be preferred [29]. This choice, however, relies on an accurate choice of the scaling parameter and good engineering knowledge. It is also possible to compute the losses directly, as explicit analytical formulas can be found [53, 94]. The drawback of using these formulas is that, while the exponents for the dependencies on the torque and the rpm are fairly constant, the proportionality term can vary from one motor architecture to another. Nonetheless, as the exponents for the dependencies on the operating parameters are fairly constant, scaling laws can be devised to obtain them from a reference case [143]. The choice was thus made to establish those scaling laws based on a regression on the efficiency maps of the EMRAX family.

From literature, the main sources of losses in an electric motor were identified as:

- **Joules losses [53]:** which are proportional to the square of the current and thus, to the torque. This results in $P_{cu} \propto Q^2$.
- **Iron losses [53, 93]:** which encompasses hysteresis losses, which are proportional to the rpm, eddy current losses, proportional to the square of the rpm, and excess losses proportional to the rpm power 1.5. This results in $P_{iron} = P_h + P_{ec} + P_{ex}$, with $P_h \propto \omega$, $P_{ec} \propto \omega^2$ and $P_{ex} \propto \omega^{1.5}$
- **Mechanical losses [53, 94]:** which include friction losses, which are proportional to the square of the rpm, and windage losses, which are proportional to the cube of the rpm. This results in $P_{mech} = P_{wdg} + P_{fr}$ with $P_{wdg} \propto \omega^3$ and $P_{fr} \propto \omega^2$.

The identification of the prevalent term among the aforementioned losses in the efficiency maps of the motor in the EMRAX family yielded the generic formula presented in Equation 3.10.

$$P_{losses} = \alpha \times Q^2 + \beta \times \omega + \gamma \times \omega^2 \tag{3.10}$$

While the scaling of the α coefficient can be found in the literature [128], a regression was used to infer the scaling of the β and γ coefficients. The resulting scaling laws are presented in 3.11.

$$\alpha^* = d^{*-4.0} \times l^{*-1.0} \tag{3.11a}$$
$$\beta^* = d^{*6.89} \times l^{*-1.96} \tag{3.11b}$$
$$\gamma^* = d^{*6.0} \times l^{*-1.60} \tag{3.11c}$$

Finally, to compute voltage and current at the input of the motor, a torque constant k_Q was assumed to link torque with current. To estimate the value of this constant for each design investigated, a scaling law was developed. This was done using the definition of the copper losses and of the torque constant, as well as the scaling laws for nominal torque, copper losses [143], and for the resistance. For the latter existing formula [128, 129] could not reproduce manufacturer's data; consequently, a regression was devised. It was, however, decided to keep the exponent on the rewinding scaling factor to 2 as is done in literature [129], which results in Eq. 3.12. This all results in the scaling law presented in Eq. 3.13.

$$R^* = U^{*2} \times {d^*_{em}}^{-2.62} \times {l^*_{em}}^{-1.12} \tag{3.12}$$

$$k_Q^* = R^{*0.5} \times {d^*_{\text{em}}}^{2} \times {l^*_{\text{em}}}^{0.5} = U^{*2} \times {d^*_{\text{em}}}^{-0.62} \times {l^*_{\text{em}}}^{-0.62} \tag{3.13}$$

For all physical quantities whose scaling laws were presented here, the chosen reference motor is the EMRAX 268 HV [2].

3.6 Sources

3.6.1 Battery packs

Battery cell chemistry and assembly

Batteries are electrochemical energy storage device which can generate electricity thanks to a chemical reaction taking place between their terminals. Of particular interest for a lot of battery-powered applications is the fact that this chemical reaction can be reversed,

[2] https://emrax.com/wp-content/uploads/2022/11/EMRAX_268_datasheet_A00.pdf, Accessed: 2025-08-02

allowing for the recharge of the battery [148]. Two main properties are usually retained when comparing battery packs: the energy density (in Wh/kg), which represents how much energy can be stored in a unit mass, and the power density (in W/kg), which represents how much power can be drawn from one unit of battery mass. The current standard chemistry for aeronautical applications is Li-Ion batteries [18]. They offer far better specific energies and power than their predecessor, lead-based and Ni-Cd batteries, and also have higher nominal voltage, reducing the requirement for the number of cells to reach high voltage networks [149].

Battery packs are an assembly of hundreds, if not thousands, of individual, smaller cells. The way these cells are assembled, in series or in parallel, defines the property of the packs and, as such, it must be considered early in the design [86, 150]. The properties of the pack can be derived from the properties of the cell using Kirchoff's circuit laws presented in Equations 3.14.

$$I_{pack} = n_{parallel} I_{cell} \tag{3.14a}$$

$$U_{pack} = n_{series} U_{cell} \tag{3.14b}$$

where I_{pack} is the current delivered by the pack in A, I_{cell} is the current delivered by the cell in A, U_{pack} is the voltage of the pack in V, U_{cell} is the voltage of the cell in V, $n_{parallel}$ is the number of cell in parallel and n_{series} is the number of cell in series.

A direct consequence of Equation 3.14 is the fact that increasing the number of cells in parallel increases the capacity of the pack. Additionally, it also decreases the amount of current that each cell has to supply. This is an additional sizing constraint to consider in the sense that each cell has a limited current throughput. In practice, the current demand on a cell is represented by the C-rate, expressed as a time, which stands for the amount of time the cell can be discharged at this rate.

The computation of the battery mass will be made using a simple packaging efficiency to account for the Battery Management System (BMS), the mechanical packaging, venting system, and isolation. State-of-the-art packaging efficiency is around 65-70 %, meaning the mass of the cells represents 65-70 % of the total mass of the pack [18].

Battery cell performances estimation

Multiple techniques for the modeling of the performances of a battery cell have been identified and reviewed in literature [49, 151, 152]. In this work, however, the cell performances will be modeled using a simple Thevenin Equivalent Circuit Model (ECM) [18, 151, 153] consisting of an open voltage source and internal resistance. More complex circuits with several resistance-capacitance (RC) networks in series [154] were also envisioned. Those circuits, however, are typically used to model transients that have far smaller time steps than

those used in the simulation of the aircraft's flight. Therefore, only a single internal resistance was considered. The data from the reference Samsung INR18650-35E cell[3] will be used to calibrate the models for the open-circuit voltage V_{oc} and the internal resistance R_{int}.

For the modeling of the Open Circuit Voltage (OCV), a simple fifth-order polynomial expression depending on the State-of-Charge (SOC) of the battery will be used [155]. The choice was made not to include a dependency on the temperature Θ for U_{oc} because experiments on similar cells have shown that this dependency only appears for very low values of the battery SOC [150]. For the estimation of the internal resistance, however, this dependency is not negligible. In this work, the assumption will be made that, while R_{int} is dependent on both the temperature and the SOC, these dependencies will be independent [156]. For the dependency on the temperature, an exponential function with a negative parameter [156] will be used. For the dependency on the SOC, a fifth-order polynomial model [141, 157] was chosen. This choice of models results in the generic formula presented in Equation 3.15.

$$U_{\text{cell}}(SOC, \Theta, I) = U_{\text{oc}}(SOC) - k_{\text{Rint},\Theta}(\Theta) \times R_{\text{int,SOC}}(SOC) \times I_{\text{cell}} \tag{3.15}$$

The variation in SOC at each time step is computed based on the current and cell capacity. High discharge rate can, however, further impact the cell capacity, which can be accounted for using a relative capacity r_C [48, 86]. This was modeled using a simple third-order polynomial fitted on manufacturer's data. The variation in SOC is then computed using Eq. 3.16.

$$\Delta SOC(t_i) = \frac{I(t_i)}{r_C(I(t_i)) \times C_{\text{nom}}} \Delta t_i \tag{3.16}$$

Battery cell aging

In addition to modeling the performances of the battery in its nominal, out-of-the-factory conditions, it is also paramount to consider the fact that, as batteries are used, they degrade because of the chemical processes taking place, inducing irreversibilities. The effect of aging on the performances of the cell is usually translated by two effects, first an increased internal resistance, and second, a reduced capacity [48, 158]. The loss of battery capacity because of aging is usually represented by the battery cell's State Of Health (SOH). A brand new cell has an SOH of 100% while a cell that has lost half of its capacity will have an SOH of 50%. Current practice in the electric mobility sector is to consider that a battery is at the end of its life when it has reached 80% of its original capacity [159].

Battery aging is a complex phenomenon influenced by factors including depth of discharge during charge/discharge cycles, temperature variations, and operational profiles [160–163]. Because it involves chemical reactions of Lithium ions, aging has linear and non-linear tendencies, where aging depends on the SOH of the battery, making it challenging to model.

[3] https://www.orbtronic.com/content/samsung-35e-datasheet-inr18650-35e.pdf, Accessed: 2024-01-26

Consequently, and as is suggested in literature [160], a focus will be made on the linear dependencies only. Aging is then usually separated into two categories: calendar aging, which happens due to side reactions even when the cell is idle, and cyclic aging, which is due to the usage of the battery. To improve predictive accuracy due to a change in cell chemistry or packaging, a model calibrated on the aging of a cell from the same family as the reference cell was selected [162]. Dependencies on major parameters, however, are respected [153]. The capacity loss is thus modeled as:

$$C_{loss} = C_{loss,calendar} + C_{loss,cyclic} = 1 - SOH/100 \tag{3.17a}$$

$$C_{loss,calendar} = f(SOC) \times exp\left(\frac{-3053}{\Theta_{storage}}\right) \times t^{0.5} \tag{3.17b}$$

$$C_{loss,cyclic} = g(DOD) \times exp\left(\frac{-4345}{\Theta_{mission}}\right) \times N_{cycle}^{0.5} \tag{3.17c}$$

where C_{loss} is the relative capacity loss, $\Theta_{storage}$ is the storage temperature in °K, t is the storage time in days, DOD is the depth of discharge, $\Theta_{mission}$ is the average temperature during the mission in °K and N_{cycle} is the number of cycles. Other dependencies, such as the throughput, the C-rate during charge and discharge [161] or the average SOC during discharge [160], won't be modeled.

3.6.2 Generators

As discussed in the introductory part of this chapter, thermal engines can be used to power a hybrid-electric architecture, in which case a conversion of mechanical power into electric power is required. That function is fulfilled by a generator. In practice, generators function the same way electric motors do, even though different topologies might be better suited for each function [143]. For this reason and for low-power applications, it was decided to take the same model for both the electric motor and the generator, as is done in some proprietary software such as GasTurb. This can be further justified by the fact that the literature review revealed that multiple flying electric aircraft use a piston ICE coupled to a motor from the EMRAX family, the one selected in this work as a reference, as a range extender [164, 165]. There is, however, a slight change that will need to be made linked with the fact that, as part of the load flow analysis method [120], generators impose the voltage on the rest of the circuit.

For higher power applications, typically generators coupled to turboshafts or turboprop, and because of a lack of available literature on the subject, a simple model based on top-down metrics was used. An efficiency value of 96% and a power density of 5 kW/kg were selected [43]. For this type of application, a separate component was added to the library of models.

This means it is the user's responsibility to use the appropriate component for the expected power range.

3.6.3 Piston Internal Combustion Engines (ICEs)

Piston ICEs have been a staple in aviation since the first flights of the Wright brothers; to this day, they are still widely used for low-speed aircraft applications. They are also the most used form of propulsion across all areas of the transportation sector [166]. Its history makes it a widespread, low-cost, and very adaptable solution [58]. Nonetheless, this type of power source also has a great deal of drawbacks, among which are high vibrations, low Time-Between-Overhaul (TBO), and harmful emissions, including noise and, with conventional fuels, CO_2 and lead [7, 58].

Similar to electric motors, piston ICE performances can be modeled using manufacturers' data, which usually comes in the form of a table or maps. The drawback of this method is the low availability of such information, combined with the discrete nature of the sample. Another method is to use an analytical expression of a four-stroke Otto cycle [167], which is the thermodynamic cycle that describes the working principle of a piston ICE [58]. The original method from the FAST-OAD-CS23 plugin will, however, be kept [91]. This method is based on the assumption that certain key characteristics stay constant on a family of technologically similar engines. In this case, the maximum Mean Effective Pressure (MEP) and the relation $SFC = f(MEP, rpm)$ were assumed to be constant. The rescaling of the engine can then be done by varying the displacement volume of the cylinders with the help of Equation 3.18, which links MEP, volume, and shaft power.

$$V_d = \frac{2 \times \pi \times n_s \times P}{\omega \times MEP} \tag{3.18}$$

where V_d is the displacement volume in m^3, n_s is the number of strokes in the engine, usually two or four, P is the shaft power in W, ω is the shaft rotation speed in rad/s, and MEP is the mean effective pressure in Pa. To allow for the analytical differentiation of the model, it was decided to approximate the SFC map with a third-order polynomial expression. This model, like other scaling laws, will have limited use outside of the range of engines it was derived on: the Continental IO-550 family. Other piston ICEs are, however, of particular interest in the General Aviation segment: the Rotax family [4]. These engines, while they have lower power outputs (160 hp at most), work under much higher rpm, enabling a higher power density. They are especially well-suited for smaller aircraft. Available models from literature [168, 169] and regression from manufacturer's data were compared with the fuel consumption extracted from Pilot Operating Handbooks (POH), which revealed a poor fit. Consequently, for Rotax engines, the SFC will be an input of the problem.

[4] https://www.flyrotax.com/p/products/engines

An important phenomenon that also has to be taken into account is the fact that the power output of the engine directly depends on the density of the air [58]. Therefore, at higher altitudes, the maximum power available will be significantly lower than at sea level. The sizing of the engine should account for that phenomenon. To model this, the Gagg-Ferrar model [170] will be used.

The computation of the dry engine mass will be made according to traditional correlations between the mass and the maximum power at sea level [58]. The installed mass of an engine is somewhat higher than its uninstalled mass, or dry mass, because to properly function, a wide variety of accessories must be installed: fuel lines, oil circuit, and nacelle/cowling. This will be accounted for using a penalty coefficient method to multiply the mass of the uninstalled engine.

Finally, and even though piston engines account for a mere .05% of aviation fuel burn (only 2% of propeller-powered flights) [171, 172], a computation of the emissions will be included. Indeed, piston ICEs have high outputs of harmful emissions due to the use of outdated combustion and fuel technologies. Even considering their low contribution to aviation fuel burn, they release around 40% of total CO emissions and 100% of lead emissions from aviation [7, 8]. Multiple approach exists for modeling emissions, ranging from using experimental data [7, 8] to detailed modeling of the combustion process [173]. Literature, however, shows that emissions profiles are very sensitive to engine, pilot actions, mixture, and atmospheric conditions [7]. Therefore, simple emission indices (EI) — a ratio between fuel burn and emissions outputs — will be considered. The species and indices considered were taken from literature [174, 175] and are summarized in Table 3.1.

Table 3.1 Value for the emissions indices considered for the operation of piston ICE.

Species	CO_2	CO	NO_X	lead	SO_X	HC	H_2O
EI (g/kg_{fuel})	2000	1000	3.14	0.794	0.42	18.867	1237

It is worth noting that, while the theoretical emission index for CO_2 should be around 3170 g/kg, the fuel is burnt in such a suboptimal way [7], that in reality, less CO_2 is produced but much more CO.

3.6.4 Gas turbines

Another type of powerplant commonly found on conventional light aircraft is gas turbines. Contrary to piston ICE, gas turbine engines suffer less from the loss of density at high altitude and can be used even at high speed. Most importantly, however, they have higher power densities, making them ideal for high power/high speed installations [58]. This is the reason why it is typically used on commuter and regional aircraft.

The estimation of the performances of gas turbines is extensively covered in literature, and, beyond a modeling through a simple fixed specific fuel consumption (SFC) and power

density [31, 176], it is mostly done using thermodynamic cycles [80, 91, 177]. It is worth noting that while top-down constant SFC methods are convenient to use, their simplicity can hide complex design trends that are paramount to the model, as this is where gains might stem from. Indeed, as gas turbines operate far from their optimal throttle ratio, their SFC increases [178], indicating that gains might be found in downsizing gas turbines for cruise conditions. Methods relying on thermodynamic cycles can be further broken down based on the level of detail taken for the modeling of rotating parts. While fixed efficiencies can be taken for the compressors, turbines, and fans with a decent level of accuracy [91], in practice, they highly depend on the operating conditions. These efficiencies are often computed using maps. A high level of detail concerning the design of rotating parts is, however, necessary to estimate those maps, making them hard to use.

Another approach commonly found is the use of specialized software or frameworks like GasTurb [16, 83, 84] or PyCycle [104]. While this approach enable high level of fidelity and, to a certain degree, the study of future gas turbine performances, it won't be retained because of high computational time and low automatibility.

The choice was made to build an existing one based on the method in the original FAST-OAD-GA framework, as it proved to yield good results on the TBM900 use case [91]. The effect of exhaust thrust was also included in the form of negative drag. Finally, the operational limits of the turboshaft presented in the original model were included as well. They will, however, be slightly reworked to allow for the resizing of the turboshaft according to each constraint. This results in the generic formulas presented in 3.19.

$$FF = f(\sigma, M, P_{req}, P_{des}, TET_{des}, OPR_{des}) \tag{3.19a}$$

$$P_{des,OPR_lim} = g(\sigma, M, P_{req}, TET_{des}, OPR_{des}, OPR_{lim}) \tag{3.19b}$$

$$P_{des,ITT_lim} = h(\sigma, M, P_{req}, TET_{des}, OPR_{des}, ITT_{lim}) \tag{3.19c}$$

$$T_{exhaust} = i(\sigma, M, P_{req}, P_{des}, TET_{des}, OPR_{des}) \tag{3.19d}$$

More information on the surrogates and the input parameters is available in Appendix B.2.

Formulas for the mass and dimensions of the turboshaft were also included. The choice was made to perform a statistical analysis and devise regressions based on data from existing turboshafts. A focus was set on the PT6A family as it is a popular choice for CS-23 category aircraft and the type of engine that is installed on some of the aircraft under study in Chapter 4. Data were found in the engine's Type Certificate DataSheet (TCDS), Pratt & Whitney's website, and in Jane's Aero Engines. It is worth noting that those data already include the mass and dimensions of a power turbine module that brings the rotation speed down to 1700-2000 rpm. The result of this statistical analysis is presented in Figure 3.2.

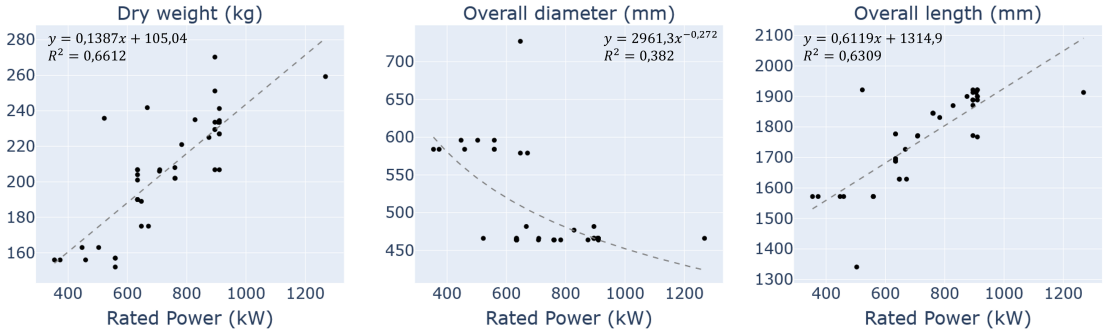

Figure 3.2 Statistical analysis on the characteristics of the PT6A turboshaft family.

Further analysis of the trends in mass, diameter, and length as functions of the rated power reveal very poor coefficient of determination. These results can be partly explained by the rationale behind the development of a new engine in the PT6 family. Indeed, while the regression we made implicitly assumes continuous evolution of the parameter as a function of the power, the reality is different. In practice, turboshaft engines are developed around a modular architecture with a lot of common parts. Power output is then adjusted by changing the number of compressor and turbine stages. Therefore, some characteristics remain constant for different values of rated power, which can be seen in Figure 3.2, where two families of architecture can be identified on the graph of the overall diameter.

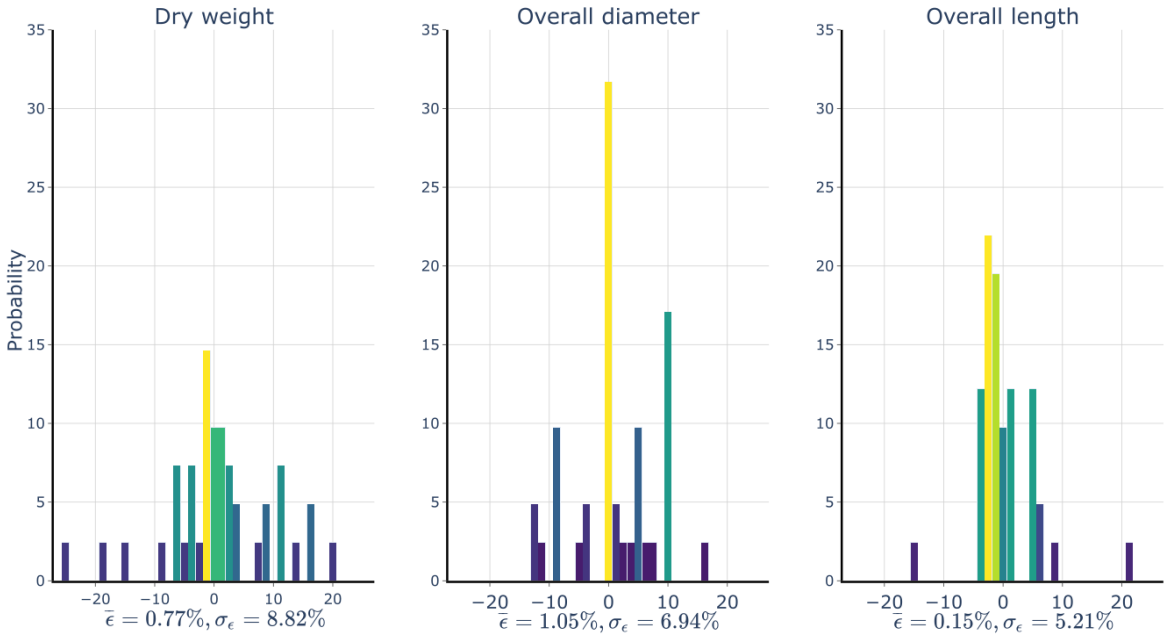

Figure 3.3 Distribution of the relative error between data and the statistical trends implemented in the framework.

The robustness of the results to those uncertainties and to the uncertainties stemming from the regression performed on the fuel consumption estimation method presented in Appendix B.2 will be investigated in Chapter 4. The repartition of the relative error is presented in Figure 3.3. The PT6A-140, with an overall diameter of 727 mm, was removed from the uncertainty distribution in Figure 3.3 because it represents an obvious outlier.

Similarly to piston ICEs, the emissions of gas turbines will be computed. Unlike piston engines, however, literature is much more extensive on the subject because it can reasonably be assumed that the model used to estimate the emissions of larger turbofan engines can be applied for turboprops and turboshafts [179–181]. These methods, which include the P3T3 method [182], the Boeing Fuel Flow Method2 [183], or the DLR method [184], work using the same principle. They are based on a set of reference EI promulgated by the International Civil Aviation Organization (ICAO) as part of its certification definition and emission database, which are then adjusted to take into account the effect of a variation of atmospheric conditions or engine operating parameters. These reference EI, however, are only mandatorily reported for engines with nominal thrusts greater than 26.7kN. While a private database from the FOI (Swedish Defence Research Agency) covering turboprop exists and while methods have been derived for smaller engine [185], the choice was made as a first approximation to use constant emission indices [181]. It is worth noting that, while CO_2 and H_2O are fairly constant throughout the flight, not accounting for engine operating parameters and atmospheric conditions can introduce up to 20% error [181]. The indices found in literature [186, 187] and used for turboshafts are reported in Table 3.2

Table 3.2 Value for the emissions indices considered for the operation of turboshafts.

Species	CO_2	CO	NO_X	SO_X	HC	H_2O
EI (g/kg_{fuel})	3155	5	11.4	0.42	0.05	1237

3.7 Connectors

For connectors, the models originally presented in the load flow analysis [120] were mostly reused but supplemented here with detailed efficiency computations and models for aircraft-level impacts.

3.7.1 Inverters and Rectifiers

Inverters and rectifiers transform DC into AC current and vice versa using a pair of switches located in each arm of the component, of which there are 3, amounting to a total of 6. By controlling the sequencing and the duration for which each of these switches is opened and closed, it becomes possible to replicate a pseudo-sinusoidal voltage. This technique is called Pulse Width Modulation (PWM). As PWM rectifiers and inverters share similar topologies,

the same models will be used for both types of components. Losses in PWM converters are essentially linked with the conduction losses and switching losses occurring in their six arms [125]. The procedure for the computation of inverters and rectifiers' losses is presented in Appendix B.3

Conduction losses, however, depend on characteristics of the Insulated-Gate Bipolar Transistor (IGBT) module, mainly resistance and gate voltage, which depend on the temperature of the component. This effect of the junction temperature on the resistance was implemented as a linear variation, as is commonly done for other electronic components. Following an analysis of the technical datasheet from the manufacturers, the same approach was adopted for the gate voltage, resulting in the formulas presented in 3.20. The coefficients for those variations were computed based on a fit of manufacturers' data [5].

$$R_{d,IGBT} = R_{d,IGBT,ref} \times (1 + \alpha_{R,IGBT} \times (\Theta_{IGBT} - \Theta_{IGBT,ref})) \tag{3.20a}$$

$$R_{d,diode} = R_{d,diode,ref} \times (1 + \alpha_{R,diode} \times (\Theta_{diode} - \Theta_{diode,ref})) \tag{3.20b}$$

$$U_{CE,0} = U_{CE,0,ref} \times (1 + \alpha_{U,IGBT} \times (\Theta_{IGBT} - \Theta_{IGBT,ref})) \tag{3.20c}$$

$$U_{D,0} = U_{D,0,ref} \times (1 + \alpha_{U,diode} \times (\Theta_{diode} - \Theta_{diode,ref})) \tag{3.20d}$$

where $R_{d,IGBT}$ is the on-state resistance of the IGBT module in Ω, $\alpha_{R,IGBT}$ is the IGBT resistance temperature scaling factor, equal to $0.0041\Omega/degK$, $R_{d,D}$ is the on-state resistance of the diode in Ω, $\alpha_{R,diode}$ is the diode resistance temperature scaling factor, equal to $0.0033\Omega/degK$, $V_{CE,0}$ is the gate voltage of the IGBT module in V, $\alpha_{V,IGBT}$: is the IGBT gate voltage temperature scaling factor, equal to $-0.00105V/degK$, $V_{D,0}$ is the gate voltage of the diode in V, $\alpha_{V,diode}$ is the diode gate voltage temperature scaling factor, equal to $-0.0022V/degK$.

The computation of the mass of the converters will be based on the sum of the masses of its individual components: three modules (each with two diodes and two IGBT modules) whose mass is computed based on a regression on manufacturer's data, a heat-sink sized with respect to the amount of heat to dissipate, a capacitor sized to limit the voltage ripple, a control card and contactors with masses computed based on manufacturer's data [125]. The role of the switching frequency as a key technological driver was also implemented.

3.7.2 DC/DC Converters

Among the possible types of DC/DC converters previously described, a buck-boost converter was considered. In the original load flow analysis method [120], converters provide the electric network with a constant voltage. In a real network, this might also be required as components like batteries or fuel cells have a voltage that can vary when power demand

[5] https://www.semikron-danfoss.com/products/product-classes/igbt-modules.html#view/table/items/20/filters/switches=gb/, Accessed: 2025-08-05

changes. Regardless of the topology retained, the computation of the duty cycle has to be considered. The duty cycle corresponds to the ratio of the time the switch is on to the total period of the signal. It directly controls the ratio of the input to the output voltage, but its formula depends on the topology. For this work, the topology represented in Figure 3.4 was chosen. While other topologies like Dual Active Bridge (DAB) converters exist and are better suited for high voltage applications [188], the relative simplicity of the selected architecture allows for explicit expression of the losses and the components' masses. Therefore, the simple architecture was kept in spite of its drawbacks.

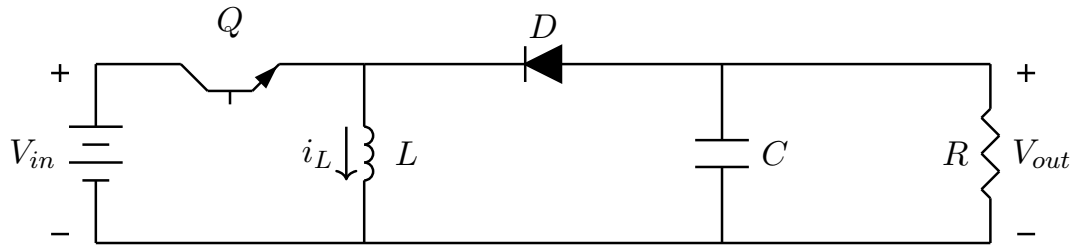

Figure 3.4 Architecture considered for the DC/DC converter, adapted from [189].

On such an architecture, the losses can be computed from the conduction losses in the inductor, in the capacitor, and in the diode, but also the losses in the IGBT modules [84, 189]. These losses depend on the Root Mean Squared (RMS) value of the current in the components, which themselves depend on the duty cycle. It can be computed with:

$$D = \frac{V_{\text{out}}}{V_{\text{out}} + V_{\text{in}}} \tag{3.21}$$

To those conduction losses, the switching losses will be added. They will be computed the same way as for the inverters and rectifiers.

The computation of the converter mass will be done by summing the masses of the diode, the IGBT module, the capacitor, the inductor, the heatsink, and the mass of a control card. The capacitor will be sized to limit the voltage ripple [130]. The inductance will be sized using scaling laws on the core and winding surface. For the other sub-components, the same methodology as the one employed for the sizing of the inverter in Section 3.7.1 will be used.

3.7.3 Cables

In electric architectures, cables are used to transmit the power between loads and sources. To achieve this purpose, the cable is built around an electric core made of, with current technologies, either copper or aluminum [148]. Both copper and aluminum have widely different electrical, mechanical, and thermal properties as shown in Table 3.3.

The sizing of the core is directly linked to the amount of current that will pass through the cables [148]. This is due to the maximum current density allowed in a cable, but it also has a

Table 3.3 Physical properties of the materials considered for the cable core.

	Copper	**Aluminium**
Electrical resistivity ρ_{elec} [Ωm]	1.724 $\times 10^{-8}$	2.65 $\times 10^{-8}$
Density ρ [kg/m^3]	8960	2700
Specific heat cp [$J/kg/degK$]	386	902
Temperature scale factor α [$\Omega/degK$]	0.00393	0.00431

link to thermal constraints. For these reasons, the National Electrical Code (NEC) released guidelines linking the maximum ampacity of a cable and its gauge in the form of a table. Similarly to what has already been done in literature [148], a regression based on this table has been created.

The issue of partial discharge is also a key point in the design of high-power transmission cable [50, 148, 190]. The consideration of those phenomena is crucial because, to lower losses proportional to current, higher voltages are sought. However, higher voltage means that more insulation is going to be required, meaning the cables will be heavier [50]. There is thus a trade-off to be made at aircraft level. The sizing of the insulation thickness will be made using a methodology developed to compute the insulation thickness required for a given voltage and core radius of a cable [50].

Two additional layers to the cable will be considered. First, a layer of copper tape will be added after the insulation, as a shield to the electromagnetic interference of the other cables. The thickness of this tape will be considered constant, and as for its value, it will be taken at 0.2 mm according to manufacturers' data [6]. The final layer we will consider is an external sheath that is there to provide protection against mechanical damage. To determine its thickness, a correlation based on the diameter of the unsheathed cable will be used [148]. For the choice of properties, it will be assumed to be made of high-density polyethylene. The final representation of the cable is given in Figure 3.5.

Having sized the radius of each layer, it becomes possible to compute the length-specific properties of the cable, such as the density, the resistance, and the heat capacity, using Equations 3.22

$$\mathcal{R} = \frac{\rho_{elec}}{A_{core}} \tag{3.22a}$$

$$m = A_{core}\rho_{core} + A_{ins}\rho_{ins} + A_{tape}\rho_{tape} + A_{sheath}\rho_{sheath} \tag{3.22b}$$

$$\mathcal{C} = A_{core}\rho_{core}cp_{core} + A_{ins}\rho_{ins}cp_{ins} + A_{tape}\rho_{tape}cp_{tape} + A_{sheath}\rho_{sheath}cp_{sheath} \tag{3.22c}$$

where $\mathcal{R}$ is the length specific resistance in Ω/m, ρ_{elec} is the core material resistivity in Ωm, A's are the cross sections in m^2, m is the length specific mass in kg/m, ρ are the densities,

[6] https://na.prysmian.com/sites/na.prysmian.com/files/media/documents/UTY-0018-R1116_Electric%20Utility%20Catalog_CANADA.pdf, Accessed 2025-08-06

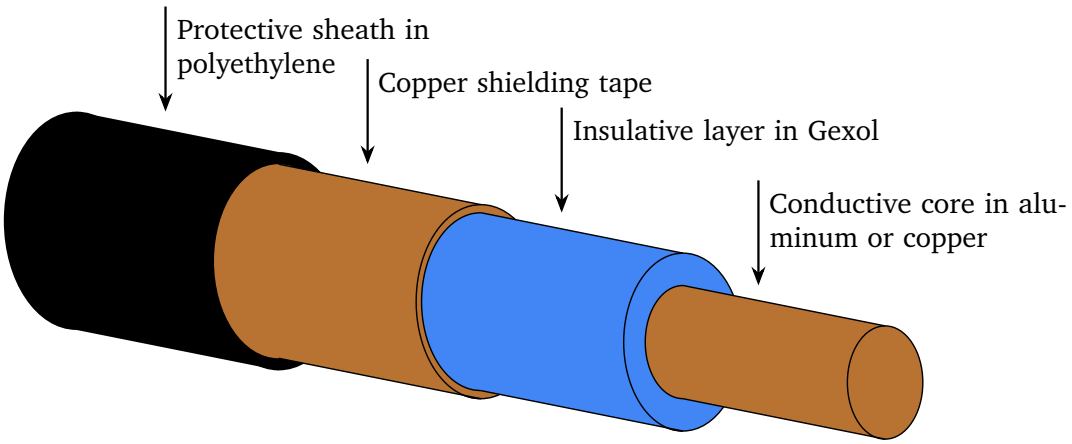

Figure 3.5 Schematized drawing of the cable.

$\mathcal{C}$ is the length specific heat capacity in J/°K/m and cp are the specific heats in J/°K/kg. We will also assume that, at both ends of the cable, there are contactors whose mass will be computed based on a regression made on available data [125].

Similarly to semiconductors, the resistance of the cable will be assumed to linearly depend on its temperature [50], which itself is a consequence of the losses in the cable.

3.7.4 Buses and Splitters

The role of the electric buses will be to combine loads from multiple sources. The splitters, on the other hand, will be used to hybridize multiple sources. It is worth noting that this component has no physical meaning; it is used here to simplify the representation of the converter's command law, which dictates how power is shared among multiple sources. In the original implementation of the load flow analysis method [120], the bus voltage is an implicit variable. Implicit variables are those that are computed as an implicit function of other variables. In OpenMDAO, those variables are handled by defining a residual $\mathcal{R}$ equation for the variable, which the solver will then attempt to drive towards zero. In the original method, the residual equation for the bus voltage is the sum of the current going in and out of the bus. As those currents are functions of the difference in voltage between the bus and connected component, they are implicitly linked with the bus voltage. Therefore, when the residuals are driven to zero with the help of the solver, Kirchhoff's law will be respected. A similar approach was used for the splitters, except that the residuals in the original *ImplicitComponent* were changed to force $\mathbb{S}$% (the split percentage) of the output current to go in the primary input and the rest to go in the secondary input resulting in Equations 3.23.

$$\mathcal{R}(V_{out}) = (V_{in,1} + V_{in,2}) - 2 \times V_{out} \tag{3.23a}$$

$$\mathcal{R}(V_{in,1}) = 100 \times I_{in,1} - \mathbb{S} \times I_{out} \tag{3.23b}$$

$$\mathcal{R}(V_{in,2}) = I_{in,1} + I_{in,2} - I_{out} \tag{3.23c}$$

In addition to specifying $\mathbb{S}$ as a percentage, it is also possible to fix a threshold power P_{th} such that: if the output power is smaller than the threshold value everything goes in the primary input, if it is greater, P_{th} power goes in the primary input and the rest goes in the secondary one. This will allow to assess powertrains where a fixed-power fuel-burning engine is complemented, in power-intensive phases, with batteries. Both operating principles are illustrated in Figures 3.6 and 3.7.

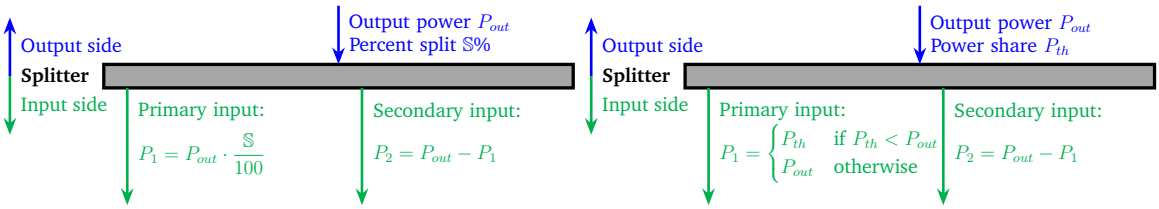

(a) In percent split mode.

(b) In power share mode.

Figure 3.6 Operating principle of the splitter.

The buses and splitters' mass and properties will be computed under the assumption that a laminated bus bar technology is considered. Laminated bus bars are made of electric cores sandwiching a layer of dielectric material for insulation. Furthermore, the issue of partial discharge in the bus bar seems to be a considerable challenge in the sizing of the insulation [191, 192]. The computation of the core cross-section area will be made according to a consideration on the maximum current that will flow through the bus [193]. The thickness of the insulation will be computed based on the adaptation to the bus bar of the methodology used for the sizing of a cable insulation according to partial discharges considerations [50].

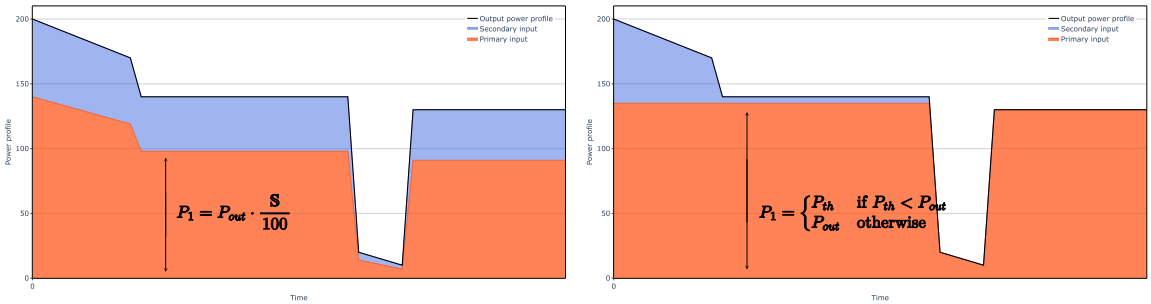

(a) In percent split mode.

(b) In power share mode.

Figure 3.7 Influence of the operating principle of the splitter on the power repartition.

3.7.5 Circuit breakers

Circuit breakers are used to identify and isolate faulty components to protect the rest of the network. Multiple technologies exist: mechanical circuit breakers, Solid State Power Controller (SSPC), or hybrid breakers. While mechanical breakers have lower on-state losses, SSPCs were preferred because of fast breaking time and prevent the formation of an electric arc when the switch is open [194]. A typical SSPC is made up of a Solid State Switching Device (SSSD) responsible for the "on"/"off" switching of the SSPC and a control center [195]. Based on this observation, we will assume that all losses happen in the SSSD, which is comprised of two IGBT modules [195].

The efficiency of the SSPC will be computed, in this work, based on the on-state losses of a diode and of an IGBT module for which the formula is available in literature [125]. However, it will be assumed to be constant and equal to its worst-case scenario. For the computation of the mass of the SSPC module, and because they account for so little compared to the rest of the component, a simple power density will be considered [196]. The "off" state of the SSPC was also implemented to allow for a reconfiguration of the powertrain and the creation of secondary power paths, should a component fail. In addition to sizing secondary branches, this will enable the opportunity to oversize the component for failure cases. The "off" state of the SSPC is simulated as an enforcement of a nil current at the output of the SSPC.

3.7.6 Gearboxes

Models for two functioning modes of gearboxes were implemented. The first type, speed reducers, serves as a way to reduce shaft rotation speed. This allows, for instance, to connect propellers that typically have a rotation speed of around 2000-3000 rpm to electric motors that benefit from running at a higher rotation speed [143]. The other type will serve as a way to sum the power of two shafts, as can be seen on some parallel hybrid powertrains, like the one on the H3PS project [7].

Both modes will, however, be based on the planetary gearbox architecture as it can be used in both cases [143, 197]. For the estimation of the performances, a constant efficiency of 0.98, representative of current technologies, will be assumed [43, 143]. This value of efficiency is coherent for single-stage gearboxes, which, given the low gear ratios needed (less than 10), will be the case for most of the propulsive architectures that will be considered. To estimate the dimensions of the gearboxes, scaling laws will be used [128]. The choice for the reference component will be a range of existing inline planetary speed reducers [8]. Even though the specifications of that range of gearbox are on the lower end of the power range for hybrid aircraft, the availability of technical data motivated that choice.

[7] https://h3ps.eu/, Accessed 2025-08-07
[8] https://www.ato.com/inline-planetary-speed-reducer-gearbox

After a review of other models available in literature [198], the choice was made to compute the mass of the gearboxes using an estimation method developed at NASA based on a survey of existing gearboxes [199]. In addition to a dependency on the gear ratio and output torque, this method also uses a technology factor to scale results. Judging from the results displayed in the original paper and from the application of that method on the selected reference gearbox, that factor highly depends on the power output and technology of the gearbox. From the results presented in the original paper, the value of that technological factor was estimated at 6.16, which will serve as the default value for the implementation.

3.7.7 Tanks and fuel system

For the modeling of the tanks and their impact on the aircraft mass, a simplified approach consisting in assuming that it does not add mass was taken. Unusable fuel, however, is accounted for using a ratio from a conventional aircraft design book [60] and bookkept in the tank mass. The mass of the rest of the fuel system is computed using a classical handbook method based on the volume of connected tanks [58]. Although tanks, by our assumptions, don't have a significant direct contribution to the OWE, the fuel inside them plays a role as a relief force for the wing sizing. Automatic interfacing with the physics-based methodology used in the original OAD framework [32] was implemented to account for that effect. Additionally, the aircraft CG and trim drag will vary to account for fuel consumption during the mission [91].

3.8 Summary

A summary of the models and modeling techniques introduced in this chapter is proposed in Table 3.4. The following code is used to indicate which approach has been retained for each model: (SL) for scaling laws, (R) for manufacturers' data regressions, (SU) for high fidelity surrogate models, and (P) for physical models. In a similar fashion to what is done in literature, scaling laws were favored for electromechanical components. Indeed, such components have many uses beyond the aeronautical sector, which makes them well-documented, with vast amounts of data available, enabling the verification of scaling laws, which, by nature, are differentiable. For components found on conventional architecture, although little data exists on actual fuel consumption, literature is also extensive with numerous modeling approaches available. To ensure analytical differentiation was available but also to prevent runtime prohibitive for preliminary design, surrogate models and regression were employed.

3.9 Conclusion and perspectives

Chapter summary

Following the description of the framework introduced in Chapter 2 and more specifically, the

Table 3.4 Summary of the models implemented.

Component type	**Component**	**Performances (Simulation models)**	**Sizing (Estimation models)**	**Slipstream (Simulation models)**	**Constraints (Eval. models)**
Propulsor	Propeller	Surrogate for C_P as a function of other dimensionless parameters built based on BEMT and ADT (SU)	Mass based on a regression on existing propeller (R), no added profile drag, CG based on location and geometrical considerations, considered a punctual load when on the wing.	Addition of increments to clean aerodynamics (P), affects C_l, C_d [34, 64, 79] and C_m [137]	Torque
Load	E-Motor	Main loss sources are computed using torque and rpm (R), using the torque constant to get voltage and current	Dimensions, mass, and physical properties from scaling laws (SL) [143] and regressions (R). Profile drag from nacelle considered, CG based on location and geometrical considerations, considered a punctual load when on the wing	NA	Torque, RPM
Source	Battery	Equivalent circuit model (R) [18], OCV as a function of SOC (R) [155], R_{int} as a function of SOC and temperature (R) [156, 157], relative capacity (R) [86]	Mass computed from cell arrangement, reference cell, and packaging efficiency [18] (R), CG, and volume based on location and geometrical considerations, profile drag from underbelly or pod when applicable, considered a punctual or a distributed load when on the wing, and depending on location	NA	State of charge, C-rate
Source	Piston ICE	Scaled consumption map (SL) [91] as a polynomial function (R)[200], power decrease with density (R)[58]	Mass from handbook method [58] (R), CG and volume based on location and geometrical considerations, profile drag from nacelle, considered a punctual load when on the wing	NA	Sea-level power
Source	Generator	Same as E-motor	Same as E-motor	NA	Torque, RPM
Source	Turboshaft	Surrogate for FF as a function of design parameters and flight conditions based on thermodynamic cycles [91]	Mass from regression on manufacturer's data (R), CG and volume based on location and geometrical considerations, profile drag from nacelle, considered a punctual load when on the wing	Residual thrust from hot air exhaust as a negative drag coefficient (SU, P)	Rated power + power due to engine limitations
Tank	Fuel tanks	CG shift as fuel is used	No mass considered only unusable fuel (R), volume and dimensions based on capacity and geometrical considerations, profile drag when podded, considered a punctual or a distributed load when on the wing, and depending on location	NA	Volume

Table 3.4 continued: Summary of the models implemented

Component type	Component	Performances (Simulation models)	Sizing (Estimation models)	Slipstream (Simulation models)	Constraints (Eval. models)
Connector	Inverter	Switching losses and conduction losses (P) [125], impact of temperature and thermal network (P)[201]	Properties and resistance based on scaling laws (SL) [202], weight based on sizing of individual components [125] (R), no profile drag, CG based on geometrical considerations, punctual load	NA	Current, voltage, frequency, losses
Connector	Rectifier	Same as Inverter	Same as Inverter	NA	Current, voltage, frequency, losses
Connector	DC/DC converter	Conduction losses in each components [189], switching losses (P) [125]	Properties and resistance based on scaling laws (SL) [202], mass based on sizing of individual components [125] (R), no profile drag, CG based on geometrical considerations, punctual load	NA	Currents, voltages, frequency, losses
Connector	Cable	Conduction losses (P), influence of temperature and thermal behavior [50]	Each layer of the cable is sized independently, length-specific properties computed (P)[50], no profile drag, CG based on geometrical considerations, punctual loads	NA	Current
Connector	Circuit breaker	Constant efficiency based on conduction losses (SL) in the worst case scenario [195]	kW/kg method for mass [196] (R), resistance with scaling law (SL), no profile drag, CG based on geometrical considerations, punctual loads	NA	Current, voltage
Connector	Buses/ Splitters	Original methodology for buses [120], power splitting based on percentage or threshold value for splitters	Weight based on core [193] and insulation [50] thickness (P), no profile drag, CG based on geometrical considerations, punctual loads	NA	Current, voltage
Connector	Fuel Systems	Fuel splitting based on percentage	Weight from handbook method (R) [58] no profile drag, CG based on geometrical considerations, punctual loads	NA	NA
Connector	Gearboxes	Fixed efficiency and speed ratio	Scaling laws based on planetary gearboxes for dimensions (SL) [128], regression for mass (R) [199]	NA	NA

formalism it proposes for the generic description of physical components models, this chapter presents the models adopted to allow for the sizing and the estimation of the performances of hybrid and all-electric configurations. As the choice was made to integrate the presented methodology in a wider framework, the choice was made to put particular emphasis on the propulsive architecture and its impacts at aircraft level, as the sizing of the aircraft is handled by the FAST-OAD ecosystem. For each component, a literature review was conducted to identify what models were most suitable, considering the need for medium fidelity and analytically differentiable models. This need, which led to considerable additional effort upstream of solving the design process, stemmed from the observation that top-down efficiencies couldn't capture some of the most beneficial interactions enabled by electric propulsion, but also because this type of model has been proven to misguide the optimizer [178]. As a result, and to benefit from the engineering knowledge gained from other sectors, a mix of higher fidelity modeling techniques was employed, ranging from scaling laws to physics-informed surrogates.

Perspectives

Regarding the models adopted for the physical components of the powertrain, further work could be done on the formulation of the model to improve robustness and improve convergence. In particular, in the OpenMDAO framework, upon which the FAST-OAD software is built, convergence is guided by the diminution of residuals. Those residuals are computed as the norm of the output vector at each step of the solver without transformation of the values. More specifically, it implies that values with vastly different orders of magnitude are considered to have equal masses in the computation of the residuals. The previous chapter highlighted, as a perspective, that the framework formalism did not implement but allowed for the co-design of the thermal management system along with the design of the propulsive architecture. In addition to that, the thermal behavior of the components of the powertrain should also be implemented. While the residuals-driven approach proposed by this framework and the load flow analysis method enabled this characterization on some select components as part of a separate work, this behavior is not implemented for all the components. In addition to affecting its efficiency, accurate estimation of the components' temperature is paramount as it affects the components' lifespan, which, in turn, will affect its environmental footprint, as will be discussed in Chapter 5. Finally, it is worth pointing out that, to enable analytical differentiation of the models, surrogate models of higher fidelity methods were frequently used. Surrogates, however, introduce model or epistemic uncertainties that can influence confidence in the final results of the sizing process. These uncertainties will be addressed in the next chapter for a specific case. However, further work is warranted to reduce these uncertainties and quantify their impact on the results.

The validity of the approach presented in Chapter 2 and the models presented in this chapter will be evaluated on a variety of validation cases, both electric and thermal, and on some prospective electrification scenarios in Chapter 4.

Part II

Emission optimized hybrid- and full-electric alternatives for General Aviation aircraft

Abstract

The second part of this manuscript addresses the study, at aircraft level, of the potential, in terms of reduction of CO_2 emissions, of the electrification of the propulsion chain in General Aviation aircraft. Chapter 4, in particular, addresses the preliminary sizing of electrified versions of existing aircraft to assess possible gains in terms of harmful pollutant emissions. The effect of the model uncertainties presented in Chapter 3 will also be investigated in this part.

Author's contribution

Conference paper

Lutz, Florent, et al. "Study of hybridisation scenarios for turboprop aircraft in the general aviation segment." 34th Congress of the International Council of the Aeronautical Sciences, Florence, Italy. 2024.

Chapter 4

Electrification scenarios for CS-23 certification category aircraft

Contents

4.1 Introduction **77**
4.2 Selection of electrification scheme for the propulsive architecture **79**
4.2.1 Aircraft use phase emissions estimation 79
4.2.2 Limitations of electric components technology maturity 80
4.2.3 Pre-selection of electrification scenario for the different applications 82
4.3 Level 1 aircraft **85**
4.3.1 Velis Electro 85
4.3.2 Comparison with the Pipistrel SW 121 88
4.4 Level 2 aircraft **90**
4.4.1 Electric version 92
4.4.2 Hybrid version 96
4.5 Level 3 aircraft **104**
4.5.1 Selection of the reference aircraft 104
4.5.2 Hybrid TBM 900 107
4.5.3 Hybrid DAHER Kodiak 115
4.6 Level 4 aircraft **119**
4.6.1 Identification of representative aircraft 119
4.6.2 Hybrid Cessna 208B 122
4.7 Conclusion and perspectives **125**

4.1 Introduction

WITH the retained methodology and framework presented in Chapter 2 and the component models presented in Chapter 3, it is now possible to study the design and

performances of hybrid and full-electric aircraft and to assess the potential of such configurations. The introductory chapters showed that, although electric aircraft have the potential for zero in-flight emissions, they have severe drawbacks, including very high mass penalties and associated range reductions. It was also demonstrated that, although hybridization still relies on a thermal machine, thus limiting the potential for reducing emissions, it can be a feasible option with smaller penalties than a fully electric configuration, while still leveraging the other benefits of electrified propulsion. It is worth noting that aircraft in the General Aviation segment can be used for a wide variety of purposes, including private and recreational flying, pilot training, agricultural crop dusting, surveying, passenger transport, and air ambulance services. Therefore, it is clear that the most suitable electrification scheme will vary greatly depending on the aircraft's requirements.

Another question left hanging is the one of the comparison basis for comparing conventional designs with electrified ones. Indeed, when new designs are introduced, they are often marketed in terms of range, fuel efficiency, or weight — as illustrated in Figure 4.1 — metrics for which electric and hybrid electric aircraft will systematically perform worse. These metrics, however, are but proxies, historically used on conventional configuration [35], for other quantities such as emissions, total energy use, operating costs, safety, and reliability, in which these new configurations could be advantageous [13].

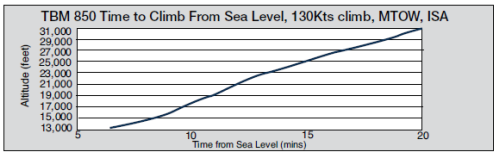

Fuel Efficiency

The TBM 850 offers both better fuel consumption and performance than typical turboprops, as well as substantially better fuel consumption and equivalent performance to typical light jets.

	PC-12	C90GT	Mustang	TBM 850
Max Cruise (Fastest speed)	267	270	342	320
Fuel Efficiency (nm per lb of fuel)	0,54	0,44	0,41	**0,72**
Conditions	8,000 lb, ISA, 16,000 ft	ISA, 20,000 ft	8,000 lb, ISA, 25,000 ft	6,300 lb, ISA, 26,000 ft

NBAA IFR Reserves (100 nm), ISA, Zero Wind, Max Cruise, Single Pilot + 3 pax				
Trip Distance (nm)	Flight Time (hr : mn)	Block Fuel (gal)	Cruise Alt (ft)	Reserve Fuel (gal)
200	0 : 44	54	16,000	50
400	1 : 26	83	26,000	50
600	2 : 04	118	31,000	50
800	2 : 43	154	31,000	50
1,000	3 : 20	189	31,000	50
1,250	4 : 07	241	31,000	50

Range

The TBM 850 provides greater range and load carrying performance than the capabilities of typical light jets particularly allowing for the likely limited availability of flight levels above FL310 across most of the continental US and Western Europe to light jets that depend on access to these "higher" flight levels to obtain their quoted cruise range performance.

NBAA Reserve Max Cruise IFR Range with 4 Adults on Board - 1,290 nm

NBAA Reserve Long Range Cruise with 4 Adults on Board - 1,466 nm

Figure 4.1 Excerpt from a marketing brochure from the TBM850.

The aim of this chapter is twofold. First, it will set out to validate the presented methodology and models through several validation cases known in literature or for which data are available online. For this purpose, the case of Pipistrel Velis Electro, among others, will be studied. Multiple conventional configurations will also be investigated for that purpose but also to provide baselines for prospective studies, which is the second *raison d'être* of this chapter. It aims to provide realistic electrification scenarios for light aircraft certified under EASA CS-23. An initial metric for comparing the electrification of propulsion systems will be presented, as well as avenues for reflection to help narrow down the design space. A

classification of General Aviation aircraft will then be discussed and will be used to select significant examples for studying the electrification of the propulsive architecture. Unless specified otherwise, data for the validation studies will be taken from the TCDS and POHs of the aircraft or from *Jane's All The World's Aircraft*. This chapter will also set out to prove that the level of fidelity retained for the component models presented in Chapter 3 can accurately capture new design opportunities offered by the electrification of the propulsive architecture that classical top-down methods cannot.

4.2 Selection of electrification scheme for the propulsive architecture

4.2.1 Aircraft use phase emissions estimation

Multiple metrics have been proposed in literature to assess the gain brought by the electrification of propulsive systems in aircraft and switch the paradigm from fuel burning engine to alternative energy sources. Cost estimation, for instance, has been proposed as a way to reconcile the expected increase in aircraft construction costs with reduced energy costs and expected carbon taxes [62, 138, 203, 204]. Literature also suggests the investigation of the use of the Thrust Specific Power Consumption (TSPC) as a way to measure powertrain efficiency regardless of the power source. Similarly, the Energy Specific Air Range (ESAR) could be used as an extension of the Specific Air Range (SAR), which has the merit of also including aircraft-level impacts [205]. Finally, the impacts on climate change from the use and the production of the energy required for the flight are also commonly used to compare designs [177, 178, 206, 207]. Because of the urgent nature of the need to reduce the impact of aviation on the environment, however, the latter will be of particular interest as a starting point in this work. Nonetheless, a more detailed analysis of the life cycle of electrified design is required [208] and will be assessed in Chapter 5.

Furthermore, as part of this study, only the GHG emissions will be evaluated, even though these emissions represent only one of the contributors to the impact of aviation on global warming. When considering the GHG emissions of an energy carrier on aircraft, the scope must go beyond simply its use by the aircraft, often called the Tank-To-Wake (TTW) pathway [177]. Indeed, a significant part of the emissions occurs upstream of the life cycle [209], in the extraction and production phase, also called the Well-To-Tank pathway (WTT). Both can be combined in the Well-To-Wake (WTW) pathway, which represents all the steps from the extraction of the energy to its use. Values for the impacts of the retained energy carrier on climate change have been accurately calculated [210] for the WTW pathway and will be used to compare the retained designs. A common way to evaluate the impact of GHG is to use the warming potential of CO_2 as a reference value for other gases such as CH_4 or N_2O. It is worth

noting that since the WTW includes the production of the energy, there can be significant variation in the impacts because of sensitivity to the region of production.

For the CO_2 impact of conventional jet fuel or Jet A-1, and because the process is well developed, there is only a slight variation on the values reported for the whole life cycle of the fuel, with values ranging from 81.1 to 94.8 $gCO_{2,eq}$/MJ. Rather than doing a study for both values of the carbon intensity of jet fuel, we will use an average of 88.7 $gCO_{2,eq}$/MJ [209]. For the carbon intensity of AvGas 100LL, one of the most common types of aviation gasoline, literature is sparser. Based on available data [211], assuming an energy density of 43.7 MJ/kg and depending on the emission index for the CO_2 (see Section 3.6.3), the carbon intensity of AvGas was computed at a value between 82.37 and 107.55 $gCO_{2,eq}$/MJ. Because detailed analysis of the impacts of the emissions of each type of fuel will ensue in Chapter 5, and for simplicity, the same value as Jet A-1 will be used. For electricity, the dependency of the carbon intensity on the method of production is even more pronounced. Values can vary between 5.7 $gCO_{2,eq}$/MJ for countries with high shares of renewable energy to 427 $gCO_{2,eq}$/MJ for countries that mainly rely on coal for energy production [212]. These values also rely on the time frame considered. Indeed, electricity mixes are predicted to change in the coming years, with a peak in fossil fuel usage before 2030 [213]. For this study, and with the goal of having a rapid EIS in mind, we will only look at today's value for the emission factor, rather than using prospective values corresponding to future years. We will consider the value for Europe, where the carbon intensity of the average electric mix is equal to 72.7 $gCO_{2,eq}$/MJ, and for France, where it is equal to 29.6 $gCO_{2,eq}$/MJ [209]. The final value retained for each energy carrier is presented in Table 4.1.

Table 4.1 Carbon intensity of all considered energy carriers.

	AvGas	**Jet A1**	**Elec. (Europe)**	**Elec. (France)**
Carbon intensity ($gCO_{2,eq}$/MJ)	88.7	88.7	72.7	29.6

4.2.2 Limitations of electric components technology maturity

As previously stated, battery energy density has been identified as a major bottleneck for the widespread use of electric aircraft [44]. Other more optimistic papers judge that a threefold increase in battery energy density, from 250 Wh/kg with current technologies to 800 Wh/kg, will still be required to power commercial aircraft on short-haul missions, even when taking into account the increased efficiencies of the powertrain [6]. Additionally, the maturity of power electronics and electric drives further prevents their use on high-power applications. Indeed, while prototypes have been shown to reach 2-3 MW of power [214], readily available electric motor remains in the hundreds of kW [215]. The first certified electric drive for CS-23 aircraft, Safran's ENGINeUS100 series, is rated at 114kW with a power density of 2.2 kW/kg. Similarly, while it was proven possible to fly a Cessna Grand Caravan purely on

electric power using a Magni500 engine, with a rated power of 560 kW, the power density didn't exceed 2.5 kW/kg. These values remain out of the bounds of what would be required for a full electric powertrain on commuter aircraft [216]. While such motors could be used to power aircraft with fewer than 10 passengers, their use on larger commuter aircraft remains unfeasible [217]. New prototypes, however, offer interesting prospects for use up until the regional market, with densities reaching between 5 kW/kg for the Siemens SP260D to 15.1 kW/kg as proposed in the HASTECS project with 2035 technologies [53]. Likewise, while current power electronics have power densities of a few kW/kg [164], prototypes using new semiconductor technologies have shown to increase that value to 50 kW/kg [218].

For smaller aircraft, however, electrified powertrains seem to be possible with current technologies. Literature shows that many manned electric aircraft are flyable, although their range and endurance are often very limited [51, 219]. In addition to that, General Aviation aircraft, as mentioned earlier, are used on a variety of missions, some with very short ranges and flight times. Consequently, gains on small GA aircraft and UAVs seem to be rather promising, even considering today's technological readiness levels [56]. This makes all the more sense knowing that the predicted range of viability of all-electric aircraft is likely to be around 50-200 miles [57], which is particularly well suited for leisure and trainer aircraft. It could also make sense for commuter aircraft, knowing that some airlines like Cape Air report that most of their flight have a range below 200 miles as shown in Figure 4.2. It is worth noting that in Figure 4.2, the acronym EAS refers to Essential Air Services and not Equivalent AirSpeed.

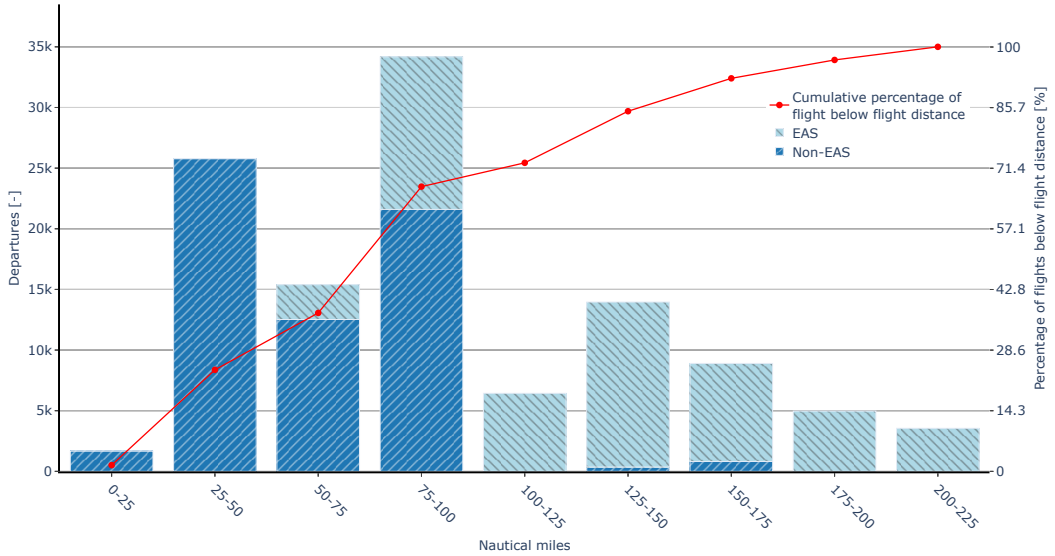

Figure 4.2 Cape Air commuter flight distribution as a function of distance, adapted from Cape Air's *Commuter Airline Perspective*, Accessed: 2025-08-13

.

Overall, it can be concluded that, while full electrification is likely to be feasible in the short term for short-range and low-passenger applications, it will require more mature electric technologies for longer ranges or applications requiring greater power. For such applications, hybrid powertrains may be more beneficial in order to mitigate the increased weight and associated increased energy use associated with all-electric flights. It is therefore proposed that multiple electrification scenarios for General Aviation aircraft be studied. While it would have been possible to classify aircraft based on their range or most common usage, this study will use, as a base, the aeroplane certification levels proposed by CS-23 [220].

4.2.3 Pre-selection of electrification scenario for the different applications

The EASA Certification Specification for Normal-Category Aeroplanes (or CS-23) defines four aeroplane certification levels based on the number of seats in the maximum passenger seating configuration of an aircraft:

- The Level 1 category encompasses aircraft with one or no passenger in addition to the pilot. This definition would include aircraft like the Pipistrel Velis Electro, the Issoire APM 20 Lionceau, or the Diamond DA20, which are mostly used as trainer aircraft.

- Then, Level 2 aircraft can accommodate between two and six passengers, which would include aircraft like the Cirrus SR22, the Cessna 172, or the Robin DR400, and while these aircraft are also used for training, they can also be used for leisure.

- Following this are the Level 3 aircraft with a seating configuration of between seven and nine passengers. This includes aircraft like the DAHER Kodiak (formerly known as the Quest Kodiak) or the Pilatus PC12, which can be utilized for small commuting routes or air ambulance services.

- Finally, the Level 4 aircraft category includes the biggest aircraft covered by the CS-23 category with up to 19 passenger seats. These aircraft, like the Cessna 208 Caravan or the DHC-6 Twin Otter, are typically used to transport passengers from local airfields to bigger hubs.

Using Breguet's range equation in its electric form, presented in Equation 4.1 [23], it is possible to get a preliminary estimate of the maximum range an electric aircraft could achieve in each level. It writes:

$$R = E^*_{\text{elec}} \times \eta_{\text{elec}} \times \frac{1}{g} \times \frac{L}{D} \times \frac{m_{\text{battery}}}{m_{\text{tot}}} \tag{4.1}$$

where E^*_{elec} is the battery energy density in Wh/kg, η_{elec} is the efficiency of the electric powertrain, $\frac{L}{D}$ is the lift-to-drag ratio, $m_{battery}$ is the battery mass in kg and m_{tot} is the aircraft total mass in kg. As a metric to assess the feasibility of a design, literature proposes the use of the derivative of the aircraft mass with respect to its design range [23]. By setting a

maximum acceptable value for that derivative, it is possible to find the maximum theoretical design range. Another acceptable criterion could be setting an upper limit on the aircraft Maximum TakeOff Mass (MTOM). While this maximum range depends on parameters such as the aerodynamics of the aircraft and the efficiency of the power train, it is also highly dependent on the design payload, even more so than with conventional aircraft. Since certification levels are defined based on seating capabilities, design payload tends to increase with level, leading to reduced achievable ranges. Figure 4.3 shows a quantitative assessment of the range sensitivity of an all-electric aircraft at each level. This was drawn under the assumption of a lift-to-drag ratio of 15, a battery energy density of 250 Wh/kg at pack level, and a powertrain efficiency of 0.73. The upper mass limit prescribed in an earlier iteration of the CS-23 has also been plotted to provide a criterion for judging the maximum achievable range. It is worth noting that, when using these criteria, the estimated range for level 1 aircraft exceeds 250 nm, but they would achieve this with an MTOM far above anything seen in this category [219], leading to an unlikely design.

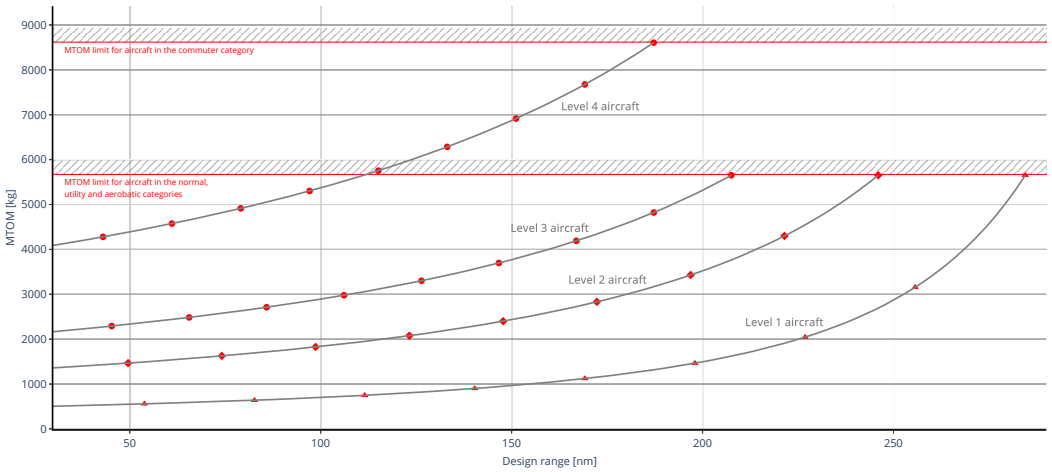

Figure 4.3 Evolution of MTOM with respect to design range for different CS-23 level electric aircraft.

While it seems possible to attain a feasible all-electric design at each level, for the higher levels, they would likely not be competitive compared to their thermal counterparts due to higher masses and, consequently, higher energy use, even at low ranges. This suggests that all-electric designs could be used for smaller aircraft, whereas a hybrid configuration would be preferable for bigger ones. To confirm this, a literature review of proposed configurations [44, 65, 77, 79, 82, 211, 219, 221–226] as well as of manned flying concepts [51, 219] has been undertaken to identify the configuration that seems to be favored for each certification level. The results presented in Figure 4.4 clearly confirm the interest in all-electric concepts for lower-level aircraft, as well as corroborating the infeasibility of all-electric concepts for aircraft with a higher payload. Additionally, while the small statistical sample does not allow

clear conclusions to be drawn with respect to levels 2 and 3, it appears that hybrid concepts are favored at level 4, as predicted.

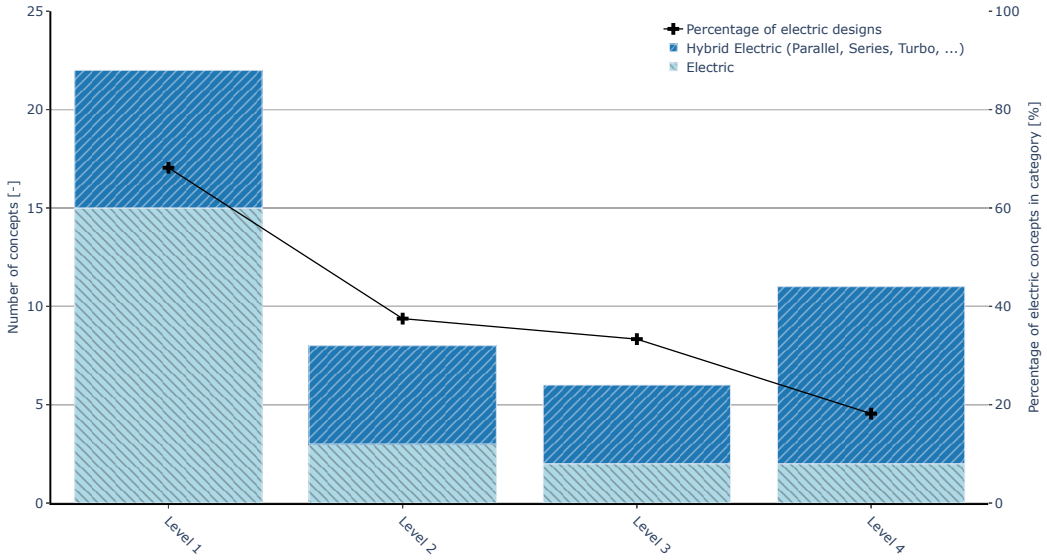

Figure 4.4 Classification of concepts identified in the literature review based on the powertrain type.

Based on the results of this literature review and the preliminary analysis of mass sensitivity with respect to the design range of each aircraft category, this work will focus on studying the full electrification of propulsion systems for aircraft in levels 1 and 2. Hybrid configurations will be evaluated on level 3 and 4 aircraft, as well as on level 2 aircraft, as this seems to strike an interesting tipping point between all-electric and hybrid concepts. For all levels, a preliminary study will be conducted to select a representative aircraft that can be used for comparison purposes and as a validation case. Furthermore, since performance reductions are to be expected for electrified concepts, the usage of the selected representative aircraft will be investigated in order to determine an appropriate design range for the all-electric or hybrid variant. The only exception to this will be level 1, where the Pipistrel Virus SW121 and the Pipistrel Virus SW128 — which we will refer to from now on using its trade name "Pipistrel Velis Electro" — will be selected. The reason for that choice is that, while strictly speaking they are certified under the Light Sport Aeroplanes category, with special conditions for the electric power plant, they have similar performances as Level 1 aircraft, and their performances and specifications are available, which is also why they will be used as a validation case.

Particular emphasis is placed in this manuscript on the effects of aircraft electrification. Accordingly, although the reference conventional configurations for all levels are still evaluated to provide a basis for comparison, only the corresponding results are presented here. A

detailed description of the sizing methodology and the results for conventional configurations is provided in Appendix C.

4.3 Level 1 aircraft

Selection of the reference aircraft

As mentioned earlier, for Level 1 aircraft, rather than selecting a representative aircraft from the certification level and studying potential scenarios for the electrification of the propulsion chain, two existing aircraft — one conventional and one electric — will be studied as validation cases. These aircraft — the Pipistrel Virus SW 121 and the Pipistrel Velis Electro — were selected because they utilize the same airframe, providing the perfect platform on which to study the retrofitting of conventional aircraft with an all-electric powertrain. Additionally, as the Pipistrel Velis Electro is a certified aircraft, the POH [1] contains a great deal of information, such as the details of its performances during the flight, its limitations, and a full description of its powertrain. For this validation study, however, the Velis Electro will not be treated as a retrofit but as if the design was made from scratch.



(a) Pipistrel Virus SW 121. (b) Pipistrel Velis Electro.

Figure 4.5 Pipistrel aircraft under consideration. Source: Pipistrel.

As previously mentioned, only the methodology for the electrified design will be discussed in the main part of this manuscript. For the reference designs, however, details are available in the Appendix. In particular, for the Virus SW 121, the results are presented in Appendix C.1.

4.3.1 Velis Electro

The Pipistrel Velis Electro, although it shares geometric features with the Pipistrel SW 121 as shown in Figure 4.5, is a full electric aircraft and, as such, has very different performances.

[1] https://www.domergue.aero/wp-content/uploads/Manuel-de-vol-Pipistrel%20-Velis-Electro.pdf, Accessed: 2025-08-19

The powertrain, as presented in the POH as well as the way it has been modeled for the purposes of this study, is illustrated in Figure 4.6. In addition to the powertrain description, information on the electric motor and battery pack structure was available in the POH or on the manufacturer's website. For this reason, and thanks to the modularity of the code, most of the sizing values for the motor and battery pack will be set as specifications and checked against the computed maximum value. The electric motor fitted on the aircraft, officially the Pipistrel E-811, appears very close in design to an engine in the EMRAX family, which is the foundation of the electric motor model presented in 3.5.1. To account for installation losses and match data available in technical documentation, a multiplicative coefficient was considered for the efficiency estimated by the original model. The final list of specifications, architectural choices, and main model assumptions used for this study is presented in Table 4.2 along with the values used on the Virus SW 121.

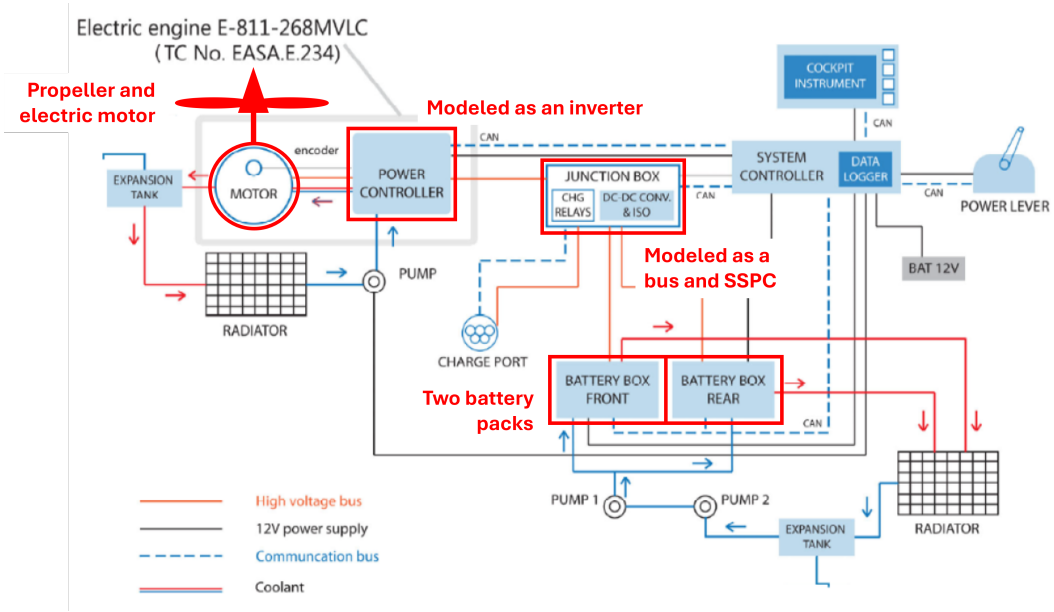

Figure 4.6 Propulsive system architecture for the Pipistrel Velis Electro, the components highlighted in red are the ones modeled in this study.

Like for the study of the Virus SW 121 described in Appendix C.1, these inputs will be fed into an MDA process. The results, in terms of performance and OAD, will then be compared against baseline values. However, even before the sizing process is run, Table 4.2 shows the fundamental impacts in terms of performance and the achievable range of switching to all-electric propulsion. It must be noted, however, that although performance has been greatly reduced, this demonstrates that all-electric flight is possible and enables an additional degree of freedom, as can be seen from the wider range of propeller Revolutions Per Minute (RPM) variation. This is limited, in conventional design, by the narrow operating range of ICEs. The main outputs of the OAD process after convergence are summarized in Table 4.3.

Table 4.2 Main input parameters for the validation study on the Pipistrel Velis Electro.

		Virus SW121	**Velis Electro**
TLAR	Design payload:	188 kg	172 kg
	Design range:	513 nm	28.6 nm
	Design mission speed:	119 KTAS	93 KTAS
	Design mission altitude:	2000 ft	2000 ft
	Approach speed:	58.5 KTAS	58.5 KTAS
Geometry	Wing aspect ratio:	12.04	12.04
Propulsion	Rotax 912 SFC:	256 g/kW/h	*NA*
	Battery structure	*NA*	96 series 12 parallel
	Propeller diameter:	1.7 m	1.64 m
	Propeller rpm:	From 2263 to 2099	From 2350 to 1780

Table 4.3 Main outputs for the FAST-OAD sizing process of the Pipistrel Velis Electro.

	FAST-OAD sizing	**Reference**	**Diff. wrt ref. (%)**
MTOM (kg)	600	600	<1
OME (kg)	428	428	<1
End of mission SOC (%)	8.4[a]	0[b]	8.4
Wing area (m^2)	9.84	9.51	3.3
HTP area (m^2)	0.98	1.02	4

[a] refer to explanations in text, [b] at the end of the mission (including reserves) the battery is empty

Further emphasis is put in the text and in Figure 4.7 on the powertrain data. The results show good agreement between the computed values and reference values for the MTOM and Operating Mass Empty (OME). Information from the POH regarding the variation of the SOC of the battery during different flight phases was also compared with the computed value. Namely, a SOC of 8.4% at the end of the mission was computed while the actual value is equal to 0%. This difference comes from the fact that the framework's reference cell has a slightly higher capacity than the one used for the Velis Electro for the same mass. Another run was made with the actual value for the cell capacity. This led to an end-of-mission SOC of 1.6%, a value much closer to the 0% expected. Comparisons were also made between technical data that were available for electric components and the data computed by the code. While the mass of the battery pack shows very good agreement with reality (computed at 75kg with a real value at approximately 70kg [2]), this mass is computed based on the cell configuration and cell mass fraction, which were input data for that sizing process. A similar remark can be made for the electric motor mass since the one installed on the Pipistrel is very close, in terms of technical characteristics, to one of the electric motors used to establish the

[2]https://www.pipistrel-aircraft.com/products/velis-electro/#1680814658914-2692ce13-a72a, Accessed: 2025-08-20

mass regression (computed at 20.4 kg and an actual value of 22.8 kg [3]). Comparisons were also made on the mass of the inverter and cables, as well as the mass of the propeller. For the former, very good agreement was found between the 7 kg published by Pipistrel and the 6.8 kg computed by the code. For the latter, a larger discrepancy is noted with a value computed at 19 kg against the 5 kg declared in the TCDS. This is largely due to the constant term in the regression, which is predominant for small propellers. Finally, the required shaft power to complete the different phases of the flight was also compared against data from the POH and shown in Figure 4.7. Although the shaft power is not exactly constant during the climb phase, we can see that the average value is very close to the Maximum Continuous Power (MCP). Likewise, during cruise and reserve, a very good agreement has been found between the computed values and the performances described in the POH.

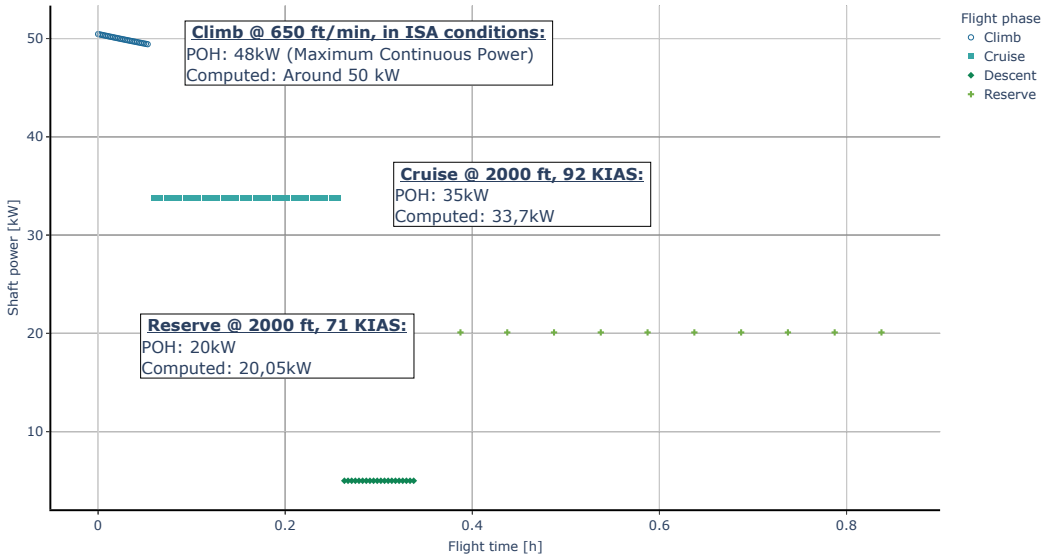

Figure 4.7 Comparison of the flight performances computed by the code with those published in the POH for the Velis Electro.

4.3.2 Comparison with the Pipistrel SW 121

In conclusion to the section dealing with Level 1 aircraft, the performance of the two representative aircraft on their design mission will be compared in terms of emissions and ESAR. However, as illustrated in Table 4.2, despite sharing the same airframe, the two designs have very different missions. To enable a fairer comparison, as is done in Life Cycle Assessment (LCA) — which will be discussed further in Chapter 5 — the aircraft will be evaluated based on their performance in relation to the same reference quantity. In LCA, this would be called the functional unit (FU). As the main goal of these aircraft is to train

[3] https://www.pipistrel.fr/aircraft/electric-flight/e-811/, Accessed: 2024-01-19

new pilots, and in accordance with what is done in the literature [227], we will consider the functional unit to be 'flying for one hour'. Consequently, instead of looking at the ESAR, we will also look at the Energy Specific Endurance (ESE). Although the developed method would enable the evaluation of the performance of the two designs on an off-design mission lasting one hour, we will instead calculate the quantity on the design mission and divide it by the flight time. It is worth pointing out that this means that the quantities will be averaged over the mission, which smooths out phases such as climb. As this could widen the gap between the short missions performed by the Velis Electro and the comparatively long mission of the Virus SW 121, the performance of the latter will also be evaluated on an off-design mission with the same range as the former. The main outputs for that analysis are presented in Table 4.4.

Table 4.4 Performances and emission metrics of the Level 1 designs.

	SW 121 (On-design)	**SW 121 (Off-design)**	**Electro**
Electricity use:	0 kWh	0 kWh	25 kWh
Fuel burn:	65.5 kg	12.86 kg	0 kg
Flight time:	5 h	0.91 h	0.97 h
Emissions:	250.5 kg$CO_{2,eq}$	49.01 kg$CO_{2,eq}$	2.66 kg$CO_{2,eq}$
Emissions per FU:	50.1 kg$CO_{2,eq}$/h	53.86 kg$CO_{2,eq}$/h	2.74 kg$CO_{2,eq}$/h
Emissions per NM:	0.49 kg$CO_{2,eq}$/NM	1.71 kg$CO_{2,eq}$/NM	0.09 kg$CO_{2,eq}$/NM
ESAR:	0.66 NM/kWh	0.19 NM/kWh	1.15 NM/kWh
ESE:	0.0063 h/kWh	0.0058 h/kWh	0.039 h/kWh

The results in Table 4.4 clearly demonstrate a significant reduction of the emission, which is linked to the change in energy vector. Even when taking into account the reduced achievable range and flight time of the Velis Electro, the emissions per hour of flight are reduced by a factor of 95%. This can be attributed to two factors. Adapting Kaya's identity written for aircraft [228], the emissions for a reference quantity can be broken down into three components relating to the number of reference quantity in one flight, the energy required for a flight (which encapsulates the flight efficiency), the emissions per unit energy (carbon intensity of the power source), this is illustrated in Equation 4.2.

$$\frac{E_X}{FU} = \left(\frac{FU}{\text{flight}}\right)^{-1} \times \frac{E}{\text{flight}} \times \frac{E_X}{E} \tag{4.2}$$

where E is the energy and E_X are the emissions. The reduction stemming from the last term, the carbon intensity of the energy carrier, has already been discussed in Section 4.2.1 and gives a first division by a factor of around 3 of the emissions per hour of flight. More interestingly, however, are the benefits coming from the combination of the first two terms, which is the energy per hour of flight, or, in other words, the ESE. Table 4.4 indeed shows a division by around 6 of the ESE, which is attributable to two effects. First, the improvement in the efficiency of the powertrain, which according to literature [23, 25] is multiplied by

a factor of 3 when switching from piston ICE to all-electric propulsion. Additionally, the Velis Electro flies slower because of the choice of motorization, making the flight longer and requiring less power, as illustrated in Appendix C.1 and Figure 4.7. A combination of those two effects can also be seen on the ESAR, which has improved by a factor of around 2. It is also worth discussing the degradation of performance metrics for the off-design mission of the Virus SW 121. There is a slight deterioration in emissions per FU and ESE, which is explained by the fact that the mission is shorter and the aircraft spends more time in climb and descent phases, where it is much less efficient. Before concluding, it is necessary to remember that those two aircraft share the same airframe and mass limitations, meaning there is no penalty associated with the increase in mass due to the batteries. All in all, the results show clear benefits of switching to all-electric aircraft for the Level 1 category, although at the cost of reduced performances and range.

4.4 Level 2 aircraft

Selection of the reference aircraft

For Level 2 and higher certification levels, as opposed to Level 1, there is no certified all-electric or hybrid aircraft. Thus, studies will focus on the selection of an accurate representative for each Level as well as a prospective study on the electrification of said representative. For Level 2, the Cirrus SR22 was selected. Although it is not the aircraft that has been produced the most, that prize belonging to the Cessna 172, also a Level 2 aircraft, data from the General Aviation Manufacturers Association (GAMA) Shipment reports [4] show that in recent years the Cirrus SR22 has been the most popular design. This is illustrated in Figure 4.8. Additionally, the Cirrus SR22 better represents the current state of the art in the General Aviation segment thanks to its high-performance capabilities, high design range, advanced avionics, protection system, and composite airframe. For these reasons, the Cirrus SR22 is better suited to personal transport than the legacy Cessna 172, which is more suited to training. It is also for these reasons that the former might not be the best candidate for total electrification with current technologies, as range and speed reduction are to be expected.

In addition to the reasons presented in the introductory paragraph of this section, the Cirrus SR22 was also chosen because it is already a reference case in the FAST-OAD ecosystem, albeit with legacy models for the powertrain [91, 226]. A detailed study on the results of the sizing process for the Cirrus SR22 is available in Appendix C.2

[4] https://gama.aero/facts-and-statistics/statistical-databook-and-industry-outlook/annual-data/, Accessed: 2025-08-20

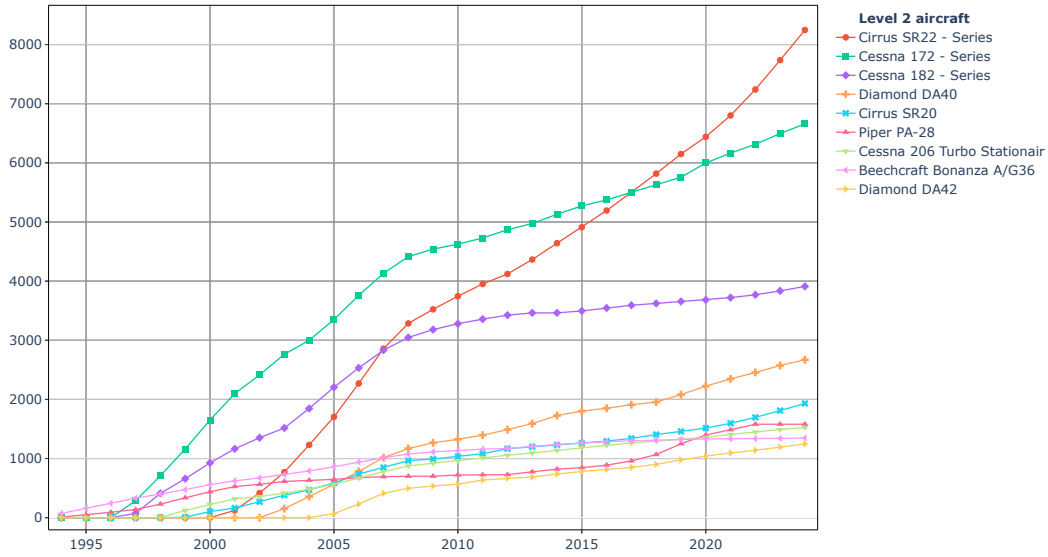

Figure 4.8 Cumulative number of piston aircraft of each type produced since 1994.

Aircraft usage

To identify a commercially relevant target for the electric and hybrid version of the Cirrus SR22, the practical uses of the conventional version were studied. To do so, data from the OpenSky network [229] will be used. The OpenSky network is a community-based receiver network that continuously collects data for air traffic research. Through this network, various databases containing flight data are made available. Two databases are of particular interest to us: a database including a list of flights, with a location of origin, a destination, and the type of aircraft used to perform this specific flight, and a database that contains a list of all known registered aircraft and their type. While the latter is fairly complete, the former heavily relies on volunteers installing receivers, making the coverage very poor in regions other than Europe, North America, and Japan. For the study of the most frequent use of the aircraft, a modified version of the 2019 OpenSky database, which has been developed as part of the creation of the AeroSCOPE tool [230], will be used. The choice was made to also include flights for the turbocharged version of the Cirrus SR22, the Cirrus SR22T, as it shares similar performances. In this modified database, more than 17000 Cirrus SR22 and SR22T flights have been registered. Out of those flights, a certain number were filtered out when the route distance could not be computed, was equal to zero (local flights and flights for which the destination or the origin was unknown), or was above the maximum range of the aircraft. After filtering, more than 7000 SR22 flights and more than 4000 SR22T flights were considered. Their distribution, as a function of the distance of the flight, is represented in Figure 4.9. Flights with a range above 600 nm were aggregated because they represent less than 2% of the total number of flights analyzed.

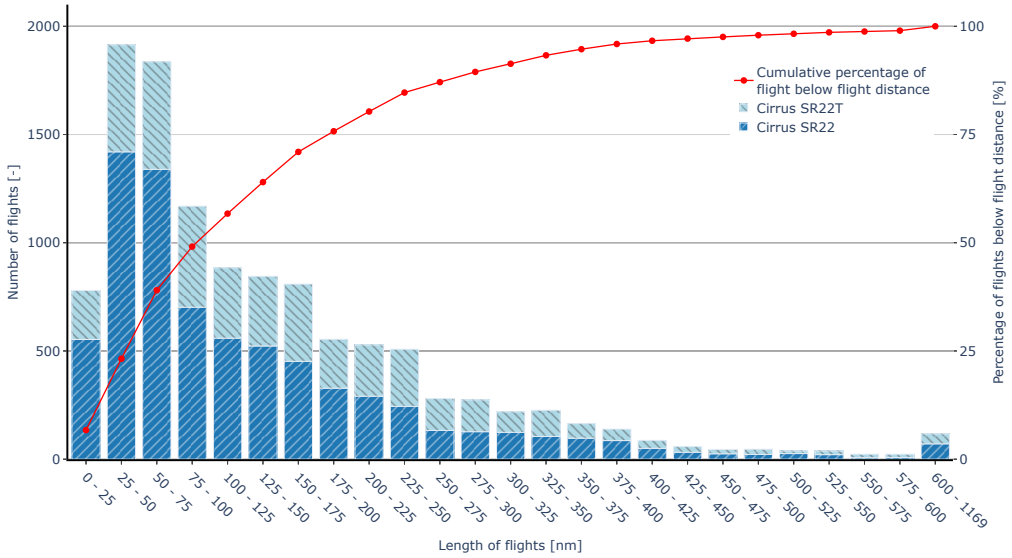

Figure 4.9 Distribution of flights for aircraft in the Cirrus SR22 Series.

The results presented in Figure 4.9 show that a vast majority of the flights occur below 200 nm, showing that missions performed with the Cirrus SR22 are good candidates for electrification. More precisely, we can see that around 50% of the flights in the database have a range lower than 100 nm. This number increases to around 80% for flights with ranges lower than 200 nm.

Results for the sizing run of the original configuration, presented in Appendix C.2, also allowed to identify two potential obstacles to the electrification of the Cirrus SR22. With the conditions set as specifications for the climb — a climb at constant Equivalent AirSpeed (EAS) with climb rates varying between 1390 ft/min a sea level and 1280 ft/min at cruise level — and descent — also at constant EAS with descent rate of 500 ft/min — the aircraft already covers 82 nm of ground distance in those phases alone. Consequently, missions with shorter ranges will require lower climb altitudes. It is also worth noting that the Cirrus SR22 is approved for Instrument Flight Rule conditions, which means it must be sized for a reserve of 45 minutes as opposed to 30 minutes for aircraft operating under Visual Flight Rules conditions like the Virus SW 121 and Velis Electro. For this reason and to improve the chances of finding a feasible design, the electric design will be sized considering 30 minutes of reserve. For the hybrid design, the original 45 minutes will be kept.

4.4.1 Electric version

Following the discussion in the previous section, it was decided to set a target range of 100 nm. The same specifications as on the original design presented in Appendix C.2 will be adopted for the climb and descent segments, and the same speed was selected for the cruise

segment despite the conclusions drawn for Level 1 aircraft. Additionally, analyzing the results for the original Cirrus SR22, presented in Appendix C.2, reveals that the required cruise power of more than 145 kW is just within the capabilities of the EMRAX348. As this is the most powerful motor in the EMRAX family, which we used to establish the regressions in the motor model, and because the electric version is expected to be heavier, thus requiring more power, issues could arise from said model. To improve confidence in the results, instead of relying on a single engine, the powertrain will be modeled with two stacked engines, which, according to EMRAX recommendations, is feasible [5]. This will be translated in the powertrain file as two engines coupled via a virtual gearbox with a mass equal to zero and an efficiency of 0.99. Given the shape selected for the electric engine mass estimation formula presented in Section 3.5.1, the results on the mass will be conservative. For the same reason, it was decided to have the sizing conditions for the electric motors, torque and rpm, as specifications in input of the process, which will then be checked after the convergence of the process. The resulting power train is presented in Figure 4.10 and the main architectural choice, as well as model assumptions considered for the sizing process of the electric version of the SR22, from here on called the eSR22, are presented in Table 4.5.

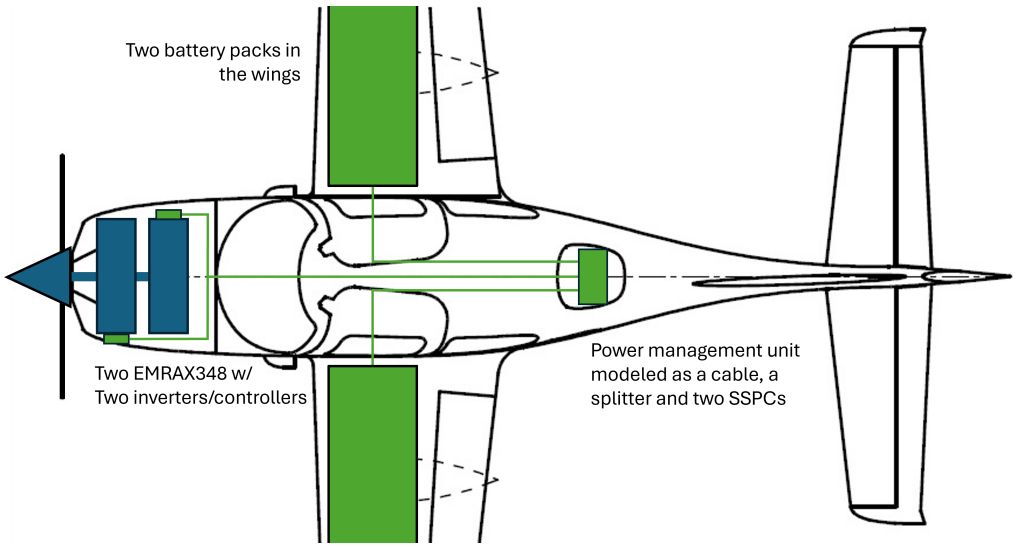

Figure 4.10 Propulsive system architecture considered for eSR22.

This choice of input parameters for the eSR22 leads to the results presented in Table 4.6. As opposed to the validation case used for the first level, an approach consisting of a design from scratch was selected here, as evidenced by the increase in aircraft mass. Indeed, the MTOM of the aircraft has increased by more than 50% which is mainly attributable to the increase in the powertrain mass, in which the ton of battery is bookkept. Results also show that, despite the fact that two EMRAX348 would have been enough to power the conventional

[5]https://emrax.com/e-motors/stacked-motor/, Accessed 2025-08-21

Table 4.5 Main input parameters for the prospective study on the eSR22.

		Cirrus SR22	**eSR22**
TLAR	Design payload:	375 kg	375 kg
	Design range:	971 nm	100 nm
	Reserve duration:	45 min	30 min
Propulsion	E-motor rated torque:	*NA*	1478 Nm
	E-motor rated rpm:	*NA*	2500 rpm
	Battery structure:	*NA*	120 series *P* parallel[a]

[a] the number of modules in parallel is adjusted by the code to satisfy the SOC constraints and the C-rate constraint, whichever is active

Cirrus SR22, the increase in mass and the choice to keep the same climb profile result in a violation of the constraint on the torque rating of the electric motor. An argument in favor of the selected configuration could be made because of the fact that, despite being above the continuous torque of the electric motor, the required torque still remains significantly below (33%) the peak torque. Additionally, thanks to the aggressive climb profile, the climb phase only lasts 6.5 min, leaving hope of managing that excess power requirement as transient. A detailed analysis of the output of the sizing process also reveals that, despite the increased power requirement, the constraint associated with energy remains the active constraint for the battery pack. Further attempts at adjusting the input of the sizing problem revealed that it would be possible to achieve a design that satisfies all constraints, albeit at the cost of a reduced cruise altitude of 2000 ft and climb rates reduced to 50% of their original values. Interestingly, this would result in a slightly degraded ESAR because of the lower cruise level. In spite of this knowledge, the original eSR22 will be retained for future analysis.

Table 4.6 Main outputs for the FAST-OAD sizing process of the eSR22.

	Cirrus SR22	**eSR22**	**Diff. wrt conventional (%)**
MTOM (kg)	1600	2477	+55
OME (kg)	990	2102	+111
Fuel burn design (kg)	233	*NA*	*NA*
Battery pack mass (kg)	*NA*	2x520	*NA*
Excess prop. power req.	3.0% of P_{rated}	75% of Q_{rated}	*NA*
Wing area (m^2)	13.3	20.2	+52
ESAR (NM/kWh)	0.34	0.54	+58

It is worth mentioning that the ESAR does not take into account the number of passengers. Thus, the figures for Level 1 and 2 aircraft (respectively in Tables 4.4 and 4.6) should not be compared as they are. Rather, it should be done by accounting for the fact that the payload is more than twice that of the Pipistrel aircraft. Finally, while the value of the ESAR still improves when switching to all-electric propulsion, it is starting to show limitations. Indeed, while for Level 1 an improvement of 75% could be observed, it is reduced here to less than

60% because of the weight penalty imposed by the battery packs. Additionally, while the electric design was found to be feasible, it was so at the cost of starkly reduced performances with achievable ranges covering merely 50% of the original design. Given the already high MTOM and the expected divergence in mass [23], the chance of finding a feasible design beyond that range is very low. Improvement could however be achieved by changing the battery chemistry, thus influencing the battery energy density, which, as a reminder, has been identified as a major bottleneck for all-electric propulsion [44, 45]. To study the effect of a change in battery technology, the sensitivity of the MTOM of the eSR22 to the design range will be studied. Another aircraft sized for the same conditions but with a higher energy density cell will also be included. For the latter, a Nickel Manganese Cobalt (NMC) pouch cell from the Ampirius catalog with an energy density of 395 Wh/kg at cell level will be retained. It's worth noting that said cell has an average lifespan of 150 cycles as opposed to the more than 500 cycles of the reference cell, leading to more frequent replacements and higher operating cost, which realistically would not be worth it. The final hypothesis which will be made for that sensitivity study, is that the electric motor won't be resized, leading to overly optimistic results at higher masses. The results are shown in Figure 4.11.

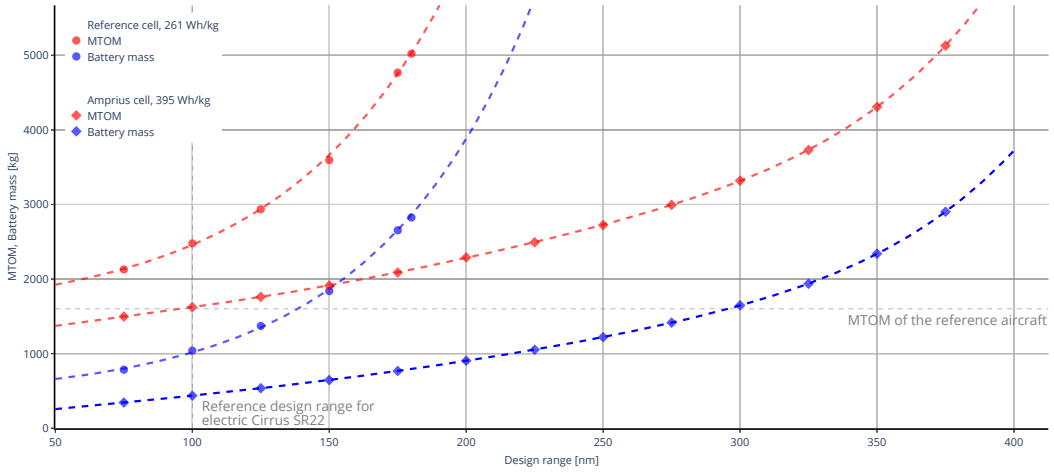

Figure 4.11 Sensitivity of the Electric Cirrus SR22 masses to the design range.

Figure 4.11 shows that no matter the design range, the MTOM of the eSR22 with the reference cell (red dots) will never be lighter than the original aircraft. In addition to that, and as predicted, the mass diverges very quickly after the 100 nm selected. For the Ampirius cell, however, we can see that MTOM similar to that of the original SR22 could be achieved with the initially selected design range. Additionally, the mass divergence occurs much later, which allows a doubling of the range with limited mass penalties. For upcoming computations with the reference cell, however, the design range of 100 nm will be kept.

4.4.2 Hybrid version

Results from the previous section lead to the conclusion that, although all electric designs could be feasible for level 2 aircraft, limitations were starting to show. Consequently, a hybrid variant of the Cirrus SR22, which will be named hSR22, was also investigated, and a range of 200 nm was retained. For the propulsive architecture, a parallel hybrid configuration was selected with the idea of mimicking the design philosophy of the H3PS project. That project, whose goal was to pioneer hybrid-electric propulsion in the General Aviation segment, replaced the conventional powertrain of a test aircraft, a Tecnam P2010, with a parallel hybrid powertrain as shown in Figure 4.12. This allowed the switch of the original Lycoming IO-360 engine for a smaller, battery-boosted Rotax 915iS, resulting in a fuel consumption decrease of between 10 and 15%.



Figure 4.12 Modified Tecnam P2010T for the needs of the H3PS project. Source: https://h3ps.eu/.

Initial processes were run by replacing the original Continental IO-550-N with an engine of the Rotax family to leverage their higher power density. However, because of the high performances of the Cirrus SR22, the power required for cruise is greater than anything the Rotax series can offer. Consequently, the approach that was adopted consisted of assuming a uniform hybridization ratio (corresponding to the *percent split* mode in Figure 3.6) during the mission, leading to smaller energy being generated by the piston ICE and a smaller power requirement, also allowing for a downsizing of the thermal engine. All components of the powertrain were sized based on their maximum value during the flight, ensuring a fitted design of the components. The hybridization ratio was then optimized for a minimization of the emissions on the design mission. A French electricity mix was selected for this study after preliminary efforts revealed that no hybrid configuration was better than the thermal one when considering a European electricity mix. This can be explained by the fact that, while increasing the contribution of electric power decreases emissions, it also increases the battery mass significantly, leading to increased weight, power demand, fuel consumption, and thus CO_2 emissions. In the case of the European electric mix, the latter effect was shown

to be preponderant. Details of the requirements, objective function, and design variables for the optimization are presented in Table 4.7. Regarding the design variables, only the share of thermal power H_P will be investigated. In the context of this optimization, it will be equivalent to the split percentage of the gearbox output power $\mathbb{S}$ that go in the primary shaft connected to the thermal machine.

Table 4.7 Specification for the hSR22 optimization problem.

Requirements	Design payload:	375 kg
	Design range:	200 nm
	Reserve duration:	45 min
	Carbon intensity electricity:	29.6 $gCO_{2,eq}$/MJ
	Carbon intensity fuel:	88.7 $gCO_{2,eq}$/MJ
Objective function	Emissions on design mission	
Design variables	Hybridization ratio, % of thermal power	$H_P \in$[80%,95%]
		$H_{P,0}$ =85%

For the optimization, COBYLA [231] was chosen as the optimizer. Although COBYLA is a gradient-free optimizer, it was retained because the optimization is relatively simple with one objective and one design variable. Additionally, and even if all models about the sizing of the powertrain and the performances of the aircraft are analytically differentiated, the aircraft design models inherited from FAST-OAD-GA are not, which led to stability and robustness issues when attempting the optimization with other optimizers like SLSQP. The shape of the objective function as well as the function evaluation carried out by the optimizer are shown in Figure 4.13.

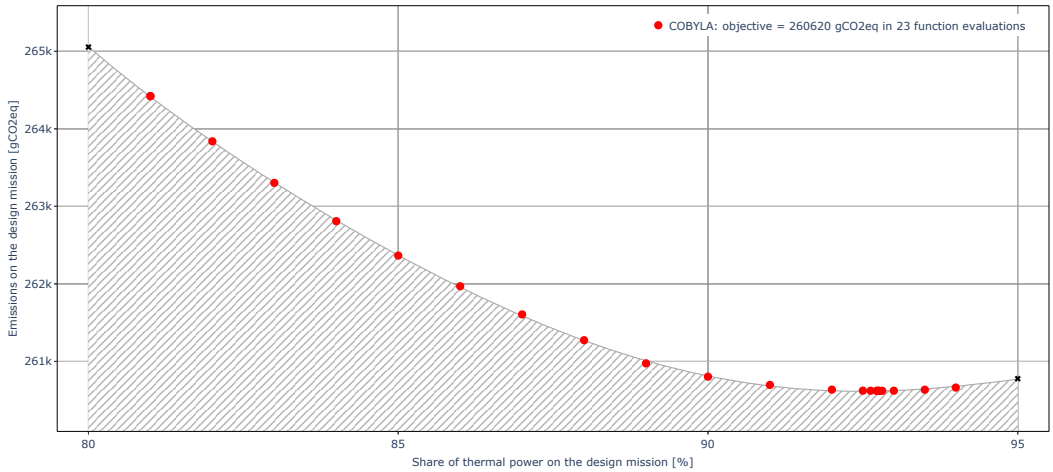

Figure 4.13 Optimization of the hybridization ratio to minimize the emission of the Cirrus SR22.

The results of the optimization show that, for a hybridization ratio of around 93%, a minimum for the objective function could be found. That minimum, evaluated at around 260 $kgCO_{2,eq}$, was however found to be only marginally better than the emissions of the reference aircraft on an off-design mission with the same parameters, which was computed to be around 261 $kgCO_{2,eq}$. That behavior can be explained with the same reasons as why no better solution could be found with a European electric mix: the weight of the battery penalizes the fuel consumption too much. Another study was carried out using another cell from the Ampirius catalog with a value of energy density of 300 Wh/kg. This cell, which is a cylindrical cell with the same dimensions as the framework's reference cell, has a comparable lifespan, making it much more likely to be used in the near future. The results of this optimization are presented in Figure 4.14 along with the shape of the objective function. The shape of the objective function with the framework's reference cell, plotted in light gray, was also kept as a comparison basis.

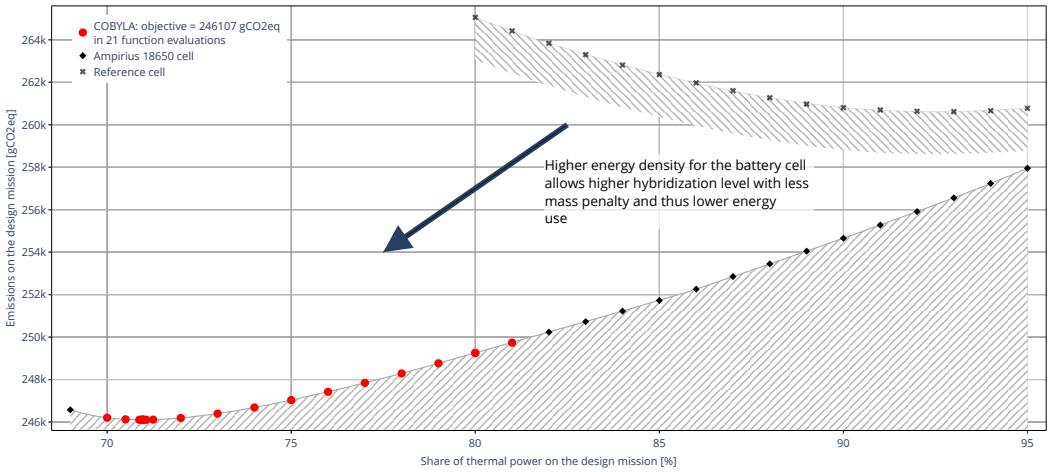

Figure 4.14 Optimization of the hybridization ratio to minimize the emission of the Cirrus SR22 with a higher energy density cell. The results with the original cell are presented as a comparison point.

Results show that even with a moderate improvement of the battery energy density, much higher hybridization can be obtained thanks to the reduced weight penalty of the battery packs [178]. This resulted in a reduction of the emissions down to 246 $kgCO_{2,eq}$ obtained for a hybridization ratio of around 71%. The characteristics of the resulting aircraft are presented in Table 4.8 along with pertinent characteristics of the original design on a 200 nm off-design mission. Even with the more advantageous battery energy density the Ampirius cell offers, the mass penalty associated with the electric powertrain remains significant, with a 41% increase in the MTOM of the aircraft. This increase in mass also coincides with a degradation of the ESAR. Going back to Equation 4.2, this means that the reduction in the emission here arises from the change in the carbon intensity of the energy vector.

Table 4.8 Main outputs for the FAST-OAD optimization process of the hSR22.

	Cirrus SR22 (Off-design)	**hSR22**	**Diff. wrt SR22 (%)**
TOM/MTOM (kg)	1433	2026	+41
OME (kg)	990	1590	+60
Fuel burn (kg)	68.3	61.5	-10
Battery pack mass (kg)	*NA*	466	*NA*
Wing area (m^2)	13.3	16.6	+25
Emissions ($kgCO_{2,eq}$)	261	246	-6
ESAR (NM/kWh)	0.24	0.23	-4

An additional exploration was carried out in which the functioning mode of the splitter was switched to a power share (see Figure 3.6) in an effort to enable the downsizing of the piston ICE. In theory, this could have led to a lighter engine and better efficiency. Computation of the performances with the original flight profile, however, showed that, while the shaft power demand was higher during climb, once the effects of altitude on the power output of the piston ICE were included, the equivalent sea level power was very close to the sizing criteria. As such, very little room for improvement was found. Additionally, inside the design space, a specific value of the threshold power was found below which the constraint for the battery pack abruptly switches between sizing for C-rate to sizing for energy, leading to a rapid increase in mass. This design was thus abandoned.

Multi mission comparison

Having determined the sizing of the hybrid-electric configuration for the design mission, it is important to keep in mind that it can be used for shorter missions, just like the reference. This is especially interesting since the hSR22 was designed to cover around 80% of the original design's missions, which is around 30% more than the eSR22, meaning it could be used to reduce emissions for all missions in between the two design ranges. Additionally, as the range decreases, there will be a surplus of energy in the battery that could be used to reduce fuel consumption further. For this reason, the performances of the hSR22 were evaluated for off-design missions with ranges of 100, 125, 150, and 175 nm. For these missions, the share of electric power was gradually increased to ensure that the battery was fully depleted at the end. Two additional constraints were however monitored. On the design mission, the electric motor has been sized for a rated power of 91kW, approximately 29% of the power required for climb. As the share of electric power in cruise increases, we can expect that this value will eventually be reached. For the same reason, the battery C-rate will also be considered a constraint, especially given the low current throughput of the selected cell. If either constraint is reached while the SOC at the end of the mission is still positive, the hybridization ratio will be changed in other phases of the mission, prioritizing low-power phases such as descent or taxi, and ultimately reserves.

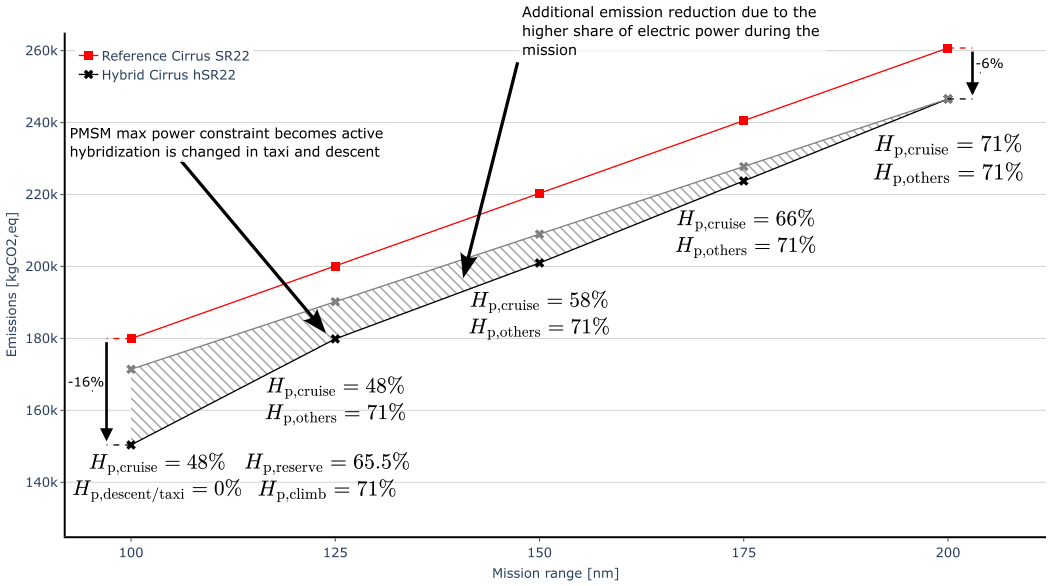

Figure 4.15 Comparison of emissions of the hSR22 on off-design missions.

The results of these evaluations are presented in Figure 4.15. They show that, for missions with ranges of more than 125 nm, the hybridization ratio in cruise can be decreased without reaching either of the two constraints that were set. At 100 nm, however, as the share of electric in cruise reaches 52%, the required electric shaft power goes above the rated power of 91 kW. Consequently, the hybridization ratios for descent and taxi were changed for the 100 nm mission. In fact, the energy requirements were so low in those phases that they could be completed using only the electric branch, with some energy left over to reduce fuel consumption during the reserve phase. Interestingly, Figure 4.15 shows that, at that point, there is a break in the emission reduction trend. This inflection is due to the relatively poor efficiency of the thermal engine in descent when compared to cruise, which we chose to electrify first. For this reason, and mostly because the descent profile has not been changed with the range, a completely electric descent can lead to significant relative gains in terms of emissions, especially those close to the ground. All in all, the results also show that thanks to this use of leftover energy, gains in terms of emissions actually vary between 6% and 16%. To get a better estimate of the average emissions reduction for those missions, a weighted average based on the number of flights in each segment, as illustrated in Figure 4.9, is proposed. The weights and emission reductions in each segment are summed up in Table 4.9 and result in a weighted average reduction of 9.5% of the emissions, noticeably higher than the 6% of the design mission.

This increase in the expected gains of hybridizing the SR22, in addition to further confirming the interest of such configurations, also illustrates the importance of accounting for the operational aspects when evaluating new designs. While it could be argued that

Table 4.9 Average emission reduction and weight for each segment. Average emissions reductions are obtained based on the average reduction of emissions for the mission at both ends of the segment.

Segments (nm)	100-125	125-150	150-175	175-200
Average emissions reduction (%)	13.1	9.5	7.7	6.5
Percentage of flights in each segment (%)	28.6	27.3	26.2	17.9

the results presented in Figure 4.15 may be difficult to achieve in practice because they require knowledge of the exact flight profile before the mission start in order to optimize energy management on-board, they demonstrate that the original hybridization choice and the impacts it had on the electric motor sizing affects the off-design energy management strategy. Better results may have been achieved if, instead of enforcing a sizing of the piston ICE and e-motor to fit exactly the conditions encountered during the design mission, they had been free to change to optimize off-design conditions. The knowledge of the flight distribution would have allowed to further refine the objective function in what is often called in literature a multimission optimization [232, 233]. This was however not further investigated. A final remark can be made on the choice of opting to decrease in priority the share of thermal power in cruise. Indeed, a "break" can be observed on the black curve of Figure 4.15, which seems to suggest that it may be more beneficial to prioritize the electrification of low-power phases. An analysis of the piston ICE SFC during descent and taxi reveals that it is significantly higher than in power-intensive phases, suggesting it may have been wiser to start by fully-electrifying those parts, even during the design mission. It would also help with the reduction of emissions during the Landing and TakeOff (LTO) cycle, which is a topic of particular interest for the improvement of the local air quality near airfields [207, 234] and may enable operations at times when conventional aircraft may otherwise be forbidden to operate due to noise constraints[6].

Forecast of hybrid design lifespan

Initial design investigations in the hybrid version of the Cirrus SR22, and more specifically, the observed improvement with the increase in the battery energy density, hinted at the question of the time frame during which hybrid designs would be preferable to all-electric ones. Indeed, the literature predicts an evolution of the energy density of Li-Ion batteries in the coming years, with values reaching between 400 and 500 Wh/kg as soon as 2035 [235, 236]. Even higher densities could be reached when switching to different cell chemistries, with predictions reaching values north of 1000 Wh/kg for Li-S and Li-air cells in the next decade. With densities high enough, all-electric designs with similar performances to the hybrid design we selected could become feasible. Additionally, given the low carbon intensity

[6]https://www.ecologie.gouv.fr/sites/default/files/documents/livret_pilotes_toussus_le_noble_dispositions_environnementales.pdf, Accessed 08-25-2025

of the electric grid, they would be preferable in terms of emissions. Results from literature posit that, depending on the TLARs, and although they enable fuel consumption reduction, hybrid powertrains should be considered only as a mid-term transitory solution given the feasibility of all-electric design with future batteries [81]. Consequently, to identify the tipping point, investigations into the feasibility of an all-electric version of the Cirrus SR22 with similar TLARs as the hybrid case initially selected were conducted for various values of the battery energy densities. The results are shown in Figure 4.16. Additionally, to study the evolution of the optimal hybridization ratio for those same densities, similar optimizations as on the reference hybrid design were conducted. The values of the optimal share of thermal power and the associated emissions are shown in Figure 4.17.

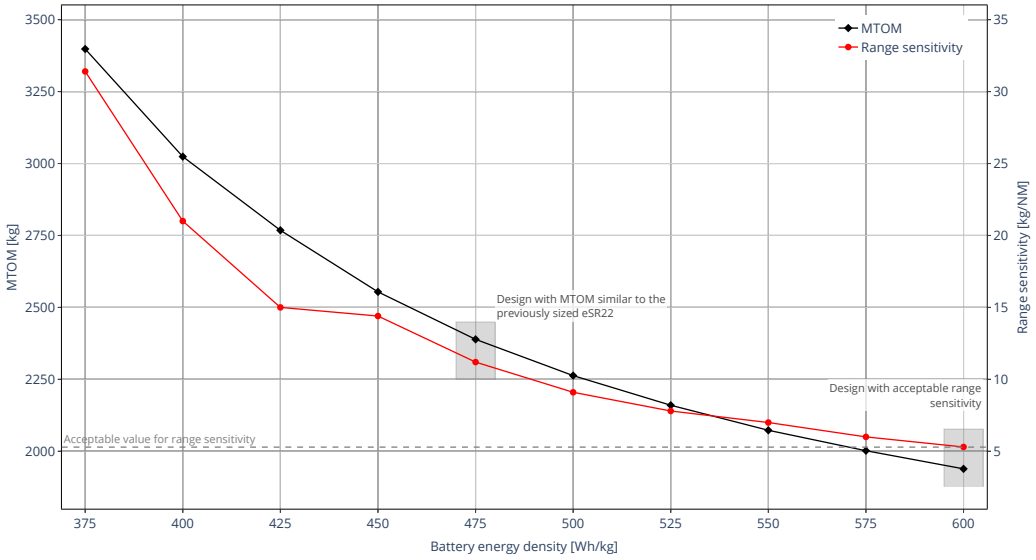

Figure 4.16 Feasibility study for a 200 nm eSR22 based on battery energy density.

As opposed to the eSR22 discussed in Section 4.4.1, and because the goal of this study is to assess the competitiveness of a future all-electric replacement for the hSR22, the same TLARs as the latter, presented in Table 4.7, will be taken. Due to the increase in design range and reserve duration, only high values of battery energy density, greater than 275 Wh/kg at cell level, were considered. Due to the prospective nature of this study, instead of relying on the models calibrated for existing components and architectures, efficiency values representative of future technologies will be considered for the other electric components. In order to find a quantifiable criterion to judge the feasibility of the designs that will be investigated here, two avenues were considered. The first one is based on the value of the aircraft's MTOM. Results presented in Section 4.4.1 showed that considerable increases in the aircraft mass needed to be accepted for an electric design to be qualified as feasible. As such, a design will be deemed feasible here if its MTOM is smaller than that of the original

eSR22. A second criterion stemming from literature [23] was also considered. This criterion, which is based on a theoretical development of the electric version of the Breguet range equation, defines a design as feasible if the MTOM does not increase too much with design range, thus preventing mass divergence. Acceptable sensitivity was computed at 5.29 kg/nm based on the application of a formula presented in literature [23] using the MTOM of the original SR22. Results from Figure 4.16 show that acceptable designs according to the second criterion can be reached only for battery energy densities of 600 Wh/kg. For this energy density, a design with an MTOM of less than two tons could be found. For the first criterion, smaller values of the battery energy density would be acceptable with feasible designs found starting at 475 Wh/kg at cell level. Only the latter will be considered as an upper bound for the next study on the hybrid designs. It is however worth noting that according to the second criterion, the eSR22 presented in Section 4.4.1 would not be deemed acceptable because of a range sensitivity of 8.4 kg/nm.

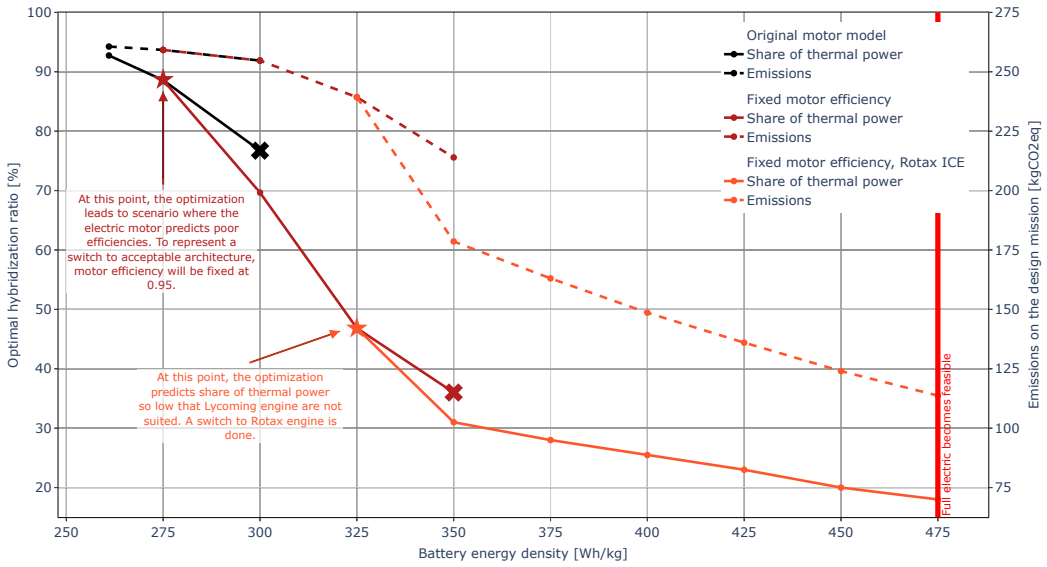

Figure 4.17 Results of the emission minimization for various battery energy densities.

The same problem inputs, powertrain, and optimization setup as discussed in Section 4.4.2 were reused here and reran for values of the battery energy density varying between that of the reference cell, 261 Wh/kg, and the feasibility threshold for all electric at 475 Wh/kg. As expected, results show that the higher the battery energy density, the higher the optimal share of electric power and the lower the emissions. There are however a few points of interest in the graph that show that improvement of the battery energy density alone is not the only thing to be considered. Indeed, while initial processes were run using the reference electric motor model, the value of the design variable led to fairly low electric power compatible with engines in the EMRAX family. For higher values of the battery energy density, however,

higher hybridization ratios are sought. This leads to not only a higher share of electric power but also to heavier aircraft, leading to increased shaft power demand on the electric motors. Because of that, the model starts predicting efficiencies below 90%, indicating that the architecture of the representative electric motor, an AFPMSM, might not be suited for higher power applications, confirming the need for further development of electric motors. To enable further analysis, a switch in electric motor technology will be assumed. This will be modeled by fixing the output efficiency of the motor to a fixed value of 95%. The mass and volume model, however, will not be changed. The switch between those two assumption scenarios is illustrated in Figure 4.17 with the red star at 275 Wh/kg. The second point of interest on the graph is located at battery energy densities of 325 Wh/kg. At that point, the optimizer is guided towards values of the share of thermal power low enough (less than 50 %) that during cruise, very little thermal power is required. At that point, like for the electric motor, the model for the internal combustion engine, and the underlying model assumptions on its four-cylinder architecture, predicts very poor value of the SFC. Actually, the value is small enough that, at that point, a smaller engine like the aforementioned Rotax family can be used. That second and last change in the assumption scenario is represented by the second cross in red on the graph. Predictably, because of the improved SFC, emissions are even lower with an even higher share of electric power. Interestingly, for some optimizations and especially at high battery energy density, the process had to be stopped manually and rerun because the optimizer was looking into designs with higher shares of electric power, leading to a divergence in the mass. This can be explained by the fact that, unlike for initial design with a majority of thermal power, those designs are very sensitive to the infamous snowball effect.

All in all, those two explorations of the sensitivity of architectures to the battery energy density reveal that, at least for Level 2 aircraft, hybrid designs are predicted to have a very small window of pertinence. Indeed, for values of the energy density achievable by 2035 according to predictions in literature, all-electric designs have been shown to be feasible and preferable to their hybrid counterparts. That contrast is even strengthened by the introduction of new and lighter cell chemistries. Questions regarding the certifiability of multiple power sources could also be raised as opposed to all-electric or all-thermal designs, further hampering the interest in hybrid designs for those configurations.

4.5 Level 3 aircraft

4.5.1 Selection of the reference aircraft

For the third level of certification under the CS-23 category, particular emphasis was placed on turboprop aircraft. While Level 3 aircraft powered by piston engine exists, like the Cessna 402, they are outdated designs not representative of current trends in the General Aviation

segment. Similar to what was done for Level 2 aircraft, shipment reports from the GAMA were analyzed to identify suitable candidates, focusing on aircraft fitted with turboprop engines. The results of this analysis are illustrated in Figure 4.18. While the results show that the Pilatus PC-12 is the most manufactured aircraft certified under Level 3, the choice was made for this part to study the DAHER TBM 900 and the DAHER Kodiak. This choice is justified by the fact that, thanks to a collaboration via the ISAAR (which stands for Innovative Solutions for Aviation Architecture and Regulations) research chaire at ISAE-SUPAERO, detailed data could be retrieved directly from the manufacturer to validate the results on the baseline. Additionally, the DAHER Kodiak remains one of the most manufactured airframes and has other characteristics that make it a suitable candidate. For one, it has similar performances as other aircraft used as test benches, such as the Cessna Grand Caravan modified by Ampaire or the full electric De Havilland Beaver operated by Harbour Air. Additionally, the aircraft has a very versatile cabin with lots of room to accommodate large batteries and flies at relatively low speeds. It also flies at low altitude, removing the need to pressurize the cabin.

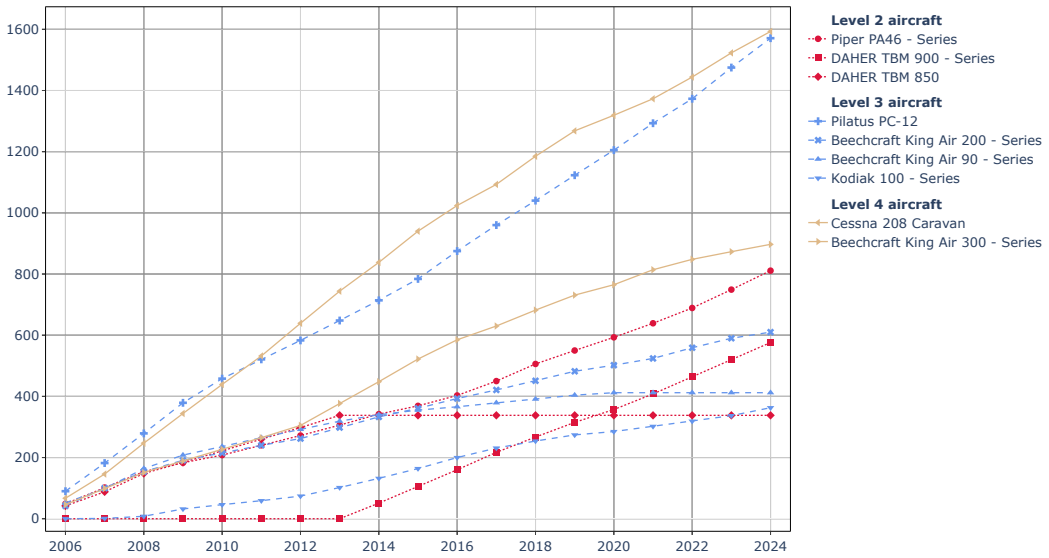

Figure 4.18 Cumulative number of turboprop aircraft of each type produced since 2006.

For the DAHER TBM700N (commercialised as the TBM900), it is worth noting that it strictly speaking does not belong in the Level 2 category. Early versions of the design are actually not even certified under the basis of the CS-23, but rather on the basis of the FAR-23, where the concept of certification level was not yet introduced in certification regulation. And while the latest aircraft in the series is explicitly certified under the CS-23 Level 2 category [7], the TCDS mentions seating capabilities of seven passengers. Thus, for the needs of this study, it will be considered as a Level 3. Additionally, this aircraft is of particular interest because it

[7] https://www.easa.europa.eu/en/document-library/type-certificates/aircraft-cs-25-cs-22-cs-23-cs-vla-cs-lsa/easaa010-daher, Accessed 25-08-2025

was chosen as a demonstrator platform for the EcoPulse project [8]. The goal of this project, co-led by Airbus, Safran, and DAHER, was to explore the potential benefits of Distributed Electric Propulsion (DEP) and to increase the maturity of key technological bricks.

The sizing process and main outputs for the TBM900 and Kodiak 100 are presented in Appendices C.3 and C.4, respectively.

DAHER TBM 900 aircraft usage

For the identification of a commercially relevant target range for the hybridized version of the DAHER TBM 900, the same approach as for the Cirrus SR22 was adopted. It is worth noting that caution was raised in the initial analysis regarding the scarcity of data in regions with poor coverage. Fortunately, the vast majority of DAHER aircraft are registered in countries where coverage is extensive, as can be seen in Figure 4.19, which increases the confidence in the relevance of the OpenSky database.

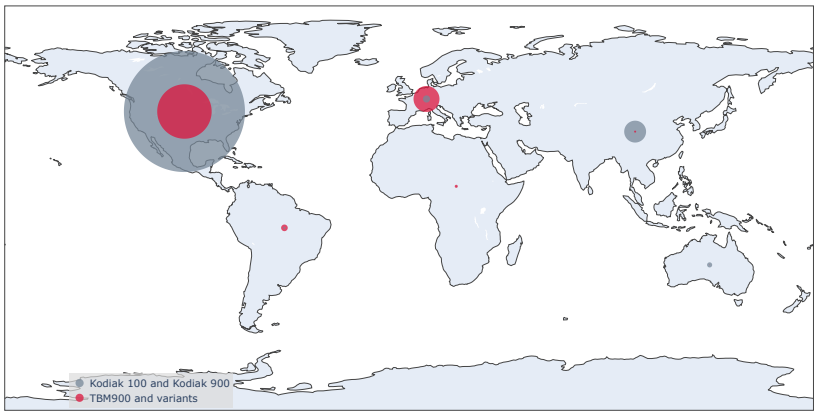

Figure 4.19 Distribution of the countries of registration of the TBM 900 and the Kodiak 100/900 [226].

Out of the 12200 DAHER TBM 900 flights in the database, around 5000 were filtered out, leaving a total of around 7000 usable TBM 900 flights. Their distribution, as a function of the distance of the flight, is represented in Figure 4.20. The results show that more than half of the flights considered for the TBM 900 have a range of 250 nm or less, which is compatible with the range achievable with today's electric technologies [57]. To improve the odds of finding a feasible hybrid design for the TBM 900, which is considered a high-performance aircraft, its performances will be studied on a different mission profile. For the climb and reserve, the same target performances as the design mission, presented in Appendix C.3, will be selected. In addition to that, and while the design mission was chosen as a max power

[8] https://www.daher.com/ecopulse-ouvre-la-voie-a-une-aviation-plus-durable/, Accessed 25-08-2025

mission, an off-design mission will be performed with the long-range cruise setting. Finally, even though the descent phase of the sizing mission was performed assuming a constant speed of 230 knots of Equivalent AirSpeed (KEAS), for the operational mission, it will be done considering a constant equivalent airspeed of 160 KEAS.

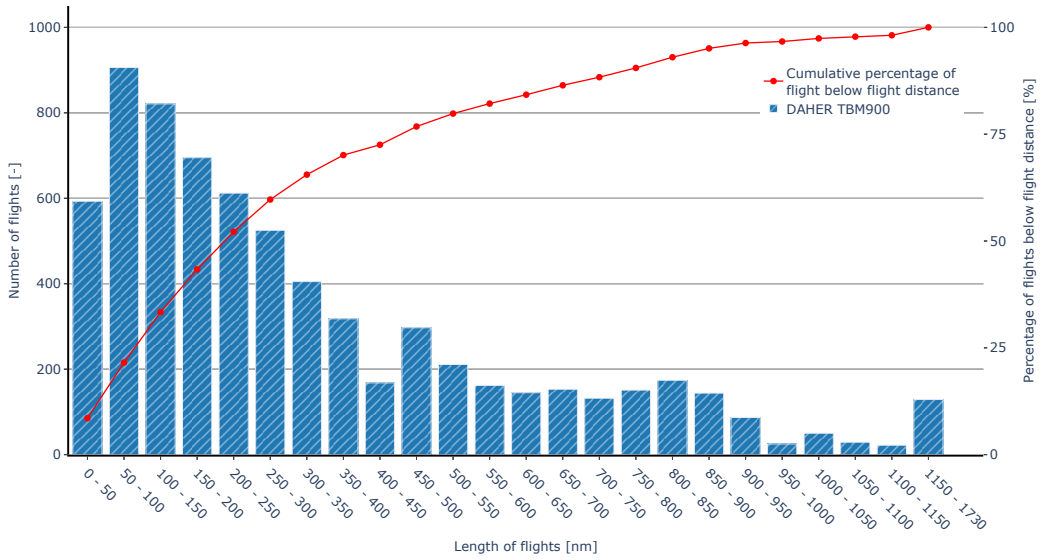

Figure 4.20 Distribution of flights for aircraft in the TBM900 Series.

4.5.2 Hybrid TBM 900

For the study of the hybridization of Level 3 aircraft, and in line with projects such as the EcoPulse or the all-electric Cessna Grand Caravan, the choice was made to adopt a pseudo-retrofit approach. In addition to de-risking the introduction of electric and hybrid designs and reducing time to certification, this approach could allow for a rapid EIS. On commercial transport aircraft, aircraft retrofit can typically be carried out during scheduled maintenance, allowing for low downtime and minimal costs [237]. In practice, this means that instead of looking for a design from scratch where the geometry is computed based on the TLARs, most of the parameters will be kept constant with only minimal change allowed on the airframe [238, 239]. Similarly, to not exceed certified load envelopes, the MTOM of the reference aircraft will be set as an upper limit for the reference design [178, 223]. The OME, however, will be allowed to vary to account for the change in powertrain. Finally, to ensure that the constraint on the MTOM is respected and as both the OME and the fuel burn on the design mission are expected to change, the payload will be adjusted following Equation 4.3. It is worth noting that the retrofit might result in a reduction of the Revenue Passenger Kilometers (RPK), thus negatively impacting scores that depend on the RPK [178].

$$PL_{\text{des}} = min(PL_{\text{max}}, MTOM_{\text{ref}} - OME - m_{\text{fuel,des}}) \tag{4.3}$$

On the original EcoPulse demonstrator, it was decided, for safety reasons, to decouple the electric propulsion part from the original turboprop. While this ensures a functional separation of the two sides of the powertrain, allowing to physically segregate the electric part during in-flight testing, this means that the architecture is far from being optimal. Additionally, with the EcoPulse being a retrofit of a DAHER TBM 900, keeping mostly the same wing, the slipstream effects coming from the use of DEP are not optimally used as would be the case with a redesign of the wing [13]. The evaluation of the EcoPulse with a design "from scratch" thus appears as a worthwhile case study. Consequently, to assess the gains of a DEP-enabled reduction of the wing area, two designs will be investigated. A first design, close to the EcoPulse, using the same airframe as the original aircraft with a turbo-electric powertrain, will be evaluated. It will include six electric motors and wing-mounted propellers as on the demonstrator. An additional propeller in the nose will also be kept, but we will consider that it does not produce any thrust. The resulting aircraft and powertrain are presented in Figure 4.21. The second design, which will be referred to as "from scratch", will have a reduced wing area as a result of the additional lift generated by DEP in low-speed conditions. An additional constraint will be added for the computation of the geometry of the wing, in that the span will be kept constant. Finally, the nose propeller will be removed, and all the thrust will be produced by the wing-mounted propeller. The resulting powertrain is presented in Figure 4.22.

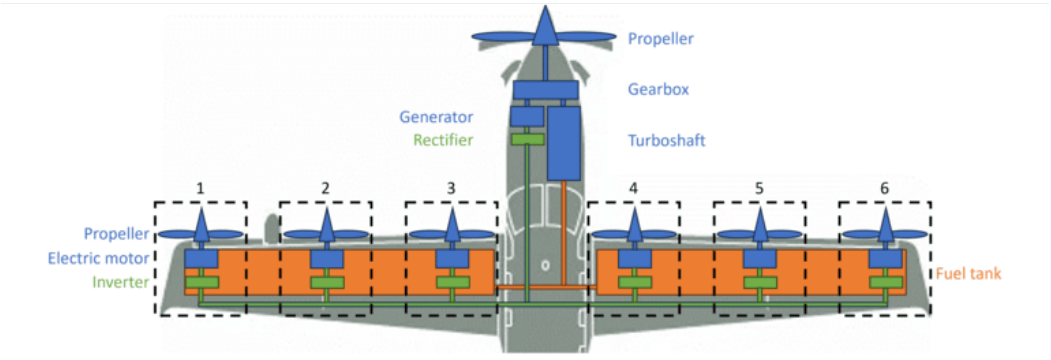

Figure 4.21 Powertrain considered for the study of EcoPulse as a retrofit.

The TLARs for both versions of the EcoPulse, resulting from the discussion in Section 4.5.1, are presented in Table 4.10. It was decided to keep the same turboshaft as the original design on the two hybrid variants; its sizing conditions and characteristics will thus be kept constant. The diameter of wing-mounted propellers and their position were estimated based on pictures of the demonstrator.

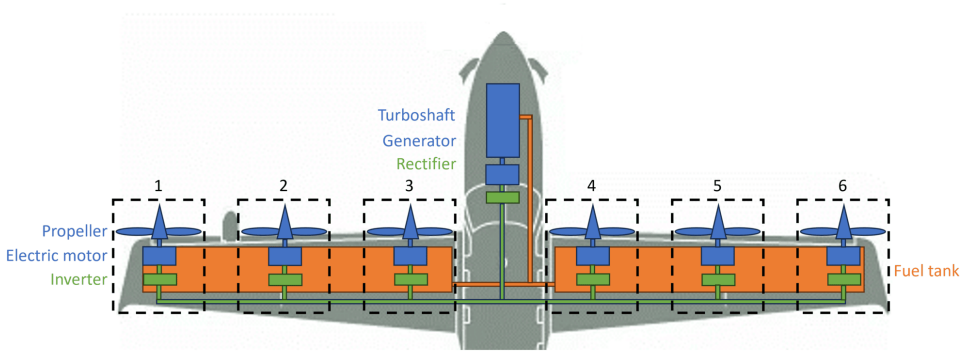

Figure 4.22 Powertrain considered for the study of EcoPulse with a design from scratch.

Table 4.10 Main input parameters for the sizing process of the EcoPulse.

TLAR	Design range (nm)	250.0
	Design mission speed (KTAS)	244
	Design mission altitude (ft)	28000
	Approach speed (KTAS)	85
Propulsion	Network Voltage (V)	800
	Turboshaft rated power (kW)	634
	Propeller diameter (m)	1.5
	Propeller rpm (-)	3000

The comparisons of the FAST-OAD sizing process's results for the hybrid design obtained with those choices to the results of the evaluation of the reference TBM900 on the same mission are presented in Tables 4.11 and 4.12.

Table 4.11 Main outputs for the FAST-OAD sizing process of the retrofit version of the EcoPulse.

	Ref. TBM900	**Retrofit EcoPulse**	**Diff. with ref.**
TOM/MTOM (kg)	3012	3378	+12%
OME (kg)	2088	2570	+23%
Payload (kg)	650	473	-27%
Propulsion chain mass (kg)	357	830	+132%
Wing mass (kg)	360	360	+0%
Wing area (m^2)	18.06	18.06	+0%
Fuel mission (kg)	273	334	+22%
Emissions ($kgCO_{2,eq}$)	1042	1277	+23%
EF ($g_{CO2}/kg_{PAX}/km$)	3.46	5.82	+68%

One notable result from the comparison of the investigated designs is that a reduction of the wing surface area of more than 1.5 m^2 could be achieved on the design from scratch. This leads to a reduced profile drag. In addition to that and because of the assumed constant wing span, this reduction in wing area is also associated with an increase in aspect ratio,

Table 4.12 Main outputs for the FAST-OAD sizing process of the EcoPulse with a design from scratch.

	EcoPulse from scratch	**Diff. w/ ref.**	**Diff. w/ retrofit**
TOM/MTOM (kg)	3378	+12%	+0%
OME (kg)	2473	+18%	-4%
Payload (kg)	585	-10%	+24%
Propulsion chain mass (kg)	725	+103%	-13%
Wing mass (kg)	375	+4%	+4%
Wing area (m^2)	16.5	-8%	-8%
Fuel mission (kg)	320	+17%	-4%
Emissions ($kgCO_{2,eq}$)	1218	+16%	-5%
EF ($g_{CO2}/kg_{PAX}/km$)	4.49	+30%	-29%

with a value going from 8.22 to around 9.00. This, in turn, is associated with a decrease in lift-induced drag. The combination of those two effects results in a lift-to-drag ratio in cruise conditions increasing from 13.06 in the original design to 14.79.

The investigated hybrid designs, however, perform worse in almost every aspect. The fuel consumed during the mission is significantly above that of the reference aircraft, with an increase of 17% for the design from scratch and an increase of more than 22% for the retrofit design. For the retrofit design, the results could have been expected given the fact that we only introduce inefficiencies in the powertrain without taking advantage of the better aerodynamics from a resized wing. For the design from scratch, however, the result is more telling. Further investigations into the efficiencies of the powertrain components reveal that the efficiency from propulsive power to turboshaft required power varies from 77% in the original design to 64% in the design from scratch. This decreased efficiency, and the added aircraft mass, outweigh the gains in terms of aerodynamics. The amplitude of said gains was evaluated by comparing the design from scratch to the retrofit one, which showed a reduction of less than 5% of the fuel consumed. It is worth noting that the losses in terms of efficiency are not only due to the losses in the electric components but also to the efficiency of the wing-mounted propellers, which is smaller due to a smaller radius.

The increase in aircraft empty mass was also investigated. Beyond the increase due to the electric components, a slight contribution can be imparted to the wing mass. Thanks to the physics-based method implemented in the FAST-OAD-GA framework and used in the FAST-OAD-CS23-HE framework [32], supplementary analysis on the reasons for those increases could be conducted. The main contributor to that increase is the skin mass, which increased because of the increased aspect ratio and reduced chord lengths. For the rest of the primary structure, gains stemming from the structural synergies from DEP were observed, although not enough to offset the increased skin mass.

In conclusion, the investigated designs for the hybridization of the EcoPulse don't seem promising with current technologies. While a significant improvement in terms of lift-to-drag

ratio could be observed, the losses stemming from the use of electric propulsion to provide thrust in cruise and the added power train mass completely outweigh those gains. Two avenues for improvements can however be identified. The first comes from the fact that it was decided to keep the same positioning and same diameters for the propulsive elements as on the demonstrator. This resulted in only 75% of the span being blown, but more importantly, in only using propulsive elements with fairly large diameters. More gains could be achieved by using a greater number of smaller propellers, as the strength of slipstream effects seems to increase with a decreasing propeller diameter [34]. This would allow to increase the lift coefficient in approach conditions and thus further decrease the wing area. This would, however, come at the cost of a reduced propeller efficiency.

Another avenue would be to increase the efficiency of the propulsion chain to reduce the fuel consumption. While little work can be done on the efficiency of the components themselves, it could be worth investigating a more complex power management scheme. For instance, and similarly to what was envisioned for the X-57, only a single nose-mounted propeller could be used in cruise conditions to attain the same powertrain efficiencies as in the original design, while wing mounted propellers could be used in low-speed conditions. This would allow to utilize the aerodynamic efficiency gains stemming from DEP without having the efficiency penalty from the electric components. The mass penalty, however, would remain.

As a concluding remark to these studies on hybrid versions of the DAHER TBM900, it is also interesting to mention the limitations of the assumptions made in the scope of the retrofit approach adopted in this work. Indeed, one of the original assumptions was that keeping a constant MTOW would lead to the same sizing load envelope, and as such, the airframe could be kept the same. The structure of aircraft, however, is sized according to a variety of factors and scenarios, one of which is when the aircraft has little to no fuel left in the tanks, depriving it of its role as a relief force for the wing [32]. As the hybrid designs that were investigated have been shown to be heavier when empty, i.e., a higher Maximum Zero Fuel Weight (MZFW), it could lead to a reshaping of the load envelope.

Robustness to uncertainties

As a preamble to the section dealing with the hybridized version of the Kodiak 100, the robustness of the design process to uncertainties will be investigated. Indeed, as highlighted in the section of Chapter 3 dealing with the modeling of the turboshaft, the statistical trends adopted for the computation of the mass, length, and diameter of the gas turbines introduced some uncertainties in the design process. This type of uncertainty, called epistemic uncertainty (as opposed to aleatory uncertainty when dealing with uncertainties on model inputs), concerns uncertainties that have to do with the modeling process. Appendix B.2, which showed the establishment of a surrogate model for the estimation of turboshaft

fuel consumption, also highlighted uncertainties stemming from the choice of the PyVPLM method. Therefore, to increase confidence in the results and to identify where to prioritize resource allocation for improvement, the robustness of the converged values presented in Appendix C.4 to those uncertainties will be investigated. To this end, the UQPCE (Uncertainty Quantification with Polynomial Chaos Expansion) package [240, 241] will be used. This package, developed by NASA, enables users to efficiently perform design under uncertainty with limited knowledge of the uncertainty quantification discipline.

The uncertainties on the turboshaft model will be represented as a multiplicative factor to the output of the statistical trends presented in Section 3.6.4 and the surrogate discussed in Appendix B.2. Following the distribution of uncertainties presented in Figure 3.3 and B.3, those multiplicative factors will be represented as variables following a normal distribution with a mean of 1.0 (meaning using the outputs of the model as is). For the standard deviation, the value will depend on the error distribution for each model. A summary of the values used for the modeling of uncertainties is given in Table 4.13. Uncertainties were sampled using a Latin Hypercube Sampling method and fed into the existing sizing process thanks to UQPCE's abilities to perform uncertainty analysis non-intrusively.

Table 4.13 Uncertain parameters.

Parameter	**Distribution**	**Mean**	**Standard deviation (%)**
Turboshaft fuel consumption	Normal	1.0	3.8
Turboshaft mass	Normal	1.0	8.82
Turboshaft length	Normal	1.0	6.94
Turboshaft diameter	Normal	1.0	5.21

The results of the uncertainty analysis are shown in Figure 4.23 in the form of the mean values obtained for the different samples as well as the confidence intervals and reference values. Results show that, despite the high standard deviation on the mass and dimensions of the turboshaft, the confidence interval is fairly narrow for the MTOM and the OME, with intervals spanning 6% and 5.8% of the mean values, respectively. For the fuel on the design mission, however, that interval is significantly wider, spanning 15% of the mean value. Nonetheless, results show that the value on the reference aircraft lies within the bounds of the confidence interval. The confidence in the output value for the wing area was also investigated, and while the interval is narrower than for the masses, just 3.5% of the mean value, indicating low dependency on the epistemic uncertainties investigated, the reference value is slightly outside of the bounds. Nonetheless, the deviation from the mean value remains small, suggesting that the sizing process is overall robust.

The UQPCE package also computes the value of total Sobol' indices, which gives the contribution of an input to the variance of an output, considering all the interactions. The rescaled Sobol' indices are also computed, allowing to identify, among the uncertain parame-

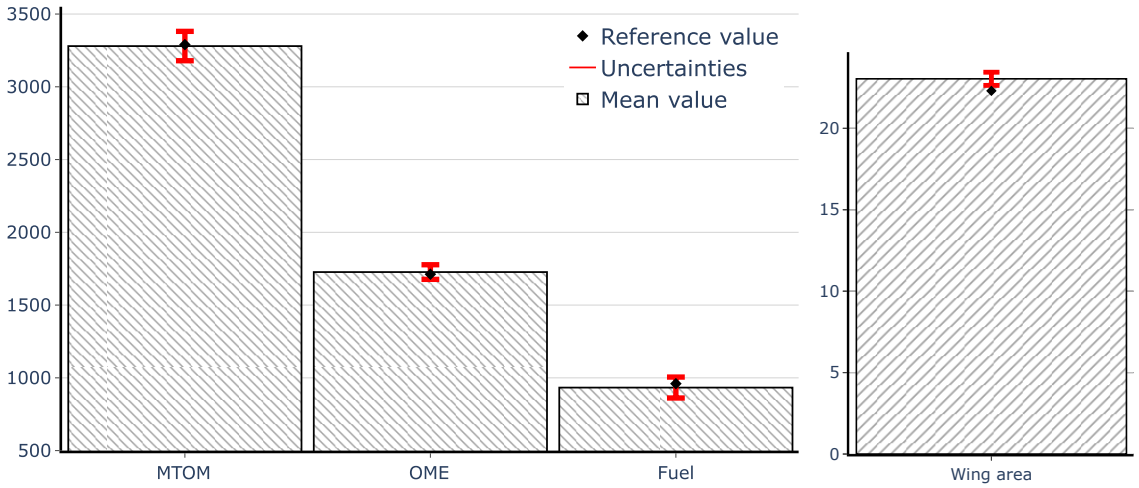

(a) Uncertainties on characteristic masses (in kg).

(b) Uncertainties on wing area (in m^2).

Figure 4.23 Uncertainties on the main outputs of the sizing process.

ters, which one has the biggest contribution to the output's uncertainty, thereby allowing to prioritize improvements. The rescaled total Sobol' indices are given in Table 4.14.

Table 4.14 Rescaled total Sobol' indices.

Uncertain Parameter	**MTOM**	**OME**	**Design fuel**	**Wing area**
Turboshaft fuel consumption	0.7291	0.080738	0.9965	0.080738
Turboshaft mass	0.27065	0.91913	3.4331×10^{-3}	0.91913
Turboshaft length	1.379×10^{-4}	1.3485×10^{-4}	6.9541×10^{-5}	1.3485×10^{-5}
Turboshaft diameter	2.039×10^{-9}	2.6584×10^{-9}	8.6043×10^{-10}	2.6584×10^{-9}

The analysis of the Sobol' indices presented in Table 4.14 shows that, for the most uncertain outputs, the MTOM and the fuel on the design mission, the uncertainty that holds the most weight is the fuel consumption. Indeed, although the deviation is small, as shown in Table 4.13, it has a direct 1:1 ratio effect on the fuel required for the flight. Additionally, as the fuel represents more than 28% of the aircraft mass at the start of the selected design mission, this uncertainty is directly passed on to the MTOM. Therefore, to increase confidence in the outputs of the sizing process and reduce uncertainties for validation and exploration cases involving gas turbines, the model was recalibrated, when possible, on known data points. Regarding the uncertainty on the aircraft's empty mass, as expected, the main contributor is the uncertainty on the turboshaft mass. It can however be seen through the snowball effect that the uncertainty of the fuel consumption on the MTOM also induces a variance of the OME. The analysis of Table 4.14 also reveals that the rescaled indices for the OME and wing area are exactly the same. This can be explained by the model adopted for the

estimation of the latter. Indeed, the wing is sized, in the developed framework, considering the equilibrium in low-speed conditions at Maximum Landing Mass (MLM). Since the MLM is a direct function of the OME and since no other uncertain parameters influencing this computation were considered, the rescaled influence is identical. Finally, the analysis of the Sobol' indices for the turboshaft length and diameter reveals that they have little to no influence on the output variance. This is also a result of the choice of models, and more importantly on the choice of the position for the turboshaft in the test case retained. Indeed, to avoid double-counting the profile drag from the nacelle and the profile drag of the nose or tail cone, when a component is at the front or back of the aircraft, its contribution to the drag coefficient is assumed to be zero, as it is assumed to be nested inside the cones. Additionally, as there is currently no consideration of the volume occupied by the components inside the different subspaces of the aircraft, the components' volumes do not influence the front or tail cone dimensions. Thus, they have no influence on their aerodynamics or mass, which explains the low value of the Sobol' indices. While the uncertainty on the turboshaft diameter is virtually non-existent, a slight dependency on the turboshaft length can still be highlighted. This stems from the ability of the developed framework to account for the effects of a change in CG. Indeed, as the CG of the turboshaft is dictated by its length and as the turboshaft accounts for around 1/8 of the aircraft's empty mass, an uncertainty on the length induces a variance of the aircraft's empty CG. This can then cause a change in the aircraft's geometry because the sizing process aims to maintain stability constraints. It also influences, to a lesser extent, the fuel consumption through a change in the trim drag, also captured by the framework.

Quest/DAHER Kodiak aircraft usage

After initial filtering of the 2200 DAHER Kodiak flights in the database, the remaining 1300 were analyzed to study the distribution of their usage. This distribution, as a function of the distance of the flight, is represented in Figure 4.24. These results show that two-thirds of the analyzed flights have a range of 100 nm or less. Because of the small sample and because at such ranges only half the flight would correspond to cruise conditions, a conservative range of 200 nm was selected for the hybrid version.

Since a significant part of the mission of the Kodiak consists in military surveillance mission[9] where long endurance is preferred, and because it would better fit the maturity of electric components available today, the long range cruise profile, consisting of a cruise at 10000ft and 120 knots of True AirSpeed, will be of particular interest. The post-processing tools of the framework were used to analyze the performances of the reference aircraft, discussed in Appendix C.4, with such a mission profile. In particular, the evolution of the power that the turboshaft needs to provide was investigated in order to better guide the choice

[9]https://specialmissionaircraft.daher.com/kodiak-platform/#aid, Accessed: 26-08-2025

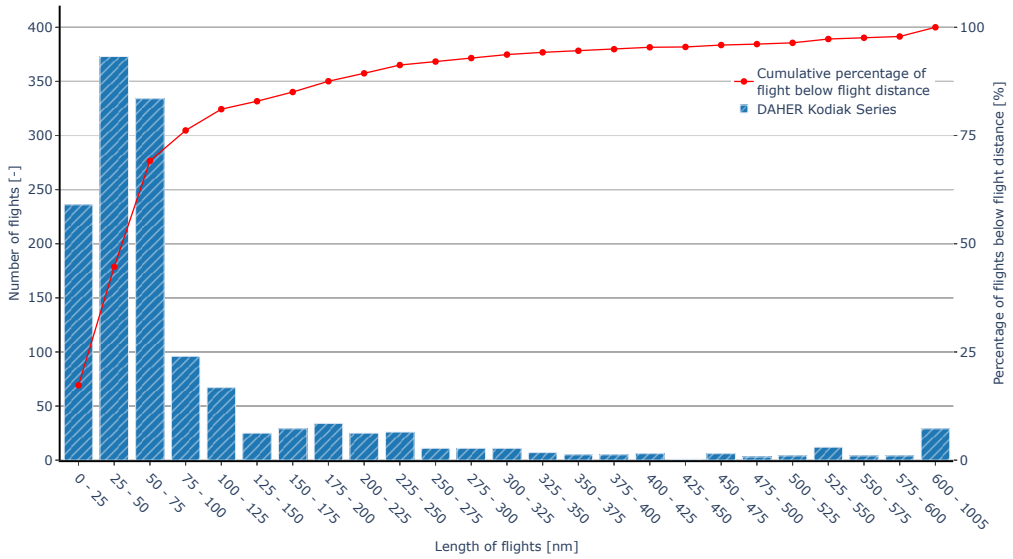

Figure 4.24 Distribution of flights for aircraft in the DAHER Kodiak Series.

for hybridizing the aircraft. A required cruise power of 200kW was computed which showed good agreement with cruise performances indicated in the POH. It is however significantly lower than the rated power, indicating a vast potential for improvement. Surprisingly, however, the power required to reach target descent performances was found to be greater than the power required for cruise. While the aircraft thrust is indeed lower, the fact that the descent airspeed was set at 160 KEAS results in a greater power required. This yields descent power decreasing from 230 to 200 kW. Results were still considered valid as the fuel consumed during descent seemed to closely match the data from the POH. The choice was however made to consider a descent speed of 140 KEAS for further computation.

4.5.3 Hybrid DAHER Kodiak

For the hybridization of the Kodiak, a parallel hybrid powertrain where the batteries would be used to boost a turboshaft in power-intensive phases was selected [226]. The reason behind this choice is that it would allow the turboshaft to be sized for cruise power and thus operate closer to its optimal point, consequently reducing emissions with only mild hybridization levels [13, 178, 242]. It's worth stressing that, as opposed to the hybridization extensively discussed for Level 2 aircraft, this will correspond to the "power share" mode presented in Figure 3.6, which will allow for a much more efficient downsizing of the thermal engine [178]. The powertrain that we will consider is presented in Figure 4.25a. The interest in this choice of propulsive architecture is confirmed by the recent start of the T.A.G.I.N.E. project, of which DAHER is one of the four stakeholders, which aims at studying the benefits of such a configuration as illustrated in Figure 4.25b.

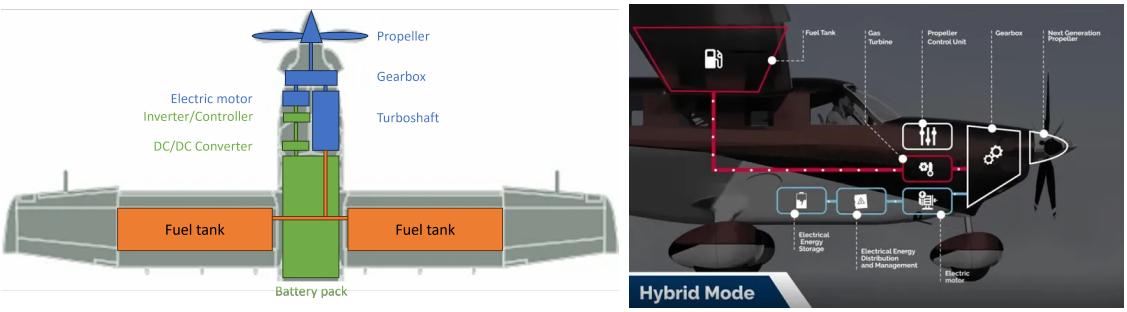

(a) Powertrain considered for this study.

(b) Powertrain considered for the T.A.G.I.N.E. project. Source: DAHER, Accessed; 2025-09-14.

Figure 4.25 Powertrain considered for the hybridization of the DAHER Kodiak.

Given the 200kW power requirement discussed in the analysis of the reference sizing mission in Appendix C.4, limited options were available for the choice of thermal engine. In particular, most turboshafts from the PT6 family have rated power way above that target. As for the remaining ones, the PT6A "Small" engines [10], SFC values seemed to indicate that they would not bring any significant gains. A review of other engines in that power range was thus conducted. This led to the choice of another turboshaft from Pratt & Whitney, the PW206B2, a helicopter engine with a flat rating at 331 kW. To ensure accuracy of the model, off-design verifications were conducted, which led to the inclusion of a correction factor of 1.11 for the engine fuel consumption estimation on this analysis. For the battery pack, which will be used only in the power-intensive climb, a high C-rate cell, the Samsung INR18650-25R, was retained instead of the reference one. For the choice of the electric network voltage, a value of 800 V was selected based on the voltage of the battery pack in the EcoPulse demonstrator. A summary of this discussion, along with the main specifications, architectural choices, and model assumptions for the sizing process, is presented in Table 4.15. The power profile resulting from the choice of hybridization is presented in Figure 4.26.

Table 4.15 Main input parameters for the sizing process of the hybrid Kodiak 100.

TLAR	Design range (nm)	200
	Design mission speed (KTAS)	120
	Design mission altitude (ft)	10000
	Approach speed (KTAS)	78
Propulsion	Network Voltage (V)	800
	Battery reference cell	Samsung INR18650-25R
	Battery cell mass fraction	0.768
	Battery min SOC (%)	20
	Engine rated power (kW)	321

[10]https://www.prattwhitney.com/en/products/general-aviation-engines/pt6a

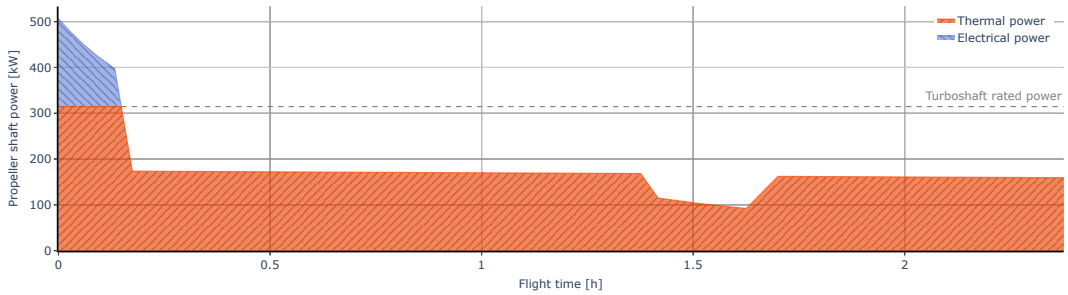

Figure 4.26 Propeller shaft power profile with each contributing source.

A comparison of the main outputs of the sizing process of the hybrid Kodiak with the performances of the reference design, presented in Appendix C.4, is shown in Table 4.16. The results show a 15% improvement in fuel consumption when compared to that of the reference Kodiak on the operational mission. While a part of that reduction is because climb is partially done with electric power (7 kg reduction), the majority is due to the reduced fuel consumed during cruise (14 kg reduction) and reserve (9 kg reduction). In terms of specific fuel consumption, having a smaller, more efficient turboshaft working closer to its optimal point allowed a reduction from 0.488 kg/h/kW to 0.382 kg/h/kW. This reduced fuel consumption is however offset by the fact that the aircraft is heavier due to the more complex propulsion chain. In turn, this means that the maximum payload of the original aircraft, 1140 kg, cannot be flown without exceeding the MTOM, resulting in a marginal decrease to 1130 kg. The emissions of both aircraft were also computed, both in terms of total emissions and in terms of Emission Factor (EF), the emissions per kg of payload per km, studied to account for the mass penalty. A clear decrease in the total emissions can be observed despite the minimal degree of energy hybridization; less than 1% of the energy comes from the electric branch. Indicatively, at maximum power, the degree of power hybridization is equivalent to 41%. However, because of the choice of hybridization scheme, this degree is not constant as opposed to what was presented for Level 2 aircraft in Section 4.4.2. It is worth noting here that, as opposed to the latter, the decrease in emissions does not come from a change in the energy vector but rather from an improvement of the ESAR enabled by the new degree of freedom introduced by electric propulsion. Similarly, a decrease in the EF, although smaller due to the penalty in payload transported, indicates that the gains in flight efficiency are not offset by the weight penalty. Those gains also indicate that the hybrid design, albeit sized for a relatively short mission at max payload, also performs better on missions where longer ranges, longer endurance, and lower payload (a surveillance mission, for instance) are preferred.

Using the detailed breakdown of the masses of the components computed by the framework, the evolution of the mass of the powertrain file was investigated. The results are shown

Table 4.16 Main outputs for the FAST-OAD sizing process of the different versions of the Kodiak.

	Ref. Kodiak	**Hybrid Kodiak**	**Diff with ref (%)**
TOM/MTOM (kg)	3113	3279	+5
OME (kg)	1727	1939	+12
Payload (kg)	1140	1130	<1
Propulsion chain mass (kg)	319	529	+65
Battery pack mass (kg)	*NA*	234	*NA*
Fuel mission (kg)	245	210	-14.3
Electricity (kWh)	0	24.8	*NA*
ESAR (NM/kWh)	0.068	0.079	+16
Emissions ($kgCO_{2,eq}$)	938	809	-13.8
EF (g_{CO2}/kg_{PAX}/km)	2.22	1.93	-13

in Figure 4.27. For readability, the masses of the inverter, DC/DC converter, and bus are aggregated under the label *PMAD* (Power Management and Distribution). Likewise, fuel tank and fuel pipes mass are aggregated under the label *Fuel system*. Results show that the mass of the propeller is constant, which was to be expected given the choice of the retrofit approach. Similarly, the expected decrease in the turboshaft mass linked with the downsizing is also observable. More interestingly, however, is the stark decrease in the fuel system mass. This is linked with the choice of model that correlates the mass of the fuel system to the volume of fuel that flows through it. Given the difference in the sizing mission considered, long range for the reference and a comparatively shorter range for the hybrid, the fuel flown through the system is much lower in the hybrid case. Figure 4.27 also shows that even considering the meager energy hybridization ratio, the mass of the battery pack is significant to the point that the electric branch weighs more than the thermal branch.

Further investigations into the energy efficiency of the resized turboshaft were conducted. Mainly, the computed SFC of the original PT6A-34 and of the PW206B2 were plotted against the shaft power using inputs representative of cruise conditions. To allow results to be better interpreted, the variation of the power in the different phases for the different design were also added. The resulting plot is shown in Figure 4.28. On the original design, high variation of the SFC can be observed with values ranging between approximately 0.33 kg/kW/h and 0.5 kg/Kw/h. More specifically, an increase of the order of 40% between the climb condition for which the turboshaft is sized and the cruise conditions was observed. When looking at the hybrid design, the interest of the engine resizing becomes apparent, for the same power required, the SFC is 20% to 25% lower. As a result of the aircraft being heavier, which is detailed in Table 4.16, it can however be seen that the average power in cruise and reserve is higher. Additionally, it is interesting to point out that, since the aircraft is heavier and less fuel is burnt, the variation in total mass is smaller during those phases. Consequently, the variations of power required are as well. Figure 4.28 also highlights the inability of top-down

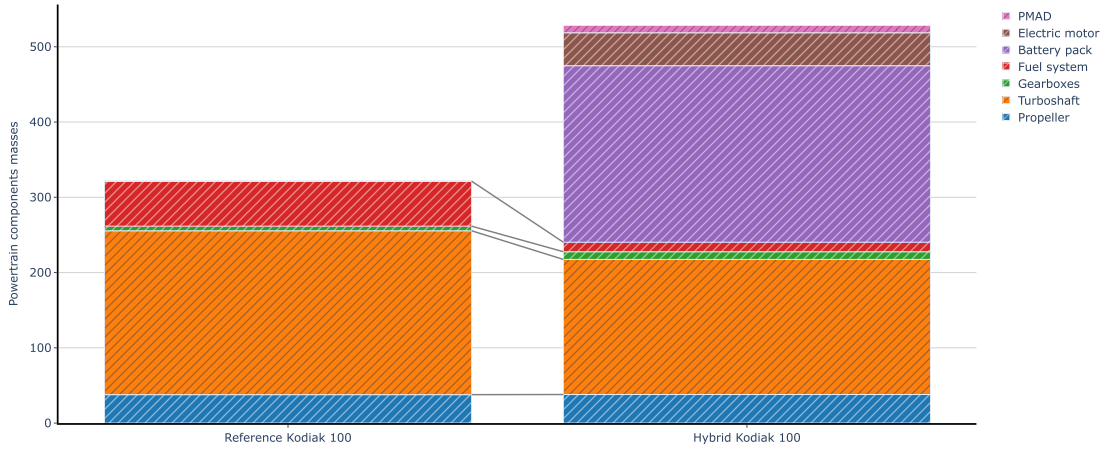

Figure 4.27 Evolution of the masses of the components of the powertrain between the Kodiak 100 and its hybrid retrofit.

SFC methods to accurately capture the benefits coming from the resizing of the engine. Indeed, a constant value for the SFC, which, for instance, could have been based on the SFC at T/O rating available in literature [243], would have led to severe underestimation of the fuel consumed. Indicatively, a time-averaged value of the SFC was plotted, and although this value can now reasonably be used for similar missions and similar engines, its computation requires knowledge of the performances of the final design, making it unusable for new configurations.

4.6 Level 4 aircraft

4.6.1 Identification of representative aircraft

For the final level of certification considered, the Cessna 208 will be investigated as, according to the analysis of the production data from the GAMA presented in Figure 4.18, it is the most produced Level 4 aircraft since 2006. More specifically, the Cessna 208B will be selected, even though a more powerful version of that airframe exists (like the Cessna Grand Caravan EX with a rated power of 867hp). One of the reasons for that choice is the availability of a POH online [11] ensuring reliable comparison for the baseline design. Additionally, it has seating capabilities that can reach up to 13 passengers in addition to the pilot. The final reason for that choice is the use of the Cessna 208B as a test platform to prove the feasibility of hybrid propulsion [12] and the associated cost savings [244]. On this test platform, named the Eco-Caravan concept, the original PT6A turboprop is meant to be replaced by a battery

[11] https://caravannation.com/208BG1000POH.pdf, Accessed: 01-09-2025
[12] https://www.ampaire.com/vehicles/eco-caravan, Accessed: 01-09-2025

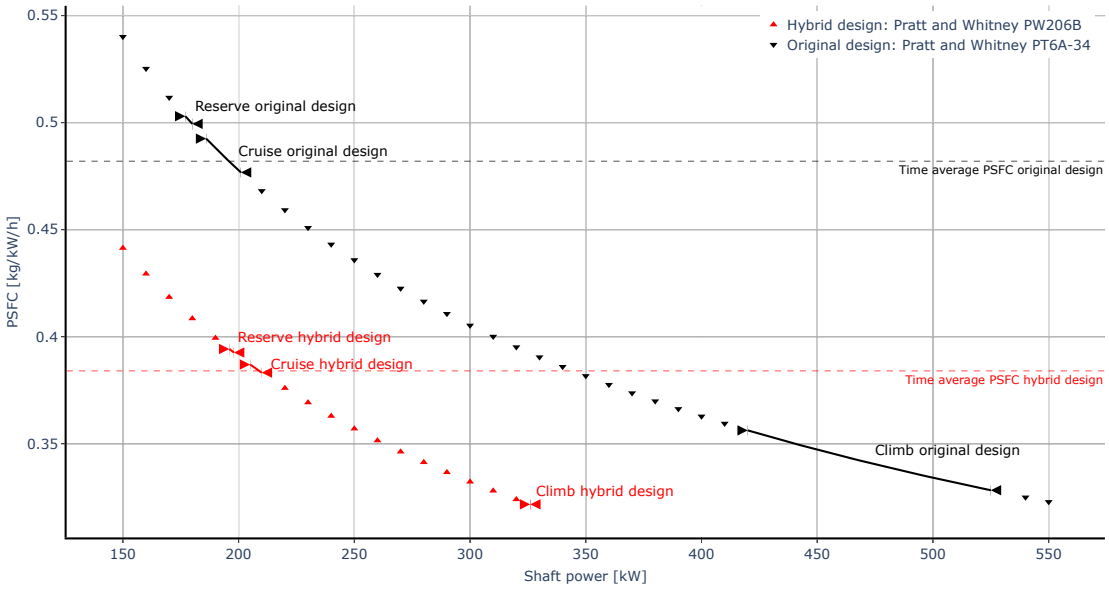

Figure 4.28 Variation of SFC and power demand for the turboshaft of the reference Kodiak 100 and its hybrid retrofit.

boosted piston engine with advertised fuel consumption gains of up to 70% thanks to the more efficient jet fuel powered piston engine [13]. Other aircraft like the DHC-6 Twin Otter or the Dornier Do228 were also considered because they were used as baselines for studies on the electrification of aviation, either in conceptual studies like the Do228 [77, 225] or as test beds like the DHC-6 [14]. In the end, however, only the Cessna 208B was retained as the representative for Level 4. The results of the sizing process of the reference configuration are discussed in Appendix C.5.

Aircraft usage

Similar to the Kodiak 100, the Cessna 208B is advertised as a multirole aircraft capable of conducting a wide variety of missions thanks to its rugged design and STOL (Short TakeOff and Landing) capabilities. It ranges from air surveillance to air ambulances, but is also primarily used for commuting activities. In the modified version of the OpenSky database that was used for this work, more than 100.000 flights were registered after filtering. It is worth noting here that, since aircraft are filtered based on their ICAO code, this number of flights includes all variants of the Cessna 208, not only the Cessna 208B. Additional filtering could have been done based on the tail numbers. However, as all variants share similar performances, this was deemed unnecessary. The repartition of these flights, as a function of the range of the mission performed, is presented in Figure 4.29. Results show that, while

[13] https://www.ampaire.com/amp-h570, Accessed: 02-09-2025
[14] https://www.ampaire.com/vehicles/eco-otter-aircraft, Accessed 01-09-2025

the aircraft can reach ranges north of 1000 nm, it is mostly used at ranges below 400 nm. Additionally, more than 90% of reported flights are below 200 nm, with that number going up to 98% for flights below 350 nm, showing consistency with the design range of the Eco-Caravan reported in literature [244].

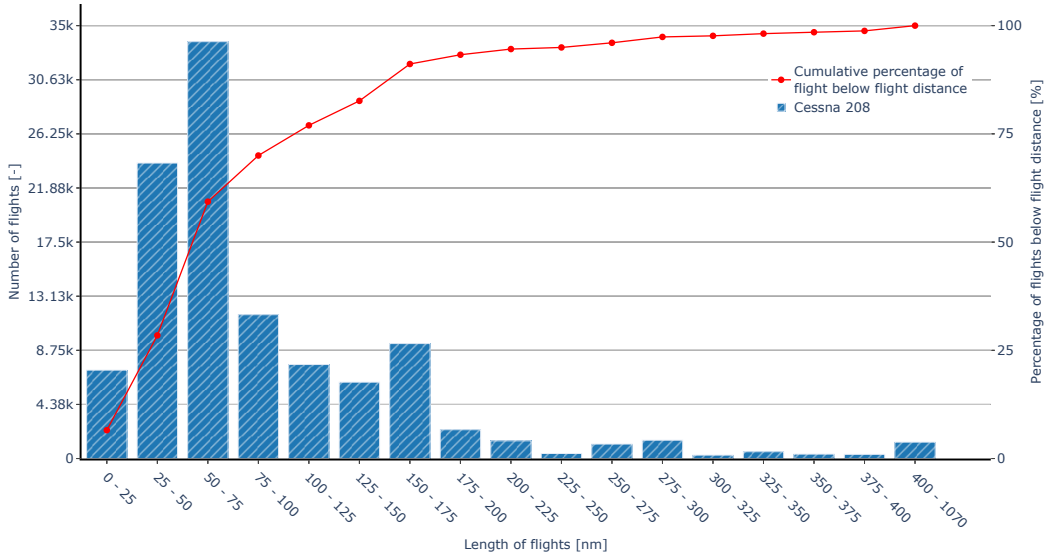

Figure 4.29 Distribution of flights for aircraft in the Cessna 208 Series.

Additional insights on the real-life use of the Cessna 208B were gained through a supplementary analysis of a database of Air Carrier Statistics in the U.S., similarly to other analyses reported in literature [245]. This database, provided by the Bureau of Transportation Statistics (BTS), contains data on domestic and international flights reported by U.S. air carriers. Since the Cessna 208B is, as already mentioned, primarily used for small commuting travels, only the domestic flights were investigated. The choice was made to only consider flights reported for the year 2025, which, as of the date of the writing of this thesis, contains the months of January to May. It is worth keeping in mind that, as this database only contains air carrier flights in the US, it might introduce small biases in the data. Nonetheless, data were still investigated, and good correlation with the data from the OpenSky database was found, with 92% of flights reported with a range of 200 nm or less and 99% of flights reported with a range of 350nm or less. Interestingly, the number of passengers on each route is also reported. Data reveal that the Cessna 208B is rarely used at full capacity, with an average of 3.4 passengers per flight. It also shows that the aircraft is used with at most 10 passengers. Based on these observations, the choice was made to select a range of 350 nm as the design range for the hybrid version that will be studied. Additionally, the performances of the obtained aircraft will be compared to the performances of the reference aircraft on that same

350 nm mission with a payload comprising 10 passengers and two pilots, rounded at 1150 kg.

4.6.2 Hybrid Cessna 208B

Case studies that have been conducted up until now, mainly those of the hSR22 and the hybrid Kodiak 100, as well as results stemming from literature [208], have shown that the hybridization scheme should be carefully considered. Indeed, and while the hSR22 was proven to be feasible considering a constant hybridization ratio throughout the mission, it led to situations where the weight penalty of the batteries rapidly outweighed the gains of changing the energy vector. More significant gains were achieved on the hybrid Kodiak 100, where the electric branch was used as a way to relieve design constraints and improve flight efficiency instead of decarbonizing the energy vector. For these reasons, and similarly to the case of the hybrid Kodiak 100 presented in Figure 4.25a, a parallel hybrid powertrain with a battery boosted thermal engine will be considered. Unlike the case of the Eco-Caravan presented in literature [244], however, the thermal machine will remain a turboprop. Results are thus expected to be similar to what was described in Section 4.5.3, but it will prove to be a valuable comparison point to further highlight the added degree of freedom introduced by electric propulsion. Two cases will be considered for this study: in the first one, the turboshaft will remain a PT6-114A as on the original design, and, in the second one, the thermal engine will be assumed to be resized to perfectly meet the design requirement from the mission and the choice of hybridization power. This should serve as additional proof that the most significant gains from hybrid propulsion come from its role as an enabler of thermal engine resizing. Similar to what was done on the hybrid Kodiak 100 case, a retrofit approach will be adopted. The constraint presented in Equation 4.3 will however be slightly altered so that a limit mass of 1150 kg, the payload for the reference aircraft on the off-design mission, will be allowed. The main differences in modeling assumptions retained for the investigation of the gains on the hybrid Cessna 208B are summarized in Table 4.17.

Preliminary runs were conducted to check whether or not, as was observed on the hybrid Kodiak 100, the reference Samsung INR18650-35E was adequate for this application. Results presented in the first column of Table 4.18 show that the sizing of the battery pack is driven by the constraint on the C-rate. Ulterior runs using another cell with a higher maximum C-rate (at the cost of a lower capacity) showed that overall, the latter was better suited.

To assess the effect of a variation of the threshold power on the performances of the hybrid design, multiple sizing processes were run with values of that power distributed through a feasible design space. The lower and upper bounds were selected based on an analysis of the propeller shaft power required on the design mission of the reference Cessna 208B presented in Appendix C.5. This showed that for cruise and reserve, approximately 285 kW were required with the selected flight profile. Based on the knowledge gained on the hSR22,

Table 4.17 Summary of the main modeling assumptions for the design investigation of the Cessna 208B.

Reference C208B (off-design)	Reference design (geometry, aerodynamics, masses, ...) Off-design range: 350nm Off-design payload: 1150kg Thermal powertrain Reference turboshaft (Design parameters fixed to ref values)
Hybrid C208B (no gas turbine resizing)	Retrofit (same geometry and masses as reference) Design range: 350nm Design payload: max. between 1150kg and limit given by Eq 4.3 Battery-boosted thermal engine Reference turboshaft (Design parameters fixed to ref values)
Hybrid C208B (gas turbine resized)	Retrofit (same geometry and masses as reference) Design range: 350nm Design payload: max. between 1150kg and limit given by Eq 4.3 Battery-boosted thermal engine Turboshaft resized according to max. mission values

Table 4.18 Active battery pack constraints for the hybrid C208.

Cell	**Parameter**	**Value**	**Constraint**
Samsung INR18650-35E	SOC_{min}	47%	>20%
	C-rate	$2.4h^{-1}$	$<2.4h^{-1}$
Battery pack mass: 322kg			
Samsung INR18650-25R	SOC_{min}	20%	>20%
	C-rate	$3.64h^{-1}$	$<8.0h^{-1}$
Battery pack mass: 258kg			

namely the rapid divergence of the battery mass when the energy constraint becomes active, only a few values below 282 kW were explored. For the upper bound of the design space, a value corresponding to the maximum climb power minus a certain margin was selected. For these reasons, only values between $\approx$ 60% and $\approx$ 85% of the original turboshaft's rated power will be explored. This ensures that the electric branch is used during the mission, ensuring that proper sizing of the component can be achieved, which prevented non plausible values from appearing in the residuals. For the comparison criteria, the emission factor was considered as it proved to be a reliable indicator to account for possible payload reductions in retrofit designs. The results of that design space exploration are shown in Figure 4.30.

The red markers, which represent the first aforementioned case, show that for values of the threshold power above 300 kW, corresponding to Zone 1.A in Figure 4.30, the mass of the powertrain is small enough that the original payload can be accommodated in the retrofit aircraft. This also means that in that first zone of the graph, the payload is not limited by the MTOM of the original design, and thus, the total mass of the hybrid design can increase.

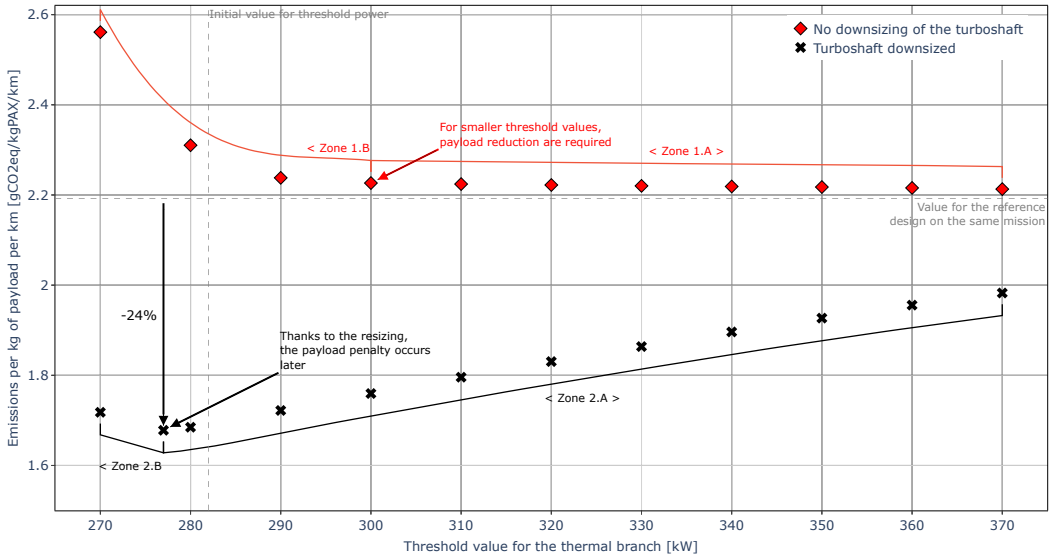

Figure 4.30 Influence of the hybridization threshold power on the emissions per kg of payload per km.

With decreasing values of the threshold power, and although the share of low-carbon energy vector increases, the added battery pack weight increases the overall energy use of the design more quickly, leading to slightly increased emissions. For values below 300 kW, however, in Zone 1.B, payload must be removed to accommodate the powertrain mass, and, as the EF is inversely proportional to the payload, there is a rapid deterioration of the score. Overall, the first case, where no resizing of the turboshaft is allowed, performs systematically worse than the original thermal design. However, when allowing for a redesign of the turboshaft, which corresponds to the black markers in Figure 4.30, a significant reduction in the total emission factor can be achieved. As discussed in Section 4.5.3, the downsizing of the thermal machine allows lighter powertrains and better fuel efficiencies during cruise and reserves, leading to lower mass penalties. As a result, the inflection point, which marks the separation between Zones 2.A and 2.B, is moved to an even lower share of thermal power, leading to reduced emissions. Once that inflection is passed, however, the same effect as on the red curve can be seen with a rapid increase in the EF in Zone 2.B. It is worth noting here that the inflection point, which marks the lowest emission factor, coincides with the point where payload starts needing to be reduced. All in all, results show that boosting the thermal machine to simply reduce the share of thermal power is not enough to significantly reduce emissions. The most significant gains come from the possibility of downsizing the turboshaft to allow it to operate at a more optimal throttle ratio, confirming known results from literature [13, 178, 242].

Remarks found in literature regarding the non-optimality of sizing the battery pack for power during takeoff and climb, resulting in leftover energy and a dead mass during other phases of the flight [178] prompted an investigation of the power profile for the case with

the optimal threshold power. The distribution of thermal and electric power, illustrated in Figure 4.31, shows that because the power required for reserve is slightly higher than that of cruise, the turboshaft alone does not provide enough power. As a result, the battery pack becomes sized to provide energy during the reserve, which was not the case for the initial run whose results were presented in Table 4.18, thus questioning the original choice of changing the battery cell. It is worth noting that this investigation on the active constraints on the battery sizing is made possible by the choice of models and the methodology implemented, which allows the quantification of state variables throughout the flight, which wouldn't have been possible with classic top-down density methods.

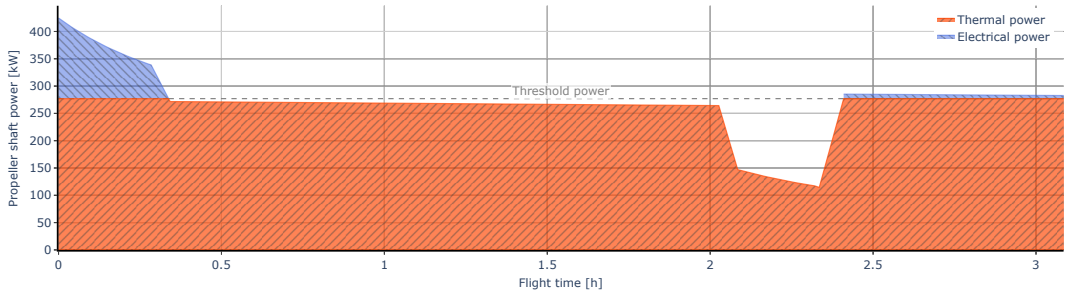

Figure 4.31 Power profile with each contributing source.

4.7 Conclusion and perspectives

Chapter summary

Utilizing the framework presented in Chapter 2 and the component models introduced in Chapter 3, this chapter was devoted to the validation of the methodology through the comparison of the results obtained with several known aircraft, both thermal and electric. This methodology was then used to investigate the benefits that could be obtained by leveraging the electrification of the powertrain and the potential synergies at aircraft level. A summary of all those cases is presented in Figure 4.32. Additionally, those investigations led to several conclusions that can be viewed through two lenses: a decarbonization lens and a methodological lens.

From a decarbonization perspective, the study of the configurations proposed for Level 1 and Level 2 showed that, when achievable, all-electric configurations had the potential to severely cut back the emissions of harmful pollutants from outdated piston engines. It additionally showed that when only small achievable ranges and payload were required, all-electric designs were preferable over hybrid designs, which yield only minor reductions in comparison. It additionally confirmed results from literature in that all electric configurations

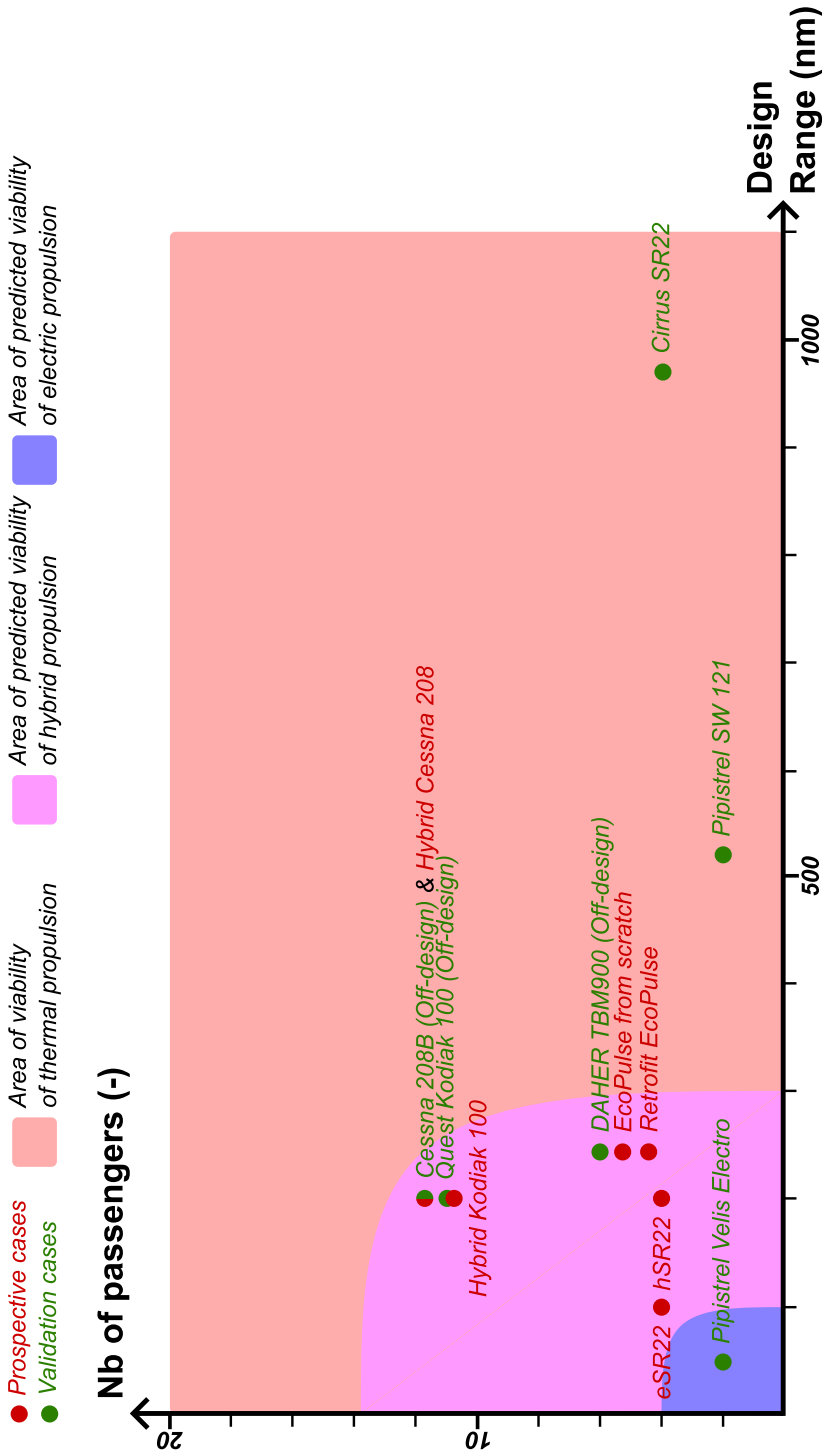

Figure 4.32 Summary of all the validation and prospective cases investigated in this Chapter.

were more energy efficient than their thermal counterparts. However, these test cases and in particular the eSR22 presented in Section 4.4.1 and 4.4.1, also showed that even considering a severe reduction in autonomy, an all-electric configuration for a 4-seater would not be possible until battery energy densities reach values forecasted for 2035.

Still, from a decarbonization perspective, the study performed with aircraft representative of the Levels 2, 3, and 4 of the CS-23 allowed to pinpoint the scenarios in which the hybridization of the propulsive architecture could be beneficial. First, from a feasibility point of view, the cases investigated showed that, while still penalized by the added mass of the electric branch, hybrid configurations were less sensitive to the mass and payload penalties highlighted for all electric configurations. Yet, the most important conclusion drawn from the analysis of those cases is the fact that using electric propulsion as a partial substitute for the energy vector is not the most beneficial use of electric propulsion; rather, it should be used to optimize the thermal branch. Indeed, the hybrid version of the Level 2 and 4 aircraft showed that replacing highly energy-dense aviation fuel with batteries led to weight penalties that, overall, increased the energy use of the aircraft. This penalty could however be offset by higher energy density batteries, but in those cases, all-electric configurations are preferable. On the other hand, the studies performed for Level 3 and 4 aircraft showed that when electrified propulsion is used to relieve design constraints on the thermal branch, with a battery-boosted thermal engine, for instance, it yielded the biggest improvement in terms of energy efficiency and emissions reduction. Some potentials in terms of structural and aerodynamic synergies were also found, but, beyond the weight penalties from distributing propulsive elements, the question of the certifiability of those configurations should be raised. Further analysis into the hybrid version of the Level 2, 3, and 4 aircraft however reveal that not all configurations are best suited for hybridization. Indeed, the biggest gains were found on the configurations and flight profiles for which there were inefficiencies in the original designs. For the Kodiak 100, for instance, gains were only achievable because there was such a big margin between the power the turboshaft was being used at and its rated power. For the Cirrus SR22, on the other hand, as the aircraft is already used at near maximum power during cruise, there is not much room for improvement. An additional conclusion that can be drawn from those analyses is that the optimal electrification scenario highly depends on the planned use of the aircraft. Indeed, not only might electrified powertrains reduce the achievable ranges, but mostly, they will yield the biggest gains when there are significant differences between design conditions and typical use cases. This all advocates for the inclusion of operational constraints directly in the design phase.

From a methodological point-of-view, this chapter confirmed the necessity for an integrated framework and its role as a key enabler in the rise of electric and hybrid aircraft. This was in particular demonstrated through the case of the EcoPulse-like aircraft with a resized wing. This case study showed that including the cross-disciplinary synergies, more specifically the interactions between aerodynamics, structures, and propulsion, could lead to significant

gains at aircraft level. This case study also showed the importance of considering the broader scope of the whole vehicle. Indeed, despite the gains from an aerodynamic and structural point of view, the evaluation of the performances at aircraft level showed overall increased fuel consumption. Additionally, this chapter, and in particular the study on the Level 4 aircraft and the Kodiak 100, reinforced the need for medium fidelity methods. More specifically, these studies showed that the most significant reduction in fuel consumption stemmed from effects that could not be captured by top-down methods.

Perspectives

Although this chapter highlighted the potential for significant reduction in terms of the release of harmful pollutants, and as pointed out in the conclusion of Chapter 2 and 3, the absence of models for the sizing and the evaluation of the impacts in terms of drag, weight and power consumption of the TMS is likely to mitigate those results. Literature shows that, when retrofitting aircraft with electrified powertrains, the TMS could increase the emissions per passenger and per kilometer by up to 27% [178]. Therefore, the computation of the impacts at aircraft level of the TMS, as well as the tradeoff in terms of component performances and lifespan, is considered a major avenue of improvement for this work.

Further analysis of the figure summarizing the test cases investigated in this chapter, Figure 4.32, also shows a lack of investigations of configurations at the edge of the CS-23 in terms of passengers. As such, this work could be rendered more exhaustive with the addition of several additional test cases in this area. The amplitude of the gains on the hybridized Cessna 208B, however, hints at the limited gains that can be attained with high payload configurations. These configurations, at the border with CS-25, could instead be improved through the additional electrification of non-propulsive functions. Indeed, given the increased power on board and knowing the impacts of the extraction of bleed air on turboprop's performances, the modeling of auxiliary systems appears as a worthwhile endeavor. This is especially interesting given the high modularity adopted in this framework and the residuals-based approach of the load flow analysis method, which would enable the co-design of propulsive and non-propulsive architectures.

The next chapter will set out to extend the scope of the analysis presented in this chapter by including the effects induced by the use of aircraft over its whole lifespan and considering impacts beyond the mere impacts on climate change of the use phase. This will be done by integrating, into the analysis method presented and used up until here, a module capable of automatically performing a Life Cycle Assessment (LCA).

Part III

Design under environmental life cycle considerations

Abstract

The third part of this manuscript proposes to extend the scope of the preliminary analysis conducted in Part II, by extending the methodology to cover all the impacts induced by the use of General Aviation aircraft. In particular, Chapter 5 proposes an adaptation of a Life Cycle Assessment (LCA) method for tight integration inside the already presented design process. This implementation will then be used to study the sensitivity of the environmental impacts to several design variables, highlighting effects that cannot be captured with traditional uses of LCA methods in the realm of the aeronautics sector.

Author's contribution

Journal paper

Pollet, Félix, et al. "A generic life cycle assessment tool for overall aircraft design." Applied Energy 399 (2025): 126514.

Workshop contribution

Lutz, Florent, et al. "Implementation of LCA models in OAD for hybrid-electric aircraft design." 4th European Workshop on MDO for Industrial Applications in Aeronautics, Toulouse, France. 2025

Chapter 5

Life Cycle Analysis

Contents

5.1 Introduction and context **131**
5.2 LCA **133**
5.3 Review of LCA use cases in the aviation sector **135**
5.3.1 Review of representative products in LCA applications 135
5.3.2 Integration into the design process 138
5.4 Application to the LCA of electrified General Aviation aircraft **140**
5.5 Application of the LCA methodology for the design of electrified aircraft . **147**
5.5.1 From CO2 emissions to Life Cycle impacts 147
5.5.2 Influence of cell chemistry choice on environmental impacts . . . 159
5.5.3 Effect of change in airframe materials 165
5.5.4 Effect of battery aging 171
5.6 Application of the LCA for the assessment of future aircraft configurations **183**
5.7 Conclusion and perspectives **191**

5.1 Introduction and context

THE previous chapter has demonstrated the capabilities of the newly developed framework to assess the design and performances of hybrid and all-electric aircraft. It was used to study prospective scenarios for the electrification of the propulsion of the different certification levels of the CS-23. With particular focus on the emissions, it was shown that for smaller aircraft, less than six passengers, all-electric designs could be achieved with today's or near-future technologies. For aircraft with more payload, hybrid powertrains were shown to be more beneficial, mostly thanks to the added degrees of freedom they introduce. These investigations, however, like many other found in literature [177, 178, 208], focused only on one stage of the life of the aircraft, its use (or operational) phase, and only on one particular impact the aircraft can have on the environment, its effect on climate change. While an

analysis of the equivalent CO_2 effect of a system can be a fair first approximation [246], especially in the transportation sector, the impact of very important processes can be obscured as a result, like the production of the components, the construction of the infrastructure, or the end of life of the system [247]. As such, focusing on the carbon intensity of the use phase is not sufficient [234], especially for new energy vectors which tend to shift impacts to other stages of the aircraft life and other categories of impacts [248].

A holistic approach, capable of comparing designs with different architectures across their whole life and in an exhaustive number of category thus appears as being of particular interest to serve as a comprehensive tool to guide the decision-making process for new propulsive architectures. Notably, Life Cycle Assessment (LCA) is a standardized multi-stage and multi-criteria methodology that has been proposed in literature as a way to compare new designs. In recent years, that methodology and its applications to electrified propulsion have been gaining more traction in literature [110, 227, 249], which advocates that a comprehensive analysis of the sustainability of those new concepts could be done using LCA [250]. Additionally, given the significant time and research required for the development of these new technologies, rigorous assessment of the impacts on the environment becomes mandatory [251]. Moreover, this approach allows to identify and avoid burden shifts [252, 253] typically associated with electric technologies that have low impacts during the use phase but require lots of rare materials and have expensive production processes. PMSM motors, for instance, require rare earth metals for the construction of the permanent magnets [254]. The same goes for the semiconductors required in the power electronics, like inverters, rectifiers, or DC/DC converters, and, of course, for the Lithium used in Li-ion batteries [255]. A rapid overview of the processes involved in the production of an electric aircraft is presented in Figure 5.1. A more detailed representation of its adaptation as part of this framework is shown in Figure 5.7.

LCA is especially interesting in the case of hybrid-electric configurations because, as it is, as of now, still at the prototype stage, designs are not yet frozen. Integrating such methodologies directly in the design process thus appears as a worthwhile endeavor to better guide that process for more sustainable aircraft [109, 234, 248]. More broadly speaking, integrating life cycle considerations earlier in the design process of novel and conventional configurations alike is a strategic challenge given the current trends in the aeronautics sector. The European Union, for instance, has edited a series of rules for various products and sectors called Product Environmental Footprint Category Rules (PEFCR), including, as of recently, drones and the space sector. This initiative was made in an effort to create "a consistent method to assess environmental impacts of products, processes, and services" and enable "informed decisions, better data sharing, more competitive, and a sustainability-driven market". More generally speaking, EASA, which has historically been tasked with implementing safety rules, is now being tasked with also enforcing rules regarding the protection of the environment [256].

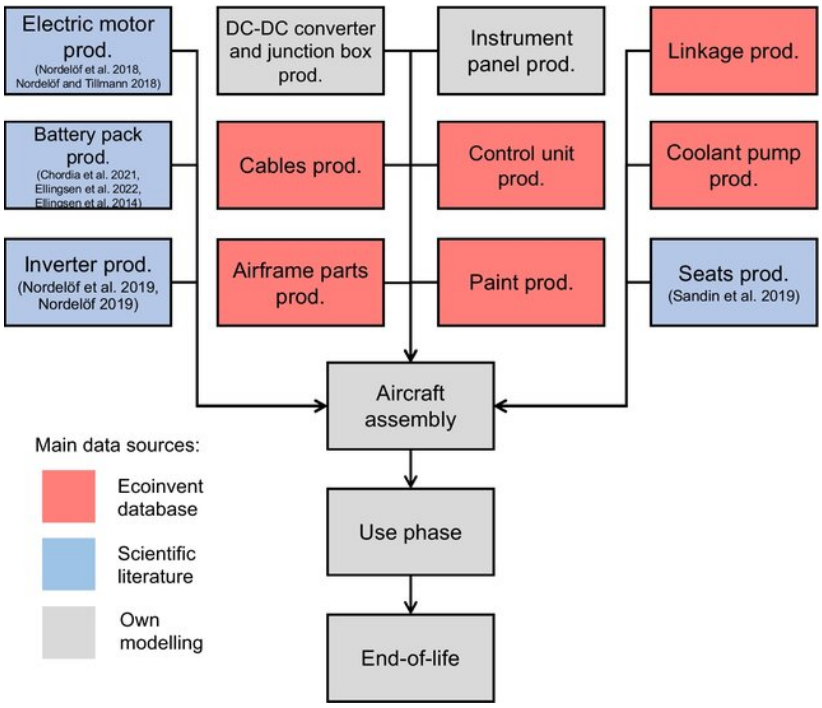

Figure 5.1 Flowchart providing an overview of the life cycle of the two-seater all-electric aircraft [227].

Given the criticality of design choices on the impacts of the final product, integrating LCA in the preliminary design phase will undoubtedly become the norm for future configurations.

This chapter aims to highlight the methodological benefits of the integration of environmental considerations in the framework. First, a review of the LCA methodology and a state-of-the-art of its utilization in the aeronautics sector will be done. Gaps in the methodologies and the lack of applications specific to hybrid and all-electric configurations will then be identified. Common hypotheses made in literature will then be reviewed to establish the assumptions to be made to enable the assessment of an electrified powertrain. Finally, the integration of the LCA module in the sizing process will be used to challenge results presented in Chapter 4, provide a reference case for hybrid-electric light aircraft, and highlight new drivers in the design of electric components.

5.2 LCA

Life Cycle Assessment is a standardized methodology that allows the assessment of the impacts of a system throughout the value chain [42] and whose principle and framework are defined by the International Organization for Standardization (ISO) in Standard 14040:2006 [257] and Standard 14044:2006 [258]. It is defined as the evaluation of the impacts of a product or system with respect to a reference function by considering the entirety of its life

cycle. It is thus a multi-stage, from cradle to grave, and multi-criteria, as it not only considers the impact on climate change but also other impacts like the depletion of resources. This thus enables comparison with different products performing the same function, but also to identify hotspots in the various stages of the life of a product [246]. An LCA is performed in four steps [246, 248, 259]:

1. **The definition of the system, scope, and goals for the analysis:** This step defines what the purpose of the LCA is (as a post-processing tool, for ecodesign, etc) and to whom it is destined. It is also in this step that the functional unit, a qualification of the function based on which the system is evaluated, is defined, along with the evaluation of the reference flow, or how much of the system is required to perform that function. In the aeronautics sector, "the transportation of one revenue passenger in a safe way over one kilometer" or "flying one hour" are commonly used. Finally, the boundaries of the system are defined to identify which contributing processes will be considered under the scope of the LCA.

2. **The inventory of emissions and extractions:** Based on the reference flow and scope defined in the first step, an inventory of all elementary exchanges with the biosphere, be they emissions or extractions, is then created. The question of data accessibility is paramount to this step for two reasons. First, manufacturers control only design parameters within their scope, and cannot act on other processes, such as the production materials or electricity. Second, the quantity of data and knowledge required to access elementary exchanges with the biosphere is colossal. In practice, databases aggregating existing processes are used to simplify this step.

3. **The analysis of the impacts:** This step consist in quantifying the effect on the environment of the emissions and extractions identified in step 2. This is done using Life Cycle Impact Assessment (LCIA) methods that model how each species damages the environment and through which pathway. Following current practice in literature, the ReCiPe2016 method and the Environmental Footprint (EF) methods will be used. To make data more interpretable, optional steps like normalization (comparing results to a reference system) and weighting (assigning relative importance to categories) can be used.

4. **The interpretation:** The fourth and final step of the LCA is the interpretation. This step involves analyzing the previously obtained results to formulate recommendations on environmental hotspots, support decision-making, and allow prioritization. Analysis of the dependency on data quality is also recommended for reliability.

These steps are highlighted in Figure 5.2 and are further detailed in Appendix D.1. In particular, common modeling assumptions found in literature when dealing with aircraft or aircraft parts are discussed. It is worth noting that even if LCA is still in relatively nascent

stages of its life, many initiatives are driving its adoption to promote eco-design of new products, such as the PEFCR for drones and eVTOL. A draft of the PEFCR applied to aircraft was made available to the public, but it has since been removed for review. It will still be occasionally referred to, as it proposes guidelines to enable fairer comparison of different aircraft designs.

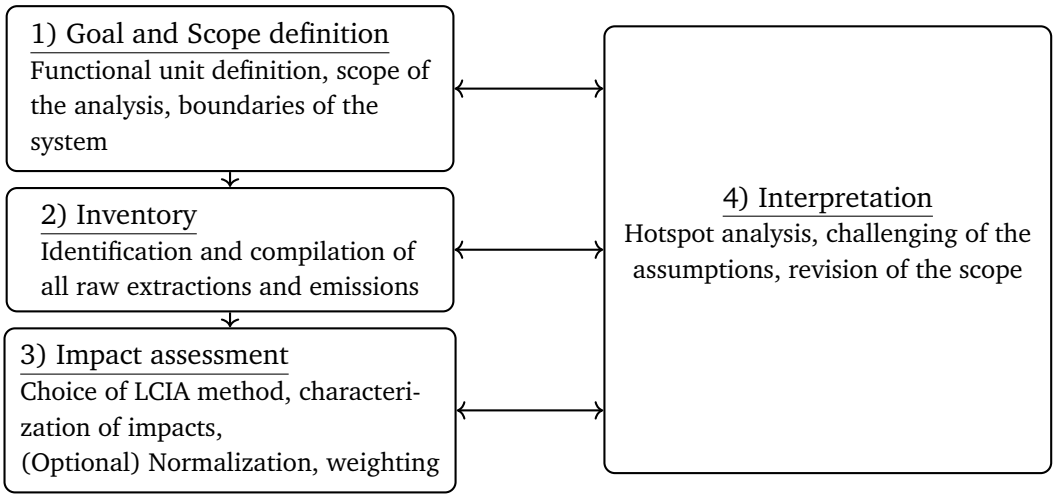

Figure 5.2 Phases of LCA, adapted from [246].

5.3 Review of LCA use cases in the aviation sector

While the previous section offered a general description of the LCA methodology, with a more detailed breakdown of the steps involved and choices required available in Appendix D.1, common practices for its application in the aeronautics sector were also briefly discussed. It was highlighted that, while LCA is still fairly new, its use is becoming increasingly popular as an answer to the growing need for tools capable of assessing the sustainability of future systems across their whole life cycle. Thus, a review of the literature pertaining to the use of LCA in aviation was conducted to identify current gaps in its use for electrified propulsion.

5.3.1 Review of representative products in LCA applications

As mentioned in the introductory section of this chapter, an analysis focusing on the CO_2 emissions is often a fair first approach to estimating the biggest contributor to the environmental impacts of a system. Based on this observation, and based on the consideration that commercial transport and freighter activities represent more than 90% of all CO_2 emissions of the global aviation sector [172], it is easy to understand why those types of aircraft are popular representatives in LCA studies in the sector of aviation. Indeed, many applications from literature have been found to deal with the analysis of the impacts of regional to wide-body

aircraft. For example, in the draft of the PEFCR, a reference product is proposed to serve as a baseline for comparison with future LCA applications. This reference, which was created as a virtual mean of different models of aircraft based on market shares, is composed of more than 95% of regional jets, single aisle, and wide body aircraft. More specifically, the share of single-aisle aircraft in the representative product is evaluated at more than 2/3. This seems to be confirmed by the large number of scientific papers focusing on single aisle aircraft [81, 110, 124, 259–261]. Bigger aircraft have also been studied with carrying capacities of up to 190 passengers in some cases [81, 252]. Regional aircraft also seem to be of particular interest because, like General Aviation, they appear as a stepping stone for the widespread introduction of more electric propulsion chains in the aviation sector. For instance, inventories applicable to assess hybrid electric ATR-type turboprop have been proposed in literature [251]. Similarly, hybrid configurations representative of the regional turboprop segment have been studied with particular focus on the LTO cycle [207]. As a significant share of emissions also stems from the transportation of freight using aircraft, some applications on that topic have also been found [262]. Other studies with a different scope have also been reviewed. It is indeed not uncommon to find studies focusing on specific sub-parts of the aircraft, such as turbine blades [263], elevators [123], trolleys, or interior panels. On the opposite end of the spectrum, studies have been undertaken to assess the impacts with a scope spanning the whole aeronautics sector [264, 265].

Incidentally, the number of analyses on the impacts of General Aviation aircraft is much smaller. Even though General Aviation as a category encompasses a broad array of usage as discussed in Chapter 4, it represents a relatively small share of the aviation market as indicated by the mere 1% share of the representative aircraft of the PEFCR that account for all General Aviation. For similar reasons and because of the trend in the electrification of aircraft, for which small regional aircraft appear as an upper limit of feasibility, very few studies have been found for configurations with an electrified powertrain. An article from the early 2020's reported that "the literature on sustainability assessment of electric aircraft is relatively scarce. Only two studies undertake analyses of electric propulsion of aircraft" [249]. Even a few years later, a review paper from 2023 [247] noted that only 4 out of 23 reviewed papers focused on hybrid and all-electric aircraft, reinforced by the observation that "studies comparing conventional and electric aircraft for short-haul flights considering different fuel options are scarce" [266]. Still, existing case studies reveal interesting insights into the impacts of electrified powertrain, including the effect of the hybridization of an A320-like [208] or the environmental damages of an all-electric 190 PAX aircraft [252] called the Ce-Liner. Both studies, however, use very aggressive assumptions on the battery energy density, not representative of current technologies. Other studies include the assessment of the hybridization of a range of aircraft covering multiple categories, going from a Boeing 777-like aircraft to a Cirrus SR-22-type aircraft [81]. A framework for comparing conventional-fueled aircraft with new energy sources has also been proposed [267], but, to date, its use is limited

to the evaluation of alternative fuels. Finally, the comparison of two versions, a full-thermal and a full-electric light aircraft, revealed deeper insights into a complete change of energy vector than a simple CO_2 emissions assessment [227].

As for applications dealing with lighter aircraft, studies have been conducted on a Piper Archer [268], a Cessna 172 [269], and on a Pipistrel Alpha Trainer [227]. They however revealed mostly the same conclusions as LCA performed on bigger aircraft, which is that most impacts stem from the production and the combustion of the fuel. Indeed, for conventional designs, most of the impacts are linked to the emissions released by the use of the fuel in the thermal machines and its production process. Consequently, the most impactful stage of the life cycle of conventional aircraft is the usage phase, which is reinforced by the high intensity of the usage of commercial aircraft, therefore making the other phases proportionally smaller. Figures reported in the literature show that the operation phase can account for up to 99.8 % of the weighted impacts [248, 249, 261, 265]. Even when looking at impact category by impact category, the average contribution of the operation phase can be as high as 77% [249]. Even when considering the ground infrastructure, which is a major contributor across multiple categories, once normalized and weighed, fuel has the biggest impact, primarily because of its impact on climate change. Because of this overwhelming presence of the impacts of fuel across multiple categories, it is not uncommon to find in literature that, to simplify the analysis, strong assumptions are made on phases other than the operational phases [259], which can go as far as only focusing on the operational phase [266]. Similarly, because fuel production and combustion were found to have the biggest impacts, studies are frequently focusing on the fuel production and combustion process itself [266, 267, 270, 271], investigating solutions like SAF, which are more virtuous when considering their whole life cycle. For these reasons, and to enable clearer assessment of other life cycle phases, the PEFCR for aircraft recommends presenting results with and without the use phase. This observation seems to be holding even for hybrid designs, where, in the case of a hybrid A320, fuel production and combustion accounted for 94% of total impacts [208]. The general conclusion is that, for conventional designs, and because the operation phase is so preponderant when compared to all other phases, any implemented measure that allows to reduced fuel consumption, even at the cost of shifts to other categories, is profitable. This conclusion is supported by literature, where most papers investigated were focusing solely on the energy efficiency of the aircraft [247]. It is also for this reason that composite materials, despite their very impactful production stage, are found to have a positive effect on the overall impacts of the aircraft [253].

Yet, that status quo is very likely to change with the advent of low-carbon energy vectors like SAF, but also because of the zero in-flight emissions enabled by the use of batteries. By virtue of proportionality, other phases will become more important to the point of going from a share of around 1% to a tenth of the total impacts [272]. The introduction of these new sources of energy is thus predicted to move the burden away from the operation phase

[248, 250]. It is especially true in the case of all-electric aircraft, as battery production is an intensive process that might cause a major shift in the impacts to the production phase [249]. Additionally, General Aviation aircraft are typically used way less intensively than their commercial counterpart making the damping of the production phase less strong, thus increasing its relative contribution. This, plus the fact that General Aviation aircraft will be early adopters of electrified powertrains, makes a comprehensive assessment of their impacts particularly interesting, especially given the scarcity of results in literature.

5.3.2 Integration into the design process

As already highlighted, LCA has started to become increasingly present in the assessment of novel configurations, although very often with a strong focus on the life cycle of the fuel and the operation phase of the aircraft. For this reason, the effort put into the modeling of the aircraft and its production phase is often minimal, with a common approach consisting in reusing and adapting existing process of the ecoinvent database [110] (in particular the *aircraft production, passenger aircraft* process). Similarly, it is not uncommon to see the bill of materials being established based on the aircraft's empty mass and the share of materials taken from a common reference aircraft. Some studies have also been conducted using the precise mass breakdown obtained thanks to direct collaboration with manufacturers [227] or by extracting data for one aircraft from various individual studies [253], which, while enabling accurate assessment of the impacts of one aircraft, does not allow prospective studies on other configurations. Alternatively, when precise data are not available, some studies have proposed the use of retro-engineered data from manufacturers or airlines to estimate energy use and adapt it, often with strong simplifying assumptions, to new energy sources [42, 266]. In those cases, where an extensive amount of data is available, professional LCA software are often used to handle the compiled inventory of emissions and extractions, including OpenLCA [110], SimaPro [81, 253], or Gabi 9.2.1 [42].

This approach, however, and in particular the use of external software, echoes an issue which was raised in Chapter 2 in that interfacing with design tools cannot be automated and that there is a risk of information loss at the interface. This issue has been raised in literature, and there are strong recommendations to address the integration of LCA in preliminary design tools [109, 110, 248, 249, 273]. Although it has been identified as a key issue for the assessment of the sustainability of new configurations [249], and even though preliminary efforts have been made, studies with exhaustive and comprehensive integration of an LCA module into an OAD tool are scarce. At the forefront of this effort, Johanning and Scholz [248] proposed a method that connects impacts across the life cycle of the aircraft to a dozen design variables, enabling a "first step towards the integration of LCA in aircraft design". This method has since been reused and extended [124, 260, 273]. Similarly, a spreadsheet-based tool named qUWick has been developed to rapidly assess the impacts of aircraft in the early

design phases to integrate it into a broader OAD framework [274]. Other approaches for integrating LCA in conceptual OAD frameworks have been proposed [208, 262], but the minimal representation of the aircraft and limited exchange of variables have been identified as key issues that could potentially introduce wide uncertainties in the LCA results [234]. Even when the integration of LCA tools is more extensive [81, 110], the time required to compile inventories and impacts is often prohibitive, relegating the LCA to a post-processing tool to evaluate a configuration optimized for other criteria.

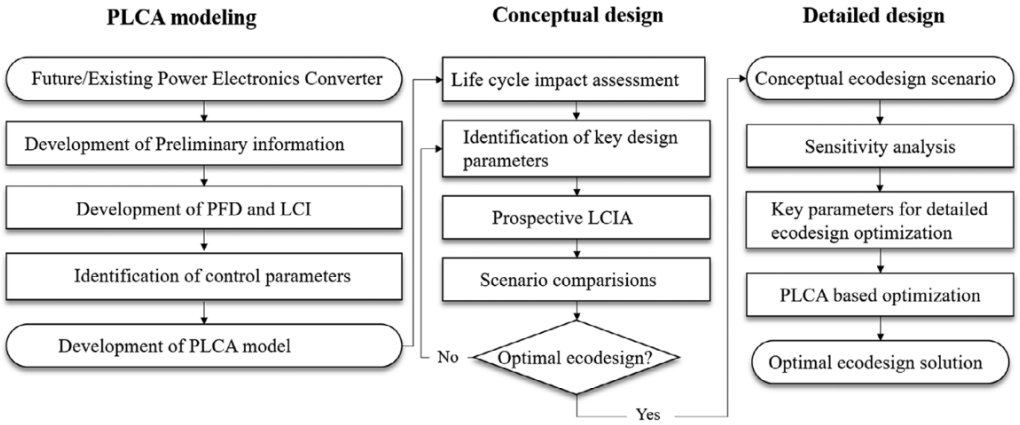

Figure 5.3 Framework of parametric life cycle assessment (PLCA) based ecodesign process for power electronic. [275].

While strictly speaking not dealing with aircraft, some noteworthy studies have been found that detail methodologies capable of minimizing the impacts of a product by challenging design variables. Fang et al. present a study on the minimization of the environmental impacts of a power electronic module [275]. The approach developed is based on the observation that, once the LCIA method has been chosen, the functions computing the impacts are essentially linear with respect to the design parameters. For instance, the impacts of x kg of controllers and y of connectors are the same as x times the impacts of one kg of controllers, and y times the impacts of one kg of connectors. This method, called Parametric Life Cycle Assessment (PLCA) and described in Figure 5.3, is essentially based on the compilation of parametric LCA functions ahead of the design process. These functions can then be reused during the design. This approach, based on creating upstream surrogates for the impact assessment [234], enables to overcome the limitations that have been identified for the use of LCA beyond simple post-processing evaluations. In its current state, however, it requires knowledge of power electronics and doesn't seem to apply to different architectures. To overcome this last problem, a modular framework has been developed to enable pre-compilation of impacts based on a user-defined configuration file, thereby allowing customization depending on aircraft architecture but also aircraft type [276]. This framework, which is itself based on the `brightway2` Python package [277] and which has been used in conjunction with FAST-OAD,

is called `lca-modeller`. Another point of interest is the fact that it has been used to evaluate the impacts of aircraft ranging from a drone to a commercial aircraft. Remarkably, as this method relies on pre-compiled symbolic functions, they enable analytic differentiation, which, as discussed in Chapter 2, is essential given the high number of design variables and objective functions.

All in all, a review of literature revealed that methodologies tightly integrating a comprehensive assessment of the impacts of new General Aviation configurations with electrified powertrains are scarce. This stems from both a clear disinterest in phases other than the operation phase, as it accounts for an overwhelming majority of impacts, and a methodological lack of interfacing between OAD and LCA tools. However, because of the introduction of new energy sources with lower emissions in the use phase and more impacts in the production phase, the former is expected to change drastically. For the second stopping point, a modular framework capable of being adapted to fit in the same ecosystem as the FAST-OAD-CS23-HE framework has been identified as a key enabler. In addition to strong cues as to its compatibility with the framework developed here, it adopts a similar modular approach through a user input configuration file, allowing customization of the content of the LCA, similarly to how the architecture of the powertrain can be configured. The implementation and the assumptions that will be made for the environmental impact assessment of hybrid and all-electric aircraft will be discussed in the next section.

5.4 Application to the LCA of electrified General Aviation aircraft

As discussed in the previous section, the `lca-modeller` package will be used for the assessment of the environmental impacts of the General Aviation aircraft sized by the FAST-OAD-CS23-HE framework. The primary feature of the `lca-modeller` framework is its ability to generate, from a user-defined configuration file specifying the structure of the LCA model, a set of algebraic functions representing the impacts of the configuration. These functions, called *lambdas* and generated by the `lca-algebraic` package [278], can then be evaluated using the foreground parameters generated by the OAD module. The ecoinvent database will also be leveraged to speed up the inventory compilation process. To proceed further, it is thus necessary to list the processes that will be considered and that are available in ecoinvent as well as assess the foreground parameters, which in essence consist in the first step of any LCA as described in the introductory part of the chapter.

Goal and scope definition

For the upcoming studies, and as opposed to what was discussed in the section on the literature review, the LCA here will be used as a tool to evaluate prospective electrified aircraft, guide the design of new configurations, and challenge architectural choices on

existing configurations. For the choice of the functional unit, and given the wide variety of missions performed by General Aviation aircraft, two functional units will be considered, depending on the aircraft. For trainer aircraft, the unit "flying one hour" will be considered. For private planes and commuters, whose function is to transport passengers over a certain distance, the "safe transportation of one revenue passenger over one kilometer" was initially considered. However, given the possible reductions in payload for the retrofit configuration investigated in Chapter 4, a derivative, the "safe transportation of 85 kg of payload over one kilometer" was retained instead. The weighting of all sub-processes contributing to the functional unit, in other word "how many" flights and "how much" aircraft are necessary to fulfill that functional unit, will be assessed based on the performances of the aircraft under consideration on a representative mission. That mission, which will either be a design or an off-design mission, will depend on the aircraft and will be specified for each study.

For the boundaries of the system, based on the recommendation of the PEFCR and the review of literature [110, 247], the use phase of the aircraft will be considered, as well as its production. For the use phase, the production of the energy, be it fuel or electricity, as well as its use during the mission, i.e., the emissions or lack thereof, will be included. Other processes linked to the accommodation of passengers will not be included as they are specific to commercial aviation. The production of the aircraft will encompass everything, ranging from the extraction of raw materials and their processing to the delivery of the aircraft to the final user, including the aircraft assembly and the testing of the aircraft. The distribution of materials to the assembly plant, as well as the construction of the assembly plant, will, however, not be considered. The End of Life (EoL) of the aircraft, as well as the impacts of infrastructures, will also not be included. For the former, literature has shown that not only were available data sparse for aircraft [247, 252, 259], but it was also the case for sub-components, especially batteries [208] and power electronics [275], which can sometimes be reused or have second lives. For the latter, General Aviation aircraft are typically operated on small airfields with grass or dirt runways and without passenger terminals and the associated energy needs. A summary of the boundaries of the system that will be considered, adapted from the PEFCR for aircraft, is shown in Figure 5.4.

Extraction and Emission Inventory

For the compilation of the elementary extractions and emissions, the capabilities of the `brightway2` framework, upon which `lca-modeller` is built, will be leveraged. The way `brightway2` works is that, rather than aggregating the inventories of all processes known in ecoinvent and then inverting the potentially massive matrix, it computes the impacts for each process and aggregates those instead based on the weights of the process tree. Consequently, it is only required to expand the process tree in such a way that the termination of the branches are ecoinvent process. For the production of the wings, fuselage, and tail planes,

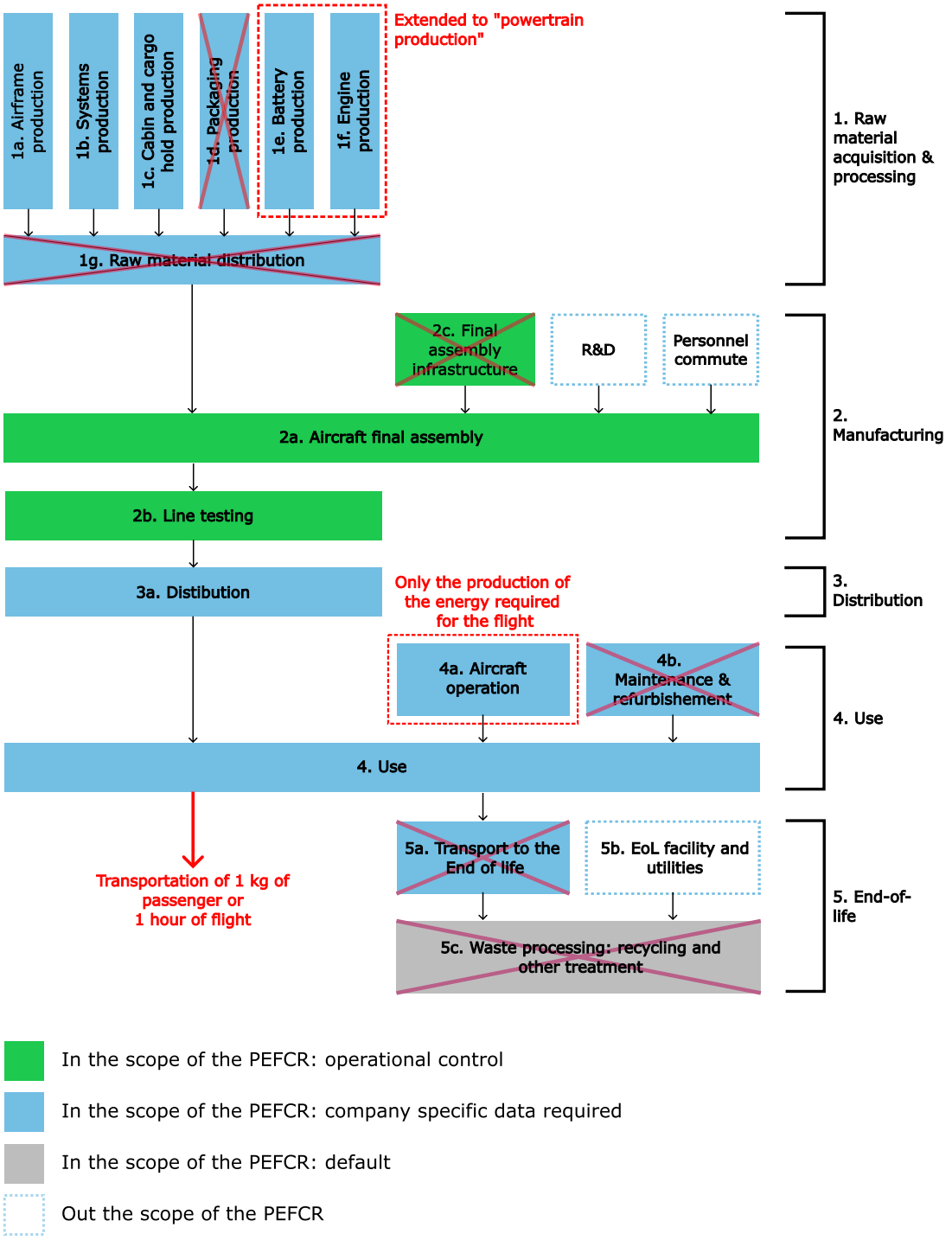

Figure 5.4 Boundaries for the LCA study of electrified General Aviation Aircraft, adapted from the initial draft of the PEFCR for aircraft.

they will be assumed to be made of a single material, which, depending on the aircraft under study, will be made of either Carbon Fiber Reinforced Plastics (CFRP) or aluminum. For the

flight controls, aluminum will also be assumed, while for the landing gear, it will be assumed to be made of steel. For those parts, since their mass is individually computed by the OAD modules from FAST-OAD_CS23, the weight on their branch in the process tree will be known. The process of shaping those materials into their final form, however, does not come without losses. Indeed, because of the production processes, there are some losses that must be considered in the LCA. These losses are commonly represented by a Buy-to-Fly (BtF) ratio that represents the ratio of the mass of material that must be purchased, or in that case produced, to the mass of the final part. This ratio, which is crucial to consider in LCA [247], depends a lot on the materials, with values that can range between 1 and 2 for composite materials to between 5 and 10 for metallic materials [253, 274, 279]. Another aspect that could have been considered is the fact that metal scraps are much easier to recycle. This, however, will not be accounted for in the model. The emissions and extraction associated with the assembly of the aircraft will also be considered. For simplicity and because of a relative lack of data on the processes of each General Aviation aircraft manufacturer, values reported in literature for the energy requirement and emissions of Volatile Organic Compounds (VOC) for a Pipistrel Alpha Electro will be used and scaled based on the aircraft's empty mass.

Other factors that are important when computing the impacts of the production of the aircraft are its expected lifespan and use. Indeed, it will dictate the number of times the aircraft will perform its design function during its life, thus affecting the weight of the production process [274]. It is also a crucial piece of data as it will allow to compute how many times certain components of the aircraft that need renewal will be built. It is especially the case for hybrid- or all-electric aircraft, for which it is predicted that longer lifetime will lead to the need for more battery replacement [227]. For commercial transport aircraft, literature reports values that range between 20 and 30 years with almost daily use when the aircraft is not undergoing maintenance [249, 251, 253, 259, 274, 280]. For General Aviation aircraft, those data were not reported in literature. Additionally, the wide variety of usage of CS-23 aircraft makes those numbers very dependent on the type and configuration. These numbers can, however, be estimated based on data from the General Aviation Survey of the Bureau of Transportation Statistics, which provides figures including the average age of the fleet and the yearly number of hours flown in previous years. The evolution of those two metrics in the past 20 years is represented in Figures 5.5 and 5.6, respectively. Assuming a uniform age distribution across the fleet, the lifetime of the aircraft will be estimated as twice the average age of the current fleet. This leads to an average expected lifetime of between 6000h for single engine piston to more than 12000h for twin engine turboprop. This is the same order of magnitude as other values reported in literature for light sports aircraft [227]. Given the importance of that parameter, however, it will be subjected to a sensitivity analysis. The analysis of the reported number of hours flown each year reveals that, on average, General Aviation aircraft are flown less than an hour a day, even for twin turboprop aircraft. It is worth noting that this database does not include aircraft used for

commercial commuting activities, which are typically used more intensively and for longer periods of time. However, since a lower lifetime will lead to more conservative results, data from the General Aviation survey will be used.

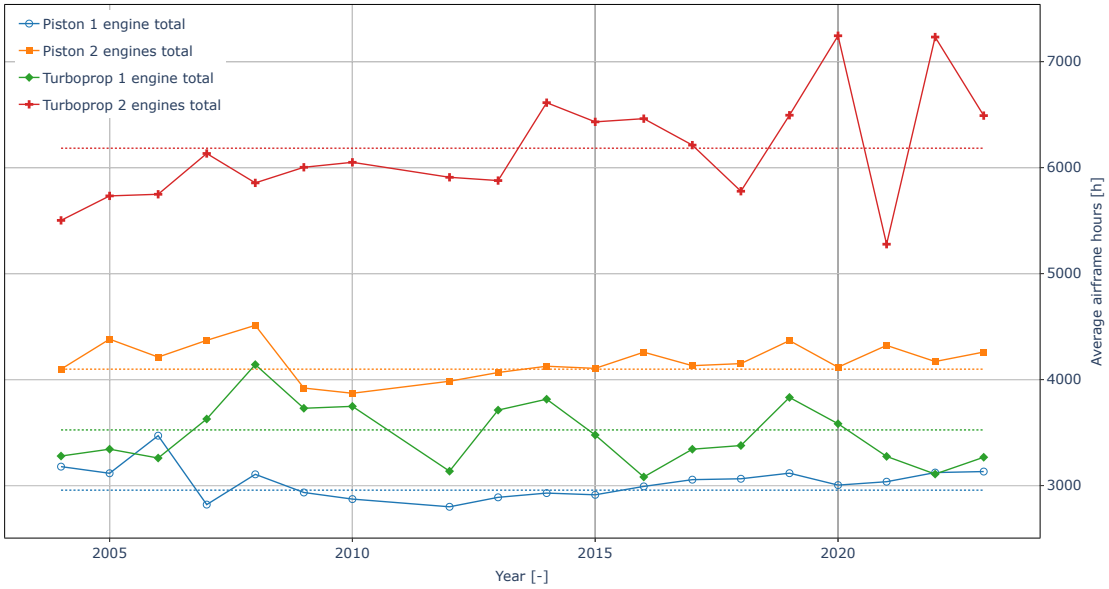

Figure 5.5 Average age of the fleet per category reported in the GA survey from the BTS.

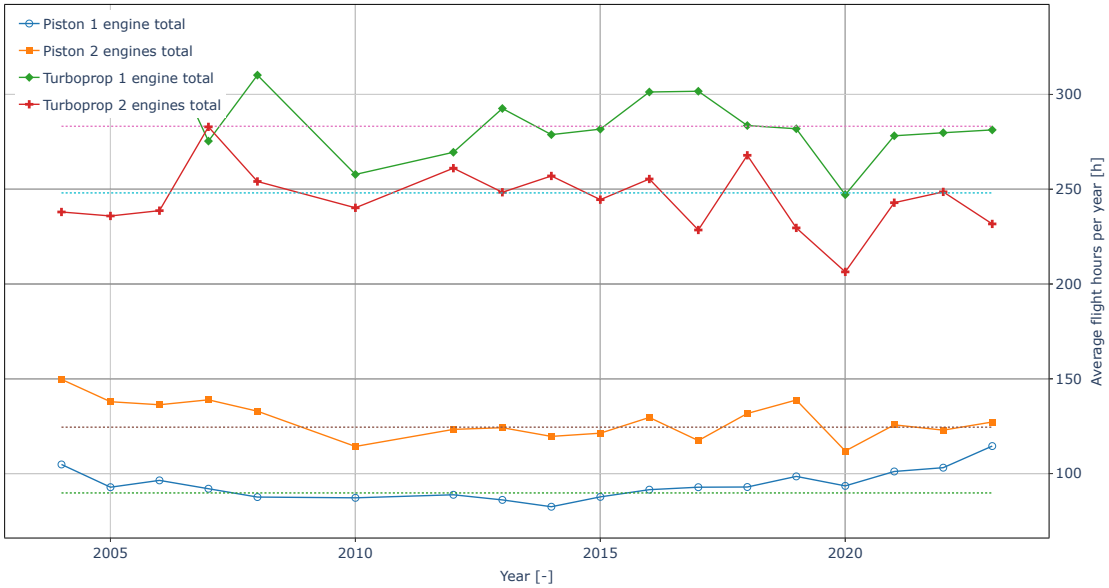

Figure 5.6 Average yearly usage of the fleet per category reported in the GA survey from the BTS.

For the production of the powertrain, different approaches were used depending on the component. For some components that had reasonable proxies, equivalent processes from the ecoinvent database were used directly. This is the case for electric machines (generator and motor), inverters, and combustion engines, for which pre-compiled inventories from the automotive sector were available. Similarly, for components such as buses, cables, or battery packs, as they have quite a wide range of applications, suitable surrogates were found in the existing database. Rectifiers and DC/DC converters were assumed to have the same manufacturing process as inverters used on cars. Finally, for the remaining components — propellers, turboshafts, gearboxes, and fuel systems — a breakdown of the material composition was found in literature [251, 281] and implemented. For these components, values for the energy requirement and emissions of the assembly process were also reported. However, the proper distinction between the requirements and emissions for materials extractions and their assembly was not clear. Consequently, the assembly was discarded to avoid counting multiple times the extraction of raw materials already available in ecoinvent, leading to potential underestimations of the impacts of the production of these components. Components renewal was also accounted for through the comparison of the component lifespan to that of the aircraft. For power electronics and electric machines, a replacement every 15 years was assumed based on values available in literature [251]. For battery packs, however, more frequent renewals are required because of the aging process discussed in Section 3.6.1. It is especially important to consider as batteries have a very impactful production process, it is expected to contribute to a significant share of the aircraft's impacts, as illustrated by LCA applications on electric drones [109]. Literature reports that, for Li-Ion, a renewal every 500 to 700 cycles will be required [227] while for other chemistries, values as high as 2000 cycles are reported [81, 274]. However, it was discussed that, in addition to cyclic aging, batteries also degrade because of side reactions that happen even when the battery is idle, and that battery lifetime could be estimated based on when the battery capacity reaches a threshold value. Depending on the application, either the aging model implemented in the framework or the fixed value will be used. The rest of the components were assumed to never need replacement.

Figure 5.4 shows that impacts stemming from line testing should also be considered. As a first approximation, those impacts will be computed based on the inventories on a reference mission for the aircraft, either design or off-design, depending on the case, and the ratio of the duration of the design mission to the duration of the tests, taken by default at 10 hours. For the distribution of the aircraft to the end user, two scenarios were considered, depending on the category of aircraft. Bigger aircraft like the TBM or the Kodiak tend to be ferried by flight to their end users. For this case, and similarly to what was done for line tests, the impacts will be computed based on the impacts on a reference mission and a ratio of the delivery range to the reference mission's range. Smaller aircraft like the Pipistrel tend to be

delivered like normal cargo. In that case, the aircraft was assumed to be delivered by train as a shipment whose mass was equal to the aircraft's empty mass.

Last but not least are the processes associated with the use phase. Based on the assumptions described in the scope and reported in Figure 5.4, impacts in the use phase are essentially linked with the production and the emissions of the energy vector and its use. Emissions stemming from the use of turboshaft and piston engines were already discussed in the section describing their respective models. It is however worth noting that a potential oversimplification of the consideration of these emissions was done. Indeed, in addition to the dependencies on the engine operating parameters, which were not considered, it will also be assumed that these species will have the same impacts regardless of the altitude at which they were emitted. Similar studies in literature often make the distinction between LTO cycle and cruise as some species are more harmful to human health when emitted close to the ground, while some others are more damaging at high altitude [207, 208, 234, 247, 253, 265, 266, 271, 282]. However, because of the difficulties of accounting for that effect in traditional LCA [282], and because General Aviation aircraft typically fly at low altitudes, that distinction won't be made here. Additionally, initial LCA runs revealed that the water vapor emitted as part of the combustion process of Jet A-1 and AvGas was accounted for as water being drawn from the ecosphere. This led to an erroneous over-representation of the operation phase in the water use impact category. Consequently, the water emitted by turboshaft and piston engines was omitted for further analysis. For the production of the Jet A-1 burnt in the turboshaft, the readily available process for kerosene will be used. For the AvGas, however, data are much scarcer; therefore, a proxy will be used [211, 267, 268]. As is done in other works found in literature, the impact of its production will be approximated based on the impacts of the production of unleaded fuel to which lead was added as a replacement for tetraethyllead [227]. For electricity, either to charge the battery for the flight or when it is required in the assembly of a component, a market group for high-voltage electricity will be used. Market groups represent a geographical average created for convenience and ease of use. Depending on the study, the particular region whose average will be used might differ. It is a key factor to define, as, depending on the geography, the method of electricity production widely differs, leading to a wide variance of the environmental impacts [246, 252, 260, 271]. The ecoinvent entries used for the background processes are listed in Appendix D.2.

The resulting process tree is shown in Figure 5.7. It is worth noting here that, similarly to what is done for the sizing and the assessment of the performances of the powertrain, processes are only added if the corresponding components are present in the powertrain file. In fact, before each initialization of the LCA module, a new LCA configuration file is created based on the contents of the powertrain file. This means that a change in the airframe materials or energy vector used is not handled by a discrete variable acting as a switch; rather, it is dynamically adapted. It has the advantage of not needing to precompile inventories for materials and background processes that are not used, but also the drawback of not having

certain variables appear as design variables to the optimizer. A corollary to the dynamic adaptation of the LCA configuration file is that, when there are multiple components of the same type, one entry is added per component instead of having one entry for all components of the same type. While this may marginally slow down the process, it enables a clear distinction of the impacts of each component of a type. In an example that will be detailed in Section 5.5.4, it will be used to identify the impacts that would stem from using two different cell chemistries for two battery packs sized for different conditions.

5.5 Application of the LCA methodology for the design of electrified aircraft

5.5.1 From CO2 emissions to Life Cycle impacts

In Chapter 4, several electrification scenarios were proposed for various reference aircraft certified under the basis of CS-23. Results showed that, for the lowest levels, as soon as an electric version was reasonably feasible, it was better than its thermal counterpart on the basis of Well-To-Wake emissions. However, that simplified approach was based only on the analysis of one stage of the life of the aircraft and only considering one impact category. With the implementation of the LCA methodology inside the OAD framework discussed in the previous section, it is now possible to have a more comprehensive overview of the implications of the electrification of the powertrain. Consequently, select test cases discussed in the previous chapter will be re-investigated under the lens of the life cycle impacts.

Comparison of the eSR22 to the baseline level 2 aircraft

For this study, both aircraft were evaluated based on their performances on their respective design mission whose parameters are reported in Table 4.5. Despite the aforementioned relevance of the use of "flying one hour" as a functional unit, this study will compare both designs on the basis of their ability to transport payload over one unit of distance. As the original aircraft is a single-engine piston, and based on the results presented on the usage of General Aviation aircraft, a lifespan of 6000h was assumed for both aircraft, even though the lack of feedback on electric configurations makes the validity of that assumption questionable. For the yearly usage, and even if the GA survey points at a value of 90 hours of flight per year, a value of 200 hours was assumed. The reason for this is that it would lead to an average lifespan of more than 60 years, which felt unrealistic even if some airframes like the Cessna 172 are still flying. Additionally, this number is based on a US average. This might introduce a bias, as there are more private users in the U.S. who use their aircraft less frequently when compared to the French or European model, where aircraft are shared by members of an aeroclub, thus leading to more intensive use. For the delivery, the aircraft was assumed to be ferried from the Cirrus manufacturing plant in Orlando, Florida, to Toulouse

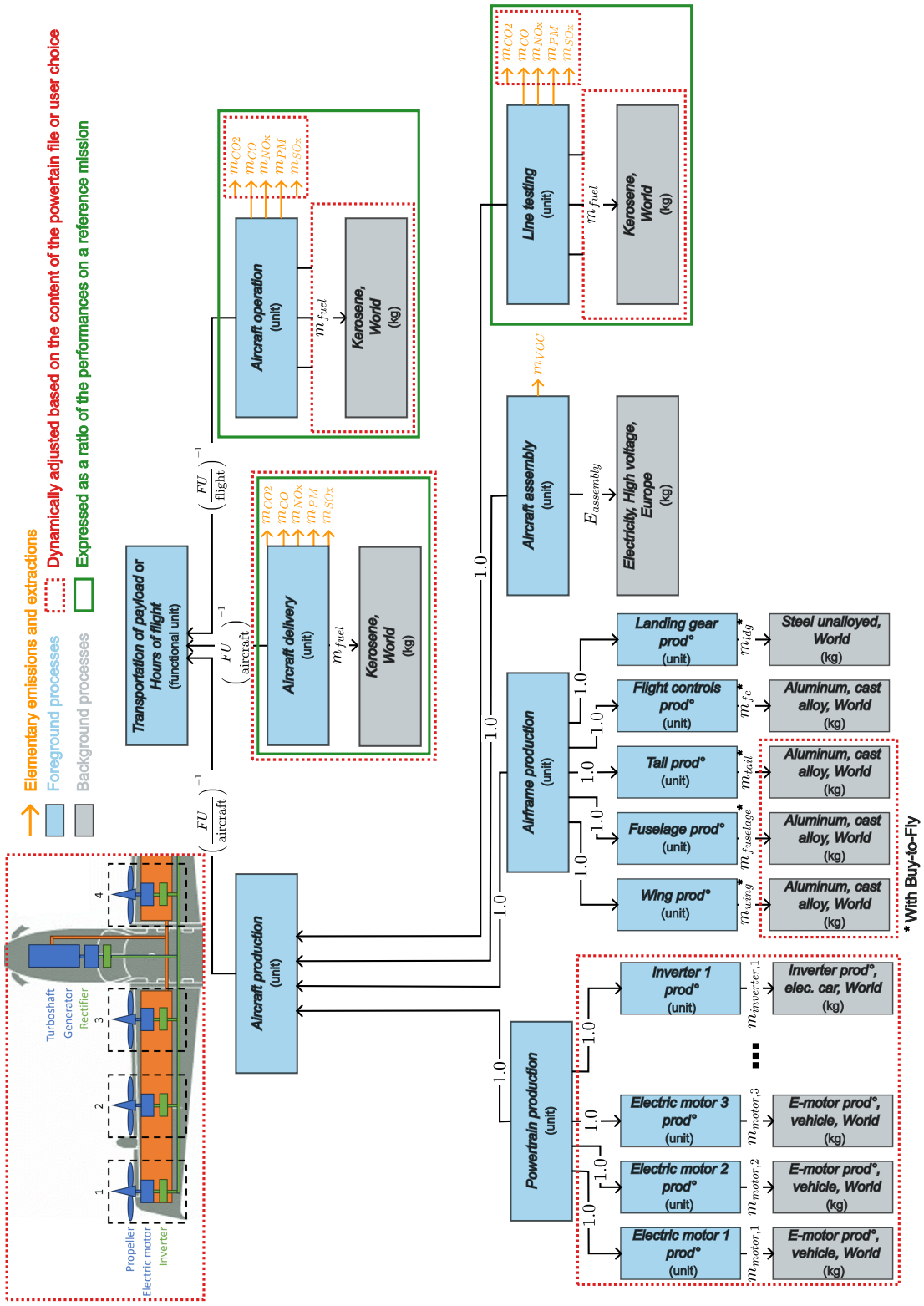

Figure 5.7 Example process tree associated with the retrofit EcoPulse presented in Section 4.5.2.

in France, leading to a rounded distance of 5000nm. The same assumption will be made for the electric aircraft, although, given the low range capabilities, that may be optimistic. For line tests, a value of 10h was taken. Concerning the Buy-to-Fly ratio, averages in the range found in literature were taken, with a value of 1.5 for the composite parts and a value of 7.5 for the metallic parts. Finally, for the battery renewal rate, a value of 700 cycles was taken in accordance with a similar study [227], and a European electric mix will be considered for their charging and for the assembly. Regarding the LCIA method, an initial study on a reference aircraft aimed at validating the assumptions was conducted. It revealed that using the EF3.1 led to extremely high values in the "human toxicity: non-carcinogenic" category, an effect attributable to the combustion of leaded fuel. Studies of the order of magnitude of the normalized impacts and comparison with values found in literature [227] revealed that there may be an over-representation of lead emissions. Consequently, for that particular study, the ReCiPe 2016 LCIA method was used.

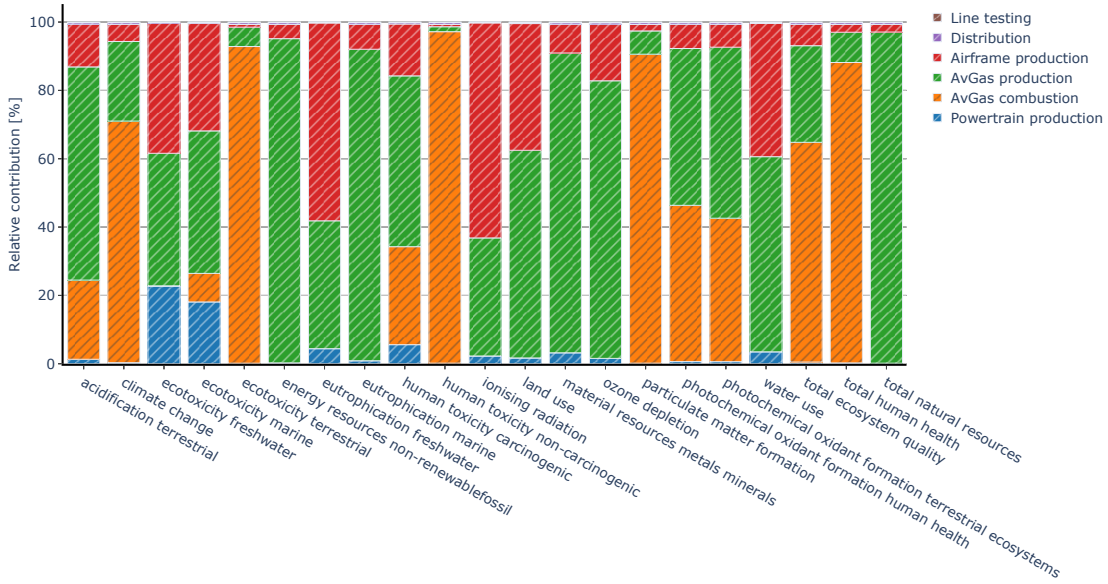

Figure 5.8 Relative contributions to each impact category for the reference Cirrus SR22.

Figure 5.8 shows the relative contribution of major sub-processes across all 18 impact categories for the reference design. The 15 midpoint indicators are on the left of the graph, and the three endpoint categories are on the right. Further information on the distinction between midpoint and endpoint impacts are available in Appendix D.1. First, focusing on the climate change category, it can be seen that, as expected from the results discussed in literature [227, 268, 269], even on conventional GA aircraft, fuel combustion and fuel production remain the biggest contributors at around 96%. The same can be said for many other categories, in particular those that are linked with the extraction and refining of the fuel. Nonetheless, it can also be seen that in many other categories, the assembly of the

airframe is one of the, if not the, biggest contributors. The reason for this is the high intensity of the composite manufacturing process. Further analysis of the endpoint impacts, which represent the combined effects at the end of the damage chain on areas of protection, however reveal that fuel-related processes remain the priority. It also shows that for conventional configurations, minimizing the impacts is equivalent to minimizing the fuel consumption, even at the cost of other phases of the life cycle.

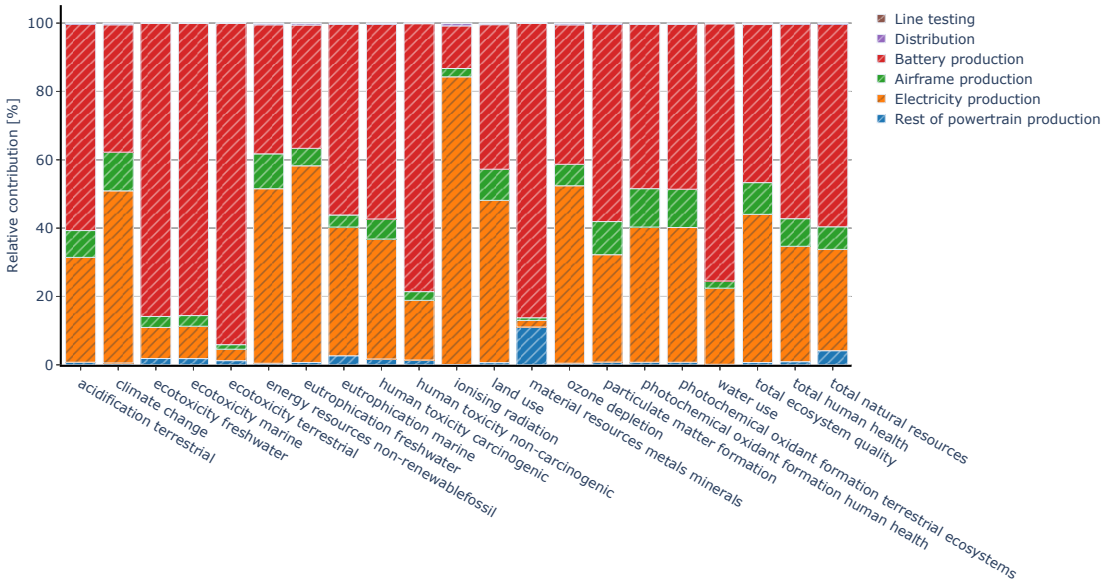

Figure 5.9 Relative contributions to each impact category for the electric Cirrus SR22.

Figure 5.9, on the other hand, shows the same analysis but for the electric version of the Cirrus SR22 discussed in Chapter 4. While for the conventional version, it was shown that the initial analysis focusing solely on the use phase yielded a reasonably accurate result, it can be seen here that neglecting the production, and more specifically, the battery production, can yield significant errors. Indeed, in most categories, the battery production process is the leading contributor. This can be explained not only by the high impacts of battery production across multiple categories but also by the mass of the pack and the need to frequently renew it during the life of the aircraft. Given the renewal rate of battery cells set as input and given the usage of the aircraft, the ton of battery cells would need to be replaced eight times throughout the life of the aircraft. The importance of the battery production process is further emphasized by the results in terms of endpoint impacts, where approximately half of all impacts are linked with the production of the battery. Interestingly as well, even though it is not as pronounced when looking at midpoints impacts because of the high relative mass of the battery, the production of the airframe becomes of significant importance at endpoints level with contributions reaching between 6% and 9%. The reason for this increase is twofold. First, the aircraft's structure is considerably heavier, with a 60% increase in the OME, meaning

more composite needs to be manufactured. The second reason is linked to the relative decrease in the processes linked to energy production. While still significant, Figure 5.9 shows that the production of electricity becomes less preponderant than the production and combustion of AvGas in Figure 5.8. This result is likely to be even more pronounced either in the future, where electric mixes are predicted to be based on more renewable energy, or had we considered a greener mix, like the French one. Both this increase in the impacts of airframe production and battery production lead to a situation where there is more balance between the contribution of the production and operation phase, indicating that minimization of impacts is not as straightforward as on conventional configurations.

Table 5.1 Main outputs for the LCA of the reference SR22 and the eSR22.

	Cirrus SR22	**eSR22**	**Diff. wrt conv. (%)**
Ecosystem quality (Species.year)	4.06×10^{-10}	6.00×10^{-10}	+47
Normalized (eq.person)	2.74×10^{-7}	4.05×10^{-7}	
Human health (DALY)	6.10×10^{-7}	3.78×10^{-7}	-38
Normalized (eq.person)	2.54×10^{-5}	1.57×10^{-5}	
Resources (USD2013)	0.015	0.011	-26
Normalized (eq.person)	5.30×10^{-7}	3.91×10^{-7}	

Results were also compared in terms of endpoint impacts. A comparison of the damage to areas of protection for the two designs is given in Table 5.1. To improve the readability of results, normalised values were also added. ReCiPe 2016 provides three sets of normalization factors based mainly on cultural perspectives: Individualist, Hierarchist, and Egalitarian. Out of these, the hierarchist approach was used as is commonly done in literature, and because it is the more neutral version in terms of subjective choices. Those normalization factors are based on the impacts of an average person; thus, normalized quantities will be expressed as the equivalent of a person. These results show that the electric design is not strictly superior to the thermal design, with a notable increase in the damage done to ecosystems. Nonetheless, it outperforms the reference in the two other endpoint categories, thus illustrating a shift of the burden. Given the different units used for each category, however, it is impossible to compare whether or not that shift is worth it. Additionally, the ReCiPe method does not provide an official weighting factor, rendering the use of a single score impossible. Still, the analysis of normalized results shows that, in terms of equivalent person, most impacts occur in the area of damage to human health with a score in the order of magnitude of 10^{-5} as opposed to 10^{-7} for the two other categories. In that particular category, the electric design has significantly lower impacts than its thermal counterpart, potentially hinting that the former is better in definitive. Indicatively, a single score assuming uniform weighting of all three categories was computed, showing a decrease from 2.59 x 10^{-5} points for the conventional design to 1.64 x 10^{-5} points for the electric one, or in other words, a 36% decrease. It is interesting to note that the preliminary analysis (considering only the operation phase, and

only the climate change impact category) on both designs revealed a 48% improvement when switching to all electric, revealing tamer, although still significant, improvements when the entire scope is considered.

Minimization of environmental impacts on the hSR22

Given the significant share of the impacts of electric configuration attributable to the production of the battery pack, revisiting the results on the hybrid SR22 discussed in Section 4.4.2 appeared worthwhile. Indeed, given the absence of consideration for the production phase and the already relatively narrow margin for improvement observed for the hybridization scheme selected, results are likely to differ once the full scope of the aircraft's life is considered. The same hypothesis as in the previous section will be taken, considering deliveries, production of the airframe and the components, as well as the renewal rate of the battery for the reference cell. Finally, the ReCiPe 2016 method will also be used.

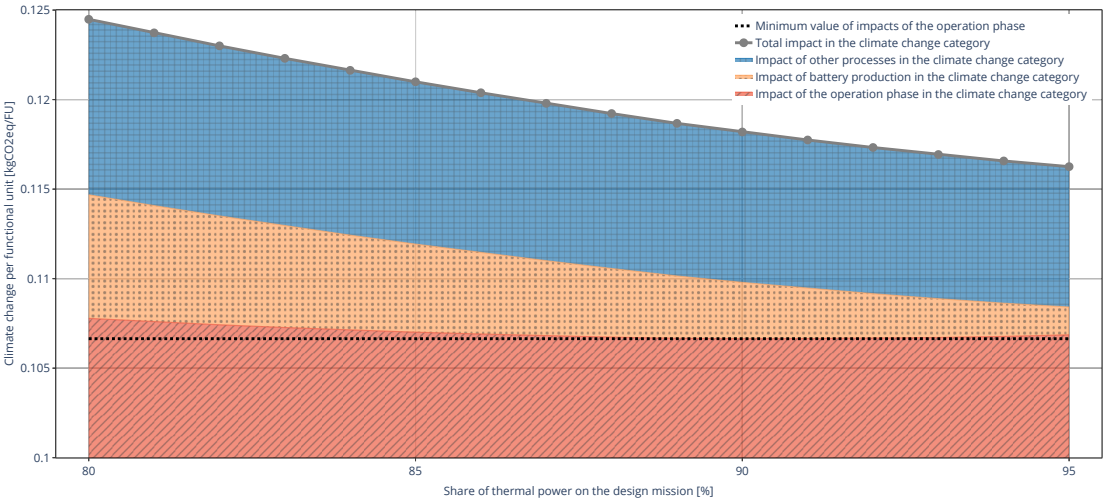

Figure 5.10 Evolution of impacts in the Climate Change category for the hybrid Cirrus SR22.

To verify consistency with the results of the preliminary analysis, the evolution of the impacts in the climate change category will first be analyzed. They are shown in Figure 5.10, whose y-axis does not start at zero for readability. In particular, the impacts stemming from processes occurring in the operation phase, which corresponds to the scope selected in Section 4.4.2, are highlighted with the red shaded area. That curve shows that, as for the original analysis, very few gains can be achieved by hybridizing with the reference cell. Indeed, just like the results shown in Figure 4.13, the variation of the objective function on the interval considered is in the order of magnitude of 1-2%. Similarly, the value of the design variable is very close to the value found for the initial analysis, with an optimum around 90%, although here, slightly higher values of the share of electric power are preferable. Finally, the order of magnitude of the results was also verified. Considering the minimum of 260

kg$CO_{2,eq}$ in Figure 4.13 and the design mission of 375kg of payload transport over 200nm, once emissions from reserves are removed, a value of 100.41 g$CO_{2,eq}$ per PAX transported over one unit distance is found, which is consistent with the values reported in Figure 5.10.

Figure 5.10 also shows the influence of the remaining processes on the evolution of the impacts in the climate change category, in particular the production of the battery which was identified as a key contributor. On the interval considered, its contribution remains fairly small when compared to the operation phase, with values varying between 1.5 g$CO_{2,eq}$ and 6.9 g$CO_{2,eq}$ as opposed to the approximately 100 g$CO_{2,eq}$ for the use phase. Despite that, the meager reduction of the impacts in the operation phase discussed previously is smaller than the rapid increase in the impacts associated with the production of the battery. This leads to an overall increase in the impacts in the climate change category when the share of electric power increases, thus contradicting the results of the initial analysis. This shows that, even when looking at only one impact category, the consideration of other life cycle stages of hybrid aircraft is paramount to assess their sustainability.

Discussions in Section 4.4.2 revealed that the low gains in the operation phase could be attributed to the rapid increase in battery mass, leading to an increase in the energy use of the aircraft. For this reason, a battery with a higher energy density was considered, which led to significantly increased gains with higher shares of electric power. In the scope of LCA, the higher energy density also means that, for the same energy, less battery needs to be produced, so the contribution of its production phase will be lower, leading to reduced overall impacts. However, for the Ampirius cell considered in Section 4.4.2, the manufacturer's catalog announces a life cycle of 600 cycles, meaning the battery will need to be replaced more often than the reference case, leading to higher production impacts across multiple categories. For those reasons, a new optimization of the hybrid Cirrus SR22 configuration with the Ampirius 18650 cell will be conducted, this time to minimize the environmental impacts. Despite the aforementioned disadvantages of using a single score, it will be used for the needs of this optimization. For that, uniform weighting across all three endpoint categories will be taken. The setup for the optimization is presented in Table 5.2.

Table 5.2 Specification for the hSR22 optimization problem using the LCA methodology.

Requirements	Design payload:	375 kg
	Design range:	200 nm
	Battery energy density:	300 Wh/kg
	Battery cycle life:	600 cycles
	Total ecosystem quality weighting	33%
	Total human health weighting	33%
	Total natural resources weighting	33%
Objective function	Environmental single score per FU	
Design variables	Hybridization ratio, % of thermal power	$H_P \in$[70%,95%]
		$H_{P,0} =$80%

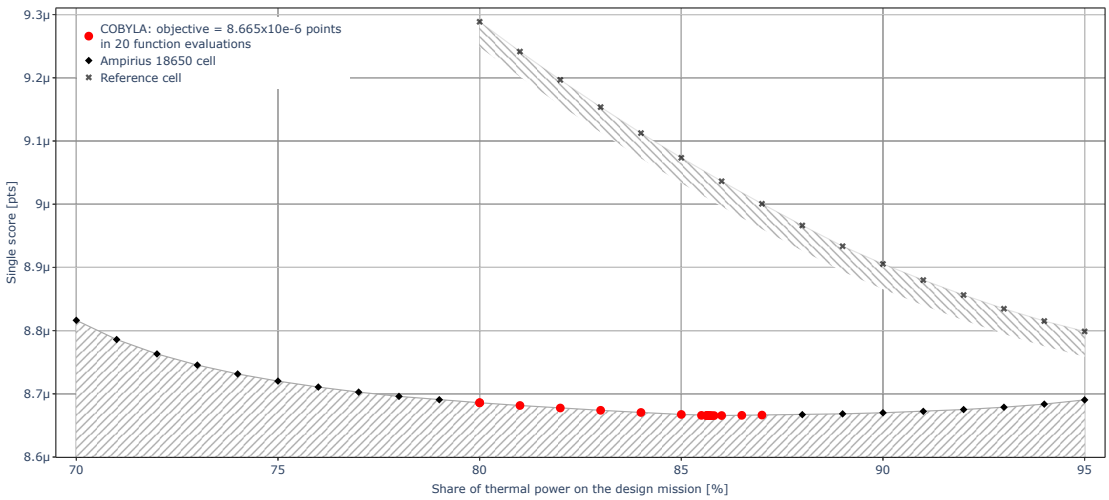

Figure 5.11 Minimization of the environmental single score for the hybrid Cirrus SR22.

The results of this optimization are shown in Figure 5.11. As was done in Figure 4.14, to better assess the evolution of the objective function with the change in battery cell, the response of the objective function with the reference cell is also shown in a lighter gray tone and using crosses as markers. Results show that, despite the need for more frequent renewal of the battery, and as was observed with the initial analysis, a lower optimum can be found. However, given the consideration of the impacts of battery production, which becomes even more pronounced as the renewal rate increases, the gains are much smaller, going from a 5% improvement considering the initial scope to a mere 1.6% improvement here. It is also interesting to point out that the optimal value was initially found for a value of the design variable corresponding to approximately a 71% share of thermal power, while here the optimal value is found at around 86%. This can be explained by the fact that, when considering the whole life cycle of the aircraft and multiple impact categories, higher battery shares lead to high impacts. Indeed, while before it was mostly linked with an increased energy demand, it is now also associated with strong impacts due to battery production, but also to the fact that a heavier aircraft increases the impacts associated with the production of the airframe.

Comparison of the hybrid Kodiak 100 to the baseline aircraft

The reduction in the anticipated gains when considering the whole life cycle of the aircraft, and in particular the propulsion, also prompted further inquiries into the hybrid design proposed for the Kodiak 100. This case is especially interesting considering that the retrofit approach led to a reduction of the payload transported, which translated into a reduction of the functional unit carried out per flight and thus per aircraft. This analysis was also motivated by a review of literature, which showed that, for bigger configurations, hybridization could

actually lead to an increase in the single score [208]. The functional unit chosen for the LCA study is the transportation of 85 kg of payload (roughly the mass of a passenger) over one kilometer with the assumption that both aircraft (the reference and the hybrid) are operated on the mission used in Section 4.5.3. The reference lifetime of the aircraft is estimated from the average age of the current single-engine turboprop fleet, provided by the General Aviation Survey of the Bureau of Transportation Statistics, at 7000 hours. A yearly use of 283 flight hours will be assumed based on the same data. As the aircraft is mostly metallic, a Buy-to-Fly ratio of 7.5 will be considered for the structure. The operation of the aircraft is assumed to take place in Europe, so the European market mix is used for the provision of kerosene and electricity. As the aircraft runs on Jet A-1, issues raised about the over-representation of lead in the impacts will not be present here. Consequently, the EF v3.1 method will be used along with the recommended normalization and weighting factors [283].

As discussed in the introductory section of this chapter, the final score is highly sensitive to the overall lifespan of the system. A preliminary analysis of the sensitivity of the conclusion to that parameter was thus conducted. The evolution of the single score for both design as a function of the aircraft's expected lifespan is shown in Figure 5.12. Values ranging from the average age of the fleet according to the BTS GA survey to twice this value were considered. Results show that, for the values considered, the relative score of both designs remains consistent, with the hybrid design presenting scores lower by 6% to 8%. Additionally, the graph reveals that, when the expected lifespan of the design is more than doubled, the single score varies by less than 8%. It is important to note that, while a fairly constant behavior is observed here, for smaller values of the aircraft lifespan, it will likely show stronger dependency. Indeed, as the needs of the production phase are essentially divided by the lifespan, their contribution increases very quickly for a short life expectancy. Interestingly, Figure 5.12 also shows the effect of the impact of battery renewal. Indeed, there is a sudden increase in the single score every 700 cycles due to the need to build a new battery. Given the average mission time of 1.86h, this would translate into an increase of the impacts linked with battery production every 1300h of flight, which shows good agreement with the results in Figure 5.12.

The normalised and weighted results for the conventional Kodiak 100 are shown in Figure 5.13, including the contributions to each impact category. The production and combustion of kerosene during the use phase remain the two main contributors across most impact categories at the single score level. The production phase, however, which includes the manufacture of the components and the assembly of the airframe, accounts for 5% of the single score, and has a significant impact in several categories (e.g., material resources). A reduction in fuel consumption, such as that offered by the hybrid-electric retrofit, is therefore expected to result in a lower single score if no significant burden shift is introduced through electrification of the powertrain, which might be the case here, given the low energy hybridization ratio.

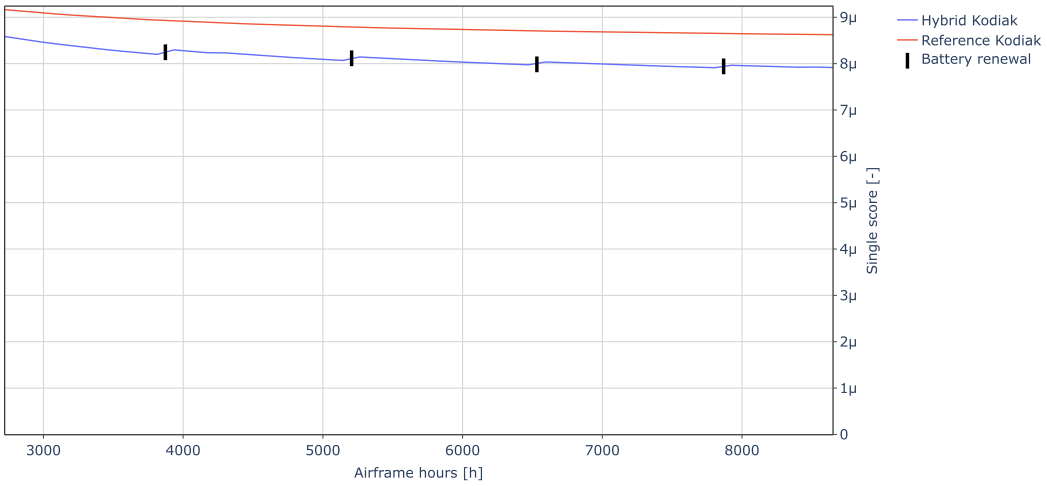

Figure 5.12 Evolution of the single score with life expectancy of the aircraft.

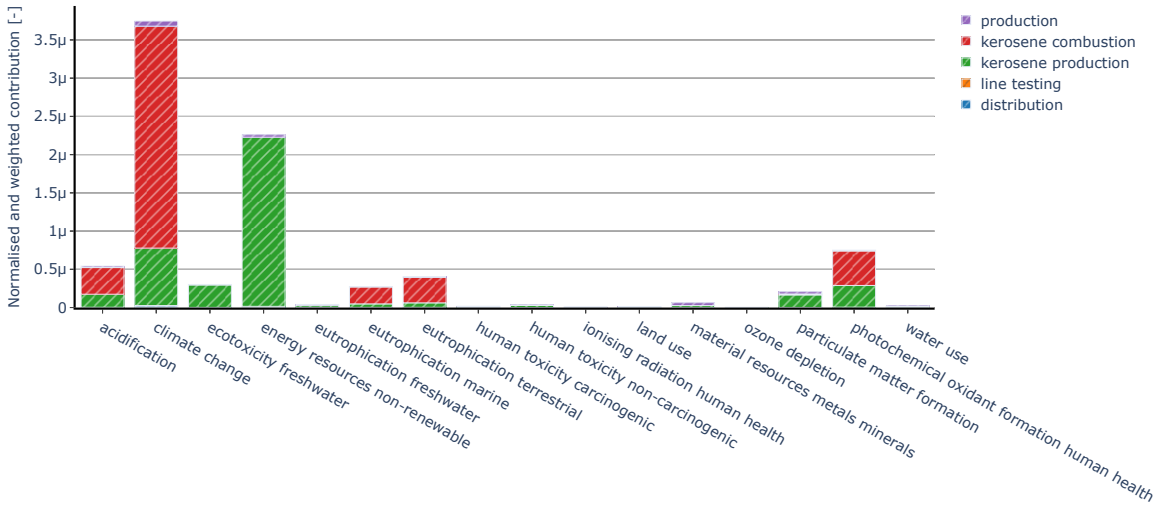

Figure 5.13 Normalised and weighted impacts for the reference Kodiak 100, expressed per pax.km.

The environmental benefits at the single score level are confirmed by the 8.1% reduction observed for the hybrid Kodiak 100, as shown in Table 5.3.

Table 5.3 Environmental single score for the two Kodiak 100 variants.

Variant	**Environmental single score**	**Relative variation**
Reference Kodiak 100	$8.68 \text{x} 10^{-6}$ pts/(pax.km)	–
Hybrid variant	$7.98 \text{x} 10^{-6}$ pts/(pax.km)	- 8.1%

However, the single score is not reduced in the same proportion as the fuel consumption, found equal to 15.1% on the mission of interest. This highlights a burden-shifting situation. Figure 5.14 provides the relative scores of the different midpoint indicators for the two architectures. The fuel savings of the hybrid-electric Kodiak 100 result in lower impacts across most environmental categories, including climate change (-13.1%) and depletion of non-renewable energy resources (-12%). However, the additional impacts of battery production lead to significant increases in some other impact categories, in particular material resources depletion (+395%) and the emission of ionizing radiation (+254%).

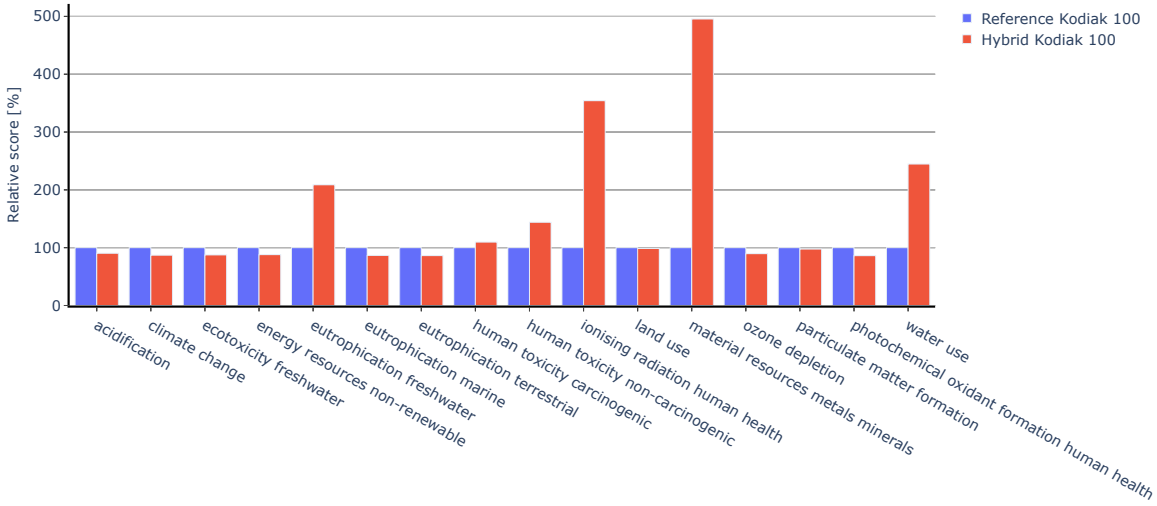

Figure 5.14 Relative comparison of the environmental impacts for the reference Kodiak 100 and the hybrid variant.

The reduction of the single score is further detailed in Table 5.4, where the variations of transport capacity (pax.km), energy intensity (kWh/pax/km), and environmental intensity (points/kWh) are reported. As a reminder, the results of the sizing process for the hybrid-electric aircraft discussed in Section 4.5.3 yield a power hybridization ratio of 41%, while the corresponding energy hybridization ratio over the mission of interest (excluding fuel reserves) is only 1.5%. Despite this micro-hybridization, the improved efficiency of the propulsion system, operating closer to its optimum, enables a 16.5% reduction in fuel consumption compared to the conventional architecture on the main route. Considering the reduction in transport capacity of the hybrid aircraft, the fuel savings are reduced to 15.7% on a passenger-kilometer basis. Taking into account the additional electricity required to power the hybrid-electric powertrain, the overall reduction in energy use per passenger-kilometer, including both energy sources, is 15.2%. Finally, the environmental intensity of energy – which refers to the environmental impacts caused by the production, storage, and, when applicable, combustion of the energy carriers – is investigated. For fossil kerosene, the carbon

intensity is equal to 333 gCO_2-eq per kWh over its life cycle, or 2.13×10^{-5} points per kWh. For electricity, the European electricity mix combined with the production of batteries to store the energy during flight results in a carbon intensity of 610 gCO_2-eq per kWh. At the single score level, this corresponds to 11.9×10^{-5} points per kWh. Overall, when combining both energy carriers, i.e., fossil kerosene and electricity, the environmental intensity of the energy mix used in the hybrid-electric Kodiak increases by 6.7% to reach 2.28×10^{-5} points per kWh.

Table 5.4 Variation of contributing factors to the single score, for the mission of interest.

	Ref. Kodiak 100	**Hybrid variant**	**Variation**
Transportation service over a flight (pax.km)	4967.7	4924.7	-0.9%
Energy per passenger-kilometre (kWh/pax/km)	0.39	0.34	-12.8%
Impact per unit energy (points/kWh)	2.13x10^{-5}	2.28x10^{-5}	$+7.0\%$

The results in Table 5.4 show that the environmental intensity of a unit of energy required for the flight is increasing. The reason for that intensification is mainly linked to the production of the battery as well as the electric mix used. Indeed, on specific impacts like climate change, it has comparable effects on its life cycle as the production and combustion of kerosene. In the end, for this case study, results demonstrate that the reduction in the single score originates from the improved design of the aircraft (i.e., better energy efficiency) rather than the direct electrification of the propulsion. This finding highlights the benefits of the comprehensive integration of an LCA module within OAD software as a tool for decision-making. Nevertheless, future work could extend the comparative assessment to off-design missions, for example, by generating payload-range diagrams and studying multi-mission variation.

Intermediate conclusions

The deepening of the analysis conducted in Chapter 4 showed that, while it provided a fair first guess on the trends of the potential of electrification of propulsion, the impacts associated with electric components, and mostly battery production, are not negligible. This effect was shown to be especially important to consider in the case where no significant reduction could be obtained in the operation phase. Since the battery production process is highly energy-intensive, the variation of impacts, even when looking only at the climate change category, can rapidly become dictated by the battery pack. Additionally, the study on the Kodiak 100 also showed that there was a significant shift of the burden in multiple other impact categories, including the depletion of mineral resources, the use of water, and the emission of ionizing radiation. Although this particular study featured an aircraft with a very low energy hybridization ratio, meaning impacts associated with electricity production and battery production remained marginal, investigation of the impacts per unit of energy showed that it can rapidly become significant when more electric energy is used. It is worth noting that the high value found for the single score per kWh of electricity is essentially due

to the high energy intensity of the battery manufacturing process and the electric mix used, which are background processes. While not under the scope of this work, these processes are likely to become less impactful with the increase in the use of renewable energy, thus pointing to the interest of performing prospective LCA, a capability the `lca-modeller` package offers and which will be used in an ulterior section.

The minimization of the single score on the hybrid Cirrus configuration also highlighted the interest of the integration of an LCA module inside an OAD framework. Indeed, it enabled the proposal of a configuration that had the overall smallest impacts considering multiple impact categories, which proved to be significantly different from the one obtained with the initial analysis. This close integration also enabled further analysis of the sources of improvement on the hybrid Kodiak. This investigation revealed that, as discussed during the preliminary analysis, the most significant gains do not stem from the change in the energy vector but from the synergies enabled by the added degrees of freedom enabled by electric propulsion. Indeed, as previously discussed, consideration of other phases of the life cycle increases the downside of electric propulsion, making them as significant as fuel related process for the computation of environmental impacts. Given the importance of battery pack related process, these studies also hint at the key tradeoffs between battery energy density and battery lifespan. While the former reduces the quantity of battery that needs to be manufactured, de facto reducing its impacts, it often comes at the cost of the latter. A smaller lifespan translates into more frequent renewal, effectively meaning that, over the lifespan of the aircraft, more battery needs to be produced. These tradeoffs will be investigated in the next section.

5.5.2 Influence of cell chemistry choice on environmental impacts

Results and discussions from Section 5.5.1 allowed to identify the production of the battery as the main contributor to the impacts of electric configurations. Test cases on hybrid platforms also revealed how the consideration of the battery renewal rate could limit even more the benefits from electrified propulsion. Literature on LCA methods applied to drones revealed that configuration sized using cells having lower energy density but considerably higher lifespan led to the lowest overall environmental score [71]. Therefore, it is proposed to study the effect of a change in battery chemistry on an electric configuration. For this study, the Pipistrel Velis Electro, using the reference Samsung INR18650-35E, a Lithium nickel manganese cobalt oxides (also abbreviated Li-NMC) cell, was considered. Literature shows that among Li-Ion batteries, Li-NMC have average lifespan and average densities [284]. Replacing the graphite anode in a conventional NMC cell with Silicon-Based materials was however shown to lead to higher energy densities [285] at the cost of a more complex manufacturing process and shorter lifespan. Among existing cells leveraging this technology, the Amprius 1.34 Ah Balanced Power + Energy cell, which was used in the prospective study

on the electric version of the Cirrus SR22 in Section 4.4.1, was selected. It has an energy density of 395 Wh/kg at cell level but a lifespan of only 150 cycles. It is worth noting that values of energy densities of up to 475 Wh/kg have been shown to be feasible [286]. At the other side of the spectrum, Skeleton Technologies advertises battery with a virtually infinite lifespan (>50000 cycles), high discharge rates but with battery densities of only 67.9 Wh/kg [1]. This high life cycle is made possible by the fact that the cell uses technologies close to those of super capacitors, also replacing the graphite anode with more sustainable materials, thus enabling the reduction of the quantities of rare materials required.

Chapter 4 revealed that the battery energy density had a significant impact on the feasibility of the design and that it could entail a significant increase in mass and energy required. Beyond the mere feasibility of the design, and with the whole life cycle now considered in the scope of the study, these induced effects also affect the impacts of other processes. Indeed, a heavier aircraft means a heavier structure, which is particularly relevant in the case of composite aircraft as discussed in Section 5.5.1. While initial investigations and the fact that the aircraft exists prove the feasibility with the reference cell and with the higher energy density cells, it is not guaranteed for the Skeleton Technologies one. Thus, a preliminary investigation into the effects of lowering the battery energy density was conducted. As an increase in weight is expected, thus leading to more power required on the electric motor and propeller, similar assumptions as those taken to enable the prospective study on the all-electric Cirrus in Section 4.4.1 will be taken. Additionally, given the nature of the cell, its rated voltage will be significantly different from the reference cell. A different cell voltage model will thus be used. For simplicity, a linear variation of the OCV between the minimal and maximal values found in the datasheet will be taken, along with a constant internal resistance. The evolution of the Velis Electro's MTOM and the mass of the battery pack for several values of the energy density spanning from 67.9 Wh/kg to 130 Wh/kg is shown in Figure 5.15.

Figure 5.15 shows that the divergence of the aircraft's masses occurs for values of the energy density above that of the Skeleton Technologies cell. It also shows that for values of energy density almost twice as big as the baseline, the aircraft is significantly heavier than the original Pipistrel Velis Electro. However, to enable comparison with the other design and given promises offered by the long longevity of the Skeleton Technologies cell, their energy density will be taken to be slightly higher than the values advertised. A value of 75 Wh/kg, just before the mass divergence, will be assumed. It will be worth keeping in mind during the analysis of the results that this cell will thus be evaluated with an advantage. All in all, the inputs presented in Table 5.5 will be used for this study.

In addition to different physical properties, these cells also have different manufacturing processes. While for the reference cell, a process could be found in the ecoinvent database,

[1] https://www.skeletontech.com/hubfs/Data_sheets/Cells/DS-SuperBattery-D35-D60-250710.pdf?hsLang=en, Accessed: 2025-10-23

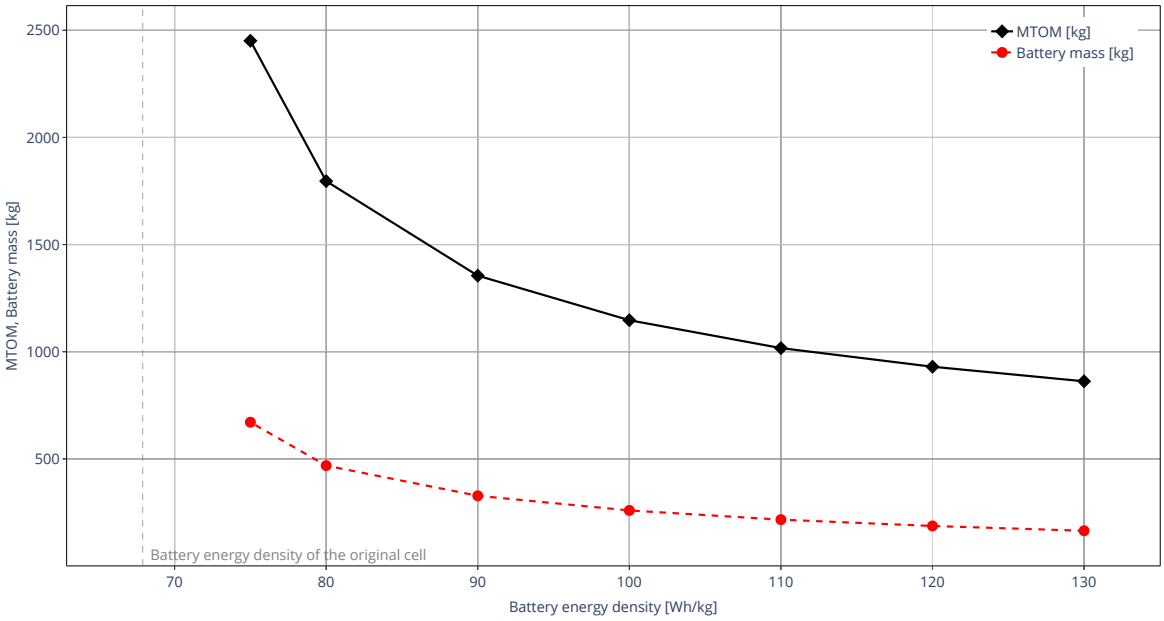

Figure 5.15 Sensitivity of the Pipistrel Velis Electro masses to the battery energy density.

Table 5.5 Characteristics of the cells considered for the Pipistrel study.

	Energy density (Wh/kg)	**Lifespan (cycles)**
Samsung INR18650-35E (ref.)	261	700
Amprius 1.34Ah Balanced Power+Energy	395	150
Skeleton Technologies SuperBattery	75	50000

it is not the case for the cell with the silicon anode or for the SuperBattery. An approach to approximate the impacts of those new anodes has been proposed in literature with an application on a Si-NMC cell [71]. It consists in building an alternate proxy by subtracting from the reference ecoinvent process for NMC cells the impacts of the anode production, and then adding the impacts of a process equivalent to a silicon anode. The original approach proposed in literature [264] will be adopted except for the production losses for the silicon nanowire, which will be assumed to be nil. A similar approach will be adopted for the SuperBattery, where the NMC cathode of the original cell will be substituted for graphite. The mass contribution of the cathode to the reference battery pack was computed based on the assumed 0.768 cell-to-pack packaging efficiency and the fact that for NMC cells, the cathode accounts for approximately 40% of the cell mass [287]. The resulting process is shown in Figure 5.16. For this study, the same functional unit was chosen for all three variants that is "flying one hour". The design mission presented in Chapter 4 was used as the reference. For the lifetime of the aircraft, a value of 4000 airframe hours was selected as per literature [227], with a yearly use of 283 hours according to the BTS's GA survey

data for single-engine piston aircraft. The airframe was assumed to be made of composite materials, and a buy-to-fly of 1.5 was considered for its production. For the electricity, a French production mix was considered. Finally, the EF v3.1 was selected for the impact assessment step with the associated normalization and weighting factors.

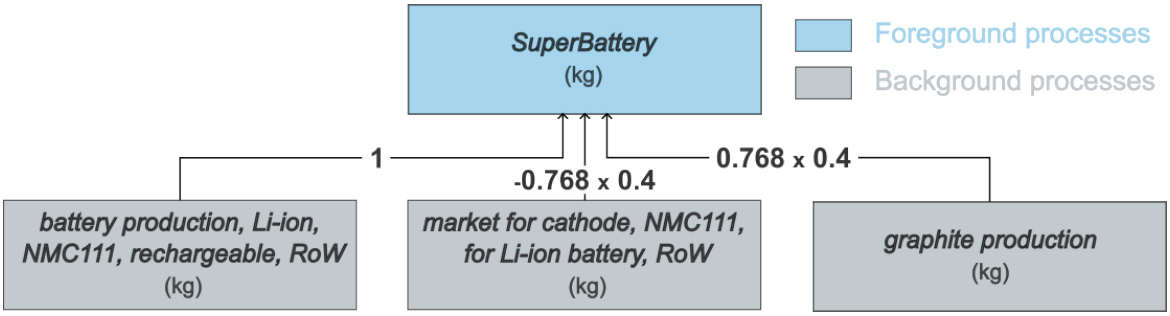

Figure 5.16 Process tree for the Skeleton Technologies SuperBattery production proxy.

The results of the coupled assessment of the overall design and their environmental impacts are presented in Table 5.6. From the previous results in this chapter, we expect a significant contribution from the battery pack, the use phase, and the airframe production. For this reason, in addition to the environmental single score and the aircraft's MTOM, the airframe mass, battery pack mass, and energy required for the mission are presented in Table 5.6.

Table 5.6 Main outputs for the sizing and LCA of the Pipistrel Velis Electro with different battery cells.

	Ref. NMC cell	**Si-NMC cell**	**SuperBattery cell**
MTOM (kg)	600	494	2450
ΔMTOM	-	-17%	+308%
Battery pack mass (kg)	149	78	1342
ΔBattery pack mass	-	-48%	+800%
Airframe mass (kg)	186	157	748
ΔAirframe mass	-	-16%	+302%
Electricity (kWh)	12.9	12.2	31.43
ΔElectricity	-	-5%	+143%
Single score (pts)	$38.7\text{x}10^{-4}$	$80.0\text{x}10^{-4}$	$47.6\text{x}10^{-4}$
ΔSingle score	-	+107%	+23%

Results in Table 5.6 show that, as expected from an OAD point of view, the Si-NMC cell brings considerable gains. The battery pack, and in consequence the aircraft, are significantly lighter than the reference, leading to a decrease in the airframe mass. By virtue of the snowball effect, this leads to a reduction, although minor, of the energy required for the design mission, leading to an even greater reduction of the battery mass. For the SuperBattery cell, masses conform to what could be expected from the preliminary analysis, whose results

are shown in Figure 5.15. Interestingly, however, both the aircraft with the Si-NMC cell and the SuperBattery cell show an increase in the environmental single score. Even more interesting is the fact that, despite presenting as a great candidate from an OAD perspective, the Pipistrel with the Si-NMC scale has a score that is twice the reference. As opposed to the version with the SuperBattery, which, even though its mass more than quadruples, shows an increase in score by merely 23%. Further analysis into the evolution of the impacts of the three designs across all impact categories available in the EF V3.1 methodology is presented in Figure 5.17.

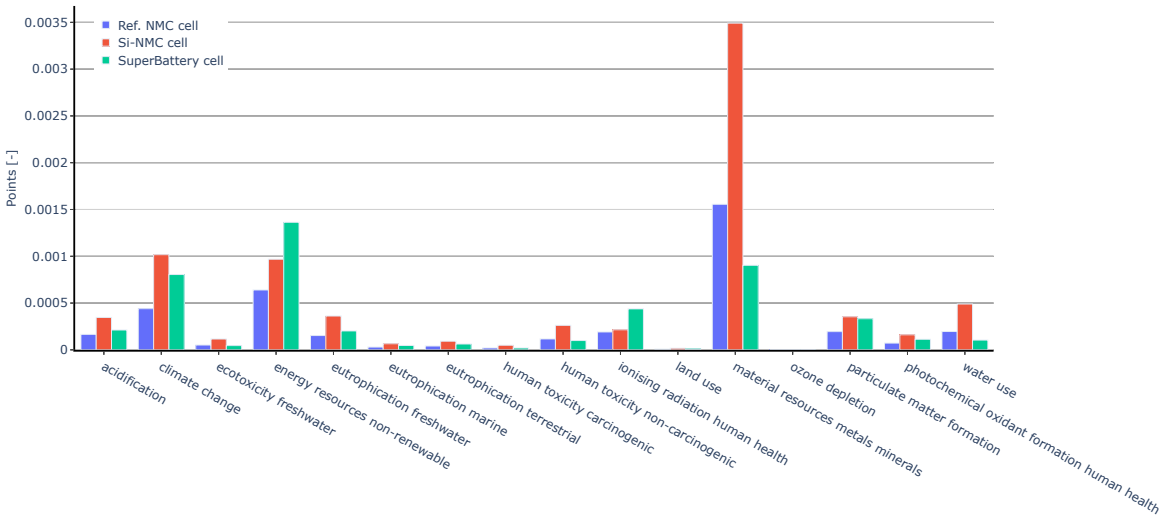

Figure 5.17 Normalized and weighted impact score for the Pipistrel Velis Electro with different battery cells.

Figure 5.17 shows that the increase in single score presented in Table 5.6 for the Si-NMC cell is essentially driven by an increase in impacts linked with the battery manufacturing process. Indeed, by breaking down the single score in terms of contributing process, the production of the battery accounts for an overwhelming 86%, reaching values that are comparable to the contribution of the fuel combustion and production on conventional aircraft. An additional reason for that result is the fact that a fairly low carbon energy mix has been considered, making the operation phase only a minor contributor (8% of the environmental single score), entailing that solutions that reduce energy use are not desirable. In terms of scores in impact categories, this translates into an increase across multiple indicators such as climate change (+127%), the depletion of non-renewable energy resources (+51%), but, more strikingly, the depletion of material and minerals (+124%). This stems from the fact that, in the lifespan considered for the whole aircraft, the battery needs to be replaced 56 times. Even considering the reduced mass, this leads to an equivalent

of 1.1 kg of battery required to perform one FU, i.e., to fly one hour. In contrast, on the reference design, only 0.48 kg is required.

On the Pipistrel with the SuperBattery cell, that number is even smaller, with a mere 0.34 kg of battery necessary. It is interesting to point out that, for the latter, given the high lifespan of the cells, other components in the powertrain (motors, inverters, ...) would need to be replaced first. Further investigation into the contribution of the battery reveals that, while the production phase is still the one with the most impacts (64% of the single score), the battery only represents 22% of the total. However, the high lifespan of the cell is not the sole reason for the stark decrease in the battery's contribution to the single score. Indeed, as pointed out earlier in the section, the manufacturing processes of the battery are different. Mainly, the SuperBattery advertises a low usage rate of rare minerals, thus explaining the decrease in the associated impact category in Figure 5.6. This is also the reason why the impact intensity of the battery, illustrated by the sum of weighted impacts across all categories for one unit of mass, is lower for the SuperBattery as illustrated in Table 5.7. This Table also shows the higher impact intensity of the Si-NMC cell, even considering no silicon losses in the anode manufacturing.

Table 5.7 Impact intensity of the battery manufacturing process for the different battery cells.

	Ref. NMC cell	**Si-NMC cell**	**SuperBattery cell**
Impact intensity (pts/kg)	0.0055	0.0062	0.0032
Variation (%)	-	+12%	-41%

The low share of impacts attributable to the battery pack in the case of the Velis Electro sized with the SuperBattery, however, raises the question of the other contributors to the single score. To answer that question, the contributors to the three highest impact categories in Figure 5.17, i.e., the depletion of non-renewable energy resources, the depletion of materials and minerals, and climate change, will be investigated. They are shown in Figure 5.18.

Figure 5.18 shows that for the Pipistrel with the SuperBattery cell, in the climate change category, the score is essentially driven by the contribution of the airframe. Because it is made of composite, and as its mass nearly quadrupled with the resizing of the aircraft with the heavier cells, its contribution has strongly increased. So much so that it is greater than the reference case altogether, which is enough to counterbalance the reduction of the battery pack contribution thanks to the more eco-friendly cell. The induced OAD effects can also be seen in the contribution of the use phase that has noticeably increased. An increase which is even more pronounced when looking at the depletion of non-renewable energy resources, where, just like the airframe in the climate change category, the use phase alone accounts for more than the whole reference combined. For the third category depicted in Figure 5.18, the depletion of minerals and metals, and since the impacts are essentially driven by the production of the battery with little to no contribution of other processes, the conclusion is

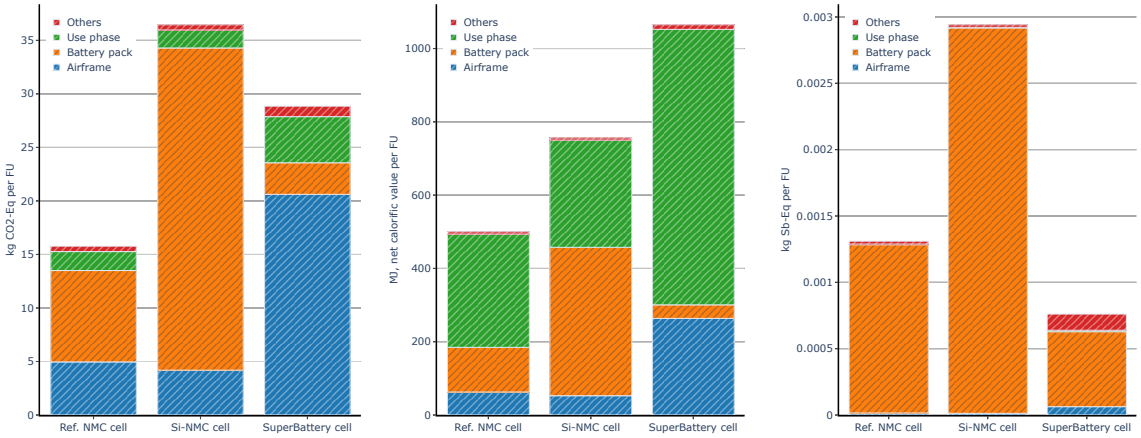

(a) Climate change. (b) Resource use, fossils. (c) Resource use, minerals and metals.

Figure 5.18 Comparison of impact magnitude in select categories for the Pipistrel Velis Electro with different battery cells.

straightforward. However, it is worth noting that the contribution of the "Others" category to that last impact category considered is significant. This is essentially linked with the increased power demand due to the increased mass, which, in turn, increases the size and mass of the inverter.

In conclusion, this case study demonstrates that for the aircraft configuration retained, the reference cell, which presents as a compromise in terms of energy density and lifespan when compared to the two other cells, yields the lowest environmental single score. However, Figure 5.18 also reveals the magnitude of the contribution of the airframe production process to the main impacts categories, which raises the question of the choice of materials for the airframe. Indeed, while composite allows for a lighter structure and fewer production losses, it also has a very energy-intensive manufacturing process. This question will be investigated in Section 5.5.3.

5.5.3 Effect of change in airframe materials

As discussed during the literature review on the use of LCA in the aviation sector, composites are a great lever to mitigate the impacts of aircraft. This was essentially linked with the fact that although composites are known to have a more intense manufacturing process, the lighter structure enables enough fuel savings that it is overall more interesting [253]. This result is a direct consequence of the overwhelming share of impacts linked with fuel production and consumption for commercial aircraft and the comparatively low share of impacts linked to production. Therefore, this conclusion might be worth questioning for configuration with a low-carbon energy vector, and for which the production phase is less

abated. As such, and even though the choice of composite materials may have been linked to other constraints like manufacturing, the Pipistrel Velis Electro presents itself as a great baseline to test the validity of that observation. A "what if" scenario [262] will be evaluated, where the structure of the aircraft will be assumed to be made out of aluminum rather than composite. The same study will also be performed on the Pipistrel SW 121 (the thermal version of the same airframe) to see if the observations made on commercial aircraft still hold. For that, the same design assumptions as those taken in Section 4.3.1 will be reused except for the 0.85 multiplicative factor on the airframe mass that was taken to account for the use of composites. For data on the aircraft usage, battery characteristics, electricity, and delivery method, the same assumptions as in Section 5.5.2 will be taken. For the BtF ratios, average values from the range found in literature will be used, with a value of 1.5 for composites and 7.5 for metallic components. As we will investigate configurations that burn AvGas for propulsion, and given the issues identified with the EF v3.1 method in that case, the ReCiPe method will be used.

Table 5.8 Main outputs for sizing of the reference Velis Electro and its metallic variant.

	Ref. Velis Electro	**Metallic version**	**Diff with ref.**
MTOM (kg)	600	661	+10%
Battery pack mass (kg)	150	162	+8%
Airframe mass (kg)	186	231	+24%
Electricity (kWh)	12.9	13.4	+4%

A comparison of the outputs of the sizing process is synthesized in Table 5.8. As expected, the metallic version of the Pipistrel Velis Electro has a significantly increased airframe mass, with an increase of 24% computed. It is worth noting that this increase is greater than the 15% that could have been expected given the multiplicative ratio previously used and can be explained by the snowball effect on the aircraft mass. Indeed, that increase in airframe mass increases the aircraft's MTOM, which increases the wing area and the loading constraints the aircraft is subjected to, thus further increasing the aircraft's mass. Interestingly, however, only a minor increase in the battery mass and energy required to perform the main route is found. As those were the other major contributors to the aircraft impacts, and depending on the impact intensity of aluminum, it might lead to a decrease in select impact categories. To further investigate that, the evolution of the scores in all midpoint impact categories proposed in the ReCiPe method is shown in Figure 5.19.

At first glance, the tradeoff mentioned above between the decreased impact intensity of the airframe manufacturing process and the increased masses and energy use does not seem worth it. Indeed noticeable increase across multiple impact categories can be seen, mainly ecotoxicity, both for freshwater and marine (+37% and +34% respectively), depletion of fossil resources (+31%), and the depletion of materials and minerals (+10%). However, this change of airframe materials also comes with a reduction in several key impact categories,

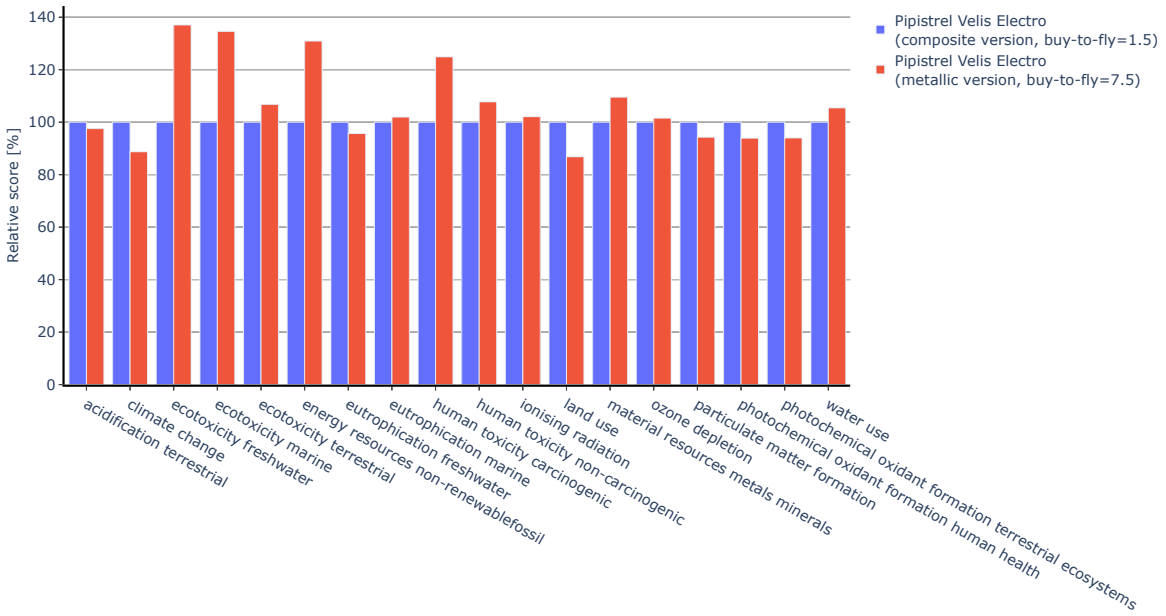

Figure 5.19 Relative comparison of the environmental impacts for the reference Velis Electro and its metallic variant.

the first of which is climate change, with an 11% decrease. This can be explained by the large contribution of the airframe to that impact category as illustrated in Figure 5.18a on the reference cell. Given the complex tradeoff between all impact categories, however, a straightforward conclusion can't be easily reached. In addition to that, and as previously discussed, the ReCiPe method doesn't provide official weighting factors. It is however possible to investigate how the midpoints impacts shown in Figure 5.19 translate at endpoint level. Furthermore, to enable easier comparison, the impacts will also be presented with their values normalized by the prescribed hierarchist normalization factor. The evolution of the scores in the three areas of protection of the ReCiPe method is shown in Table 5.9.

Table 5.9 Evolution of endpoint impacts for the reference Velis Electro and its metallic variant.

	Ref. Velis Electro	**Metallic version**	**Diff with ref.**
Ecosystem quality (Species.year)	$9.93\text{x}10^{-8}$	$8.55\text{x}10^{-8}$	-14%
Normalized (eq.person)	$6.71\text{x}10^{-5}$	$5.78\text{x}10^{-5}$	
Human health (DALY)	$6.33\text{x}10^{-5}$	$6.27\text{x}10^{-5}$	-1%
Normalized (eq.person)	$2.63\text{x}10^{-3}$	$2.61\text{x}10^{-3}$	
Natural resources (USD2013)	1.87	1.93	+3%
Normalized (eq.person)	$6.67\text{x}10^{-5}$	$6.91\text{x}10^{-5}$	

Table 5.9 shows similar behavior as for midpoints impacts in Figure 5.19 in that there is no clear answer as to which solution is best. However, a couple of interesting remarks can be

made. First, it is worth noting that changing the airframe has very little influence on the score in the human health area of protection; the analysis can thus focus on the depletion of natural resources and the ecosystem quality. For those impacts, the amplitude of the normalized score and its evolution are very similar. This means that unless significantly more value is given to one area, and since the decrease in the impacts on the ecosystem quality is greater than the increase in the depletion of natural resources, the change of airframe material is beneficial. This is reinforced by the fact that most midpoint categories contribute only to the human health and ecosystem quality endpoint category in ReCiPe (more information about the links between midpoint and endpoint impacts is given in the appendix, more specifically in Figure D.3) Therefore, since the latter barely changed and the former decreased significantly, the combination of the evolution of most of the impacts depicted in Figure 5.19 is desirable. This is however nuanced by the unambiguous increase of the two remaining midpoint impacts and their associated increase in the depletion of natural resources.

The same analysis was carried out on the Pipistrel Velis SW121. However, as opposed to what was done in Chapter 4 and since the goal is not here to compare the thermal version to the electric version, the design mission of the SW121 will be considered. A preliminary analysis of the amplitude of the contribution of each process to the midpoint impact categories proposed by ReCiPe was first conducted, similarly to what was done on the Cirrus SR22 in Figure 5.8. It is worth recalling here that the contribution of the production of the composite airframe was already identified as a major contributor. Given the even lower lifespan considered for the Velis Electro, we can thus expect that contribution to be greater in that case. The results for that preliminary analysis are shown in Figure 5.20. It shows that the score in a significant number of categories is driven by the production of the airframe. Significant variation can thus be expected.

The outputs of the sizing process and the normalized impacts in the three endpoint categories are reported in Table 5.10. Additionally, the evolution of the score in all midpoint categories is shown in Figure 5.21. From an OAD perspective, results are consistent with the case of the electric configuration, although it is worth noting here that the snowball effect is weaker here. This is due to the higher energy density of the energy vector. The consequence is that the heavier airframe and thus heavier MTOM induce a smaller added mass due to the energy, here merely 2 kg as opposed to the added 12 kg of battery mass reported in Table 5.8.

Results in Figure 5.21 show a strong increase in two of the impact categories that were already pointed out in the all-electric case. Indeed, the score in the freshwater and marine ecotoxicity has increased by 289% and 229%, respectively. This effect, which was an order of magnitude smaller in the case of the Velis Electro, can be explained by a displacement of the impacts linked with the change of materials. Its amplitude can be explained here by the fact that the airframe already accounts, in the baseline case, for more than 40 % of the impacts. In the electric case, these categories are also largely affected by the battery pack production, so much so that they represent a significantly smaller share (only 5%). For the

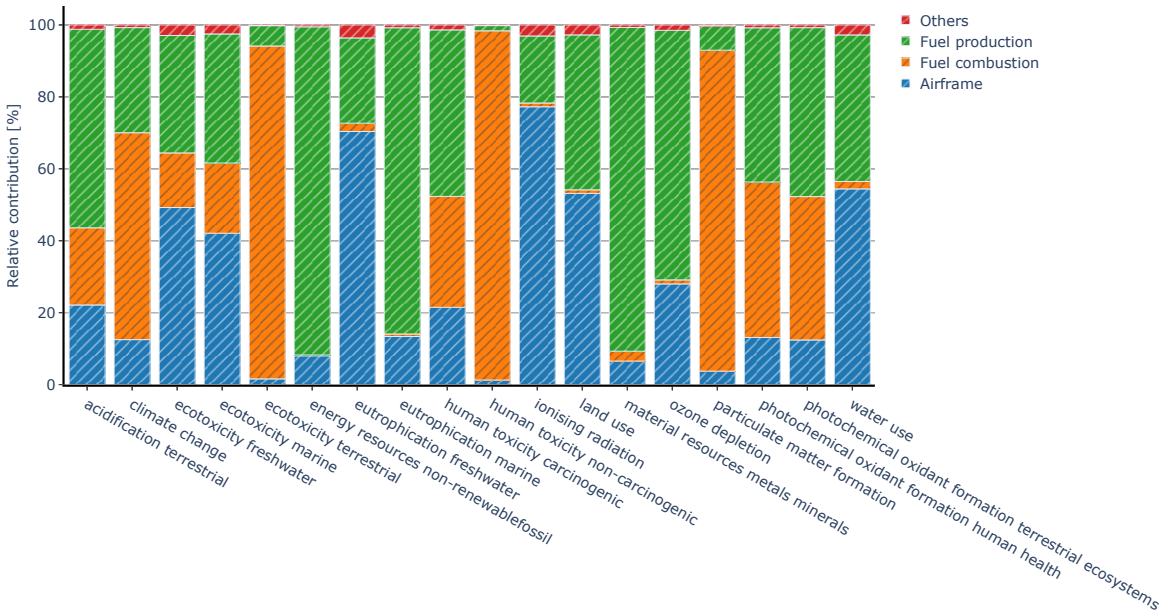

Figure 5.20 Relative contributions to each impact category for the reference Pipistrel SW121.

Table 5.10 Main outputs for the sizing process and LCA of the reference SW121 and its metallic variant.

	Ref. SW121	**Metallic version**	**Diff with ref.**
MTOM (kg)	589	640	+9%
Airframe mass (kg)	202	250	+20%
Fuel (kg)	58.6	60.3	+3%
Ecosystem quality (eq.person)	$1.16x10^{-4}$	$1.11x10^{-4}$	-5%
Human health (eq.person)	$1.22x10^{-2}$	$1.23x10^{-2}$	+1%
Natural resources (eq.person)	$2.65x10^{-4}$	$2.66x10^{-4}$	+0%

remaining categories, it is mainly interesting to highlight the relative variation in the climate change category. While in the previous case, abandoning composite materials allowed for a reduction of more than 11%, in the case of the thermal SW121, because of the carbon intensity of the fuel and the low usage of the airframe, that reduction is only equal to 4%. In terms of damage to protection areas, this translates into only minor changes, as can be seen in Table 5.10 with little to no change in endpoint categories other than ecosystem quality. Even there, the reduction is only equal to a mere 5%, which could easily be shadowed by uncertainties in the characterization factors.

To further look into the validity of those results, their sensitivity to the lifespan was investigated. More specifically, since it drives most of the impacts for the thermal configuration, the impacts in the climate change category were analyzed. As shown in Figure 5.20, the score in the climate change category is essentially linked with the contribution of the airframe

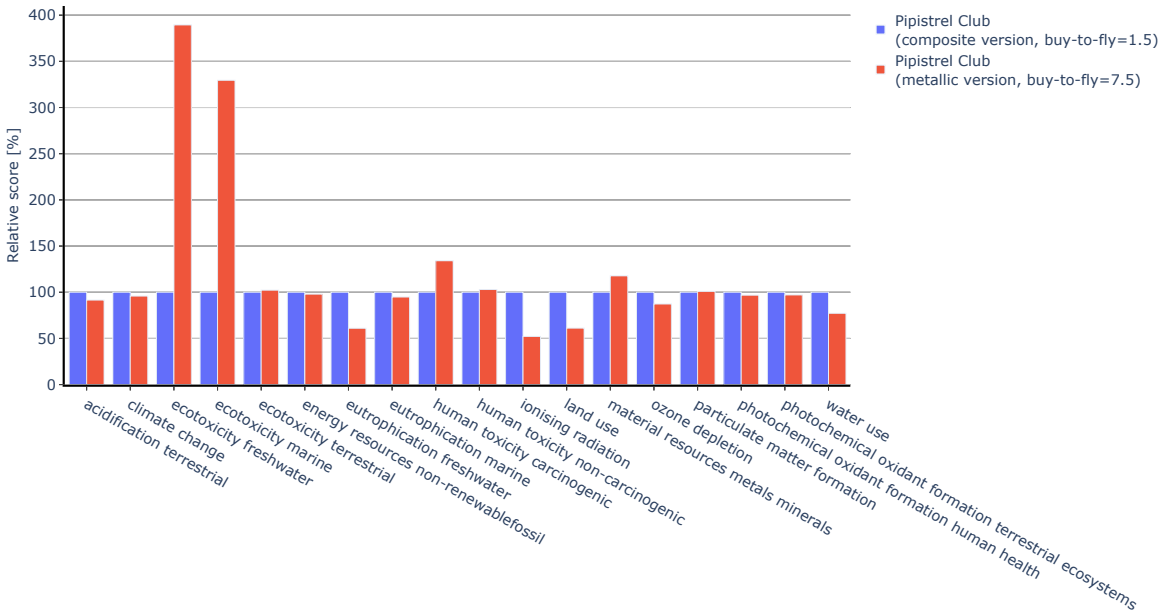

Figure 5.21 Relative comparison of the environmental impacts for the reference SW121 and its metallic variant.

production and the contribution of the fuel, mainly its combustion and production, both of which are linked to the fuel quantity. Therefore, the score can be expressed by Equation 5.1

$$IS_{\text{climate change}} = IS_{\text{fuel, climate change}} + IS_{\text{airframe, climate change}} \tag{5.1}$$

where IS is the impact score. Those two terms can then be developed to make the dependency on foreground parameters explicit, which becomes:

$$IS_{\text{climate change}} = \frac{m_{fuel}}{\text{flight}} * \left(\frac{FU}{\text{flight}}\right)^{-1} * (IF_{\text{production}} + IF_{\text{combustion}}) + \frac{m_{\text{airframe}}}{\text{aircraft}} * \left(\frac{FU}{\text{aircraft}}\right)^{-1} * BtF_{\text{material}} * IF_{\text{material}} \tag{5.2}$$

where IF is the impact factor which characterizes the impacts of foreground processes imported from ecoinvent or which are rebuilt by the framework in the selected category and the $\frac{\cdot}{\text{flight}}$ and $\frac{\cdot}{\text{aircraft}}$ fractions represent a quantity per flight or per aircraft, respectively. Upon closer inspection, all the terms in this expression are known. Besides the impact factors for which data are available in the database we selected, the rest are either inputs or results from the sizing process. The number of FU per flight will remain constant for both configurations, as the design mission was kept, whereas the mass of fuel per flight and the mass of the airframe have both been calculated by the process. The remaining term, the

number of functional units performed over the life of the aircraft, is, given our choice of functional unit, equal to the lifespan of the aircraft expressed in hours. Using this equation with the values reported in Table 5.10, it is thus possible to find the value of the aircraft lifespan after which keeping a composite structure is more beneficial. This can be found by looking for the value of $\left(\frac{FU}{\text{aircraft}}\right)^{-1}$ for which the impact score with the composite airframe and with the metallic airframe is equal. This value is found to be equal to approximately 10500 h, or in other words, as long as the aircraft is expected to fly less than 10500 h during its lifetime, the metallic airframe will yield fewer impacts in the climate change category than the composite one. It is worth noting, however, that this analysis was conducted considering only one impact category, especially one where the airframe originally had a significant contribution and where the switch from composite to metallic yielded great benefit.

As a conclusion to this section, it is essential to point out that the amplitude of the impact reduction when switching between composite and metallic structure were very small, and as such, the robustness of the conclusion to the assumptions shall be challenged. Mainly, we assumed that in order to perform the "what if" scenario, the only changes that were needed were the process for the manufacturing of the airframe (including the BtF ratio) and the impact on the airframe mass. More specifically, the aerodynamic computations were never challenged, although composites allow for significantly smoother surfaces and higher aspect ratio wings. Thus, it could be argued that aerodynamic penalties, and therefore higher fuel consumption, should have been incurred by the metallic structure. An argument in favor of the metallic structure could also be made regarding the lack of consideration of the end-of-life of the aircraft. Indeed, metallic scraps are more easily recycled than composite leftover thus giving an edge to metallic structures. A final concluding remark would be the investigation of other types of composites. Indeed, the results of this Section hinged on the high energy intensity of the CFRP production. However, different types of composites called bio-composites have been shown to have great potential thanks to a reduction by a factor of 5 of the energy required for production [288].

5.5.4 Effect of battery aging

In addition to the concluding remark of Section 5.5.2 on the influence of the airframe, arguments about the sensitivity of the design solution to the cell lifespan were made. In that regard, the literature reviewed in Section 3.6.1 showed that it depended on the conditions in which the battery packs were used. More specifically, the selected model showed a dependency on the temperature of the cells and the DoD for the cyclic aging and a dependency on the storage SoC for the calendar aging. As a preliminary analysis, the coherence of the model with values reported in literature for the Velis Electro [227] was checked. For easier comparison with the values used so far, expressed in cycles, and to include the calendar aging, the unit equivalent cycles, consisting of a discharge cycle during the mission plus the time between

missions, will be used. During the first part of an equivalent cycle, only cyclic aging will be considered, while in the second part, only calendar aging will be considered. To compute the time between cycles, the yearly usage reported in the GA survey from the BTS will be used. For conditions related to calendar aging, the battery will be assumed to be stored in a "ready-to-use" state, i.e., with a SOC of 100%, and will be assumed to be stored at 25°C. For the cyclic aging, which depends on the DoD at the end of the main route, it will be a result of the performance estimation. Regarding the temperature, as a thermal model is yet to be implemented, a constant value of 23°C will be assumed. As discussed in Section 3.6.1, the battery will be assumed to be renewed after losing 20% of its initial capacity. A summary of all those conditions is presented in Table 5.11. Except for the DoD on the main route, the rest of the conditions will be assumed to remain constant for all subsequent test cases.

Table 5.11 Main input parameters for the battery aging model.

General	Capacity loss at End of Life	20% of C_{init}
Cyclic aging	Cell temperature during mission[a]	23°C
	Start of main route SoC[a]	100%
	End of main route SoC[b]	55%
	Main route DoD[b,c]	45%
Calendar aging	Storage SoC[a]	100%
	Storage temperature[a]	25°C
	Average time between cycles[a]	0.607 days

[a]: Input parameters

[b]: Outputs of the sizing process

[c]: The DoD here and used in the aging model refers to the amplitude of the discharge on one cycle, not the current discharge state

Given the mission profile and the choice of input parameters, a battery cell lifespan of 900 equivalent cycles is estimated using the implemented model, which gives a slightly more optimistic value than the 700 cycles reported in literature [227]. Despite this slight difference, this model will be further used to investigate the impact of performances on the lifespan of the aircraft. It is however worth recalling that the battery lifespan largely depends on the temperature, which we assumed. For instance, on the SuperBattery used in a previous section, the cell lifespan is reportedly divided by a factor of 4 when the average temperature in use goes from 25°C to 45 °C.

Optimization of aircraft performances for longer battery lifespan

As mentioned in the introductory part of this section, one of the deciding parameters for the battery lifespan is the amplitude of the discharge during the mission. As such, it was deemed worth investigating whether over-sizing the battery could lead to an increase in the lifespan, which would yield benefits. Indeed, increasing the number of cells for the same requirement in energy leads to an overall smaller depth of discharge at the cost of an increased mass.

To investigate that trade-off, the Velis Electro will be used as a baseline platform. Although the framework developed allows to explicitly set the number of cells in series as input, thus allowing to showcase an effect of an increase in that number on the lifespan, a different approach will be retained. Instead, the value of the SoC at the beginning of the mission will be changed to a decreasing value. As the requirement on the SoC at the end of the mission will remain the same, this will thus result in lower discharge amplitude. Values of the starting SoC on the design mission between 100% (the reference case) and 80% were investigated. For each of those, an aircraft with the same inputs and TLARs as the Velis Electro will be sized, and its environmental impacts will be investigated. The aircraft will be assumed to have a lifespan of 4000 h with a yearly use of 283 h as per the BTS data on GA aircraft. For the structure, and as the point of this analysis is more focused on the performance's impact on the battery lifespan, a BtF ratio of 1.0 will be assumed. The EF V3.1 LCIA method will be used along with the recommended normalization and weighting factors in order to provide a single score for interpretability. The variation of the predicted battery lifespan, the battery mass required for one functional unit, and the total single score for the described case are presented in Figure 5.22.

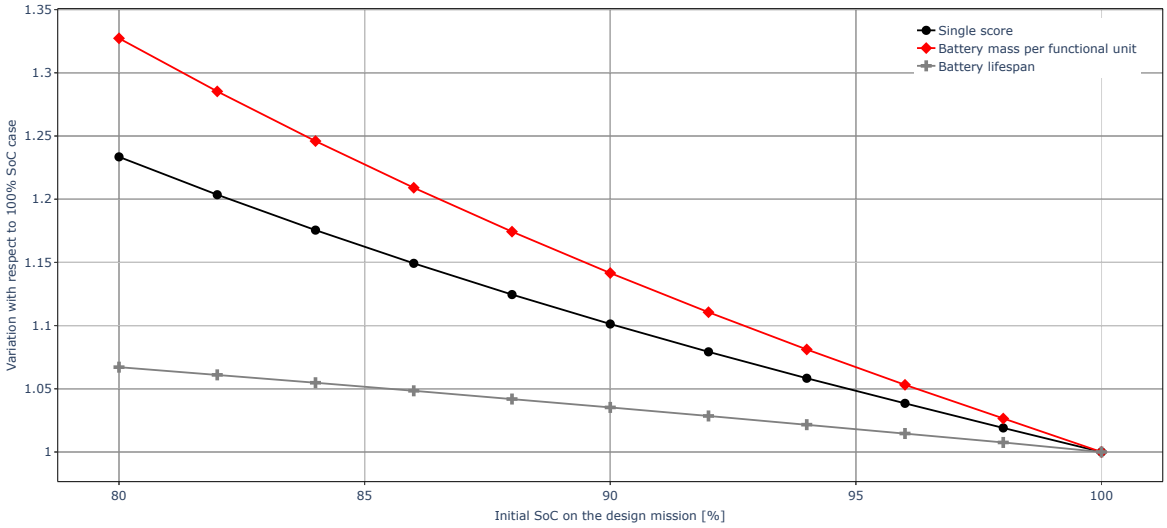

Figure 5.22 Variation of battery lifespan, battery mass per FU, and single score for decreasing SoC at the start of the mission.

Results show that, as expected, the lifespan of the battery pack increases with respect to the baseline case when the starting SoC is reduced. In the case where the battery starts the design mission charged at 80%, the lifespan is increased by about 7%. The increase in mass, however, is much faster. It is worth noting that Figure 5.22 does not show the increase in mass directly; rather, it shows the increase in the mass required to perform one functional unit, as

this is the weight on the branch of the process tree that will impact the battery production process. That quantity is computed by Equation 5.3.

$$\frac{m_{\text{battery}}}{FU} = m_{\text{battery}} \times \frac{N_{\text{battery}}}{\text{aircraft}} \times \frac{\text{aircraft}}{FU} = m_{\text{battery}} \times \frac{\text{flight}}{\text{aircraft}} \times \lceil \frac{\text{flight}}{N_{\text{cycles,battery}}}^{-1} \rceil \times \frac{\text{aircraft}}{FU} \tag{5.3}$$

The mass required to perform one functional unit can thus be seen as a quantity combining the lifespan of the cell with its mass, which is the goal of this study. In particular, Equation 5.3 shows that it depends on the number of battery pack that needs to be produced during the life of the aircraft, represented by the term $\frac{N_{battery}}{\text{aircraft}}$. Thus, as long as the change in cell number does not cause a need for an increased or decreased number of battery renewals, that quantity is proportional to the battery mass. As there is no sudden "break" in the red curve in Figure 5.22, this is the situation encountered in this study. Therefore, it does not seem like increasing the number of cells is beneficial in this scenario. This is reinforced by the fact that the cell lifespan increases more slowly (by about 7%) than the number of cells (about 33%), meaning that, even if the rounding up was not considered in Equation 5.3, it would not be advantageous. Further investigations into the cyclic aging of the battery were conducted because the calendar aging will not be affected due to the choice of inputs. The model adopted and presented in Equation 3.17 reveals that, given the absence of thermal modeling, the cyclic aging is mostly dependent on a function of the DoD. This function, which has been approximated in literature [162] as a third-order polynomial, appears to have a very small derivative around the points that have been explored in this study, meaning a small change in the DoD on the mission leads to only small improvements on the lifespan. This is illustrated in Figure 5.23.

The analysis of Figure 5.23 confirms that the battery of the Pipistrel is used in a region where the derivative with respect to DoD is not at a maximum and that bigger variations can be attained when the battery is fully discharged. This remark echoes an observation on the fact that the energy allocated to carrying out the reserves takes up half of the state of charge of the two batteries, as shown in Table 5.11. It might therefore be interesting to investigate whether the initial choice of energy distribution was optimal or whether having one battery solely for the main route and one battery solely for the reserve might not yield reduced environmental impacts.

This particular configuration was looked into next. The same assumptions regarding the OAD and the LCA were kept, except for the power management strategy. The battery located at the rear of the aircraft was selected to provide all the energy required during the main route, while the front battery will provide the energy during reserves. Therefore, from an aging point of view and under the assumption that reserves will seldom be used, the front battery will only suffer the effects of calendar aging. Initial analysis into this configuration, which will henceforth be referred to as Pipistrel Velis Electro+, led to the realization that

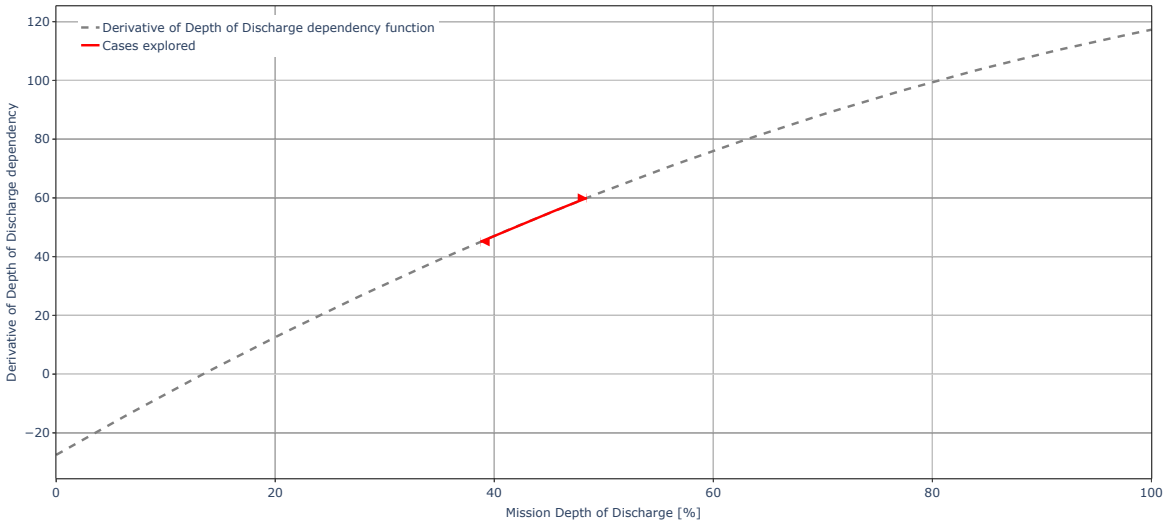

Figure 5.23 Derivative, with respect to DoD, of the function representing the effect of DoD on the cyclic aging.

using a single battery pack did not allow to meet the original required climb performances. For this reason, a more power-dense cell, the Samsung INT18650-25R presented in Appendix C.6, will be used for the main battery pack. We will additionally assume that the aging model remains valid for this cell. It is also worth noting that, as opposed to the baseline case where both packs have the same configuration, the same cell, and are used the same way, thereby meaning they provide the same voltage at each point of the flight, it will not be the case anymore. Therefore, since both batteries are connected to the same bus, a regulation of the voltage is required. This will be simulated by two DC/DC converters added between the battery and the splitter. For simplicity, their efficiency will be assumed constant, and their mass will be computed based on a power density representative of today's technologies [43]. A summary of the assumptions changed by this study is synthesized in Table 5.12.

Table 5.12 Added assumptions for the sizing of the Pipistrel Velis Electro+.

Mission	Climb hybridization ratio[a]	100%
	Cruise hybridization ratio[a]	100%
	Descent hybridization ratio[a]	100%
	Reserve hybridization ratio[a]	0%
	Others phases hybridization ratio[a]	100%
Propulsion	Battery pack 1 cell	Samsung INR18650-25R
	Battery pack 2 cell	Samsung INR18650-35E
	DC/DC converter efficiency	98% [43]
	DC/DC converter power density	15 kW/kg[43]

[a]: the hybridization ratio is equivalent here to the percent of the total power provided by the main battery

These assumptions yield the results presented in Table 5.13. From an OAD perspective, the aircraft is way heavier with an increase of about 55kg in the MTOM. This is mostly attributable to the increase in the battery mass, which totals to an added 30 kg. The reasons for that increase are twofold. First, the mass of the secondary battery pack (with the same cell as the reference case) has increased because more energy needs to be stored. This is due to both the increased energy demand due to the increased weight, but also because the energy required for reserve is greater than half of the energy required throughout the mission (which is what was stored in the battery before). For the primary battery pack, the increase is mostly linked with the required change of battery cell. Indeed, the Samsung INR18650-25R has an energy density of 200 Wh/kg or, in other words, a decrease of 23% of the energy density. The effect on the battery lifespan is also quite noticeable, with an increase in the secondary battery lifespan that leads to only needing one renewal through the lifespan of the aircraft. For the primary battery, used more intensively, the reduction of the lifespan is also quite noticeable. This, however, was expected, and the influence of the oversizing of the primary battery in this configuration will be investigated next. The same range of starting SoC as the previous case was investigated, leading to the results presented in Figure 5.24.

Table 5.13 Main outputs for sizing of the Velis Electro+.

	Ref. Velis Electro	**Velis Electro+**	**Diff with ref.**
MTOM (kg)	600	656	+9.3%
Battery pack 1 mass (kg)	75	100	+33.3%
Battery pack 1 lifespan (cycles$_{eq}$)	898	566	-37.0%
Battery pack 2 mass (kg)	75	80	+6.7%
Battery pack 2 lifespan (cycles$_{eq}$)	898	5222	+481%
Electricity (kWh)	12.9	13.6	+5.4%
Single Score (pts)	31.1x10^{-4}	35.9x10^{-4}	+15.4%

Results show that, as opposed to the original case where improvement of the lifespan of only a few percent could be found, because the battery is now used in a region where it is much more sensitive to the depth of discharge, increases by up to 25% can be achieved. Additionally, as opposed to the original case, a sudden break in the red curve representing the need for less renewal can also be observed. The fact that these breaks are now observable is mostly linked to the small lifespan of the primary battery pack's cells. Indeed, the number of renewals is an inverse function of the cell's lifespan, as shown in Equation 5.3, therefore it varies much more quickly for lower values. Interestingly, a significant reduction of the single score can be achieved going from a starting SoC of 100% to 98%, i.e., with a small oversizing of the number of cells. In addition to attesting to the importance of a precise assessment of the cell's lifespan, this reveals a great dependency, even greater than on conventional configurations, on the aircraft's expected lifespan. More precisely, there is a dependency on the ratio between the battery lifespan and the number of cycles the aircraft is expected

to carry out during its life. This highlights the need for strategies to better plan the life of the aircraft. At the very least, it encourages considering, after a certain number of battery renewals, whether the aircraft is expected to last until the next renewal of the battery pack. It also advocates for easing the reuse of batteries, at the cell or pack level, to avoid having to decommission new packs because the airframe stops flying immediately after a renewal. Although this case demonstrates the interest of oversizing the battery packs to prolong their lifetime, when compared to the original design, it yields a greater environmental single score. This increase is mostly due to the increase in the mass of battery required to perform one functional unit. More precisely, the mass of the primary battery pack alone required for one FU is greater than both battery packs in the reference scenario. In addition to that and even despite the low carbon mix selected, the added electricity requirement and increased airframe mass also significantly increase.

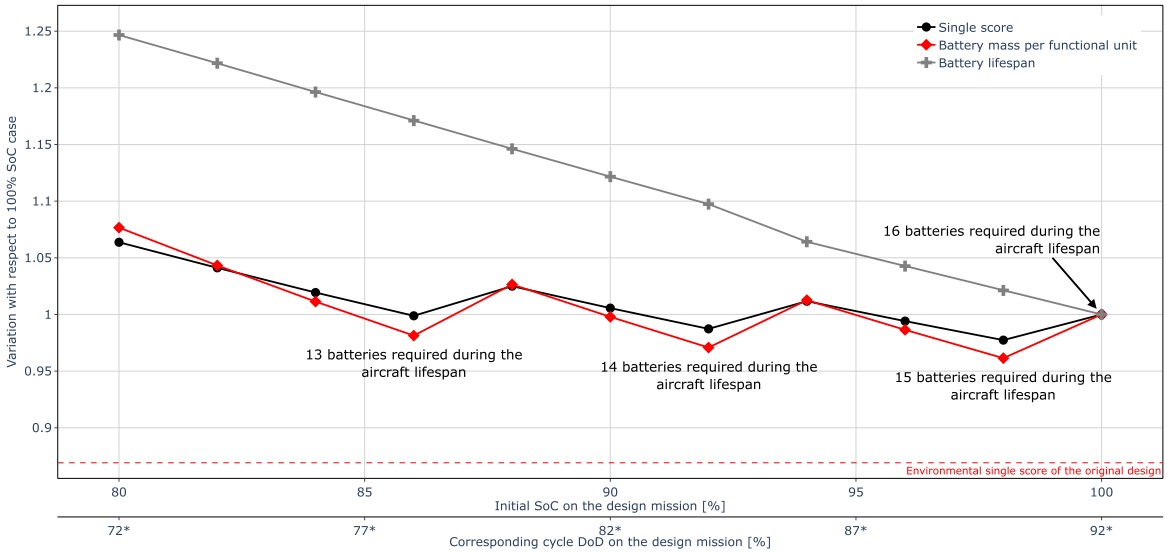

Figure 5.24 Variation of battery lifespan, battery mass per FU, and single score for decreasing SoC at the start of the mission for the Velis Electro+.

Optimal combination of battery cell chemistries

This previous case study illustrated the potential of specializing the batteries to better control how to optimize their contribution to the environmental impacts. Nonetheless, due to the choice of cells, the mass of the aircraft increased, leading to increased energy demands and thus increased battery mass. Section 5.5.2 highlighted that using a higher battery energy density cell could lead to lower mass at the cost of batteries being more sensitive to cyclic aging. However, as underlined by the case of the Pipistrel Velis Electro+, the secondary battery, used for reserve, is only subjected to calendar aging. Thus, this pack represents a prime candidate for using Si-NMC cells. A final case, which will be called the Pipistrel Velis

Electro++, and which will use the Si-NMC cell for the secondary pack, will be investigated. Identical assumptions as for the previous cases will be taken regarding the aircraft usage, the LCIA methods, and the BtF. A key assumption that will be made is the fact that the aging model will be assumed to be identical for the Si-NMC cell. Although research has shown that considerable improvement in the calendar life of Si-NMC cells is possible [289], state-of-the-art tends to show that the typical values for current Si-NMC cells are around one year. Therefore, this last assumption might be overly optimistic. For the manufacturing process of the cell, a similar proxy as presented in 5.5.2 will be used. The resulting aircraft is presented in Table 5.14.

Table 5.14 Main outputs for sizing of the Velis Electro++.

	Velis Electro	**Velis Electro+**	**Velis Electro++**
MTOM (kg)	600	656	591
Battery pack 1 mass (kg)	75	100	96
Battery pack 1 lifespan ($cycles_{eq}$)	898	566	566
Battery pack 2 mass (kg)	75	80	42
Battery pack 2 lifespan ($cycles_{eq}$)	898	5222	5222
Electricity (kWh)	12.9	13.6	13.1
Single Score (pts)	31.1x10^{-4}	35.9x10^{-4}	33.3x10^{-4}

A clear improvement of the environmental single score can be seen going from the Velis Electro+ to the Velis Electro++. This decrease is mostly attributable to the reduction of the impacts of the reserve battery pack ($\approx$ a 1x10^{-4} decrease). There are, however, also reductions that are linked to the induced effects of the lighter secondary battery pack. Indeed, using the Si-NMC has allowed for a significant reduction of the MTOM and airframe mass. Surprisingly, though, the energy required for the main route, while lower than for the Velis Electro+, is higher than that of the reference aircraft. This is linked to the efficiency of the additional converters that were added to regulate the difference in voltage between the two batteries. Nonetheless, despite the reduced mass, the original Pipistrel Velis Electro exhibits an overall better environmental single score. The oversizing of the battery was also investigated, but, similarly to the results presented in Figure 5.24, only improvements of 5% of the single score could be found.

Although the investigation of the Velis Electro+ and Electro++ did not yield an improvement in the single score, this section showed the strong influence that the desired performances can have on the lifespan of the cell and thus on its impacts. Therefore, precise knowledge of the expected missions of the aircraft is paramount to minimizing damage to the environment. This need has already been highlighted in literature, with other authors advocating for an evaluation of the impacts on a number of missions rather than a single one [259, 276]. Though this need has only been discussed for conventional airframes due to the varying flight efficiency on the different missions inside the payload range diagram, it is even

more crucial for electrified aircraft. Indeed, as was just shown, in addition to impacting the flight efficiency, the performances also impact the longevity of battery cells. Thus, computing the cell's lifespan based on an array of significant mission profiles seems like an interesting avenue of research. While this area of improvement will not be further pursued in this work, it reinforces the need for multi-mission assessment of new configurations [232].

Effect of aging on the aircraft's ability to perform its function

The conclusion of the previous section highlighted that, as opposed to what is mostly done in literature, where studies are carried out on a single representative mission, multiple mission profiles ought to be considered. Additionally, the previous part highlighted the strong impact of battery usage on its lifespan through the depletion of its capacity. The combination of these two points, however, calls attention to the fact that the reverse effect, that is, the effect of aging on the performances, is seldom taken into account. Indeed, the hypothesis of using only a single flight profile throughout the aircraft's lifetime implicitly assumes that it will be achievable regardless of the state of the battery. However, as discussed in Section 3.6.1, aging causes a loss of capacity, thereby meaning the aircraft will fly smaller distances. This reduction of the range, in turn, means that the aircraft is less able to fulfill its functional unit, which, as discussed, tends to increase the impacts. This section will investigate how accounting for those effects influences the environmental impacts of electric aircraft. To do so, the effects of the degradation of the state of health of the batteries on the achievable ranges of a reference aircraft will be investigated. This will then be translated into how many times the functional unit is fulfilled during the life of the aircraft considering this reduced flight distance. For this study, the reference Pipistrel was considered, and a particular focus on the battery will be done, as this was shown to be the component most sensitive to the need for renewal.

As a first step for this analysis, the achievable range at different states of health of the battery will be computed. To do so, starting from the reference design sized in Chapter 4, the off-design performances of the aircraft for SoH between 100% and 80% will be investigated. More specifically, the range that leads to a SoC of 0% at the end of the mission, including reserves, will be computed. This approach is made possible by the modular nature of the framework. The ability of the framework to solve a design problem or inverse problem, that is, to find a design that matches the operational requirements, has already been extensively shown in previous chapters. The framework, however, is also capable of solving a direct or analysis problem, which is to evaluate the performances of a given design. This was illustrated in Section 4.4.2 where the off-design performances of a hybrid SR22 sized for 200 nm were evaluated for shorter missions with varying hybridization ratios. In this case, the Velis Electro found as an output of the sizing problem will be used as an input of the analysis

problem, with the sole difference being the varying SoH of the battery. This approach is illustrated in Figure 5.25.

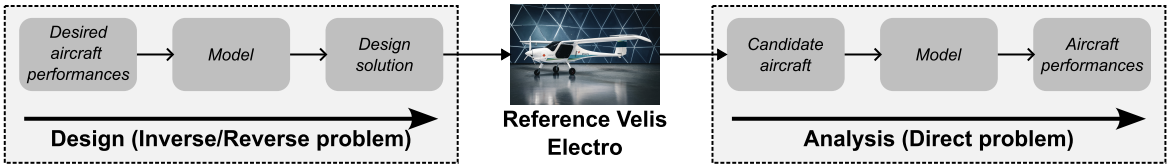

Figure 5.25 Approach adopted to evaluate the effect of SoH on the performances of the Velis Electro. Adapted from Figure 2.1 in Pollet et al. [276].

The required performances in climb, descent, and reserve will be assumed to remain the same. Therefore, any reduction in the apparent capacity of the cell will translate into a reduction in the length of the cruise phase. In addition to the already discussed effect on the reduction of the achievable range, and more specifically, the achievable flight time, it will also affect the average energy use for a flight hour. In fact, as the energy required to perform one functional unit is obtained by averaging on a representative flight, changing the repartition between climb, cruise, and descent will affect the average. Consequently, both of these parameters, the flight time and average energy required for one hour of flight, will be assessed. The results of that preliminary study are presented in Figure 5.26 and 5.27.

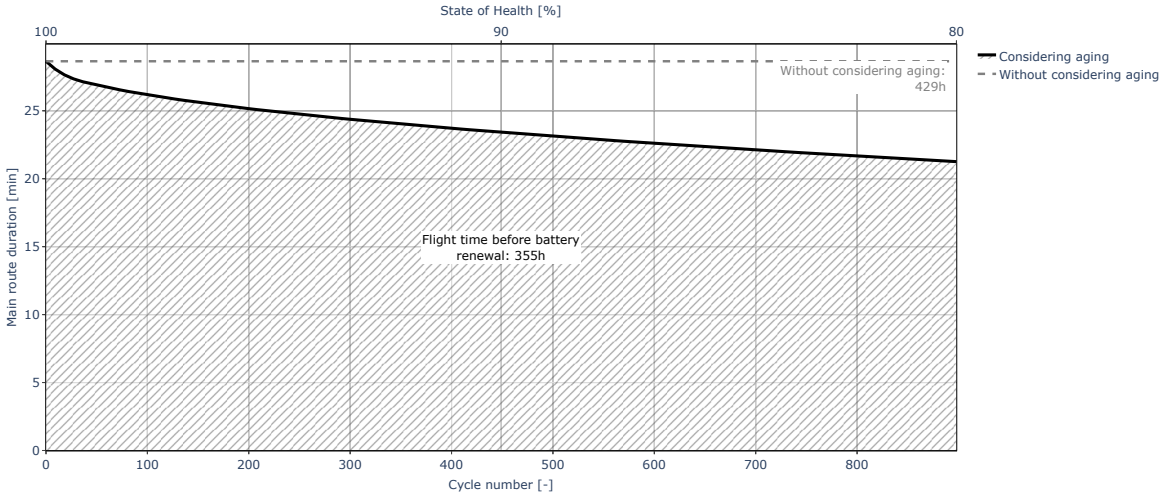

Figure 5.26 Effect of battery aging on flight performances. The main x-axis represents the number of cycles since renewal, the secondary axis shows the corresponding SoH.

Results in Figure 5.26 show that, as expected, battery aging leads to a progressive reduction in achievable flight time. For reference, the grey dashed line representing the initial case where aging effects on performances are neglected was also added. Since the chosen functional unit (FU) for the Velis Electro is “one hour of flight,” the total number of FUs achievable over the battery’s lifetime corresponds to the integral of the flight-time curve as a function of the SoH. In the case where degradation of performances is accounted for, this

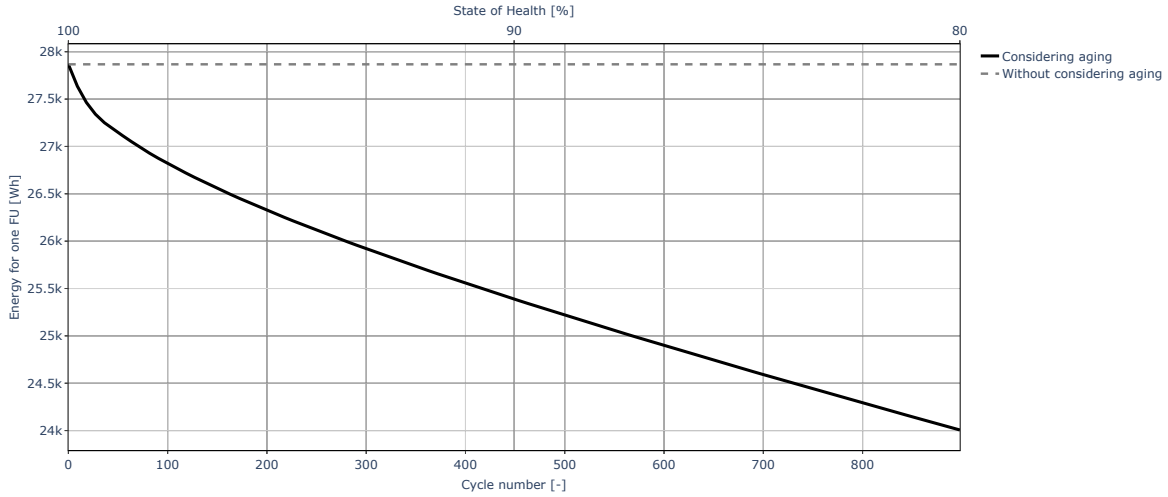

Figure 5.27 Effect of battery aging on average energy required for one FU.

total is represented by the shaded area. From this observation, the effect under investigation is clearly visible by the difference in areas between the two curves. Quantitatively, a reduction of around 17% of the number of FU that can be achieved during the battery's lifetime is computed. Regarding the trend of the curve, the rapid decrease at high SoH is explained by the model adopted, which shows a dependency on the square root of time.

Interestingly, Figure 5.27 shows that the older the battery gets, the lower the energy required to perform a functional unit. This is fairly unexpected as cruise is usually the phase of the flight in which the energy use is optimized [290]. Further investigations into the matter revealed that, given the imposed constraints on the climb and descent phases, the time-averaged power during phases other than cruise was smaller than the power in cruise. As such, reducing the size of the cruise segment tends to reduce the average power required during the fulfillment of one FU, thus reducing energy needs. Considering those two effects, a new LCA of the Pipistrel was conducted to assess the impacts of not considering the effect of cell aging on the performance. The evolution of the impacts in all the categories of the EF v3.1 LCIA is shown in Figure 5.28.

As the aging process mostly impacts the rate of renewal of the battery and the change in energy used to perform one functional unit, the increase in the score in the different impact categories is not uniform, as remaining contributions remain similar. For categories in which the main contributing process is the production of electricity, impact tends to remain quite similar and even decrease, given the computed gain in energy efficiency (-2.4% in ionizing radiation). For other categories, an increase between a few percent and up to 19% for the depletion of metals and minerals can be seen. In terms of the environmental single score, considering the suggested normalization and weighting factors, this translates in an increase of 12.5%. While this increase is not enough to question the gains brought by electrification highlighted in the study proposed in 5.5.1, it definitely calls attention to the inclusion of

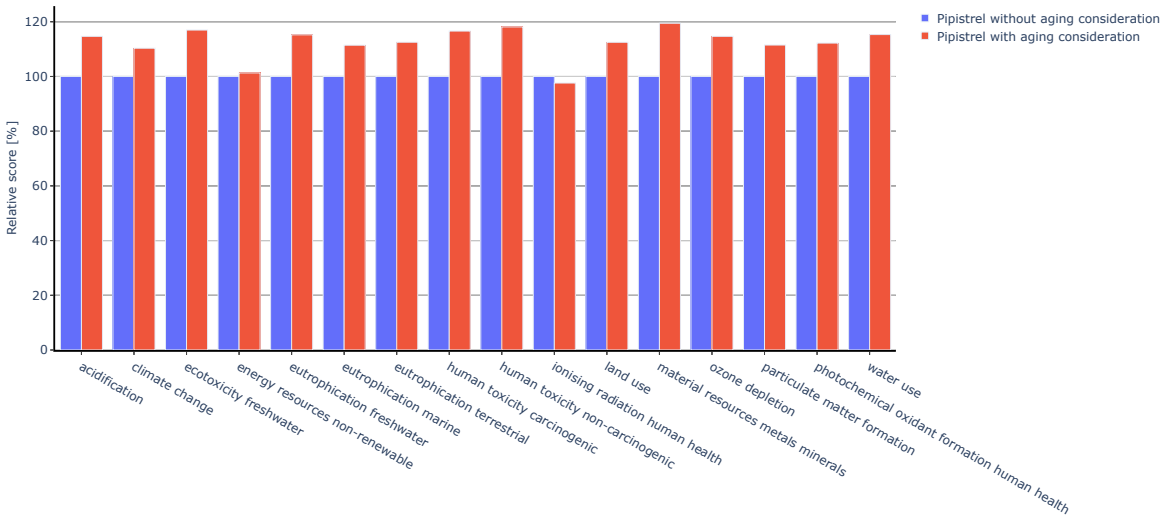

Figure 5.28 Effect of battery aging on score in EF V3.1 impact categories.

those considerations when evaluating the viability of all-electric and hybrid configurations. It is worth noting that the amplitude of these variations is highly case dependent, as it depends on the constraints imposed on the climb and descent segments, but also on the requirements to conserve the 30-minute reserve. Serendipitously, this study also strengthened the need for a clear definition of the functional unit and the alignment of the planned performances with it. Indeed, in that case, the FU was defined as "flying one hour". This definition included the time spent in climb and descent. As the aging of the battery led to a reduction in the energy available for the flight, and to keep the climb and descent profile intact, it was decided to reduce the time spent in cruise. Knowing that the energy required to perform the functional unit is obtained as a time average on the flight, and as this average is lower in climb and descent than in cruise, the aging of the battery is actually beneficial in terms of energy per hour of flight. This, in turn, hinted at the fact that adopting a see-saw flight profile could be better suited to minimize the energy required. Alternatively, it could also be advocated that the functional unit should have been changed to be more precise, like "flying one hour level". All in all, this case study reiterates the need for clear knowledge, both of the expected flight profiles during the life of the aircraft and of the aircraft's lifespan itself. It also highlights the capabilities of the design framework to both propose a design solution but also evaluates the performances of a reference aircraft under off-design conditions.

5.6 Application of the LCA for the assessment of future aircraft configurations

In addition to the electrification scenarios that have been investigated in Chapter 4 under the light of current technological level, this framework allows to study possible configurations with future technologies and assess their life cycle impacts. In this final section, the feasibility and benefits in terms of reducing the environmental impacts of an electric commuter aircraft will be investigated. Specifically, we will study the next generation of electric components and the predicted evolution of the technologies that comprise them. Particular focus will be placed on silicon carbide-based switching modules for power electronics, material evolution in electric motors, and battery cell chemistries. For future technologies, a horizon of 2040 will be selected.

Regarding the changes to the switching module inside the power electronics, and as discussed in Appendix B.3, the model adopted for the modeling of losses inside power converters is calibrated with respect to currently used Silicon IGBT modules. Silicon Carbide MOFSETs, however, have been shown to be more efficient and to allow higher power densities [291]. As the power converters have been implemented with Silicon IGBT modules, the effect of the use of SiC MOFSET will be modeled as a multiplication of the original model, rather than a new one altogether. To evaluate the amplitude of that change, the evolution of some key performance metrics will be evaluated for two modules with the same requirements: a voltage rating of 1200V and a current rating of 200A. For the characteristics of SiC-based modules, publicly available data from an existing module will be used[2], whereas for the Silicon module, the results of the model presented in Appendix B.3 will be taken. It is worth noting that a review of existing module have shown limited current ratings, incompatible with future power requirements. As the goal of this study is to assess future configurations, it can be assumed that such components will be available in the future.

Results found in literature regarding the reduction of losses are confirmed by the comparison, which shows a decrease by a factor of 4 to 6 in the energy losses due to switching. Additionally, minor reductions in the on-state resistances are found at the cost of an increase in gate voltage. At the level of the power electronics, literature predicts an increase in the switching frequency up to values of 100 kHz. A summary of the assumptions made regarding the predicted evolution of the characteristics in power electronics is given in Table 5.15.

Concerning the model used for the sizing of the electric motor, due to the use of scaling law and the implicit assumption that components will remain in the same "family", it is not possible to infer the evolution of performance metrics for future technologies. Incidentally, another reason limits the use of the current motor model for prospective scenarios. Indeed, in line with the discussions conducted in Section 4.4.2, the model leads to poor predictions

[2]https://www.infineon.com/assets/row/public/documents/60/49/infineon-ff3mr12km1h-s-datasheet-en.pdf, Accessed: 2026-02-11

Table 5.15 Predicted evolutions of characteristics in power electronics.

	Characteristic	2040 evolution wrt current tech.
IGBT/SiC MOFSET	Gate voltage (V)	+200%
	On-state resistance (Ω)	-15%
	Turn-on/-off energy (J)	-75%
Diode	Gate voltage (V)	+200%
	On-state resistance (Ω)	-15%
	Reverse recovery energy (J)	-83%
Converter level	Switching frequency (kHz)	+730%

when the required power exceeds that of the biggest engine in the EMRAX family, hinting at a possible limitation for the motor's architecture. For those reasons, a second electric model was implemented in FAST-OAD-CS23-HE based on the Surface-Mounted PMSM architecture (SM-PMSM) [53]. This model, which relies on analytical equations, has been developed to identify the breakthroughs required for future electric motor technologies. In addition to that, the original implementation of that model provides values for state-of-the-art electric motors (2025) and a scenario for the evolution of the technological parameters in the year 2035. The values of the latter will be used as being representative of the year 2040 for our scenario. A summary of the characteristics used and their evolution for our scenario is given in Table 5.16

Table 5.16 Predicted evolutions of characteristics in electric motors [53].

Characteristic	**2025 scenario**	**2040 scenario**
Tangential stress σ (Pa)	50000	70000
Current density j_{RMS} (A/mm^2)	8.1	20
Surface current density K_m (kA/m)	111.1	155.5
Number of pole pairs p (-)	2	4

For current battery technology, the Ampirius cells already extensively discussed will be used as their energy density offers the best chances of finding feasible designs. Regarding prospects in battery technologies, the next generation of cells is predicted to abandon the currently used Li-Ion for different chemistries offering better performance: Metal-air, Li-S, and Sodium-Ion batteries [292]. While metal-air batteries appear as an interesting candidate because of their high theoretical energy densities, possibly reaching values similar to gasoline, they will not be investigated further because of their very low expected lifespans [292]. Instead, particular focus will be set on Li-S and Sodium-Ion batteries as they have higher energy densities and higher lifespans.

Current state of the art for Li-S cells shows that minor degradation of the cell capacity can be achieved even after 1000 cycles, all the while showing energy densities 2-3 times higher than that of current Li-Ion cells [293]. In theory, even higher values of the energy density, around 2600 Wh/kg, could be reached [292, 294], but estimates on the practical

values achievable show that a value around 1300 Wh/kg [295] could be reached in the future. Additionally, literature shows that Li-S batteries have significantly lower impacts than Li-Ion ones in almost all categories, thanks to their lower rare-earth mineral contents [296, 297].

Similarly, Sodium-Ion batteries are expected to have lower impacts than Lithium-Ion thanks to the replacement of rare Lithium with Sodium, which is far more abundant [298–300], de facto reducing impacts in the depletion of mineral resources category. While current Sodium-Ion batteries require high temperatures to function, cells usable at room temperature are expected to become available after 2030 [292]. Additionally, projections regarding the energy density and lifespan of Sodium-Ion cells showed values between 380 and 700 Wh/kg and 6000 to 12000 cycles, respectively [292]. In addition to reinforcing previous conclusions regarding the mandatory tradeoff between the cell's longevity and energy content, the difference in value for those two chemistries also hints at the interest of investigating said tradeoff for future configurations. A summary of the evolution in terms of battery cells characteristics is given in Tables 5.17

Table 5.17 Predicted evolutions of characteristics in battery cells.

Characteristic	**Li-Ion (2025)**	**Li-S (2040)**	**Sodium-Ion (2040)**
Energy density (Wh/kg)	395	1300	700
Lifespan (cycles)	150	1000	12000
Nominal voltage (V)	3.7	2.2 [294]	2.7 [301]

Some assumptions regarding the manufacturing process of the airframe will also be made. Indeed, Section 5.5.3 showed that the metallic materials had potential in terms of reduction of life cycle impacts despite their very poor BtF ratios. The rise of additive manufacturing, and its use for metallic materials, however promise little to no manufacturing losses. Numerically speaking, provided that certain technological barriers are removed, ratios ranging between 1 and 3 are achievable [302].

The effect of prospective reduction of the impacts of inventories under future policy scenarios will also be considered. This will be achieved using `lca-modeller` interfacing capabilities with the `premise` package [303]. This package allows for the alignment of life cycle inventories from the ecoinvent database to match the output results of Integrated Assessment Models (IAM), which simulate the evolution of the world economies. In particular, the REgional Model of Investment and Development (REMIND) IAM [304] will be used as it focuses on the development of the energy sector and the implications for our world climate. Regarding the socio-economic pathway, a balanced scenario considering intermediate challenge for adaptation and mitigation is selected. Inventories will be projected to the year 2025 for the current technological scenario and to the year 2040 for the future technological scenario.

For the aircraft's TLAR, geometrical parameters, flight profile, and LCA specifications, the Kodiak 100 will be used as a reference. Some severe range reduction, consistent with the

discussion conducted in Chapter 4, will however be expected. Preliminary investigations into the feasibility of a Kodiak-100-like aircraft with current technologies led to a feasible range of merely 100 nm with a reduced payload. For future technologies, however, more ambitious ranges were considered. For the high energy density Li-S cells, a range of 600 nm was selected to cover 99% of the flights made with the current Kodiak 100 (See Figure 4.24). For the Sodium-Ion cells, a less ambitious range of 200 nm was selected. Although it is smaller than for the Li-S, it still covers more than 80% of the current needs for Kodiak 100. The resulting TLARs are presented in Table 5.18. Finally, regarding the electric mix, a European grid will be considered.

Table 5.18 Main TLARs for the sizing process and LCA of the electric commuter aircraft.

	2025 w/ Li-Ion	2040 w/ Li-S	2040 w/ Sodium-Ion
Design range (nm)	100.0	600.0	200.0
Design mission speed (KTAS)	120	120	120
Design mission altitude (ft)	10000	10000	10000
Reserve duration (min)	45	45	45
Approach speed (KTAS)	78	78	78
Payload (kg)	700	860	860

The results in terms of overall aircraft design are presented in Table 5.19. In addition to aircraft-level values, performance metrics for the components impacted by the technological scenario we considered will also be listed. It is worth noting that despite the ambitious ranges for 2040 technologies, no process encountered a divergence of the masses. Additionally, all the resulting designs are deemed feasible according to the criterion proposed in literature regarding MTOM sensitivity to the range [23]. For 2025 technology, however, that criterion is not validated.

Table 5.19 Main outputs for the sizing of the electric commuter aircraft.

	2025 w/ Li-Ion	2040 w/ Li-S	2040 w/ Sodium-Ion
MTOM (kg)	3616	3934	3765
OME (kg)	2916	3074	2905
Design mission energy (kWh)	366	1343	571
ESAR (NM/kWh)	0.273	0.446	0.350
Battery pack mass (kg)	2x570	2x574	2x527
E-motor power density (kW/kg)	5.4	15.3	15.0
E-motor rated power (kW)	577	631	575
Inverter power density (kW/kg)	62	103	103

Results presented in Table 5.19 confirm the interest in increasing the energy density of batteries to achieve higher ranges. For the particular flight profile we selected, which, as discussed in Section 4.5.2, results in very low power during cruise, this leads to very good flight efficiency, which is apparent in the drastic improvement of the ESAR. Additionally, the

efficiency of the electric powertrain is only marginally altered by the change in required power during cruise as opposed to the original thermal case presented in 4.28. The technological assumptions and their impact on the component metrics are also apparent through the increase in the power densities, allowing lower masses for higher power ratings. These lower component masses, in addition to the improved flight efficiency, additionally hint at a reduction of the environmental impacts. Indeed, as discussed in previous cases, the increased densities and efficiencies lead to lower masses of components to manufacture, thus less impact. In previous studies, this was counterbalanced by lower lifespans and higher airframe masses. In this study, however, the higher densities do not come at the cost of lower lifespan for the cells, and for the latter, a more advantageous BtF ratio was taken, so much so that the added structural mass is not detrimental to the overall impacts. This is illustrated by the great decrease in the environmental single scores presented in Table 5.20.

Table 5.20 Environmental single score of the electric commuter aircraft.

	2025 w/ Li-Ion	2040 w/ Li-S	2040 w/ Sodium-Ion
Single score (pts)	3.37x10^{-5}	2.15x10^{-6}	1.72x10^{-6}
ΔSingle score	-	-94%	-95%

Results in Table 5.20 show that the current version of the electric commuter aircraft has an impact that is an order of magnitude above that of the two future configurations, illustrating the potential of the introduction of new technologies for the future of electric aircraft. It is also interesting to point out that, even though they are not strictly speaking the same aircraft, the current version shows a higher environmental single score than the thermal Kodiak 100, whose results are described in Table 5.3. On the other hand, regarding the two future technological scenarios, the one using the Sodium-Ion cell appears to have lower environmental impacts than the Li-S cells despite the lower energy density and ESAR. Further inquiries into the major contributors confirm that, as evidenced by the results in Section 5.5.2, the depletion of mineral resources remains a major contributor to the single score, which is itself mostly a result of the battery manufacturing process. The normalized and weighted contribution of each impact category to the single score for the three configurations is presented in Figure 5.29.

It is worth noting in Figure 5.29 that some contributions were cut off from the graph because of the high contrast between the 2025 and 2040 technologies. More specifically, there is a division by around 50 of the impacts in the category linked with the depletion of mineral resources. Equation 5.4, a development of Equation 5.3, provides a conceptual explanation of the reasons for that decrease and the contributions.

$$\frac{\text{ESS}_{\text{batteries}}}{FU} = \frac{\text{ESS}_{\text{battery}}}{m_{\text{battery}}} \times \text{N}_{\text{battery}} \times \frac{m_{\text{battery}}}{E_{\text{battery}}} \times \frac{E_{\text{battery}}}{FU} \tag{5.4}$$

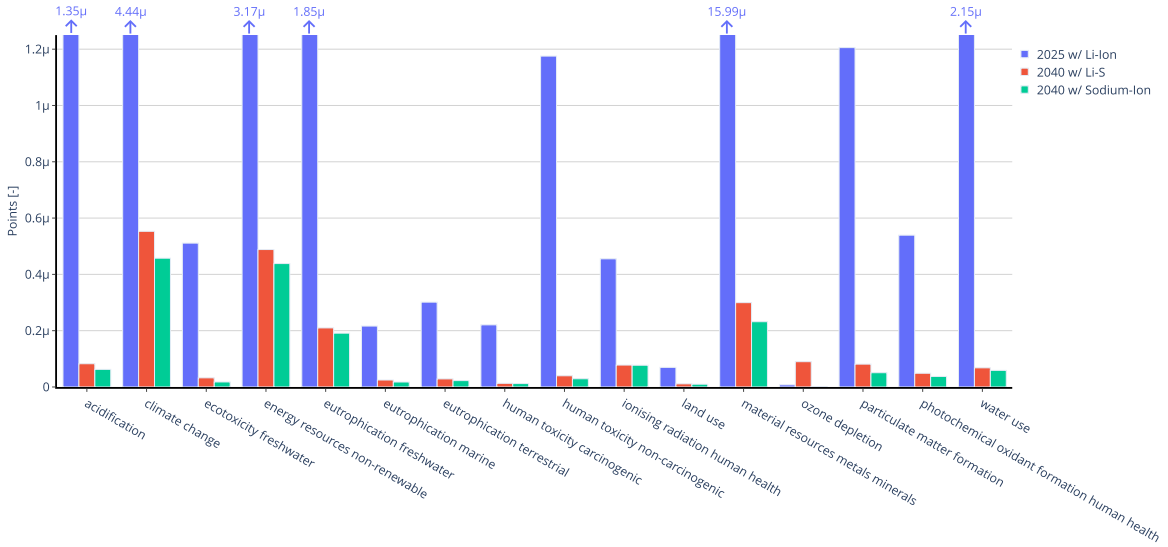

Figure 5.29 Normalized and weighted impact score for an electric commuter aircraft with various technological assumptions.

Equation 5.4 shows that the reduction of the impacts associated with the battery comes from four factors. The first one is linked with the manufacturing process of the battery, which is not only impacted by the change in cell chemistry but also by the projection, through the `premise` package, of the life cycle inventory to a more virtuous technological scenario. The second term is a direct consequence of the assumed prolonged lifespan of both chemistries. Similarly, the evolution of the third term follows from the assumed increase in energy density for both cells. Finally, the fourth term can be interpreted as the energy efficiency to perform the functional unit. It stems from the increase in flight efficiency and payload capabilities, which are both indirect consequences of the increased energy density, only quantifiable thanks to the tight coupling of LCA and OAD. It is worth noting that, among those 4 terms, only the last three are foreground data — in the sense that they are influenced by the design process — whereas the first is a consequence of uncontrolled inventories. The order of magnitude of the variation for those three last terms is presented in Table 5.21.

Table 5.21 Evolution of the factors contributing to the environmental score of the battery manufacturing process.

	N_{batt}	m_{batt}/E_{batt}	E_{batt}/FU
2040 w/ Li-S wrt 2025	x0.042	x0.303	x0.781
2040 w/ Sodium-Ion wrt 2025	x0.021	x0.564	x0.799

The results in Table 5.21 show that the Li-S battery outperforms the Sodium-Ion battery on the last two terms. The biggest contributor to the reduction of battery impacts, however, is the increase in cell longevity, a criterion in which the Sodium-Ion battery performs better.

This result confirms the conclusion of Section 5.5.2 regarding the need for cell balancing good lifespan and reasonable energy density. Additionally, it shows that, once the energy density threshold for a feasible design is met, prioritizing longer cell lifespans becomes more interesting. It also advocates for a focus of battery research towards cells with better aging characteristics. On top of that, this study shows another interesting result regarding the number of battery renewals necessary. More specifically, according to the usage selected for the increase — selected through the number of maximum airframe hours and yearly hours flown — only one Sodium-ion battery would be required, against two Li-S batteries. Besides being indicative of the potential of high lifespan cells, this result might be surprising given the difference in input lifespan for the two cell chemistries (1000 for Li-S vs 12000 for Sodium-Ion). This difference stems from the fact that, lacking data regarding the usage of commuter aircraft, it was approximated as an average amount of flight hours per year. As the Li-S battery allows for longer missions, it stays airborne longer, thus fewer flights, and consequently fewer cycles, are required to achieve the input yearly number of hours flown. While this is obviously a limitation of the model, which artificially prolongs the life of the Li-S cell, it also reinforces the need to have, as an input of the design process, an accurate knowledge of the usage of aircraft, possibly in the form of a Concept of Operations (ConOps).

Thanks to this reduction of the quantity of battery pack required to perform the functional unit, the share of the environmental impacts associated with the manufacturing of the battery decreases from an overwhelming 88% in the 2025 scenario to only 25% and 4%, for the Li-S and Sodium-Ion, respectively. More interestingly, in the case of the Sodium-Ion, that contribution is comparable to that of other components like power electronics. Regarding the identification of the other contributing processes, the relative contributions to each impact category of all processes are shown in Figures 5.30 and 5.31 for the Li-S and Sodium-Ion scenarios, respectively.

Figures 5.30 and 5.31 confirm the reduction of the relative importance of the battery manufacturing process in the environmental impacts of the electric commuter aircraft. Additionally, the impacts of the assumptions made on the airframe manufacturing process are also noticeable, with a division by a factor of around 10. More interesting, however, is the fact that the biggest share of impacts now comes from the production of the electricity required to perform the mission. Indeed, despite the assumed reduction in the impact intensity thanks to the projection of the inventories with `premise` — going from 2.65x10^{-5} pts/kWh to 1.41x10^{-5} pts/kWh — the even bigger reduction to all other contributors makes it a proportionally more important process. Further reductions could be obtained by switching the source of the electric mix used to a more environmentally friendly one, like the French mix, or to a more virtuous scenario for 2040. This preponderance of the impacts associated with energy production also hints at the interest of energy efficiency, a criterion in which the design with Li-S cells performs marginally better than the Sodium-Ion one according to the results in Table 5.21. Despite that, results show that the Sodium-Ion design has an

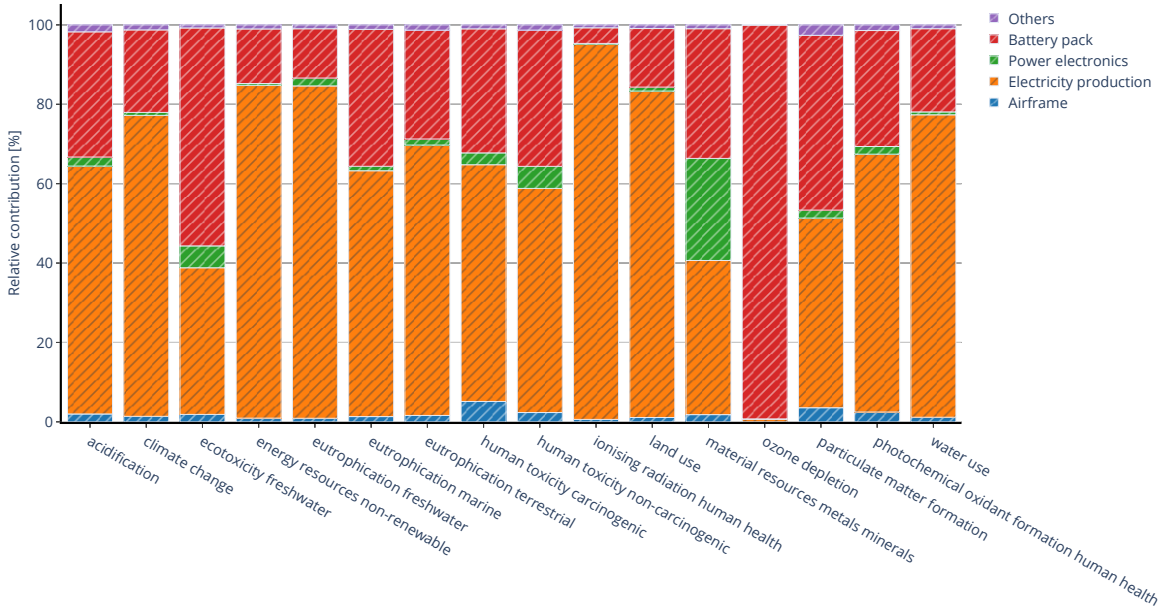

Figure 5.30 Relative contributions to each impact category for the electric commuter aircraft with Li-S battery.

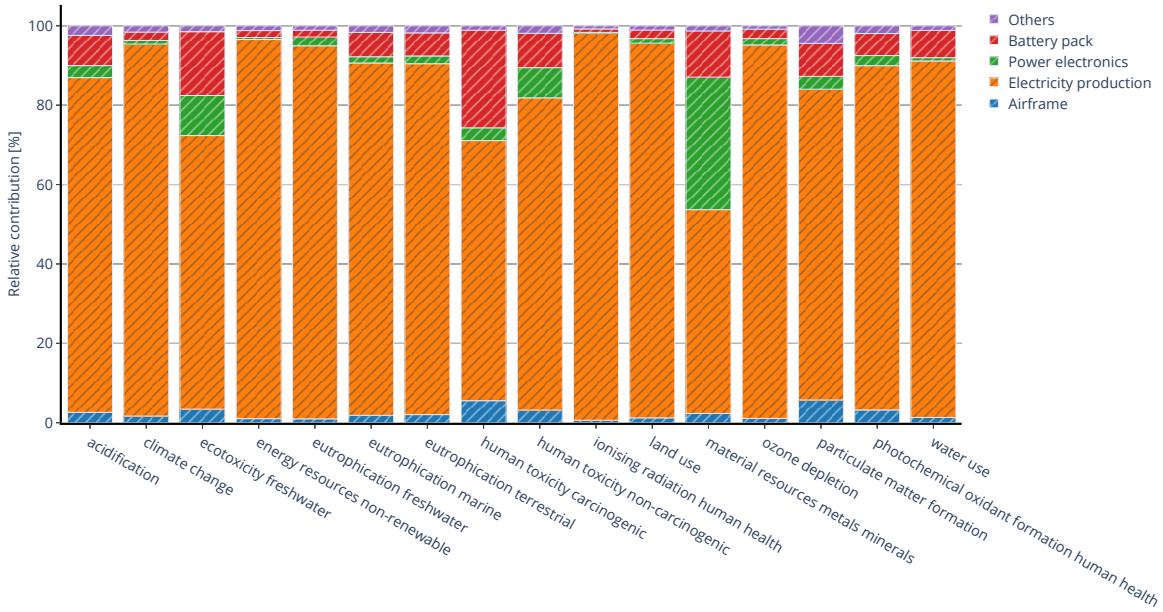

Figure 5.31 Relative contributions to each impact category for the electric commuter aircraft with Sodium-Ion battery.

overall lower environmental single score, echoing the preliminary conclusions made in this section regarding the interest of prolonging lifespan beyond a certain threshold value for the

energy density. While it is not in the scope of this work, the question of the cost of those new configurations is also worth mentioning. Besides the research and development costs, it appears that Sodium-Ion cells could be more expensive on a kWh basis when compared to traditional Li-Ion cells [301]. Although this may delay entry into service, those cells could prove advantageous in the long term, particularly in the event of a lithium shortage.

5.7 Conclusion and perspectives

Chapter summary

This chapter started with the observation that the analyses conducted in the Chapter 4 were limited, in terms of scope, to the use phase of the aircraft. This observation was put in parallel to the fact that electric components, in addition to potentially shorter lifespans, could require resources that impact the environment through different damage pathways. Finally, it was also observed that CS-23 certification category aircraft tend to be used less intensively than their commercial counterparts. This all culminated in the conclusion that manufacturing impacts should be accounted for in the electrification of such aircraft. From here, and given the traction gained by LCA methods in recent years, it was proposed to include such a methodology in the design process presented in previous chapters in order to enable a more comprehensive evaluation of electrified configurations' impacts on the environment. A literature review was then conducted to identify how LCA methods were used in the aeronautics sector. A few conclusions were drawn, the first of which was that most use cases investigated concerned transport aircraft and that, given the severity of impacts linked to the use phase, it was a common assumption to focus solely on the production and combustion of fuel. From a methodological point of view, it was also observed that LCA was mostly used as a post-processing tool after the design phase and that, therefore, the influence of design variables on the environmental impacts was rarely investigated. Finally, this review also allowed to identify that the use of LCA methods was most prevalent for the identification of impacts of existing design, rather than tools to help compare prospective configurations.

The conclusions of the literature review led to the implementation, embedded in the FAST-OAD-CS23-HE framework, of an LCA module leveraging the `lca-modeller` package to match the modularity offered by the graph-based description of the powertrain. This module was then used to identify the environmental impacts of CS-23 certification category aircraft, of prospective configurations with electrified powertrains, but most importantly, to identify design drivers for the minimization of said impacts. One of the first major conclusions highlighted thanks to this module was that, while the reduced scope considered in Chapter 4 provided a fair first guess on the point of lowest environmental impacts, the impacts linked with the manufacturing of batteries, even at low hybridization levels, were not negligible. For the same configurations, this leads to significantly different optimum points depending

on the scope considered. For this reason, the impacts of the battery manufacturing process were further investigated, and more specifically, the tradeoff between battery lifespan and energy density was looked into. Based on the cell chemistries under consideration, it was concluded that battery lifespan had a direct influence on the environmental impacts, but that energy density could prevent the feasibility of the design. Therefore, batteries offering a middle ground between energy density and lifespan were preferable for the configurations investigated. These investigations led to auxiliary observations on the magnitude of the impacts associated with airframe production for configurations with low utilization rates, like CS-23 aircraft. In particular, for the configuration investigated, and even though they allow for smaller impacts in the use phase, the use of composite materials was computed to lead to configurations with higher overall environmental scores because of their highly energy-intensive production process. Based on the importance of the environmental impacts of batteries, Section 5.5.4 proposed further investigations into the design drivers of the battery aging process. It revealed that over-sizing the battery to enable lower discharge depth and thus prolong the cells' lifetime led to overall higher impacts due to the added battery mass and the induced effects on the aircraft. Several combinations of cell chemistries and battery utilization schemes were then proposed in an effort to lower environmental impacts by allowing the use of high-energy-density cells in low cyclic usage situations. While none of the proposed schemes allowed for a reduction in the overall impacts, it enable the identification of several key avenues of improvement. Finally, based on the observations that the effect of cell aging on the aircraft's ability to fulfill its function was seldom taken into account, the amplitude of the error margin it induced was investigated. Results revealed that foregoing that effect, which is an implicit assumption found in literature, could lead to an underestimation of impacts by up to 20%. In the final section, future scenarios for electric commuter aircraft were investigated with ambitious technological advancement assumed for the power electronics, electric motor, cell chemistries, and airframe. Sodium-Ion cells were shown to be a strong candidate for future cell chemistry thanks to their very high lifespan and acceptable energy densities. In the end, due to the strong influence of aircraft usage on the battery's lifespan, the conclusion of Chapter 4 regarding the need to include operational considerations in the design showed a renewed interest.

Perspectives

Among all the conclusions drawn in this chapter, perhaps the most important one regarding the potential of electrified aircraft was the importance of the environmental impacts of the processes linked with battery production. However, the study of the impacts of different cell chemistries revealed that there was an important tradeoff to consider between cell mass and lifespan. It was also shown that, among the cells considered, there was not much room for improvement in all variations of the Li-Ion chemistry. Therefore, other chemistries, Sodium-Ion

and Li-S, were investigated and showed great potential. For this reason, it is recommended as an avenue of improvement for this work to investigate additional battery chemistries. Literature shows that, among future cell chemistries of interest, Li-Air could be an interesting candidate to consider. Indeed, not only could they offer higher energy densities, but they would also require fewer rare earth minerals [81], thus further lowering the environmental effects of the battery manufacturing. The question of their lifespan, however, potentially lower than that of Li-Ion cells [305], ought to be considered. Additionally, given the two chapters supporting the addition of realistic operational considerations early in the design process, further investigations into the usage of aircraft are also recommended. Mainly, a multi-mission weighted minimization of the environmental impacts, considering the most frequent flight profiles, in the form of a payload range diagram, should be investigated.

Regarding the framework and the methodology, a major next development identified is the inclusion, along with the LCA module, of a Life Cycle Cost (LCC) module to allow for the assessment of the costs of the aircraft. Indeed, as pointed out in the introduction, old performance metrics used as proxies in conventional configurations cannot be used for electric aircraft. Therefore, in areas where electric designs could outperform their thermal counterparts, like costs, accurate estimation should be sought. Additionally, literature has highlighted the complementary nature of LCA and LCC [42, 123, 124, 208, 246], thus further highlighting the need for such an approach. As for the LCA method itself and its implementation in this framework, several recommendations can also be made. First is the fact that, while the current module helps the decision-making process when comparing the relative importance of two or more designs across multiple environmental impact categories, it does not include the notion of the environment's ability to carry those effects. It is thus proposed to add the notion of planetary boundaries, often referred to as absolute sustainability assessment, into the framework to address that issue. Finally, literature also advocates for the inclusion of societal issues in the LCA framework [246]. This, in conjunction with the addition of an LCC module, could allow to perform Life Cycle Sustainability Assessment (LCSA), which is defined as the evaluation of environmental, economic, and social issues [249].

Part IV

Conclusions and perspectives

Chapter 6

Conclusion

6.1 Summary

This thesis provides an exploration of the potential of electrified aircraft propulsion for the reduction of the environmental impacts of CS-23 aircraft. It investigates that potential through a critical review of design methodologies, the proposition of an integrated framework to address multidisciplinary synergies at aircraft level, and uses that framework to identify the best electrification scenarios candidates at each level of the certification.

Chapter 1 of this thesis introduced the context of the electrification of aircraft propulsive architectures and its potential in terms of energy efficiency optimization and the reduction of harmful pollutant emissions. It also highlighted the pros and cons of electrified aircraft propulsion and began pinpointing the need for new methods to allow for the design of such configurations.

Part I then fully addressed the question of the sizing and the evaluation of the performances of aircraft with electrified propulsive architectures. Chapter 2 reviewed methodologies that have been proposed in literature to answer the question of how to design electric and hybrid aircraft and classified them. Out of the proposed categories, integrated frameworks were highlighted as key enablers due to their ability to model multidisciplinary systems and optimize them. In light of the pros and cons highlighted in Chapter 1, open-source integrated frameworks were then investigated to identify gaps in modeling and optimization capabilities. This review was used to justify the need for an open-source integrated framework with middle-fidelity models capable of dynamic reconfiguration to allow for the sizing of the vast array of configurations proposed for the electrification of aircraft in the CS-23 segment. An approach that leverages the modularity of the load flow analysis method and the models from the FAST-OAD framework was then proposed to enable a graph-based description of the powertrain to be used as user input, thus allowing easy reconfiguration of the design process. The modularity of the developed framework, aptly named FAST-OAD-CS23-HE, allows for the modeling of any propulsive architecture made up of any of the physical components presented in Chapter 3. This chapter also presented the middle fidelity models implemented

in the framework. It was also described how these models, which leverage a variety of approaches to make use of disciplinary knowledge, allow to propagate the different impacts of the installation of electric components onboard aircraft to allow vehicle-level optimization.

The recently developed framework and models were then used in Part II of this manuscript to propose alternatives to reduce the emissions of polluting species by aircraft designed under the CS-23 category. In particular, Chapter 4 proposed multiple scenarios for the electrification of aircraft based on the certification levels proposed in the CS-23. Hybrid and all-electric alternatives to existing candidate aircraft were investigated, along with their potential for emissions reduction, with a particular focus on CO_2. This part also used the FAST-OAD-CS23-HE framework to highlight the magnitude of the gains that can be obtained by leveraging the added degrees of freedom enabled by the electrification of the propulsion. It also showed how medium fidelity models are essential to capture the multidisciplinary synergies that electric propulsion allows to leverage.

Finally, Part III extended the scope of the analysis by including environmental considerations in the design process. More specifically, Chapter 5 looked into the implementation of a Life Cycle Assessment module in the FAST-OAD-CS23-HE framework. A review of the uses of LCA in the aeronautics sector was first conducted and used to conclude that such a method should be used to avoid cases of burden shifting, which can be masked when the scope is too limited. It also highlighted that LCA is usually used as a post-process tool to highlight hotspots in existing designs and is rarely embedded in the design process of novel configurations. The newly implemented LCA module was then used to gain further insights into the environmental impacts of electrified aircraft. Particular emphasis was put on the materials of the airframe, as well as the battery and the design variables that affect its aging process.

6.2 Answer to the research questions

The contribution of this work to the research into the field of electrified aircraft design is best exemplified through the answer it brings to the research questions highlighted in Chapter 1.

Research questions

RQ1. *What disciplines and components linked with electrified propulsion should be considered for accurate assessment at aircraft level?*

In order to fully propagate the effect of electrified propulsive architectures at aircraft level and fully grasp the potential of such configurations, the design process should consider several disciplines not found in traditional methodologies. In addition to the classic triptych between aerodynamics, weight, and performances, it was

shown that the modeling of noise emissions, environmental impacts over the life cycle, costs, evaluation of safety aspects, assessment of geometrical considerations, and the sizing of the thermal management systems were all key considerations. While the framework developed here does not include in its current state all of the considerations listed here, the methodology developed allows for easy interfacing with additional disciplines and even provides a pseudo-interface with other software in the form of a powertrain description file.

RQ2. *Are traditional design methodologies suited for the sizing of electrified aircraft? What disciplines of coupling are present/missing?*

Traditional aircraft design methodologies typically use empirical formulas built by aggregating statistical data from existing aircraft and traditionally only consider a limited amount of couplings across disciplines. For these reasons, they are unable to evaluate innovative configurations that fall outside of the bounds present in the database upon which they were built. They also fail to capture the multidisciplinary synergies from which the most gains can be expected for electrified aircraft. While some existing methodologies have been shown to be adaptable to capture a few of those effects, this work proposes the use of an integrated framework leveraging medium-fidelity physical models. This type of approach allows to assess those synergies and to capture the relieved design constraints that electrified aircraft propulsion enables while still maintaining low enough computational time compatible with the assessment of a variety of configurations.

RQ3. *How can MDAO methods and integrated OAD frameworks be adapted to assess hybrid and all-electric aircraft?*

MDAO is a key enabler for the sizing and evaluation of hybrid and all-electric aircraft, thanks to its ability to handle design problems with multiple coupled disciplines. Integrated frameworks, which largely build upon MDAO techniques, further build upon these capabilities by centralizing all disciplines in a single entity, thus eliminating manual interfaces between engineering knowledge-based software while keeping reasonable computational time, allowing for the evaluation of a large number of configurations. This work however proposes and implements several other key avenues of improvement. First, it advocates for the use of medium fidelity models for the physical components of the powertrain. This sort of models, while allowing for the capture of design trends invisible to top-down methods, also allows for analytical differentiation. This, in turn, enables the use of gradient-based approaches with reasonable computational time and numerical error, which, as was discussed, is paramount given the number of variables in the design process. Additionally, this

work builds on the physical models used in the original framework to ensure that multidisciplinary synergies are accurately represented and can be optimized. Finally, models and their implementation are built to be reusable to ensure consistency across the design process.

RQ4. *How to enable the assessment of a great number of configurations and order of magnitudes of power?*

Reviewing the concepts proposed for the electrification of the propulsion of aircraft led to the realization that a wide variety of architectures were envisioned and that those architectures could span several orders of magnitude. Additionally, multiple approaches are considered for the introduction of electrified aircraft in the fleet, from the retrofit of existing airframes to blank sheet designs. Therefore, the design processes adopted for the sizing of electric aircraft should be easily adaptable to reflect that diversity. This thesis proposes the use of a modular OAD framework coupled to a load flow analysis method, which enable for the assessment of a virtual infinite number of propulsive architectures. It additionally advocates for the representation of the powertrain using a graph-based approach in a human-readable file that serves as a pseudo-user interface, and which allows for the design process to be dynamically reconfigured depending on the architecture under study. Regarding the order of magnitude, the use of medium fidelity models, as opposed to top-down methods, allows for better capture of the scale effects of physical components. However, these low-fidelity approaches are useful to allow for a multi-fidelity simulation of the powertrain and, more specifically, to allow for a smart initialization of the variables in the design process, thus increasing robustness of the framework to multiple orders of magnitude of power.

RQ5. *Given the wide variety of usage of aircraft in the General Aviation, what electrification scenario should be considered?*

Using the framework developed in this thesis, realistic scenarios for the electrification of the propulsion of aircraft using current technologies were investigated and compared in terms of their energy efficiency and their CO_2 emissions. These investigations revealed that, similarly to conclusions found in literature, when all-electric powertrains were feasible, they were preferable to any other that included a thermal machine. The feasibility space, however, proved to be very narrow given the energy density of currently available battery cells. Regarding hybrid powertrains, this thesis showed their potential for several configurations. The most important finding of this work, however, is that hybrid powertrains yield the most significant improvement in energy efficiency and emissions reductions when they are not used as substitutes

for the energy vector. Rather, they are most beneficial when they are used to relieve design constraints on thermal machines or as a way to leverage multidisciplinary synergies.

RQ6. *How to conciliate the expected limitations of electrified propulsion with credible operational scenarios?*

The literature review conducted on existing concepts for electrified aircraft propulsion revealed that achievable ranges for all-electric configurations were an order of magnitude below those of their thermal counterpart. Additionally, investigations into hybrid configurations revealed that, depending on the hybridization scheme, and even considering major range reduction, they could be significantly heavier. This work however showed that while CS-23 aircraft are typically sized for longer ranges, they are in practice used for much shorter distances, typically compatible with electric technologies. While electric propulsion will surely not be suited to replace all thermal designs, the example of the Level 1 aircraft shows that there is a market for electric propulsion: the trainer segment. These aircraft typically require low power, low endurance, and limited seating capabilities. Regarding hybrid configurations and echoing the answer to the fifth research question, electric propulsion could be easily integrated into credible operational scenarios so long as they are not used as a substitute energy vector but rather to optimize thermal machines. This was shown to come at the cost of payload, but could significantly lower the hourly fuel consumption, which could be suited for specific usage like surveillance.

RQ7. *How to integrate, in the sizing process, design constraints stemming from manufacturing considerations? What is the influence on the vehicle?*

A survey of the concepts and demonstrators proposed for the integration within the fleet of aircraft with electrified propulsion revealed that two approaches were commonly adopted: either new designs from scratch or retrofit aircraft leveraging existing cells with novel propulsive architecture. While the latter could offer significant benefit from an industrial point-of-view — tooling already available, easier certification, rapid EIS — it significantly affects the traditional sizing process by setting numerous parameters and thus considerably limiting the design space. In this work, however, by leveraging the modularity of the OAD framework, it was shown to be possible to dynamically adapt the sizing process to allow for both approaches. Additionally, the constraints on the characteristic masses were handled by allowing the framework to reduce the payload in the case that the increase in the aircraft's empty mass led to exceeding the MTOM. In terms of impacts on the design of the vehicle, results on distributed configurations have shown that the reuse of

existing airframes did not lead to significant gains, as they did not allow to leverage the multidisciplinary synergies. In other cases, however, retrofit was shown to be a viable option, leading to significant gains if range penalties and minor payload reduction were acceptable. Nonetheless, this conclusion, which is drawn from the retrofit studies conducted on Level 3 and 4 aircraft, proves to be true only when the electrification of the powertrain is used to relieve design constraints on the thermal branch, rather than as an addition to it.

RQ8. *Is the evaluation of the impacts on climate change emission during the use of General Aviation aircraft enough to assess its sustainability?*

It was found in literature that a common practice was to compare designs through the amount of pollutants they emitted during their use phase, including or not, the production of the fuel. The use of Life Cycle Assessment, however, allowed to challenge those assumptions as it enables the coverage of the whole life cycle of the aircraft and also includes a wider range of impact categories. While for commercial, both approaches lead to essentially the same results due to the preponderance of impacts linked with the production and combustion fuel, essentially leading to the need to minimize fuel consumption, it was shown to be significantly different for electrified CS-23 aircraft. Indeed, not only are those aircraft typically less intensively used, leading to higher impacts of the manufacturing phase, but they also introduce new contributors that affect different damage pathways. More specifically, the manufacturing of the battery was shown to be a major contributor due to the high baseline impacts and the need for frequent renewal. They were also shown to contribute to widely different categories in addition to climate change, mainly the depletion of mineral resources. Therefore, the reduced scope commonly used to assess the sustainability of aircraft is not sufficient for aircraft in the General Aviation segment, and an LCA is required.

RQ9. *How can the environmental footprint of aircraft be tightly integrated in the design process?*

Reviewing the use of LCA in the realms of the aeronautics sector led to the realization that it was mostly used as a post-processing tool after the design phase or applied to existing configurations as opposed to being a tool to guide the design process of novel configurations. This shortcoming mainly stemmed from the issue of the amount of data required to perform an LCA and its availability. In order to extend its use, this thesis proposes the use of a Python package coupled to a life cycle inventory database to create pre-compiled parametric functions for the impact assessment. These pre-compiled functions allow to reduce the number of expensive calls to

the database, which makes possible and practical to implement an LCA module. Additionally, following the modularity of the framework, these parametric functions are adapted based on the contents of the powertrain description file. This allows a precise breakdown of the contributions and clear identification of the parameters driving those impacts.

RQ10. *What design drivers and aircraft specifications should be considered when minimizing the impacts?*

With the implementation of the LCA module in the framework, several analyses were conducted to identify the parameters that had the most significant influence on the environmental impacts. As opposed to the commercial transport sector, the choice of the airframe materials was shown to be non-evident. Indeed, given the preponderance of impacts linked with the use phase for CS-25 aircraft, any choice that can reduce fuel consumption will be beneficial. CS-23 aircraft, on the other hand, have a significant share of their impacts coming from the manufacturing phase. Materials with highly energetic manufacturing processes, like composite materials, have thus proven to be less beneficial. The biggest impacts have been shown to come from the battery manufacturing process, as it is not only a heavy component but also one that needs frequent renewal. Therefore, parameters that influence the lifespan of the cells were proven to have a first-order influence, the first of which was the utilization of the cells. While it was shown to be impossible to minimize the impacts by oversizing the cells to reduce depths of discharge, those studies renewed the interest in a precise knowledge of the expected flight profiles of the aircraft, as it directly influences the degradation of the cell's capacity and thus the endurance of the aircraft.

6.3 Perspectives for future work

While this framework brings significant advances in the research into the design of electrified aircraft, it is also acknowledged that several avenues of improvement exist.

First of all, as discussed across all the intermediate conclusions to the different chapters of this manuscript, a critical limitation exists in the form of a lack of modeling of thermal management systems. The weight, drag, and power draw from the thermal management system have been highlighted in literature to have a major impact at aircraft level, thus making its modeling a critical next step. Additionally, this work, and in particular Chapter 3, has shown how accurate estimation of the components' thermal behavior was critical, not only because it influenced the performances of said components but also because of its influence on the components' lifespan. The latter was shown to be of particular interest, especially for

the battery cells, because of its importance in the computation of the environmental impacts of electrified aircraft. Although it is a clear limitation of the framework, its implementation was shown to be possible thanks to the residuals-driven approach adopted.

Another topic of interest that could be pursued as a refinement of this thesis is the notion of architecture optimization. Indeed, while this framework allows for the optimization of a selected architecture, nothing guarantees that the selected architecture is the most optimal one. The easy reconfiguration of the problem and the powertrain description file, which acts as a pseudo user interface, would enable the interfacing of this framework with other software capable of generating architectures based on a set of high-level functional requirements. In addition to proposing architecture that would optimize a given objective at aircraft level, this could also be used as a way to evaluate the reliability of these architectures and thus include safety aspects as a requirement for the optimization of the design.

Finally, although the methodology developed already allows for the evaluation of a virtually infinite number of architectures, the library of components upon which those architectures are built should be extended. Most importantly, while this work focused mainly on hybridization between thermal machines and battery-powered electric branches, the question of hydrogen based powertrain was never addressed. Hydrogen has gained a lot of traction in recent years, thanks to its superior energy density when compared to batteries and even fossil fuels, meaning it has the potential to overcome the rapid increase in mass incurred by batteries. This observation is strengthened by the great number of hydrogen-based concepts that have been proposed in literature. The modeling of non propulsive element has also been identified as a key avenue of improvement for this work. Indeed, with the increase in terms of on-board electric power brought by the electrified powertrains, the electrification of non-propulsive functions could also show great potential. It is especially interesting because non-propulsive functions typically incur heavy penalties on thermal machines in the form of bleed air. To assess the potential of these concepts, it thus becomes interesting to model components other than those of the propulsive architecture.

In conclusion, it could also be said that this work could benefit from an exploration of more test cases. While a significant number of test cases were investigated in Chapters 4 and 5, the summary of those cases in Figure 4.32 highlights a lack of test cases with a high number of passengers. Additionally, most cases were optimized based on their ability to transport passengers. However, given the wide variety of usages in the CS-23 category, it could also be worth looking into a configuration with high endurance and low payload. Additionally, the investigations conducted in Chapter 5 on alternate materials for the airframe led to interesting conclusions regarding the use of composite for aircraft with low energy vectors. Therefore, additional inquiries in that direction would be worth investigating.

Contributions

Journal articles

Lutz, F., Jezegou, J., Budinger, M. and Reysset, A., 2025. Open-Source Framework for Sizing Hybrid and Electric General Aviation Aircraft. Journal of Aircraft, 62(2), pp.381-395.
Pollet, Félix, et al. "A generic life cycle assessment tool for overall aircraft design." Applied Energy 399 (2025): 126514.

Conference articles

Lutz, Florent, et al. "FAST-OAD-GA: an open-source extension for Overall Aircraft Design of General Aviation aircraft." ICAS 2022. 2022.
Lutz, Florent, et al. "Study of hybridisation scenarios for turboprop aircraft in the general aviation segment." 34th Congress of the International Council of the Aeronautical Sciences, Florence, Italy. 2024.

Workshop presentations

Lutz, Florent, et al. "Implementation of LCA models in OAD for hybrid-electric aircraft design." 4th European Workshop on MDO for Industrial Applications in Aeronautics, Toulouse, France. 2025

Teaching

- Supervision of 9 400h student projects on: the design of hybrid-electric commuter aircraft, the design of H2 powered aircraft, the creation of a surrogate for modeling slipstream effects and airfoil performances, and the dynamic sequencing of models in MDAO problems.
- Creation of a 4h classes for MDAO applications in the context of Overall Aircraft Design at ISAE-SUPAERO.
- Creation of a dedicated pedagogical interface for FAST-OAD and use in engineering classes at ISAE-SUPAERO

References

[1] C.-F. Schleussner *et al.*, "Science and policy characteristics of the Paris Agreement temperature goal," en, *Nature Climate Change*, vol. 6, no. 9, pp. 827–835, Sep. 2016, Number: 9 Publisher: Nature Publishing Group, ISSN: 1758-6798. DOI: 10.1038/nclimate3096. [Online]. Available: https://www.nature.com/articles/nclimate3096 (visited on 01/13/2023).

[2] U. S. C. H. C. o. S. a. Technology, *The State of Climate Change Science 2007: Hearings Before the Committee on Science and Technology, House of Representatives, One Hundred Tenth Congress, First Session, February 8, April 17, and May 15, 2007*, en. U.S. Government Printing Office, 2008, Google-Books-ID: YqXmNrZQwfEC, ISBN: 978-0-16-081004-6.

[3] G. Santos, "Road transport and CO2 emissions: What are the challenges?" en, *Transport Policy*, vol. 59, pp. 71–74, Oct. 2017, ISSN: 0967-070X. DOI: 10.1016/j.tranpol.2017.06.007. [Online]. Available: https://www.sciencedirect.com/science/article/pii/S0967070X17304262 (visited on 01/13/2023).

[4] D. S. Lee *et al.*, "Aviation and global climate change in the 21st century," en, *Atmospheric Environment*, vol. 43, no. 22, pp. 3520–3537, Jul. 2009, ISSN: 1352-2310. DOI: 10.1016/j.atmosenv.2009.04.024. [Online]. Available: https://www.sciencedirect.com/science/article/pii/S1352231009003574 (visited on 01/13/2023).

[5] D. S. Lee *et al.*, "The contribution of global aviation to anthropogenic climate forcing for 2000 to 2018," en, *Atmospheric Environment*, vol. 244, p. 117 834, Jan. 2021, ISSN: 1352-2310. DOI: 10.1016/j.atmosenv.2020.117834. [Online]. Available: https://www.sciencedirect.com/science/article/pii/S1352231020305689 (visited on 01/13/2023).

[6] F. Afonso *et al.*, "Strategies towards a more sustainable aviation: A systematic review," *Progress in Aerospace Sciences*, vol. 137, p. 100 878, 2023, ISSN: 0376-0421. DOI: https://doi.org/10.1016/j.paerosci.2022.100878. [Online]. Available: https://www.sciencedirect.com/science/article/pii/S0376042122000707.

[7] T. Rindlisbacher, "Aircraft piston engine emissions, summary report," *Switzerland: Federal Department of the Environment, Transport, Energy and Communications DETEC Federal Office of Civil Aviation FOCA Aviation Policy and Strategy Environmental Affairs*, 2007.

[8] T. Kumar *et al.*, "Response surface methodology application in optimization of performance and exhaust emissions of ron 98, aviation gasoline 100ll and the blends in lycoming o-320 engine," *Fuel*, vol. 256, p. 115 909, 2019, ISSN: 0016-2361.

DOI: https://doi.org/10.1016/j.fuel.2019.115909. [Online]. Available: https://www.sciencedirect.com/science/article/pii/S001623611931261X.

[9] W. R. Graham, C. A. Hall, and M. Vera Morales, "The potential of future aircraft technology for noise and pollutant emissions reduction," en, *Transport Policy*, Air Transportation and the Environment, vol. 34, pp. 36–51, Jul. 2014, ISSN: 0967-070X. DOI: 10.1016/j.tranpol.2014.02.017. [Online]. Available: https://www.sciencedirect.com/science/article/pii/S0967070X14000481 (visited on 01/13/2023).

[10] E. Commission, D.-G. for Research, Innovation, D.-G. for Mobility, and Transport, *Flightpath 2050 – Europe's vision for aviation – Maintaining global leadership and serving society's needs*. Publications Office, 2011. DOI: https://data.europa.eu/doi/10.2777/50266.

[11] K. Suder, "Overview of the nasa environmentally responsible aviation project's propulsion technology portfolio," in *48th AIAA/ASME/SAE/ASEE Joint Propulsion Conference & Exhibit*. American Institute of Aeronautics and Astronautics, 2012. DOI: 10.2514/6.2012-4038. eprint: https://arc.aiaa.org/doi/pdf/10.2514/6.2012-4038. [Online]. Available: https://arc.aiaa.org/doi/abs/10.2514/6.2012-4038.

[12] M. Schneider, *Tracking of Aviation Emissions & Fuel Efficiency Improvements/ Market Based Measures*, Mar. 2015. [Online]. Available: https://www.icao.int/Meetings/EnvironmentalWorkshops/Documents/2015-Warsaw/6_2_Tracking-of-Aviation-Emissions-and-Fuel-Efficiency-Improvements-MBMs.pdf (visited on 01/20/2023).

[13] M. D. Moore, "Misconceptions of electric aircraft and their emerging aviation markets," in *52nd Aerospace Sciences Meeting*. American Institute of Aeronautics and Astronautics, 2014. DOI: 10.2514/6.2014-0535. eprint: https://arc.aiaa.org/doi/pdf/10.2514/6.2014-0535. [Online]. Available: https://arc.aiaa.org/doi/abs/10.2514/6.2014-0535.

[14] R. Kelsey, *Electric Cessna Grand Caravan in Development to Fly by 2024*, en, Section: Electrification and Sustainability, Jul. 2021. [Online]. Available: https://www.aviationtoday.com/2021/07/20/electric-cessna-grand-caravan-development-fly-2024/ (visited on 01/20/2023).

[15] J. L. Felder, *NASA Electric Propulsion System Studies*, NTRS Author Affiliations: NASA Glenn Research Center NTRS Meeting Information: EnergyTech 2015; 2015-11-30 to 2015-12-02; undefined NTRS Report/Patent Number: GRC-E-DAA-TN28410 NTRS Document ID: 20160009274 NTRS Research Center: Glenn Research Center (GRC), Nov. 2015. [Online]. Available: https://ntrs.nasa.gov/citations/20160009274 (visited on 01/27/2023).

[16] C. Pornet and A. Isikveren, "Conceptual design of hybrid-electric transport aircraft," *Progress in Aerospace Sciences*, vol. 79, pp. 114–135, 2015, ISSN: 0376-0421. DOI: https://doi.org/10.1016/j.paerosci.2015.09.002. [Online]. Available: https://www.sciencedirect.com/science/article/pii/S0376042115300130.

[17] C. L. Bowman, J. L. Felder, and T. Marien, "Turbo- and hybrid-electrified aircraft propulsion concepts for commercial transport," in *2018 AIAA/IEEE Electric Aircraft Technologies Symposium (EATS)*, 2018, pp. 1–8.

[18] A. R. Gnadt, R. L. Speth, J. S. Sabnis, and S. R. Barrett, "Technical and environmental assessment of all-electric 180-passenger commercial aircraft," *Progress in Aerospace Sciences*, vol. 105, pp. 1–30, 2019, ISSN: 0376-0421. DOI: https://doi.org/10.1016/j.paerosci.2018.11.002. [Online]. Available: https://www.sciencedirect.com/science/article/pii/S0376042118301179.

[19] H. D. Kim, A. T. Perry, and P. J. Ansell, "A review of distributed electric propulsion concepts for air vehicle technology," in *2018 AIAA/IEEE Electric Aircraft Technologies Symposium (EATS)*, 2018, pp. 1–21.

[20] X. Zhang, C. L. Bowman, T. C. O'Connell, and K. S. Haran, "Large electric machines for aircraft electric propulsion," en, *IET Electric Power Applications*, vol. 12, no. 6, pp. 767–779, 2018, _eprint: https://onlinelibrary.wiley.com/doi/pdf/10.1049/iet-epa.2017.0639, ISSN: 1751-8679. DOI: 10.1049/iet-epa.2017.0639. [Online]. Available: https://onlinelibrary.wiley.com/doi/abs/10.1049/iet-epa.2017.0639 (visited on 01/27/2023).

[21] X. Roboam *et al.*, *Hastecs : Hybrid aircraft : research on thermal and electric components and systems*, en. Oct. 2021. DOI: https://doi.org/10.3030/715483. [Online]. Available: https://ut3-toulouseinp.hal.science/hal-03407214 (visited on 02/22/2023).

[22] E. J. Adler and J. R. Martins, "Energy demand comparison for carbon-neutral flight," *Progress in Aerospace Sciences*, vol. 152, p. 101 051, 2025, ISSN: 0376-0421. DOI: https://doi.org/10.1016/j.paerosci.2024.101051. [Online]. Available: https://www.sciencedirect.com/science/article/pii/S0376042124000770.

[23] M. Hepperle, "Electric flight-potential and limitations," *Energy Efficient Technologies and Concepts of Operation*, pp. 22–24, 2012, NATO STO-MP-AVT-209.

[24] J. Benzaquen, J. He, and B. Mirafzal, "Toward more electric powertrains in aircraft: Technical challenges and advancements," *CES Transactions on Electrical Machines and Systems*, vol. 5, no. 3, pp. 177–193, Sep. 2021, Conference Name: CES Transactions on Electrical Machines and Systems, ISSN: 2096-3564. DOI: 10.30941/CESTEMS.2021.00022.

[25] M. A. Rendón, C. D. Sánchez R., J. Gallo M., and A. H. Anzai, "Aircraft Hybrid-Electric Propulsion: Development Trends, Challenges and Opportunities," en, *J Control Autom Electr Syst*, vol. 32, no. 5, pp. 1244–1268, Oct. 2021, ISSN: 2195-3899. DOI: 10.1007/s40313-021-00740-x. [Online]. Available: https://doi.org/10.1007/s40313-021-00740-x (visited on 01/27/2023).

[26] P. Schmollgruber *et al.*, "Multidisciplinary Exploration of DRAGON: An ONERA Hybrid Electric Distributed Propulsion Concept," in *AIAA Scitech 2019 Forum*, ser. AIAA SciTech Forum, American Institute of Aeronautics and Astronautics, Jan. 2019. DOI: 10.2514/6.2019-1585. [Online]. Available: https://arc.aiaa.org/doi/10.2514/6.2019-1585 (visited on 01/27/2023).

[27] J. Hermetz, M. Ridel, and C. Doll, "Distributed electric propulsion for small business aircraft a concept-plane for key-technologies investigations.," in *30th Congress of the International Council of the Aeronautical Sciences, ICAS 2021*, Sep. 2016. [Online]. Available: https://www.icas.org/icas_archive/ICAS2016/data/papers/2016_0461_paper.pdf (visited on 12/02/2025).

[28] IATA, *Aircraft technology roadmap to 2050*, en, 2021. [Online]. Available: https://www.iata.org/contentassets/8d19e716636a47c184e7221c77563c93/Technology-roadmap-2050.pdf (visited on 02/10/2023).

[29] R. McDonald, "Electric Propulsion Modeling for Conceptual Aircraft Design," in *52nd Aerospace Sciences Meeting*. American Institute of Aeronautics and Astronautics, Jan. 2014, Journal Abbreviation: 52nd Aerospace Sciences Meeting Publication Title: 52nd Aerospace Sciences Meeting, ISBN: 978-1-62410-256-1. DOI: 10.2514/6.2014-0536. eprint: https://arc.aiaa.org/doi/pdf/10.2514/6.2014-0536. [Online]. Available: https://arc.aiaa.org/doi/abs/10.2514/6.2014-0536.

[30] ICAO, *Independent Expert Integrated Technology Goals Assessment and Review for Engines and Aircraft*, en, 2019. [Online]. Available: http://www.icscc.org.cn/upload/file/20200603/20200603140731_33885.pdf (visited on 02/10/2023).

[31] B. J. Brelje and J. R. Martins, "Development of a conceptual design model for aircraft electric propulsion with efficient gradients," in *2018 AIAA/IEEE Electric Aircraft Technologies Symposium*. American Institute of Aeronautics and Astronautics, Jul. 2018. DOI: 10.2514/6.2018-4979.

[32] R. Alonso Castilla, F. Lutz, J. Jézégou, and E. Bénard, "Wing structural model for overall aircraft design of distributed electric propulsion general aviation and regional aircraft," *Aerospace*, vol. 9, no. 1, 2022, ISSN: 2226-4310. DOI: 10.3390/aerospace9010005. [Online]. Available: https://www.mdpi.com/2226-4310/9/1/5.

[33] K. R. Moore and A. Ning, "Distributed electric propulsion effects on existing aircraft through multidisciplinary optimization," in *2018 AIAA/ASCE/AHS/ASC Structures, Structural Dynamics, and Materials Conference*. American Institute of Aeronautics and Astronautics, Jan. 2018. DOI: 10.2514/6.2018-1652. eprint: https://arc.aiaa.org/doi/pdf/10.2514/6.2018-1652. [Online]. Available: https://arc.aiaa.org/doi/abs/10.2514/6.2018-1652.

[34] M. D. Patterson, "Conceptual Design of High-Lift Propeller Systems for Small Electric Aircraft," en, Accepted: 2016-08-22T12:21:51Z Publisher: Georgia Institute of Technology, Ph.D. dissertation, Georgia Institute of Technology, May 2016.

[35] F. M. Capristan and N. J. Blaesser, "Analysis of the Parallel Electric-Gas Architecture with Synergistic Utilization Scheme (PEGASUS) Concept," English, NASA, Technical Report 20190030874, Aug. 2019. [Online]. Available: https://ntrs.nasa.gov/citations/20190030874 (visited on 04/11/2023).

[36] K. A. Deere, J. K. Viken, S. Viken, M. B. Carter, M. Wiese, and N. Farr, "Computational Analysis of a Wing Designed for the X-57 Distributed Electric Propulsion Aircraft," en, in *35th AIAA Applied Aerodynamics Conference*, Denver, Colorado: American Institute of Aeronautics and Astronautics, Jun. 2017, ISBN: 978-1-62410-501-2. DOI: 10.2514/6.2017-3923. [Online]. Available: https://arc.aiaa.org/doi/10.2514/6.2017-3923 (visited on 02/10/2023).

[37] A. Magrini, E. Benini, H.-D. Yao, J. Postma, and C. Sheaf, "A review of installation effects of ultra-high bypass ratio engines," en, *Progress in Aerospace Sciences*, vol. 119, p. 100 680, Nov. 2020, ISSN: 0376-0421. DOI: 10.1016/j.paerosci.2020.100680. [Online]. Available: https://www.sciencedirect.com/science/article/pii/S0376042120300920 (visited on 02/10/2023).

[38] D. K. Hall, A. C. Huang, A. Uranga, E. M. Greitzer, M. Drela, and S. Sato, "Boundary Layer Ingestion Propulsion Benefit for Transport Aircraft," *Journal of Propulsion and Power*, vol. 33, no. 5, pp. 1118–1129, Sep. 2017, Publisher: American Institute of Aeronautics and Astronautics, ISSN: 0748-4658. DOI: 10.2514/1.B36321. [Online]. Available: https://arc.aiaa.org/doi/10.2514/1.B36321 (visited on 04/13/2023).

[39] N. G. M. Moirou, D. S. Sanders, and P. Laskaridis, "Advancements and prospects of boundary layer ingestion propulsion concepts," en, *Progress in Aerospace Sciences*, vol. 138, p. 100 897, Apr. 2023, ISSN: 0376-0421. DOI: 10.1016/j.paerosci.2023.100897. [Online]. Available: https://www.sciencedirect.com/science/article/pii/S0376042123000131 (visited on 04/13/2023).

[40] A. Kuśmierek, C. Galiński, and W. Stalewski, "Review of the hybrid gas - electric aircraft propulsion systems versus alternative systems," *Progress in Aerospace Sciences*, vol. 141, p. 100 925, 2023, Special Issue on Green Aviation, ISSN: 0376-0421. DOI: https://doi.org/10.1016/j.paerosci.2023.100925. [Online]. Available: https://www.sciencedirect.com/science/article/pii/S0376042123000416.

[41] J. Scheelhaase, S. Maertens, and W. Grimme, "Synthetic fuels in aviation – Current barriers and potential political measures," en, *Transportation Research Procedia*, INAIR 2019 - Global Trends in Aviation, vol. 43, pp. 21–30, Jan. 2019, ISSN: 2352-1465. DOI: 10.1016/j.trpro.2019.12.015. [Online]. Available: https://www.sciencedirect.com/science/article/pii/S2352146519305824 (visited on 04/14/2023).

[42] Y. Liang, W. Zhang, and C. Li, "Assessing the deployment of electric aircraft from energy, environmental, and economic perspectives," *Sustainability*, vol. 17, no. 12, 2025, ISSN: 2071-1050. DOI: 10.3390/su17125453. [Online]. Available: https://www.mdpi.com/2071-1050/17/12/5453.

[43] M. Pettes-Duler, "Conception intégrée optimale du système propulsif d'un avion régional hybride électrique," Theses, Institut National Polytechnique de Toulouse - INPT, Apr. 2021. [Online]. Available: https://theses.hal.science/tel-04170659.

[44] B. Yang, F. Lou, and N. L. Key, "Conceptual design of a 10-passenger thin-haul electric aircraft," in *2020 AIAA/IEEE Electric Aircraft Technologies Symposium (EATS)*, 2020, pp. 1–18.

[45] N. Gray, S. McDonagh, R. O'Shea, B. Smyth, and J. D. Murphy, "Decarbonising ships, planes and trucks: An analysis of suitable low-carbon fuels for the maritime, aviation and haulage sectors," *Advances in Applied Energy*, vol. 1, p. 100 008, 2021, ISSN: 2666-7924. DOI: https://doi.org/10.1016/j.adapen.2021.100008. [Online]. Available: https://www.sciencedirect.com/science/article/pii/S2666792421000019.

[46] V. Palladino, N. Bartoli, V. Pommier-Budinger, E. Benard, P. Schmollgruber, and A. Jordan, "Optimization of a hydrogen-based hybrid propulsion system under aircraft performance constraints," *Chinese Journal of Aeronautics*, vol. 36, no. 5, pp. 41–56, 2023. DOI: https://doi.org/10.1016/j.cja.2023.02.019.

[47] T. Planès, V. Habrard, S. Delbecq, V. Pommier-Budinger, and E. Benard, "Thermal management system models for overall aircraft design," in *AIAA AVIATION 2021 FORUM*, _eprint: https://arc.aiaa.org/doi/pdf/10.2514/6.2021-2428, American Institute of Aeronautics and Astronautics, Aug. 2021. DOI: 10.2514/6.2021-2428.

[Online]. Available: https://arc.aiaa.org/doi/abs/10.2514/6.2021-2428 (visited on 04/19/2023).

[48] A. Hubert, C. Forgez, and P.-A. Yvars, "Designing the architecture of electrochemical energy storage systems. a model-based system synthesis approach," *Journal of Energy Storage*, vol. 54, p. 105 351, 2022. DOI: https://doi.org/10.1016/j.est.2022.105351Âš.

[49] A. Nikolian *et al.*, "Lithium Ion Batteries—Development of Advanced Electrical Equivalent Circuit Models for Nickel Manganese Cobalt Lithium-Ion," en, *Energies*, vol. 9, no. 5, p. 360, May 2016, Number: 5 Pub isher: Multidisciplinary Digital Publishing Institute, ISSN: 1996-1073. DOI: 10.3390/en9050360. [Online]. Available: https://www.mdpi.com/1996-1073/9/5/360 (visited on 11/14/2022).

[50] E. Aretskin-Hariton, M. Bell, S. Schnulo, and J. S. Gray, "Power cable mass estimation for electric aircraft propulsion," in *AIAA AVIATION 2021 FORUM*. American Institute of Aeronautics and Astronautics, 2021. DOI: 10.2514/6.2021-3021. eprint: https://arc.aiaa.org/doi/pdf/10.2514/6.2021-3021. [Online]. Available: https://arc.aiaa.org/doi/abs/10.2514/6.2021-3021.

[51] B. J. Brelje and J. R. Martins, "Electric, hybrid, and turboelectric fixed-wing aircraft: A review of concepts, models, and design approaches," *Progress in Aerospace Sciences*, vol. 104, pp. 1–19, 2019, ISSN: 0376-0421. DOI: https://doi.org/10.1016/j.paerosci.2018.06.004. [Online]. Available: https://www.sciencedirect.com/science/article/pii/S0376042118300356.

[52] A. W. Schäfer *et al.*, "Technological, economic and environmental prospects of all-electric aircraft," en, *Nature Energy*, vol. 4, no. 2, pp. 160–166, Feb. 2019, Number: 2 isher: Nature Publishing Group, ISSN: 2058-7546. DOI: 10.1038/s41560-018-0294-x. [Online]. Available: https://www.nature.com/articles/s41560-018-0294-x (visited on 04/19/2023).

[53] S. Touhami, "Analytical sizing models to assess the performances of high specific power electric motors for hybrid aircraft," Ph.D. dissertation, Laplace Institute, 2020. [Online]. Available: https://theses.hal.science/tel-04170761/.

[54] T. Planès, "Du dimensionnement de systèmes et d'architectures en conception avion à la simulation de scénarios prospectifs durables pour le transport aérien," These de doctorat, Toulouse, ISAE, Dec. 2022. [Online]. Available: https://www.theses.fr/2022ESAE0059 (visited on 04/19/2023).

[55] A. K. Jeyaraj and S. Liscouët-Hanke, "A safety-focused system architecting framework for the conceptual design of aircraft systems," *Aerospace*, vol. 9, no. 12, p. 791, 2022. DOI: https://doi.org/10.3390/aerospace9120791.

[56] C. Friedrich and P. Robertson, "Hybrid-Electric Propulsion for Aircraft," *Journal of Aircraft*, vol. 52, no. 1, pp. 176–189, Jan. 2015, Publisher: American Institute of Aeronautics and Astronautics, ISSN: 0021-8669. DOI: 10.2514/1.C032660. [Online]. Available: https://arc.aiaa.org/doi/10.2514/1.C032660 (visited on 01/27/2023).

[57] J. S. Langford and D. K. Hall, "Electrified aircraft propulsion," *Bridge*, vol. 50, no. 2, pp. 21–27, Jun. 2020, ISSN: 0737-6278. [Online]. Available: https://www.nae.edu/File.aspx?id=234402 (visited on 08/13/2025).

[58] S. Gudmundsson, *General Aviation Aircraft Design : Applied Methods and Procedures Ed. 2*. Elsevier Science, 2021, ISBN: 978-0-12-818465-3. [Online]. Available: https://univ.scholarvox.com/catalog/book/docid/88930616 (visited on 07/29/2025).

[59] J. Roskam, *Airplane design*. DARcorporation, 1985.

[60] D. P. Raymer, *Aircraft Design: A Conceptual Approach, Seventh Edition*, en. Reston, VA: American Institute of Aeronautics and Astronautics, Inc., Aug. 2024, ISBN: 978-1-62410-729-0. DOI: 10.2514/4.107290. [Online]. Available: https://arc.aiaa.org/doi/book/10.2514/4.107290 (visited on 07/30/2025).

[61] L. M. Nicolai and G. E. Carichner, *Fundamentals of Aircraft and Airship Design*. Blacksburg, Virginia: American Institute of Aeronautics and Astronautics, Inc., 2010, ISBN: 978-1-60086-751-4. DOI: 10.2514/4.867538. [Online]. Available: https://arc.aiaa.org/doi/abs/10.2514/4.867538 (visited on 04/20/2023).

[62] V. Marciello *et al.*, "Evaluating the economic landscape of hybrid-electric regional aircraft: A cost analysis across three time horizons," *Energy Conversion and Management*, vol. 312, p. 118 517, 2024, ISSN: 0196-8904. DOI: https://doi.org/10.1016/j.enconman.2024.118517. [Online]. Available: https://www.sciencedirect.com/science/article/pii/S0196890424004588.

[63] V. MARCIELLO, F. OREFICE, F. NICOLOSI, D. CILIBERTI, and P. DELLA VECCHIA, "Design of hybrid-electric aircraft with fault-tolerance considerations," *Chinese Journal of Aeronautics*, vol. 36, no. 2, pp. 160–178, 2023, ISSN: 1000-9361. DOI: https://doi.org/10.1016/j.cja.2022.05.014. [Online]. Available: https://www.sciencedirect.com/science/article/pii/S1000936122001066.

[64] R. de Vries, M. Brown, and R. Vos, "Preliminary Sizing Method for Hybrid-Electric Distributed-Propulsion Aircraft," *Journal of Aircraft*, vol. 56, no. 6, pp. 2172–2188, Nov. 2019, Publisher: American Institute of Aeronautics and Astronautics, ISSN: 0021-8669. DOI: 10.2514/1.C035388. [Online]. Available: https://arc.aiaa.org/doi/10.2514/1.C035388 (visited on 04/21/2023).

[65] D. F. Finger, C. Braun, and C. Bil, "An initial sizing methodology for hybrid-electric light aircraft," in *2018 Aviation Technology, Integration, and Operations Conference*. American Institute of Aeronautics and Astronautics, Jun. 2018. DOI: 10.2514/6.2018-4229. eprint: https://arc.aiaa.org/doi/pdf/10.2514/6.2018-4229. [Online]. Available: https://arc.aiaa.org/doi/abs/10.2514/6.2018-4229.

[66] M. Drela, "Tasopt 2.00—transport aircraft system optimization," *Massachusetts Inst. of Technology, Rept. Cooperative Agreement Number NNX08AW63A, Cambridge, MA*, 2010.

[67] K. Patryniak, M. Collu, and A. Coraddu, "Multidisciplinary design analysis and optimisation frameworks for floating offshore wind turbines: State of the art," *Ocean Engineering*, vol. 251, p. 111 002, 2022, ISSN: 0029-8018. DOI: https://doi.org/10.1016/j.oceaneng.2022.111002. [Online]. Available: https://www.sciencedirect.com/science/article/pii/S0029801822004267.

[68] A. B. Lambe and J. R. R. A. Martins, "Extensions to the design structure matrix for the description of multidisciplinary design, analysis, and optimization processes," en, *Struct Multidisc Optim*, vol. 46, no. 2, pp. 273–284, Aug. 2012, ISSN: 1615-1488. DOI: 10.1007/s00158-012-0763-y. [Online]. Available: https://doi.org/10.1007/s00158-012-0763-y (visited on 04/21/2023).

[69] C. David, S. Delbecq, S. Defoort, P. Schmollgruber, E. Benard, and V. Pommier-Budinger, "From fast to fast-oad: An open source framework for rapid overall aircraft design," *IOP Conference Series: Materials Science and Engineering*, vol. 1024, no. 1, p. 012 062, 2021. DOI: 10.1088/1757-899X/1024/1/012062. [Online]. Available: https://dx.doi.org/10.1088/1757-899X/1024/1/012062.

[70] J. R. R. A. Martins and A. Ning, *Engineering Design Optimization*. Cambridge, UK: Cambridge University Press, 2022, ISBN: 9781108833417. DOI: 10.1017/9781108980647. [Online]. Available: https://mdobook.github.io.

[71] F. Pollet, "Design optimization of unmanned aerial vehicles: a multidisciplinary approach with uncertainty, fault-tolerance, and environmental impact assessments," Theses, ISAE-SUPAERO, 2024. [Online]. Available: https://hal.science/tel-04657928.

[72] S. Delbecq, "Knowledge-Based Multidisciplinary Sizing and Optimization of Embedded Mechatronic Systems - Application to Aerospace Electro-Mechanical Actuation Systems," These de doctorat, Toulouse, INSA, Nov. 2018. [Online]. Available: https://www.theses.fr/2018ISAT0034 (visited on 04/12/2023).

[73] J. R. R. A. Martins and J. T. Hwang, "Review and unification of methods for computing derivatives of multidisciplinary computational models," *AIAA Journal*, vol. 51, no. 11, pp. 2582–2599, 2013. DOI: 10.2514/1.J052184. eprint: https://doi.org/10.2514/1.J052184. [Online]. Available: https://doi.org/10.2514/1.J052184.

[74] S. Kaneko, M. G. Arnson, H. Hajdik, G. Cinar, J. Martins, and A. Uranga, "Gradient-based mdao framework for advanced aircraft concepts," in *AIAA SCITECH 2026 Forum*. American Institute of Aeronautics and Astronautics, 2026. DOI: 10.2514/6.2026-1302. eprint: https://arc.aiaa.org/doi/pdf/10.2514/6.2026-1302. [Online]. Available: https://arc.aiaa.org/doi/abs/10.2514/6.2026-1302.

[75] M. M. Noel, "A new gradient based particle swarm optimization algorithm for accurate computation of global minimum," *Applied Soft Computing*, vol. 12, no. 1, pp. 353–359, 2012, ISSN: 1568-4946. DOI: https://doi.org/10.1016/j.asoc.2011.08.037. [Online]. Available: https://www.sciencedirect.com/science/article/pii/S1568494611003206.

[76] J. Bradbury *et al.*, *JAX: Composable transformations of Python+NumPy programs*, version 0.3.13, 2018. [Online]. Available: http://github.com/jax-ml/jax.

[77] F. Orefice, F. Nicolosi, P. D. Vecchia, and D. Ciliberti, "Aircraft conceptual design of commuter aircraft including distributed electric propulsion," in *AIAA AVIATION 2020 FORUM*. American Institute of Aeronautics and Astronautics, Jun. 2020. DOI: 10.2514/6.2020-2627. eprint: https://arc.aiaa.org/doi/pdf/10.2514/6.2020-2627. [Online]. Available: https://arc.aiaa.org/doi/abs/10.2514/6.2020-2627.

[78] H. L. Silva *et al.*, "A multidisciplinary design optimization for conceptual design of hybrid-electric aircraft," en, *Structural and Multidisciplinary Optimization*, vol. 64, no. 6, pp. 3505–3526, Dec. 2021, ISSN: 1615-1488. DOI: 10.1007/s00158-021-03033-8. [Online]. Available: https://doi.org/10.1007/s00158-021-03033-8 (visited on 04/21/2023).

[79] D. F. Finger, C. Braun, and C. Bil, "Case Studies in Initial Sizing for Hybrid-Electric General Aviation Aircraft," in *2018 AIAA/IEEE Electric Aircraft Technologies Symposium (EATS)*, Jul. 2018, pp. 1–22.

[80] M. Iwanizki, M. Arzberger, M. Plohr, D. Silberhorn, and T. Hecken, "Conceptual Design Studies of Short Range Aircraft Configurations with Hybrid Electric Propulsion," in *AIAA Aviation 2019 Forum*, ser. AIAA AVIATION Forum, American Institute of Aeronautics and Astronautics, Jun. 2019. DOI: 10.2514/6.2019-3680. [Online]. Available: https://arc.aiaa.org/doi/10.2514/6.2019-3680 (visited on 04/21/2023).

[81] J. Ribeiro *et al.*, "Environmental assessment of hybrid-electric propulsion in conceptual aircraft design," *Journal of Cleaner Production*, vol. 247, p. 119 477, 2020, ISSN: 0959-6526. DOI: https://doi.org/10.1016/j.jclepro.2019.119477. [Online]. Available: https://www.sciencedirect.com/science/article/pii/S0959652619343471.

[82] A. M. Stoll and G. V. Mikic, "Design studies of thin-haul commuter aircraft with distributed electric propulsion," in *16th AIAA Aviation Technology, Integration, and Operations Conference*. American Institute of Aeronautics and Astronautics, 2016. DOI: 10.2514/6.2016-3765. eprint: https://arc.aiaa.org/doi/pdf/10.2514/6.2016-3765. [Online]. Available: https://arc.aiaa.org/doi/abs/10.2514/6.2016-3765.

[83] J. Hoelzen *et al.*, "Conceptual Design of Operation Strategies for Hybrid Electric Aircraft," en, *Energies*, vol. 11, no. 1, p. 217, Jan. 2018, Number: 1 isher: Multidisciplinary Digital Publishing Institute, ISSN: 1996-1073. DOI: 10.3390/en11010217. [Online]. Available: https://www.mdpi.com/1996-1073/11/1/217 (visited on 02/17/2023).

[84] M. Pohl *et al.*, "Preliminary design of integrated partial turboelectric aircraft propulsion systems," *Journal of the Global Power and Propulsion Society*, vol. 6, pp. 1–23, 2022. DOI: 10.33737/jgpps/145907. [Online]. Available: https://doi.org/10.33737/jgpps/145907.

[85] S. Karpuk and A. Elham, "Influence of Novel Airframe Technologies on the Feasibility of Fully-Electric Regional Aviation," en, *Aerospace*, vol. 8, no. 6, p. 163, Jun. 2021, Number: 6 isher: Multidisciplinary Digital Publishing Institute, ISSN: 2226-4310. DOI: 10.3390/aerospace8060163. [Online]. Available: https://www.mdpi.com/2226-4310/8/6/163 (visited on 04/21/2023).

[86] P. Vratny, C. Gologan, C. Pornet, A. Isikveren, and M. Hornung, "Battery pack modeling methods for universally-electric aircraft," in *4th CEAS Air & Space Conference*, Sep. 2013.

[87] C. Pornet *et al.*, "Methodology for Sizing and Performance Assessment of Hybrid Energy Aircraft," *Journal of Aircraft*, vol. 52, no. 1, pp. 341–352, Jan. 2015, Publisher: American Institute of Aeronautics and Astronautics, ISSN: 0021-8669. DOI: 10.2514/1.C032716. [Online]. Available: https://arc.aiaa.org/doi/10.2514/1.C032716 (visited on 04/21/2023).

[88] J. M. Vegh, E. Botero, M. Clarke, J. Smart, and J. Alonso, "Current capabilities and challenges of ndarc and suave for evtol aircraft design and analysis," in *AIAA Propulsion and Energy 2019 Forum*. American Institute of Aeronautics and Astronautics, Aug. 2019. DOI: 10.2514/6.2019-4505.

[89] E. S. Hendricks and J. S. Gray, "pyCycle: A Tool for Efficient Optimization of Gas Turbine Engine Cycles," en, *Aerospace*, vol. 6, no. 8, p. 87, Aug. 2019, Number: 8 isher: Multidisciplinary Digital Publishing Institute, ISSN: 2226-4310. DOI: 10.3390/aerospace6080087. [Online]. Available: https://www.mdpi.com/2226-4310/6/8/87 (visited on 04/26/2023).

[90] S. Karpuk, V. Mosca, C. Liu, and A. Elham, "Development of a multi-fidelity design, analysis, and optimization environment for future transport aircraft," in *AIAA SCITECH 2022 Forum*. American Institute of Aeronautics and Astronautics, 2022. DOI: 10.2514/6.2022-0686. [Online]. Available: https://arc.aiaa.org/doi/abs/10.2514/6.2022-0686.

[91] F. Lutz, J. Jézégou, A. Reysset, A. Busteros Ramos, and V. Pommier-Budinger, "FAST-OAD-GA: an open-source extension for Overall Aircraft Design of General Aviation aircraft," in *ICAS 2022*, Stockholm, Sweden, Sep. 2022. [Online]. Available: https://hal.science/hal-03828230.

[92] F. M. Capristan, D. Caldwell, R. Condotta, and B. Petty, "Aircraft analysis using the layered and extensible aircraft performance system (leaps)," NASA, Tech. Rep., 2020. [Online]. Available: https://ntrs.nasa.gov/citations/20200001143.

[93] M. Golzar, H. Van Khang, M. M. Hubert Choux, and A. M. Midtbø Versland, "Experimental investigation of efficiency map for an inverter-fed surface-mount permanent magnet synchronous motor," in *2019 8th International Conference on Renewable Energy Research and Applications (ICRERA)*, IEEE, 2019, pp. 551–556. DOI: https://doi.org/10.1109/ICRERA47325.2019.8996549.

[94] S. Wang, Y. Li, Y.-Z. Li, and K. Xiong, "Analysis of power loss of permanent magnet synchronous motors in more-electric-aircraft considering the impact of temperature," in *2018 IEEE/ASME International Conference on Advanced Intelligent Mechatronics (AIM)*, ISSN: 2159-6255, Jul. 2018, pp. 1184–1189. DOI: 10.1109/AIM.2018.8452450.

[95] A. De Marco, M. Di Stasio, P. Della Vecchia, V. Trifari, and F. Nicolosi, "Automatic modeling of aircraft external geometries for preliminary design workflows," en, *Aerospace Science and Technology*, vol. 98, p. 105 667, Mar. 2020, ISSN: 1270-9638. DOI: 10.1016/j.ast.2019.105667. [Online]. Available: https://www.sciencedirect.com/science/article/pii/S1270963819316943 (visited on 04/26/2023).

[96] G. Cinar, M. Emeneth, and D. N. Mavris, "A methodology for sizing and analysis of electric propulsion subsystems for unmanned aerial vehicles," in *54th AIAA Aerospace Sciences Meeting*. American Institute of Aeronautics and Astronautics, 2016. DOI: 10.2514/6.2016-0216. eprint: https://arc.aiaa.org/doi/pdf/10.2514/6.2016-0216. [Online]. Available: https://arc.aiaa.org/doi/abs/10.2514/6.2016-0216.

[97] G. La Rocca, J. Jansen, and T. Zill, "Investigation of multi-fidelity and variable-fidelity optimization approaches for collaborative aircraft design," in *CEAS 2013*, Jan. 2013.

[98] J. Jepsen, P. D. Ciampa, and B. Nagel, "Avoiding inconsistencies between data models in collaborative aircraft design processes," in *DLRK 2016*, Jan. 2016.

[99] M. Hoogreef, R. de Vries, T. Sinnige, and R. Vos, "Synthesis of aero-propulsive interaction studies applied to conceptual hybrid-electric aircraft design," in *AIAA Scitech 2020 Forum*. American Institute of Aeronautics and Astronautics, Jan. 2020. DOI: 10.2514/6.2020-0503. eprint: https://arc.aiaa.org/doi/pdf/10.2514/6.2020-0503. [Online]. Available: https://arc.aiaa.org/doi/abs/10.2514/6.2020-0503.

[100] M. Zimmnau, F. Schültke, and E. Stumpf, "UNICADO: Multidisciplinary analysis in conceptual aircraft design," en, *CEAS Aeronautical Journal*, vol. 14, no. 1, pp. 75–89, Jan. 2023, ISSN: 1869-5582, 1869-5590. DOI: 10.1007/s13272-022-00620-3. [Online]. Available: https://link.springer.com/10.1007/s13272-022-00620-3 (visited on 09/28/2025).

[101] D. P. Wells, B. L. Horvath, and L. A. McCullers, "The Flight Optimization System Weights Estimation Method," NASA, Tech. Rep. NASA/TM-2017-219627/VOL1, Jun. 2017, NTRS Author Affiliations: NASA Langley Research Center, ATK Space Systems Document ID: 20170005851 Research Center: Langley Research Center (LaRC). [Online]. Available: https://ntrs.nasa.gov/citations/20170005851 (visited on 04/27/2023).

[102] J. R. Welstead, D. Caldwell, R. Condotta, and N. Monroe, "An overview of the layered and extensible aircraft performance system (leaps) development," in *2018 AIAA Aerospace Sciences Meeting*. American Institute of Aeronautics and Astronautics, 2018. DOI: 10.2514/6.2018-1754. eprint: https://arc.aiaa.org/doi/pdf/10.2514/6.2018-1754. [Online]. Available: https://arc.aiaa.org/doi/abs/10.2514/6.2018-1754.

[103] E. Adler and J. R. Martins, "Aerostructural wing design optimization considering full mission analysis," in *AIAA SCITECH 2022 Forum*. American Institute of Aeronautics and Astronautics, 2022. DOI: 10.2514/6.2022-0382. eprint: https://arc.aiaa.org/doi/pdf/10.2514/6.2022-0382. [Online]. Available: https://arc.aiaa.org/doi/abs/10.2514/6.2022-0382.

[104] E. Aretskin-Hariton *et al.*, "Multidisciplinary optimization of a transonic truss-braced wing aircraft using the aviary framework," in *AIAA SCITECH 2024 Forum*. American Institute of Aeronautics and Astronautics, 2024. DOI: 10.2514/6.2024-1084. eprint: https://arc.aiaa.org/doi/pdf/10.2514/6.2024-1084. [Online]. Available: https://arc.aiaa.org/doi/abs/10.2514/6.2024-1084.

[105] T. MacDonald *et al.*, "Suave: An open-source environment enabling unconventional vehicle designs through higher fidelity," in *55th AIAA Aerospace Sciences Meeting*. American Institute of Aeronautics and Astronautics, 2017. DOI: 10.2514/6.2017-0234. eprint: https://arc.aiaa.org/doi/pdf/10.2514/6.2017-0234. [Online]. Available: https://arc.aiaa.org/doi/abs/10.2514/6.2017-0234.

[106] J. L. Kerrebrock, *Aircraft engines and gas turbines*, eng, 2nd ed. Cambridge, Massachusetts: MIT Press, 1992, ISBN: 978-0-262-27705-1.

[107] F. Pollet, S. Delbecq, M. Budinger, J.-M. Moschetta, and J. Liscouët, "A common framework for the design optimization of fixed-wing, multicopter and vtol uav configurations," in *33rd Congress of the International Council of the Aeronautical Sciences*, 2022. [Online]. Available: A%20common%20framework%20for%20the%20design%20optimization%20of%20fixed-wing,%20multicopter%20and%20VTOL%20UAV%20configurations.

[108] V. Habrard, V. Pommier-Budinger, I. Hazyuk, J. Jézégou, and E. Benard, "Thermal management system modeling for preliminary design of fuel cell-based aircraft," in *AIAA AVIATION 2023 Forum*. American Institute of Aeronautics and Astronautics, 2023. DOI: 10.2514/6.2023-4303. eprint: https://arc.aiaa.org/doi/pdf/10.2514/6.2023-4303. [Online]. Available: https://arc.aiaa.org/doi/abs/10.2514/6.2023-4303.

[109] F. Pollet, M. Budinger, S. Delbecq, J.-M. Moschetta, and T. Planès, "Environmental Life Cycle Assessments for the Design Exploration of Electric UAVs," in *Aerospace Europe Conference 2023 – 10th EUCASS – 9th CEAS*, Lausanne, Switzerland, 2023. DOI: 10.13009/EUCASS2023-548. [Online]. Available: https://hal.science/hal-04229799.

[110] A. Fabre, T. Planès, S. Delbecq, V. Budinger, and G. Lafforgue, "Life cycle assessment models for overall aircraft design," in *AIAA SCITECH 2022 Forum*. American Institute of Aeronautics and Astronautics, 2022. DOI: 10.2514/6.2022-1028. eprint: https://arc.aiaa.org/doi/pdf/10.2514/6.2022-1028. [Online]. Available: https://arc.aiaa.org/doi/abs/10.2514/6.2022-1028.

[111] F. Brenner, J. Mangold, D. Eisenhut, N. Moebs, and A. Strohmayer, "Deriving a year 2040 reference aircraft from a modern turboprop, implemented and calibrated in suave," *Journal of Physics: Conference Series*, vol. 2526, no. 1, p. 012 009, 2023. DOI: 10.1088/1742-6596/2526/1/012009. [Online]. Available: https://doi.org/10.1088/1742-6596/2526/1/012009.

[112] A. Sgueglia, P. Schmollgruber, E. Benard, N. Bartoli, and J. Morlier, "Preliminary sizing of a medium range blended wing-body using a multidisciplinary design analysis approach," in *MATEC Web of Conferences*, EDP Sciences, vol. 233, 2018, pp. 1–9. DOI: https://doi.org/10.1051/matecconf/201823300014.

[113] J. S. Gray, J. T. Hwang, J. R. Martins, K. T. Moore, and B. A. Naylor, "Openmdao: An open-source framework for multidisciplinary design, analysis, and optimization," *Structural and Multidisciplinary Optimization*, vol. 59, pp. 1075–1104, 2019. DOI: https://doi.org/10.1007/s00158-019-02211-z.

[114] L. McCullers, "Aircraft configuration optimization including optimized flight profiles," *NASA. Langley Research Center Recent Experiences in Multidisciplinary Analysis and Optimization, Part 1*, 1984. [Online]. Available: https://ntrs.nasa.gov/citations/19870002310.

[115] D. Hague, "Gasp-general aviation synthesis program. volume 1: Main program. part 1: Theoretical development," NASA, Tech. Rep., 1978. [Online]. Available: https://ntrs.nasa.gov/citations/19810010562.

[116] T. W. Lukaczyk *et al.*, "Suave: An open-source environment for multi-fidelity conceptual vehicle design," in *16th AIAA/ISSMO Multidisciplinary Analysis and Optimization Conference*. American Institute of Aeronautics and Astronautics, 2015. DOI: 10.2514/6.2015-3087. eprint: https://arc.aiaa.org/doi/pdf/10.2514/6.2015-3087. [Online]. Available: https://arc.aiaa.org/doi/abs/10.2514/6.2015-3087.

[117] R. Singh, J. Freeman, P. Osterkamp, M. Green, A. Gibson, and B. Schiltgen, "Challenges and opportunities for electric aircraft thermal management," *Aircraft Engineering and Aerospace Technology*, vol. 86, no. 6, pp. 519–524, Sep. 2014, ISSN: 1748-8842. DOI: 10.1108/AEAT-04-2014-0042. eprint: https://www.emerald.com/aeat/article-pdf/86/6/519/281133/aeat-04-2014-0042.pdf. [Online]. Available: https://doi.org/10.1108/AEAT-04-2014-0042.

[118] C. DAVID *et al.*, *Fast-aircraft-design/fast-oad: V1.8.4*, version v1.8.4, Aug. 2025. DOI: 10.5281/zenodo.16928377. [Online]. Available: https://doi.org/10.5281/zenodo.16928377.

[119] A. Seabridge and I. Moir, *Design and development of aircraft systems* (Aerospace series), eng, Third edition. Hoboken, NJ: John Wiley & Sons, 2020, ISBN: 978-1-119-61150-9.

[120] E. S. Hendricks, J. Chapman, and E. Aretskin-Hariton, "Load flow analysis with analytic derivatives for electric aircraft design optimization," in *AIAA Scitech 2019 Forum*, 2019, p. 1220. DOI: https://doi.org/10.2514/6.2019-1220.

[121] T. Prosvirnova *et al.*, "The altarica 3.0 project for model-based safety assessment," *IFAC Proceedings Volumes*, vol. 46, no. 22, pp. 127–132, 2013, 4th IFAC Workshop on Dependable Control of Discrete Systems, ISSN: 1474-6670. DOI: https://doi.org/10.3182/20130904-3-UK-4041.00028. [Online]. Available: https://www.sciencedirect.com/science/article/pii/S1474667015339999.

[122] P. Bamrah, S. Liscouet-Hanke, A. Tfaily, and A. Tamayo, "Zonal safety and particular risk analysis for aircraft conceptual design," in *AIAA AVIATION 2023 Forum*. 2023. DOI: 10.2514/6.2023-4197. eprint: https://arc.aiaa.org/doi/pdf/10.2514/6.2023-4197. [Online]. Available: https://arc.aiaa.org/doi/abs/10.2514/6.2023-4197.

[123] E. A. Calado, M. Leite, and A. Silva, "Integrating life cycle assessment (LCA) and life cycle costing (LCC) in the early phases of aircraft structural design: An elevator case study," en, *The International Journal of Life Cycle Assessment*, vol. 24, no. 12, pp. 2091–2110, Dec. 2019, ISSN: 1614-7502. DOI: 10.1007/s11367-019-01632-8. [Online]. Available: https://doi.org/10.1007/s11367-019-01632-8 (visited on 07/30/2024).

[124] A. Johanning and D. Scholz, "Conceptual aircraft design based on lifecycle assesssment," in *International Council of the Aeronautical Sciences Congress 2014*, ser. 29th Congress of the International Council of the Aeronautical Sciences, 2014, ISBN: 3-932182-80-4. [Online]. Available: http://hdl.handle.net/20.500.12738/935.

[125] X. Giraud, "Méthodes et outils pour la conception optimale des réseaux de distribution d'électricité dans les aéronefs," These de doctorat, Toulouse, INSA, Feb. 2014. [Online]. Available: https://www.theses.fr/2014ISAT0004 (visited on 07/18/2022).

[126] B. Dimitrov, K. Hayatleh, S. Barker, G. Collier, S. Sharkh, and A. Cruden, "A Buck-Boost Transformerless DC–DC Converter Based on IGBT Modules for Fast Charge of Electric Vehicles," *Electronics*, vol. 9, no. 3, 2020, ISSN: 2079-9292. DOI: 10.3390/electronics9030397.

[127] FAA, "14 CFR Part 25 – Airworthiness Standards: Transport Category Airplanes," en, Federal Aviation Administration, Technical Report, Jan. 2023. [Online]. Available: https://www.ecfr.gov/current/title-14/chapter-I/subchapter-C/part-25 (visited on 12/02/2025).

[128] M. Budinger, J. Liscouët, F. Hospital, and J.-C. Maré, "Estimation models for the preliminary design of electromechanical actuators," *Proceedings of the Institution of Mechanical Engineers, Part G: Journal of Aerospace Engineering*, vol. 226, no. 3, pp. 243–259, 2012. DOI: 10.1177/0954410011408941.

[129] S. Stipetic, D. Zarko, and M. Popescu, "Ultra-fast axial and radial scaling of synchronous permanent magnet machines," *IET Electric Power Applications*, vol. 10, no. 7, pp. 658–666, 2016. DOI: https://doi.org/10.1049/iet-epa.2016.0014.

[130] F. Sanchez, S. Delbecq, M. Budinger, and I. Hazyuk, "Modelling and design approaches for the preliminary design of power electronic converters," in *ELECTRIMACS*, Toulouse, France, 2017. [Online]. Available: https://hal.science/hal-02044400.

[131] M. A. Bouhlel, J. T. Hwang, N. Bartoli, R. Lafage, J. Morlier, and J. R. Martins, "A python surrogate modeling framework with derivatives," *Advances in Engineering Software*, vol. 135, p. 102 662, 2019, ISSN: 0965-9978. DOI: https://doi.org/10.1016/j.advengsoft.2019.03.005. [Online]. Available: https://www.sciencedirect.com/science/article/pii/S0965997818309360.

[132] G. Yamauchi and W. Johnson, "Trends of reynolds number effects on two-dimensional airfoil characteristics for helicopter rotor analyses," NASA, Tech. Rep., 1983. [Online]. Available: https://ntrs.nasa.gov/citations/19830016201.

[133] T. Von Karman, "Compressibility effects in aerodynamics," *Journal of spacecraft and rockets*, vol. 40, no. 6, pp. 992–1011, 2003. DOI: https://doi.org/10.2514/2.7046.

[134] J. D. Hoyos, J. H. Jiménez, C. Echavarría, J. P. Alvarado, and G. Urrea, "Aircraft propeller design through constrained aero-structural particle swarm optimization," *Aerospace*, vol. 9, no. 3, 2022, ISSN: 2226-4310. DOI: 10.3390/aerospace9030153.

[135] EASA, *CS-P Amendment 2 - Certification Specifications and Acceptable Means of Compliance for Propellers (CS-P)*, en, Jul. 2020. [Online]. Available: https://www.easa.europa.eu/en/document-library/certification-specifications/cs-p-amendment-2 (visited on 07/31/2025).

[136] L. L. M. Valdhuis, "Propeller Wing Aerodynamic Interference," Ph.D. dissertation, Delft University of Technology, 2005. [Online]. Available: https://resolver.tudelft.nl/uuid:8ffbde9c-b483-40de-90e0-97095202fbe3 (visited on 07/30/2025).

[137] T. Bouquet and R. Vos, "Modeling the propeller slipstream effect on lift and pitching moment," in *55th AIAA Aerospace Sciences Meeting*. American Institute of Aeronautics and Astronautics, 2017. DOI: 10.2514/6.2017-0236. eprint: https://arc.aiaa.org/doi/pdf/10.2514/6.2017-0236. [Online]. Available: https://arc.aiaa.org/doi/abs/10.2514/6.2017-0236.

[138] V. Cusati, S. Corcione, F. Nicolosi, and Q. Zhang, "Improvement of take-off performance for an electric commuter aircraft due to distributed electric propulsion," *Aerospace*, vol. 10, no. 3, 2023, ISSN: 2226-4310. DOI: https://doi.org/10.3390/aerospace10030276. [Online]. Available: https://www.mdpi.com/2226-4310/10/3/276.

[139] G. Lei, J. Zhu, Y. Guo, C. Liu, and B. Ma, "A Review of Design Optimization Methods for Electrical Machines," en, *Energies*, vol. 10, no. 12, p. 1962, Dec. 2017, Number: 12 Pub isher: Multidisciplinary Digital Publishing Institute, ISSN: 1996-1073. DOI: 10.3390/en10121962. [Online]. Available: https://www.mdpi.com/1996-1073/10/12/1962 (visited on 05/02/2023).

[140] E. Gundabattini, A. Mystkowski, A. Idzkowski, R. S. R., and D. G. Solomon, "Thermal mapping of a high-speed electric motor used for traction applications and analysis of various cooling methods—a review," *Energies*, vol. 14, no. 5, 2021, ISSN: 1996-1073. DOI: 10.3390/en14051472. [Online]. Available: https://www.mdpi.com/1996-1073/14/5/1472.

[141] Q. Chen, D. Liang, Y. Liu, and Q. Wang, "Design and multi-object optimisation of axial flux interior pmsm for ev and hev applications," *The Journal of Engineering*, vol. 2017, no. 13, pp. 2215–2220, 2017. DOI: https://doi.org/10.1049/joe.2017.0724. eprint: https://ietresearch.onlinelibrary.wiley.com/doi/pdf/10.1049/joe.2017.0724. [Online]. Available: https://ietresearch.onlinelibrary.wiley.com/doi/abs/10.1049/joe.2017.0724.

[142] L. Shao, R. Navaratne, M. Popescu, and G. Liu, "Design and construction of axial-flux permanent magnet motors for electric propulsion applications—a review," *IEEE Access*, vol. 9, pp. 158 998–159 017, 2021. DOI: 10.1109/ACCESS.2021.3131000.

[143] J. Thauvin, "Exploring the design space for a hybrid-electric regional aircraft with multidisciplinary design optimisation methods," Ph.D. dissertation, Institut National Polytechnique de Toulouse, 2018. [Online]. Available: https://theses.hal.science/tel-04221777/.

[144] S. Stipetic, D. Zarko, and M. Popescu, "Scaling laws for synchronous permanent magnet machines," in *2015 Tenth International Conference on Ecological Vehicles and Renewable Energies (EVER)*, 2015, pp. 1–7. DOI: 10.1109/EVER.2015.7113006.

[145] Y. P. Yang and G. Y. Shih, "Optimal design of an axial-flux permanent-magnet motor for an electric vehicle based on driving scenarios," *Energies*, vol. 9, no. 4, 2016, ISSN: 1996-1073. DOI: 10.3390/en9040285. [Online]. Available: https://www.mdpi.com/1996-1073/9/4/285.

[146] A. Mahmoudi, W. L. Soong, G. Pellegrino, and E. Armando, "Efficiency maps of electrical machines," in *2015 IEEE Energy Conversion Congress and Exposition (ECCE)*, 2015, pp. 2791–2799. DOI: 10.1109/ECCE.2015.7310051.

[147] O. Winter, C. Kral, and E. Schmidt, "Design and loss assessment of air cored axial flux permanent magnet machines," in *2013 International Electric Machines & Drives Conference*, 2013, pp. 602–606. DOI: 10.1109/IEMDC.2013.6556156.

[148] S. Stückl, "Methods for the Design and Evaluation of Future Aircraft Concepts Utilizing Electric Propulsion Systems," Ph.D. dissertation, Technische Universität München, 2016. [Online]. Available: https://mediatum.ub.tum.de/1255732 (visited on 08/02/2025).

[149] H. Budde-Meiwes *et al.*, "A review of current automotive battery technology and future prospects," *Proceedings of the Institution of Mechanical Engineers, Part D: Journal of Automobile Engineering*, vol. 227, no. 5, pp. 761–776, 2013. DOI: 10.1177/0954407013485567. eprint: https://doi.org/10.1177/0954407013485567. [Online]. Available: https://doi.org/10.1177/0954407013485567.

[150] J. C. Chin, S. L. Schnulo, T. B. Miller, K. P. Prokopius, and J. S. Gray, "Battery performance modeling on maxwell x-57," in *AIAA Scitech 2019 Forum*, 2019. [Online]. Available: https://api.semanticscholar.org/CorpusID:160031914.

[151] G. Saldaña, J. I. San Martín, I. Zamora, F. J. Asensio, and O. Oñederra, "Analysis of the current electric battery models for electric vehicle simulation," *Energies*, vol. 12, no. 14, p. 2750, 2019. DOI: https://doi.org/10.3390/en12142750.

[152] M. Wang and M. Mesbahi, "Energy Management for Electric Aircraft via Optimal Control: Cruise Phase," in *2020 AIAA/IEEE Electric Aircraft Technologies Symposium (EATS)*, Aug. 2020, pp. 1–15.

[153] H. Beltran, P. Ayuso, N. Vicente, B. Beltran-Pitarch, J. Garcia-Canadas, and E. Perez, "Equivalent circuit definition and calendar aging analysis of commercial li (nixmnycoz) o2/graphite pouch cells," *Journal of Energy Storage*, vol. 52, p. 104 747, 2022. DOI: https://doi.org/10.1016/j.est.2022.104747.

[154] K. Luo, X. Chen, H. Zheng, and Z. Shi, "A review of deep learning approach to predicting the state of health and state of charge of lithium-ion batteries," *Journal of Energy Chemistry*, vol. 74, pp. 159–173, 2022, ISSN: 2095-4956. DOI: https://doi.org/10.1016/j.jechem.2022.06.049. [Online]. Available: https://www.sciencedirect.com/science/article/pii/S2095495622003564.

[155] I. Baccouche, S. Jemmali, B. Manai, N. Omar, and N. Essoukri Ben Amara, "Improved ocv model of a li-ion nmc battery for online soc estimation using the extended kalman filter," *Energies*, vol. 10, no. 6, p. 764, 2017. DOI: https://doi.org/10.3390/en10060764.

[156] L. Chen *et al.*, "Estimation the internal resistance of lithium-ion-battery using a multi-factor dynamic internal resistance model with an error compensation strategy," *Energy Reports*, vol. 7, pp. 3050–3059, 2021. DOI: https://doi.org/10.1016/j.egyr.2021.05.027.

[157] M. Clarke and J. J. Alonso, "Lithium–ion battery modeling for aerospace applications," *Journal of Aircraft*, vol. 58, no. 6, pp. 1323–1335, 2021. DOI: https://doi.org/10.2514/1.C036209.

[158] S. Barcellona, S. Colnago, G. Dotelli, S. Latorrata, and L. Piegari, "Aging effect on the variation of li-ion battery resistance as function of temperature and state of charge," *Journal of Energy Storage*, vol. 50, p. 104 658, 2022. DOI: https://doi.org/10.1016/j.est.2022.104658.

[159] M. Etxandi-Santolaya, L. C. Casals, and C. Corchero, "Extending the electric vehicle battery first life: Performance beyond the current end of life threshold," *Heliyon*, vol. 10, no. 4, e26066, 2024, ISSN: 2405-8440. DOI: https://doi.org/10.1016/j.heliyon.2024.e26066. [Online]. Available: https://www.sciencedirect.com/science/article/pii/S2405844024020978.

[160] B. Xu, A. Oudalov, A. Ulbig, G. Andersson, and D. S. Kirschen, "Modeling of lithium-ion battery degradation for cell life assessment," *IEEE Transactions on Smart Grid*, vol. 9, no. 2, pp. 1131–1140, 2018. DOI: 10.1109/TSG.2016.2578950.

[161] W. Vermeer, G. R. Chandra Mouli, and P. Bauer, "A comprehensive review on the characteristics and modeling of lithium-ion battery aging," *IEEE Transactions on Transportation Electrification*, vol. 8, no. 2, pp. 2205–2232, 2022. DOI: 10.1109/TTE.2021.3138357.

[162] Y. Chen, Y. He, Z. Li, and L. Chen, "A combined multiple factor degradation model and online verification for electric vehicle batteries," *Energies*, vol. 12, no. 22, 2019, ISSN: 1996-1073. DOI: 10.3390/en12224376. [Online]. Available: https://www.mdpi.com/1996-1073/12/22/4376.

[163] J. Schmalstieg, S. Käbitz, M. Ecker, and D. U. Sauer, "A holistic aging model for li(nimnco)o2 based 18650 lithium-ion batteries," *Journal of Power Sources*, vol. 257, pp. 325–334, 2014, ISSN: 0378-7753. DOI: https://doi.org/10.1016/j.jpowsour.2014.02.012. [Online]. Available: https://www.sciencedirect.com/science/article/pii/S0378775314001876.

[164] M. Kalwara, M. Kuźniar, and M. Orkisz, "A rotating piston engine with electric generator in serial hybrid propulsion system for use in light aircraft," *Combustion Engines*, vol. 187, no. 4, pp. 42–45, Oct. 2021, Publisher: Polish Scientific Society of Combustion Engines, ISSN: 2300-9896, 2658-1442. DOI: 10.19206/CE-141353. [Online]. Available: http://www.combustion-engines.eu/A-rotating-piston-engine-with-electric-generator-in-serial-hybrid-propulsion-system,141353,0,2.html (visited on 03/10/2023).

[165] I. Geiß, S. Notter, A. Strohmayer, and W. Fichter, "Optimized operation strategies for serial hybrid-electric aircraft," in *2018 Aviation Technology, Integration, and Operations Conference*, 2018, p. 4230. DOI: https://doi.org/10.2514/6.2018-4230.

[166] F. Leach, G. Kalghatgi, R. Stone, and P. Miles, "The scope for improving the efficiency and environmental impact of internal combustion engines," en, *Transportation Engineering*, vol. 1, p. 100 005, Jun. 2020, ISSN: 2666-691X. DOI: 10.1016/j.treng.2020.100005. [Online]. Available: https://www.sciencedirect.com/science/article/pii/S2666691X20300063 (visited on 05/08/2023).

[167] E. Harrison, S. Min, H. Jimenez, and D. N. Mavris, "Implementation and validation of an internal combustion engine and propeller model for general aviation aircraft performance studies," in *15th AIAA Aviation Technology, Integration, and Operations Conference*. American Institute of Aeronautics and Astronautics, 2015. DOI: 10.2514/6.2015-2850. eprint: https://arc.aiaa.org/doi/pdf/10.2514/6.2015-2850. [Online]. Available: https://arc.aiaa.org/doi/abs/10.2514/6.2015-2850.

[168] Grabowski, Łukasz, Siadkowska, Ksenia, and Skiba, Krzysztof, "Simulation research of aircraft piston engine rotax 912," *MATEC Web Conf.*, vol. 252, p. 05 007, 2019. DOI: 10.1051/matecconf/201925205007. [Online]. Available: https://doi.org/10.1051/matecconf/201925205007.

[169] M. Otkur, "Altitude performance and fuel consumption modelling of aircraft piston engine rotax 912 s/uls," *Journal of Advanced Research in Applied Sciences and Engineering Technology*, vol. 23, no. 1, pp. 18–25, 2021.

[170] R. F. Gagg and E. V. Farrar, "Altitude Performance of Aircraft Engines Equipped with Gear-Driven Superchargers," English, SAE International, Warrendale, PA, SAE Technical Paper 340096, Jan. 1934, ISSN: 0148-7191, 2688-3627. DOI: 10.4271/340096. [Online]. Available: https://www.sae.org/publications/technical-papers/content/340096/ (visited on 05/08/2023).

[171] M. Masiol and R. M. Harrison, "Aircraft engine exhaust emissions and other airport-related contributions to ambient air pollution: A review," *Atmospheric Environment*, vol. 95, pp. 409–455, 2014, ISSN: 1352-2310. DOI: https://doi.org/10.1016/j.atmosenv.2014.05.070. [Online]. Available: https://www.sciencedirect.com/science/article/pii/S1352231014004361.

[172] B. Graver, K. Zhang, and D. Rutherford, "Emissions from commercial aviation, 2018," *International Council on Clean Transportation*, 2019.

[173] D. G. Goodwin, R. L. Speth, H. K. Moffat, and B. W. Weber, *Cantera: An Object-oriented Software Toolkit for Chemical Kinetics, Thermodynamics, and Transport Processes*, version 2.5.1, Feb. 2021. DOI: 10.5281/zenodo.4527812.

[174] European Environment Agency., *EMEP/EEA air pollutant emission inventory guidebook 2023: technical guidance to prepare national emission inventories.* eng. LU: Publications Office, 2023, ISBN: 978-92-9480-098-5. [Online]. Available: https://data.europa.eu/doi/10.2800/795737 (visited on 07/16/2024).

[175] M. T. Kalivoda and M. Kudrna, "Methodologies for estimating emissions from air traffic," *MEET Project (underlagsrapport till MEET)*, 1997.

[176] E. Roux, "Pour une approche analytique de la dynamique du vol," Ph.D. dissertation, ISAE-SUPAERO, 2005.

[177] V. Palladino, A. Jordan, N. Bartoli, P. Schmollgruber, V. Pommier-Budinger, and E. Benard, "Preliminary studies of a regional aircraft with hydrogen-based hybrid propulsion," in *AIAA AVIATION 2021 FORUM Session: Advanced Propulsion Concepts*, Online, United States: American Institute of Aeronautics and Astronautics, Aug. 2021, AIAA 2021–2411. DOI: 10.2514/6.2021-2411. [Online]. Available: https://hal.science/hal-03690045.

[178] R. Quiben Figueroa, R. Cavallaro, and A. Cini, "Feasibility studies on regional aircraft retrofitted with hybrid-electric powertrains," *Aerospace Science and Technology*, vol. 151, p. 109 246, 2024, ISSN: 1270-9638. DOI: https://doi.org/10.1016/j.ast.2024.109246. [Online]. Available: https://www.sciencedirect.com/science/article/pii/S1270963824003778.

[179] A. Filippone and B. Parkes, "Evaluation of commuter airplane emissions: A european case study," *Transportation Research Part D: Transport and Environment*, vol. 98, p. 102 979, 2021, ISSN: 1361-9209. DOI: https://doi.org/10.1016/j.trd.2021.102979. [Online]. Available: https://www.sciencedirect.com/science/article/pii/S1361920921002777.

[180] C. Eyers *et al.*, "Aero2k global aviation emissions inventories for 2002 and 2025," 2004.

[181] S. AIR5715, "Procedure for the calculation of aircraft emissions," *AEROSPACE INFORMATION REPORT*, 2009.

[182] P. Norman *et al.*, "Development of the technical basis for a new emissions parameter covering the whole aircraft operation: Nepair," *European Commission, Luxembourg City, Luxembourg, Final Technical Report No. NEPAIR/WP4/WPR/01*, 2003.

[183] D. DuBois and G. C. Paynter, ""fuel flow method2" for estimating aircraft emissions," *Sae Transactions*, pp. 1–14, 2006, ISSN: 0148-7191. DOI: https://doi.org/10.4271/2006-01-1987.

[184] A. Dopelheuer and M. Lecht, "Influence of engine performance on emission characteristics," in *Gas Turbine Engine Combustion, Emissions and Alternative Fuels, Proceedings of the RTO/AVT Symposium: Lisboa, Portugal*, Citeseer, 1998, pp. 12–16.

[185] A. Filippone and N. Bojdo, "Statistical model for gas turbine engines exhaust emissions," *Transportation Research Part D: Transport and Environment*, vol. 59, pp. 451–463, 2018, ISSN: 1361-9209. DOI: https://doi.org/10.1016/j.trd.2018.01.019. [Online]. Available: https://www.sciencedirect.com/science/article/pii/S1361920917304716.

[186] S. L. Baughcum, D. J. Sutkus, and S. C. Henderson, "Year 2015 Aircraft Emission Scenario for Scheduled Air Traffic," National Aeronautics and Space Administration, Tech. Rep. NAS 1.26:207638, Mar. 1998, NTRS Author Affiliations: Boeing Commercial Airplane Co. NTR Document ID: 19980055200 NTR Research Center: Langley Research Center (LaRC). [Online]. Available: https://ntrs.nasa.gov/citations/19980055200 (visited on 07/17/2024).

[187] B. Y. Kim *et al.*, "System for assessing aviation's global emissions (sage), part 1: Model description and inventory results," *Transportation Research Part D: Transport and Environment*, vol. 12, no. 5, pp. 325–346, 2007, ISSN: 1361-9209. DOI: https://doi.org/10.1016/j.trd.2007.03.007. [Online]. Available: https://www.sciencedirect.com/science/article/pii/S1361920907000387.

[188] W. Xu, R. y. Yu, Z. Guo, and A. Q. Huang, "Design of 1500v/200kw 99.6% efficiency dual active bridge converters based on 1700v sic power mosfet module," in *2020 IEEE Energy Conversion Congress and Exposition (ECCE)*, 2020, pp. 6000–6007. DOI: 10.1109/ECCE44975.2020.9235903.

[189] H. A. Hairik, A. K. AbdulAbass, and K. A. Abbas, "Dc/dc buck-boost converter efficiency and power dissipation calculation at operating points not included in the datasheet," *Journal of Multidisciplinary Engineering Science and Technology (JMEST), ISSN*, pp. 2458–9403, 2019.

[190] G. Parent, M. Rossi, S. Duchesne, and P. Dular, "Determination of Partial Discharge Inception Voltage and Location of Partial Discharges by Means of Paschen's Theory and FEM," *IEEE Transactions on Magnetics*, vol. 55, no. 6, pp. 1–4, Jun. 2019, Conference Name: IEEE Transactions on Magnetics, ISSN: 1941-0069. DOI: 10.1109/TMAG.2019.2902374.

[191] Z. Yuan *et al.*, "Insulation design and optimization of laminated busbar for more electric aircraft motor drive under high altitude and depressurized environments," in *2020 AIAA/IEEE Electric Aircraft Technologies Symposium (EATS)*, 2020, pp. 1–9.

[192] Z. Yuan *et al.*, "Design of partial-discharge-free busbar for more-electric aircraft application with low pressure condition," in *2021 IEEE Applied Power Electronics Conference and Exposition (APEC)*, 2021, pp. 1178–1182. DOI: 10.1109/APEC42165.2021.9487285.

[193] M. Khan, P. Magne, B. Bilgin, S. Wirasingha, and A. Emadi, "Laminated busbar design criteria in power converters for electrified powertrain applications," in *2014 IEEE Transportation Electrification Conference and Expo (ITEC)*, 2014, pp. 1–6. DOI: 10.1109/ITEC.2014.6861841.

[194] X. Pei, O. Cwikowski, D. S. Vilchis-Rodriguez, M. Barnes, A. C. Smith, and R. Shuttleworth, "A review of technologies for mvdc circuit breakers," in *IECON 2016 - 42nd Annual Conference of the IEEE Industrial Electronics Society*, 2016, pp. 3799–3805. DOI: 10.1109/IECON.2016.7793492.

[195] Z. Liu, R. Fuller, and W. Pearson, "SSPC Technologies for Aircraft High Voltage DC Power Distribution Applications," English, SAE International, Warrendale, PA, SAE Technical Paper 2012-01-2213, Oct. 2012, ISSN: 0148-7191, 2688-3627. DOI: 10.4271/2012-01-2213. [Online]. Available: https://www.sae.org/publications/technical-papers/content/2012-01-2213/ (visited on 08/07/2025).

[196] G. Valente *et al.*, "Design methodology and parametric design study of the on-board electrical power system for hybrid electric aircraft propulsion," in *The 10th International Conference on Power Electronics, Machines and Drives (PEMD 2020)*, vol. 2020, 2020, pp. 448–454. DOI: 10.1049/icp.2021.1126.

[197] J. Koster, C. Humbargar, E. Serani, A. Velazco, D. Hillery, and L. Makepeace, "Hybrid electric integrated optimized system (helios) - design of a hybrid propulsion system for aircraft," in *49th AIAA Aerospace Sciences Meeting including the New Horizons Forum and Aerospace Exposition*. American Institute of Aeronautics and Astronautics, 2011. DOI: 10.2514/6.2011-1011. eprint: https://arc.aiaa.org/doi/pdf/10.2514/6.2011-1011. [Online]. Available: https://arc.aiaa.org/doi/abs/10.2514/6.2011-1011.

[198] R. Willis, "Lightest-weight gears," *Product engineering*, vol. 5, pp. 64–75, 1963.

[199] A. D. Anderson *et al.*, "System weight comparison of electric machine topologies for electric aircraft propulsion," in *2018 AIAA/IEEE Electric Aircraft Technologies Symposium (EATS)*, 2018, pp. 1–16.

[200] *Closed-Loop Design for Hybrid Powertrains*, vol. Volume 3: 19th International Conference on Advanced Vehicle Technologies; 14th International Conference on Design Education; 10th Frontiers in Biomedical Devices, International Design Engineering Technical Conferences and Computers and Information in Engineering Conference, American Society of Mechanical Engineers, Aug. 2017, V003T01A024. DOI: 10.1115/DETC2017-67404.

[201] L. Tan, P. Liu, C. She, P. Xu, L. Yan, and H. Quan, "Heat dissipation characteristics of igbt module based on flow-solid coupling," *Micromachines*, vol. 13, no. 4, p. 554, 2022. DOI: https://doi.org/10.3390/mi13040554.

[202] F. Sanchez, M. Budinger, and I. Hazyuk, "DIMENSIONAL ANALYSIS AND SURROGATE MODELS FOR THERMAL MODELLING OF POWER ELECTRONIC COMPONENTS," in *Electrimacs*, Toulouse, France, Jul. 2017. [Online]. Available: https://insa-toulouse.hal.science/hal-02044714.

[203] E. Stefana, E. De Paola, L. Pustina, R. Patriarca, F. Mastroddi, *et al.*, "Ensuring the next generation green aircraft'sustainability from the design phase via a life cycle cost analysis," in *ICAS Proceedings-34th Congress of the International Council of the Aeronautical Sciences*, International Council of the Aeronautical Sciences, 2024.

[204] E. Espinosa-Juárez, C. Jouannet, K. Amadori, and A. S. Mata, "Comparative analysis on aircraft direct operating cost models," in *AIAA AVIATION FORUM AND ASCEND 2025*. American Institute of Aeronautics and Astronautics, 2025. DOI: 10.2514/6.2025-3499. eprint: https://arc.aiaa.org/doi/pdf/10.2514/6.2025-3499. [Online]. Available: https://arc.aiaa.org/doi/abs/10.2514/6.2025-3499.

[205] A. Seitz, O. Schmitz, A. T. Isikveren, and M. Hornung, *Electrically powered propulsion: comparison and contrast to gas turbines*. Deutsche Gesellschaft für Luft-und Raumfahrt-Lilienthal-Oberth eV Bonn, Germany, 2012.

[206] S. Byahut, A. Pundarika, and A. Uranga, "Modeling well-to-wake life-cycle co2 emissions for electrified aircraft," in *AIAA AVIATION 2021 FORUM*. American Institute of Aeronautics and Astronautics, 2021. DOI: 10.2514/6.2021-2410. eprint: https://arc.aiaa.org/doi/pdf/10.2514/6.2021-2410. [Online]. Available: https://arc.aiaa.org/doi/abs/10.2514/6.2021-2410.

[207] K. Abu Salem, G. Palaia, *et al.*, "Environmental implications of hybrid-electric regional aircraft: Emissions and climate change," in *34th Congress of the International Council of the Aeronautical Sciences, ICAS 2024*, International Council of the Aeronautical Sciences, 2024.

[208] A. E. Scholz, D. Trifonov, and M. Hornung, "Environmental life cycle assessment and operating cost analysis of a conceptual battery hybrid-electric transport aircraft," en, *CEAS Aeronaut J*, vol. 13, no. 1, pp. 215–235, Jan. 2022, ISSN: 1869-5582, 1869-5590. DOI: 10.1007/s13272-021-00556-0. [Online]. Available: https://link.springer.com/10.1007/s13272-021-00556-0 (visited on 09/02/2025).

[209] S. Delbecq, J. Fontane, N. Gourdain, T. Planès, and F. Simatos, "Sustainable aviation in the context of the paris agreement: A review of prospective scenarios and their technological mitigation levers," *Progress in Aerospace Sciences*, vol. 141, p. 100 920, 2023, Special Issue on Green Aviation, ISSN: 0376-0421. DOI: https://doi.org/10.

1016/j.paerosci.2023.100920. [Online]. Available: https://www.sciencedirect.com/science/article/pii/S0376042123000362.

[210] M. Prussi, M. Yugo, L. De Prada, M. Padella, R. Edwards, and L. Lonza, *JEC well-to-tank report V5 – JEC well-to-wheels analysis – Well-to-wheels analysis of future automotive fuels and powertrains in the European context*. Publications Office, 2020. DOI: doi/10.2760/959137.

[211] J. Hospodka, H. Bínová, and S. Pleninger, "Assessment of all-electric general aviation aircraft," *Energies*, vol. 13, no. 23, 2020, ISSN: 1996-1073. DOI: 10.3390/en13236206. [Online]. Available: https://www.mdpi.com/1996-1073/13/23/6206.

[212] G. Wernet, C. Bauer, B. Steubing, J. Reinhard, E. Moreno-Ruiz, and B. Weidema, "The ecoinvent database version 3 (part I): Overview and methodology," en, *Int J Life Cycle Assess*, vol. 21, no. 9, pp. 1218–1230, Sep. 2016, ISSN: 0948-3349, 1614-7502. DOI: 10.1007/s11367-016-1087-8. [Online]. Available: http://link.springer.com/10.1007/s11367-016-1087-8 (visited on 09/11/2025).

[213] International Energy Agency (IEA), "World energy outlook 2023," IEA, Paris, Tech. Rep., 2023, Licence: CC BY 4.0 (report); CC BY-NC-SA 4.0 (Annex A). [Online]. Available: https://www.iea.org/reports/world-energy-outlook-2023.

[214] A. Barzkar and M. Ghassemi, "Components of electrical power systems in more and all-electric aircraft: A review," *IEEE Transactions on Transportation Electrification*, vol. 8, no. 4, pp. 4037–4053, 2022. DOI: 10.1109/TTE.2022.3174362.

[215] J. Z. Bird, "A review of electric aircraft drivetrain motor technology," *IEEE Transactions on Magnetics*, vol. 58, no. 2, pp. 1–8, 2022. DOI: 10.1109/TMAG.2021.3081719.

[216] E. Sayed *et al.*, "Review of electric machines in more-/hybrid-/turbo-electric aircraft," *IEEE Transactions on Transportation Electrification*, vol. 7, no. 4, pp. 2976–3005, 2021. DOI: 10.1109/TTE.2021.3089605.

[217] N. Madavan, "A nasa perspective on electric propulsion technologies for large commercial aircraft," in *International Conference on Electrical Systems for Aircraft, Railway, Ship Propulsion and Road Vehicles and the International Transportation Electrification Conference (ESARS-ITEC)*, Accessed: 2025-08-13, 2016. [Online]. Available: https://ntrs.nasa.gov/api/citations/20180008723/downloads/20180008723.pdf.

[218] K. Yamaguchi, "Design and evaluation of sic-based high power density inverter, 70kw/liter, 50kw/kg," in *2016 IEEE Applied Power Electronics Conference and Exposition (APEC)*, 2016, pp. 3075–3079. DOI: 10.1109/APEC.2016.7468302.

[219] C. Riboldi and F. Gualdoni, "An integrated approach to the preliminary weight sizing of small electric aircraft," *Aerospace Science and Technology*, vol. 58, pp. 134–149, 2016, ISSN: 1270-9638. DOI: https://doi.org/10.1016/j.ast.2016.07.014. [Online]. Available: https://www.sciencedirect.com/science/article/pii/S1270963816303601.

[220] EASA, *CS-23 Amendment 6 and AMC & GM to CS-23 Issue 4*, en, Mar. 2023. [Online]. Available: https://www.easa.europa.eu/en/document-library/certification-specifications/cs-23-amendment-6-and-amc-gm-cs-23-issue-4 (visited on 08/13/2025).

[221] I. Geiß and R. Voit-Nitschmann, "Sizing of the energy storage system of hybrid-electric aircraft in general aviation," en, *CEAS Aeronautical Journal*, vol. 8, no. 1, pp. 53–65, Mar. 2017, ISSN: 1869-5590. DOI: 10.1007/s13272-016-0220-5. [Online]. Available: https://doi.org/10.1007/s13272-016-0220-5 (visited on 03/10/2023).

[222] F. Orefice *et al.*, "Design of hybrid-electric small air transports," *IOP Conference Series: Materials Science and Engineering*, vol. 1226, no. 1, p. 012 075, Feb. 2022. DOI: 10.1088/1757-899X/1226/1/012075. [Online]. Available: https://dx.doi.org/10.1088/1757-899X/1226/1/012075.

[223] A. Rolando, F. Salucci, L. Trainelli, C. E. Riboldi, and Y. Khan, "On the design of an electric-powered microfeeder aircraft," in *Aerospace Europe Conference 2020*, Feb. 2020.

[224] A. T. Isikveren *et al.*, "Pre-design of a commuter transport utilising voltaic-joule/brayton motive power systems," *The Aeronautical Journal*, vol. 122, no. 1248, pp. 205–237, 2018. DOI: 10.1017/aer.2017.126.

[225] P. Wassink, G. Atanasov, C. Hesse, and B. Fröhler, "Conceptual design of silent electric commuter aircraft," in *32nd Congress of the International Council of the Aeronautical Sciences, ICAS 2021*, The International Council of the Aeronautical Sciences, 2021.

[226] F. Lutz, J. Jézégou, M. Budinger, and A. Reysset, "Study of hybridisation scenarios for turboprop aircraft in the general aviation segment," in *34th Congress of the International Council of the Aeronautical Sciences, Florence, Italy*, The International Council of the Aeronautical Sciences, 2024.

[227] R. Arvidsson, A. Nordelöf, and S. Brynolf, "Life cycle assessment of a two-seater all-electric aircraft," en, *Int J Life Cycle Assess*, vol. 29, no. 2, pp. 240–254, Feb. 2024, ISSN: 0948-3349, 1614-7502. DOI: 10.1007/s11367-023-02244-z. [Online]. Available: https://link.springer.com/10.1007/s11367-023-02244-z (visited on 02/26/2025).

[228] T. Planès, S. Delbecq, V. Pommier-Budinger, and E. Bénard, "Simulation and evaluation of sustainable climate trajectories for aviation," *Journal of Environmental Management*, vol. 295, p. 113 079, 2021, ISSN: 0301-4797. DOI: https://doi.org/10.1016/j.jenvman.2021.113079. [Online]. Available: https://www.sciencedirect.com/science/article/pii/S0301479721011415.

[229] M. Schäfer, M. Strohmeier, V. Lenders, I. Martinovic, and M. Wilhelm, "Bringing up opensky: A large-scale ads-b sensor network for research," in *IPSN-14 Proceedings of the 13th International Symposium on Information Processing in Sensor Networks*, 2014, pp. 83–94. DOI: 10.1109/IPSN.2014.6846743.

[230] A. Salgas, J. Sun, S. Delbecq, T. Planès, and G. Lafforgue, "Compilation of an open-source traffic and co2 emissions dataset for commercial aviation," *Journal of Open Aviation Science*, vol. 1, no. 2, Oct. 2023. DOI: 10.59490/joas.2023.7201. [Online]. Available: https://journals.open.tudelft.nl/joas/article/view/7201.

[231] M. J. D. Powell, "A direct search optimization method that models the objective and constraint functions by linear interpolation," in *Advances in Optimization and Numerical Analysis*. Dordrecht: Springer Netherlands, 1994, pp. 51–67, ISBN: 978-94-015-8330-5. DOI: 10.1007/978-94-015-8330-5_4. [Online]. Available: https://doi.org/10.1007/978-94-015-8330-5_4.

[232] R. P. Liem, G. K. W. Kenway, and J. R. R. A. Martins, "Multimission aircraft fuel-burn minimization via multipoint aerostructural optimization," *AIAA Journal*, vol. 53, no. 1, pp. 104–122, 2015. DOI: 10.2514/1.J052940. eprint: https://doi.org/10.2514/1.J052940. [Online]. Available: https://doi.org/10.2514/1.J052940.

[233] A. Yang, Y. Lyu, J. Li, and R. P. Liem, "Operation-aware aircraft wing design using cluster-based multipoint aerodynamic shape optimization," *Journal of Aircraft*, vol. 62, no. 6, pp. 1531–1547, 2025. DOI: 10.2514/1.C038291. eprint: https://doi.org/10.2514/1.C038291. [Online]. Available: https://doi.org/10.2514/1.C038291.

[234] K. Mazur, M. Saleh, and M. Hornung, "Integrating life cycle assessment in conceptual aircraft design: A comparative tool analysis," *Aerospace*, vol. 11, no. 1, 2024, ISSN: 2226-4310. DOI: 10.3390/aerospace11010101. [Online]. Available: https://www.mdpi.com/2226-4310/11/1/101.

[235] M. Hasan *et al.*, "Advancing energy storage: The future trajectory of lithium-ion battery technologies," *Journal of Energy Storage*, vol. 120, p. 116 511, 2025, ISSN: 2352-152X. DOI: https://doi.org/10.1016/j.est.2025.116511. [Online]. Available: https://www.sciencedirect.com/science/article/pii/S2352152X25012241.

[236] N. Wahler, L. Radomsky, L. V. Hanisch, R. Mallwitz, M. Henke, and A. Elham, "A credibility-based criterion for the assessment of futuristic aircraft concepts," in *ICAS 2022*, Stockholm, Sweden, Sep. 2022. [Online]. Available: https://www.icas.org/icas_archive/ICAS2022/data/papers/ICAS2022_0850_paper.pdf.

[237] C. Müller, K. Kieckhäfer, and T. S. Spengler, "The influence of emission thresholds and retrofit options on airline fleet planning: An optimization approach," *Energy Policy*, vol. 112, pp. 242–257, 2018, ISSN: 0301-4215. DOI: https://doi.org/10.1016/j.enpol.2017.10.022. [Online]. Available: https://www.sciencedirect.com/science/article/pii/S0301421517306456.

[238] T. Effing, F. Schültke, and E. Stumpf, "HLFC-optimized retrofit aircraft design of a medium-range reference configuration within the AVACON project," en, *CEAS Aeronaut J*, vol. 12, no. 2, pp. 441–456, Apr. 2021, ISSN: 1869-5582, 1869-5590. DOI: 10.1007/s13272-021-00510-0. [Online]. Available: https://link.springer.com/10.1007/s13272-021-00510-0 (visited on 08/19/2025).

[239] J. Mukhopadhaya, "Performance analysis of fuel cell retrofit aircraft," *ICCT White Paper*, 2023.

[240] B. D. Phillips, J. N. Schmidt, R. D. Falck, and E. Aretskin-Hariton, "Design under uncertainty for conceptual aircraft design leveraging analytical gradients," in *AIAA SCITECH 2025 Forum*. American Institute of Aeronautics and Astronautics, 2025. DOI: 10.2514/6.2025-1956. eprint: https://arc.aiaa.org/doi/pdf/10.2514/6.2025-1956. [Online]. Available: https://arc.aiaa.org/doi/abs/10.2514/6.2025-1956.

[241] B. D. Phillips, J. Schmidt, R. D. Falck, and E. D. Aretskin-Hariton, "End-to-end uncertainty quantification with analytical derivatives for design under uncertainty," *Journal of Aircraft*, vol. 0, no. 0, pp. 1–9, 0. DOI: 10.2514/1.C037976. eprint: https://doi.org/10.2514/1.C037976. [Online]. Available: https://doi.org/10.2514/1.C037976.

[242] M. Hoogreef, R. Vos, R. de Vries, and L. L. Veldhuis, "Conceptual assessment of hybrid electric aircraft with distributed propulsion and boosted turbofans," in *AIAA Scitech 2019 Forum*. American Institute of Aeronautics and Astronautics, 2019. DOI: 10.2514/6.2019-1807. eprint: https://arc.aiaa.org/doi/pdf/10.2514/6.2019-1807. [Online]. Available: https://arc.aiaa.org/doi/abs/10.2514/6.2019-1807.

[243] *Jane's aero-engines 2021-2022*, eng. 2021, OCLC: 1391845841, ISBN: 978-0-7106-3367-5.

[244] V. Cusati, M. Di Stasio, G. Lucci, and Q. Zhang, "Evaluating hybrid-electric aircraft viability: The ampaire eco caravan cost analysis," *Transportation Research Part D: Transport and Environment*, vol. 144, p. 104 759, 2025, ISSN: 1361-9209. DOI: https://doi.org/10.1016/j.trd.2025.104759. [Online]. Available: https://www.sciencedirect.com/science/article/pii/S1361920925001695.

[245] Francesco Salucci, Dominik Karbowski, and Nirmit Prabhakar, "ANALYZING THE IMPACTS OF SUSTAINABLE POWERTRAINS FOR SHORT-HAUL COMMUTER AIRLINES," in *ICAS Proceedings-34th Congress of the International Council of the Aeronautical Sciences*, International Council of the Aeronautical Sciences, Sep. 2024.

[246] P. P. et Universitaires Romandes (PPUR), Ed., *Analyse du cycle de vie: comprendre et réaliser un écobilan*, fre, 3e édition mise à jour et augmentée. Lausanne: Presses polytechniques et universitaires romandes, 2017, OCLC: 981762754, ISBN: 978-2-88915-135-6.

[247] D. Keiser, L. H. Schnoor, B. Pupkes, and M. Freitag, "Life cycle assessment in aviation: A systematic literature review of applications, methodological approaches and challenges," *Journal of Air Transport Management*, vol. 110, p. 102 418, 2023, ISSN: 0969-6997. DOI: https://doi.org/10.1016/j.jairtraman.2023.102418. [Online]. Available: https://www.sciencedirect.com/science/article/pii/S0969699723000613.

[248] A. Johanning and D. Scholz, *A first step towards the integration of life cycle assessment into conceptual aircraft design*, 2013. [Online]. Available: http://hdl.handle.net/20.500.12738/1372.

[249] S. Pinheiro Melo *et al.*, "Sustainability assessment and engineering of emerging aircraft technologies—challenges, methods and tools," *Sustainability*, vol. 12, no. 14, 2020, ISSN: 2071-1050. DOI: 10.3390/su12145663. [Online]. Available: https://www.mdpi.com/2071-1050/12/14/5663.

[250] M. Rolinck *et al.*, "A concept for blockchain-based lca and its application in the context of aircraft mro," *Procedia CIRP*, vol. 98, pp. 394–399, 2021, The 28th CIRP Conference on Life Cycle Engineering, March 10 – 12, 2021, Jaipur, India, ISSN: 2212-8271. DOI: https://doi.org/10.1016/j.procir.2021.01.123. [Online]. Available: https://www.sciencedirect.com/science/article/pii/S2212827121001530.

[251] N. Thonemann *et al.*, "Prospective life cycle inventory datasets for conventional and hybrid-electric aircraft technologies," *Journal of Cleaner Production*, vol. 434, p. 140 314, 2024, ISSN: 0959-6526. DOI: https://doi.org/10.1016/j.jclepro.2023.140314. [Online]. Available: https://www.sciencedirect.com/science/article/pii/S0959652623044724.

[252] K. Plotner, L. Miltner, P. Jochem, H. Kuhn, and M. Hornung, "Environmental life cycle assessment of universally-electric powered transport aircraft," in *Deutscher Luft- und Raumfahrtkongress 2016 (DLRK 2016)*, Braunschweig, Deutschland, Sep. 2016.

[253] A. J. Timmis *et al.*, "Environmental impact assessment of aviation emission reduction through the implementation of composite materials," en, *Int J Life Cycle Assess*, vol. 20, no. 2, pp. 233–243, Feb. 2015, ISSN: 0948-3349, 1614-7502. DOI: 10.1007/s11367-014-0824-0. [Online]. Available: http://link.springer.com/10.1007/s11367-014-0824-0 (visited on 09/12/2025).

[254] E. Gundabattini, A. Mystkowski, A. Idzkowski, R. S. R., and D. G. Solomon, "Thermal mapping of a high-speed electric motor used for traction applications and analysis of various cooling methods—a review," *Energies*, vol. 14, no. 5, 2021, ISSN: 1996-1073. DOI: 10.3390/en14051472. [Online]. Available: https://www.mdpi.com/1996-1073/14/5/1472.

[255] O. A. Towoju and F. A. Ishola, "A case for the internal combustion engine powered vehicle," *Energy Reports*, vol. 6, pp. 315–321, 2020, The 6th International Conference on Power and Energy Systems Engineering, ISSN: 2352-4847. DOI: https://doi.org/10.1016/j.egyr.2019.11.082. [Online]. Available: https://www.sciencedirect.com/science/article/pii/S2352484719309977.

[256] G. G. Pratama, "Crossroads Between Safety and Environmental Protection: EASA is not Merely a Specialized Safety Agency," en, *AILA*, vol. 50, no. Issue 1, pp. 23–44, Feb. 2025, ISSN: 0927-3379. DOI: 10.54648/AILA2025002. [Online]. Available: https://kluwerlawonline.com/journalarticle/Air+and+Space+Law/50.2/AILA2025002 (visited on 02/06/2026).

[257] I. O. for Standardization, *Environmental management: life cycle assessment; Principles and Framework*. ISO, 2006.

[258] I. O. for Standardization, *Environmental management-Life cycle assessment-Requirements and guidelines*. ISO, 2006.

[259] A. Rahn, K. Wicke, and G. Wende, "Using discrete-event simulation for a holistic aircraft life cycle assessment," *Sustainability*, vol. 14, no. 17, 2022, ISSN: 2071-1050. DOI: 10.3390/su141710598. [Online]. Available: https://www.mdpi.com/2071-1050/14/17/10598.

[260] A. Johanning and D. Scholz, "Comparison of the potential environmental impact improvements of future aircraft concepts using life cycle assessment," in *CEAS Air & Space Conference 2015*, ser. Challenges in European Aerospace : 5th CEAS Air & Space Conference, 2015, p. 80. DOI: 10.48441/4427.2159. [Online]. Available: http://hdl.handle.net/20.500.12738/434.

[261] S. Howe, A. Kolios, and F. Brennan, "Environmental life cycle assessment of commercial passenger jet airliners," *Transportation Research Part D: Transport and Environment*, vol. 19, pp. 34–41, 2013, ISSN: 1361-9209. DOI: https://doi.org/10.1016/j.trd.2012.12.004. [Online]. Available: https://www.sciencedirect.com/science/article/pii/S1361920913000047.

[262] G. Parolin, A. T. Borges, L. C. Santos, and A. V. Borille, "A tool for aircraft eco-design based on streamlined life cycle assessment and uncertainty analysis," *Procedia CIRP*, vol. 98, pp. 565–570, 2021, The 28th CIRP Conference on Life Cycle Engineering, March 10 – 12, 2021, Jaipur, India, ISSN: 2212-8271. DOI: https://doi.org/10.1016/j.procir.2021.01.152. [Online]. Available: https://www.sciencedirect.com/science/article/pii/S2212827121001827.

[263] R. Veeramanikandan, S. Nithish, G. Sivaraj, and S. Vinodh, "Life cycle assessment of an aircraft component: A case study," *International Journal of Industrial and Systems Engineering*, vol. 27, no. 4, pp. 485–499, 2017. DOI: 10.1504/IJISE.2017.087835. eprint: https://www.inderscienceonline.com/doi/pdf/10.1504/IJISE.2017.087835. [Online]. Available: https://www.inderscienceonline.com/doi/abs/10.1504/IJISE.2017.087835.

[264] F. Pollet, T. Planès, and S. Delbecq, "A Comprehensive Methodology for Performing Prospective Life Cycle Assessments of Future Air Transport Scenarios," in *34th Congress of the International Council of the Aeronautical Sciences*, Florence, Italy, Sep. 2024. [Online]. Available: https://hal.science/hal-04703961.

[265] B. Cox, W. Jemiolo, and C. Mutel, "Life cycle assessment of air transportation and the swiss commercial air transport fleet," *Transportation Research Part D: Transport and Environment*, vol. 58, pp. 1–13, 2018, ISSN: 1361-9209. DOI: https://doi.org/10.1016/j.trd.2017.10.017. [Online]. Available: https://www.sciencedirect.com/science/article/pii/S1361920917300482.

[266] A. Barke, C. Thies, S. P. Melo, F. Cerdas, C. Herrmann, and T. S. Spengler, "Comparison of conventional and electric passenger aircraft for short-haul flights – a life cycle sustainability assessment," *Procedia CIRP*, vol. 105, pp. 464–469, 2022, The 29th CIRP Conference on Life Cycle Engineering, April 4 – 6, 2022, Leuven, Belgium., ISSN: 2212-8271. DOI: https://doi.org/10.1016/j.procir.2022.02.077. [Online]. Available: https://www.sciencedirect.com/science/article/pii/S2212827122000774.

[267] P. Su-ungkavatin, L. Tiruta-Barna, and L. Hamelin, "Methodological framework for life cycle assessment of sustainable aviation (sa) systems," *Science of The Total Environment*, vol. 885, p. 163 881, 2023, ISSN: 0048-9697. DOI: https://doi.org/10.1016/j.scitotenv.2023.163881. [Online]. Available: https://www.sciencedirect.com/science/article/pii/S0048969723025020.

[268] C. M. Richard, "Life Cycle Analysis Frameworks in Sustainable Aviation," Master of Applied Science, Carleton University, Ottawa, Ontario, 2024. DOI: 10.22215/etd/2024-16346. [Online]. Available: https://repository.library.carleton.ca/concern/etds/3n204046x (visited on 02/26/2025).

[269] S. Ekici, O. Altuntaş, and T. Karakoc, "Life cycle assessment of a maintenance process for a training aircraft," in *8th International Exergy, Energy and Environment Symposium*, Antalya, Turkey, May 2016.

[270] B. W. Kolosz, Y. Luo, B. Xu, M. M. Maroto-Valer, and J. M. Andresen, "Life cycle environmental analysis of 'drop in' alternative aviation fuels: A review," *Sustainable Energy Fuels*, vol. 7, pp. 3229–3263, 2020. DOI: 10.1039/C9SE00788A. [Online]. Available: http://dx.doi.org/10.1039/C9SE00788A.

[271] H. Nojoumi, I. Dincer, and G. Naterer, "Greenhouse gas emissions assessment of hydrogen and kerosene-fueled aircraft propulsion," *International Journal of Hydrogen Energy*, vol. 34, no. 3, pp. 1363–1369, 2009, ISSN: 0360-3199. DOI: https://doi.org/10.1016/j.ijhydene.2008.11.017. [Online]. Available: https://www.sciencedirect.com/science/article/pii/S0360319908015048.

[272] N. Thonemann, E. Pierrat, K. M. Dudka, K. Saavedra-Rubio, A. L. S. Tromer Dragsdahl, and A. Laurent, "Towards sustainable regional aviation: Environmental potential of hybrid-electric aircraft and alternative fuels," *Sustainable Production and Consumption*, vol. 45, pp. 371–385, 2024, ISSN: 2352-5509. DOI: https://doi.org/10.1016/j.spc.2024.01.013. [Online]. Available: https://www.sciencedirect.com/science/article/pii/S2352550924000137.

[273] K. Kossarev, A. E. Scholz, P. Egerer, and M. Hornung, "Comparison of environmental life cycle impact assessment methods for future aircraft designs," in *AIAA AVIATION 2022 Forum*. American Institute of Aeronautics and Astronautics, 2022. DOI: 10.2514/6.2022-3659. eprint: https://arc.aiaa.org/doi/pdf/10.2514/6.2022-3659. [Online]. Available: https://arc.aiaa.org/doi/abs/10.2514/6.2022-3659.

[274] E. Dallara, J. Kusnitz, and M. Bradley, "Parametric life cycle assessment for the design of aircraft," *SAE International Journal of Aerospace*, vol. 6, no. 2, pp. 736–745, 2013, ISSN: 1946-3855. DOI: https://doi.org/10.4271/2013-01-2277. [Online]. Available: https://doi.org/10.4271/2013-01-2277.

[275] L. Fang, Y. Rosset, B. Sarrazin, P. Lefranc, and M. Rio, "Parametric lca model for power electronic ecodesign process: Addressing mosfet-si and hemt-gan technological issues," *IET Power Electronics*, vol. 18, no. 1, e12844, 2025. DOI: https://doi.org/10.1049/pel2.12844. eprint: https://ietresearch.onlinelibrary.wiley.com/doi/pdf/10.1049/pel2.12844. [Online]. Available: https://ietresearch.onlinelibrary.wiley.com/doi/abs/10.1049/pel2.12844.

[276] F. Pollet, F. Lutz, T. Planès, S. Delbecq, and M. Budinger, "A generic life cycle assessment tool for overall aircraft design," *Applied Energy*, vol. 399, p. 126 514, 2025, ISSN: 0306-2619. DOI: https://doi.org/10.1016/j.apenergy.2025.126514. [Online]. Available: https://www.sciencedirect.com/science/article/pii/S0306261925012449.

[277] C. Mutel, "Brightway: An open source framework for life cycle assessment," *Journal of Open Source Software*, vol. 2, no. 12, p. 236, 2017. DOI: 10.21105/joss.00236. [Online]. Available: https://doi.org/10.21105/joss.00236.

[278] R. Jolivet *et al.*, "Lca_algebraic: A library bringing symbolic calculus to LCA for comprehensive sensitivity analysis," en, *Int J Life Cycle Assess*, vol. 26, no. 12, pp. 2457–2471, Dec. 2021, ISSN: 0948-3349, 1614-7502. DOI: 10.1007/s11367-021-01993-z. [Online]. Available: https://link.springer.com/10.1007/s11367-021-01993-z (visited on 09/29/2025).

[279] J. Bachmann, C. Hidalgo, and S. Bricout, "Environmental analysis of innovative sustainable composites with potential use in aviation sector—A life cycle assessment review," en, *Science China Technological Sciences*, vol. 60, no. 9, pp. 1301–1317, Sep. 2017, ISSN: 1674-7321, 1869-1900. DOI: 10.1007/s11431-016-9094-y. [Online]. Available: http://link.springer.com/10.1007/s11431-016-9094-y (visited on 04/24/2025).

[280] L. Rupcic, E. Pierrat, K. Saavedra-Rubio, N. Thonemann, C. Ogugua, and A. Laurent, "Environmental impacts in the civil aviation sector: Current state and guidance," *Transportation Research Part D: Transport and Environment*, vol. 119, p. 103 717, 2023, ISSN: 1361-9209. DOI: https://doi.org/10.1016/j.trd.2023.103717. [Online]. Available: https://www.sciencedirect.com/science/article/pii/S1361920923001141.

[281] O. Balli, "Life cycle assessment and exergoenvironmental analyses for making a decision in the fuel selection for aero-engines: An application for a medium-size turboprop engine (m-tpe)," *Energy Conversion and Management*, vol. 266, p. 115 813, 2022, ISSN: 0196-8904. DOI: https://doi.org/10.1016/j.enconman.2022.115813. [Online]. Available: https://www.sciencedirect.com/science/article/pii/S0196890422006094.

[282] E. Schwartz and I. Kroo, "Aircraft design: Trading cost and climate impact," in *47th AIAA Aerospace Sciences Meeting including The New Horizons Forum and Aerospace Exposition*. American Institute of Aeronautics and Astronautics, 2012. DOI: 10.2514/6.2009-1261. eprint: https://arc.aiaa.org/doi/pdf/10.2514/6.2009-1261. [Online]. Available: https://arc.aiaa.org/doi/abs/10.2514/6.2009-1261.

[283] A. K. Cerutti, R. Pant, and S. Sala, *Development of a weighting approach for the environmental footprint*. Publications Office, 2018. DOI: doi/10.2760/945290.

[284] T. Le Varlet, O. Schmidt, A. Gambhir, S. Few, and I. Staffell, "Comparative life cycle assessment of lithium-ion battery chemistries for residential storage," *Journal of Energy Storage*, vol. 28, p. 101 230, 2020, ISSN: 2352-152X. DOI: https://doi.org/10.1016/j.est.2020.101230. [Online]. Available: https://www.sciencedirect.com/science/article/pii/S2352152X19309880.

[285] G. G. Eshetu *et al.*, "Production of high-energy Li-ion batteries comprising silicon-containing anodes and insertion-type cathodes," en, *Nat Commun*, vol. 12, no. 1, p. 5459, Sep. 2021, ISSN: 2041-1723. DOI: 10.1038/s41467-021-25334-8. [Online]. Available: https://www.nature.com/articles/s41467-021-25334-8 (visited on 10/23/2025).

[286] Y. Guo *et al.*, "A high-voltage and low-solvating electrolyte towards promising micro-si/ni-rich nmc full cells," *Energy Storage Materials*, vol. 67, p. 103 258, 2024, ISSN: 2405-8297. DOI: https://doi.org/10.1016/j.ensm.2024.103258. [Online]. Available: https://www.sciencedirect.com/science/article/pii/S2405829724000850.

[287] O. Winjobi, Q. Dai, and J. Kelly, "Update of bill-of-materials and cathode chemistry addition for lithium-ion batteries in greet 2020," *Systems Assessment Group, Energy Systems Division, Argonne National Laboratory, llinois, USA*, 2020.

[288] K. Ramachandran, C. L. Gnanasagaran, and A. Vekariya, "Life cycle assessment of carbon fiber and bio-fiber composites prepared via vacuum bagging technique," *Journal of Manufacturing Processes*, vol. 89, pp. 124–131, 2023, ISSN: 1526-6125. DOI: https://doi.org/10.1016/j.jmapro.2023.01.068. [Online]. Available: https://www.sciencedirect.com/science/article/pii/S1526612523000944.

[289] Y. Zhang *et al.*, "Silicon anodes with improved calendar life enabled by multivalent additives," *Advanced Energy Materials*, vol. 11, no. 37, p. 2 101 820, 2021. DOI: https://doi.org/10.1002/aenm.202101820. eprint: https://advanced.onlinelibrary.wiley.com/doi/pdf/10.1002/aenm.202101820. [Online]. Available: https://advanced.onlinelibrary.wiley.com/doi/abs/10.1002/aenm.202101820.

[290] A. Filippone, "Comprehensive analysis of transport aircraft flight performance," *Progress in Aerospace Sciences*, vol. 44, no. 3, pp. 192–236, 2008, ISSN: 0376-0421. DOI: https://doi.org/10.1016/j.paerosci.2007.10.005. [Online]. Available: https://www.sciencedirect.com/science/article/pii/S0376042107000826.

[291] M. Su, C. Chen, S. Sharma, and J. Kikuchi, "Performance and cost considerations for sic-based hev traction inverter systems," in *2015 IEEE 3rd Workshop on Wide Bandgap Power Devices and Applications (WiPDA)*, 2015, pp. 347–350. DOI: 10.1109/WiPDA.2015.7369032.

[292] K. Itani and A. De Bernardinis, "Review on new-generation batteries technologies: Trends and future directions," *Energies*, vol. 16, no. 22, 2023, ISSN: 1996-1073. DOI: 10.3390/en16227530. [Online]. Available: https://www.mdpi.com/1996-1073/16/22/7530.

[293] X.-B. Cheng *et al.*, "Polysulfide shuttle control: Towards a lithium-sulfur battery with superior capacity performance up to 1000 cycles by matching the sulfur/electrolyte loading," *Journal of Power Sources*, vol. 253, pp. 263–268, 2014, ISSN: 0378-7753. DOI: https://doi.org/10.1016/j.jpowsour.2013.12.031. [Online]. Available: https://www.sciencedirect.com/science/article/pii/S037877531301999X.

[294] F. Zhao, J. Xue, W. Shao, H. Yu, W. Huang, and J. Xiao, "Toward high-sulfur-content, high-performance lithium-sulfur batteries: Review of materials and technologies," *Journal of Energy Chemistry*, vol. 80, pp. 625–657, 2023, ISSN: 2095-4956. DOI: https://doi.org/10.1016/j.jechem.2023.02.009. [Online]. Available: https://www.sciencedirect.com/science/article/pii/S2095495623000888.

[295] W. Cao, J. Zhang, and H. Li, "Batteries with high theoretical energy densities," *Energy Storage Materials*, vol. 26, pp. 46–55, 2020, ISSN: 2405-8297. DOI: https://doi.org/10.1016/j.ensm.2019.12.024. [Online]. Available: https://www.sciencedirect.com/science/article/pii/S240582971931102X.

[296] Y. Deng, J. Li, T. Li, X. Gao, and C. Yuan, "Life cycle assessment of lithium sulfur battery for electric vehicles," *Journal of Power Sources*, vol. 343, pp. 284–295, 2017, ISSN: 0378-7753. DOI: https://doi.org/10.1016/j.jpowsour.2017.01.036. [Online]. Available: https://www.sciencedirect.com/science/article/pii/S0378775317300368.

[297] S. Wickerts, R. Arvidsson, A. Nordelöf, M. Svanström, and P. Johansson, "Prospective Life Cycle Assessment of Lithium-Sulfur Batteries for Stationary Energy Storage," en, *ACS Sustainable Chem. Eng.*, vol. 11, no. 26, pp. 9553–9563, Jul. 2023, ISSN: 2168-0485, 2168-0485. DOI: 10.1021/acssuschemeng.3c00141. [Online]. Available: https://pubs.acs.org/doi/10.1021/acssuschemeng.3c00141 (visited on 02/12/2026).

[298] S. Zhang, B. Steubing, H. Karlsson Potter, P.-A. Hansson, and Å. Nordberg, "Future climate impacts of sodium-ion batteries," *Resources, Conservation and Recycling*, vol. 202, p. 107 362, 2024, ISSN: 0921-3449. DOI: https://doi.org/10.1016/j.resconrec.2023.107362. [Online]. Available: https://www.sciencedirect.com/science/article/pii/S0921344923004962.

[299] J. Peters, D. Buchholz, S. Passerini, and M. Weil, "Life cycle assessment of sodium-ion batteries," en, *Energy Environ. Sci.*, vol. 9, no. 5, pp. 1744–1751, 2016, ISSN: 1754-5692, 1754-5706. DOI: 10.1039/C6EE00640J. [Online]. Available: https://xlink.rsc.org/?DOI=C6EE00640J (visited on 02/11/2026).

[300] S. Wickerts, R. Arvidsson, A. Nordelöf, M. Svanström, and P. Johansson, "Prospective life cycle assessment of sodium-ion batteries made from abundant elements," *Journal of Industrial Ecology*, vol. 28, no. 1, pp. 116–129, 2024. DOI: https://doi.org/10.1111/jiec.13452. eprint: https://onlinelibrary.wiley.com/doi/pdf/10.1111/jiec.13452. [Online]. Available: https://onlinelibrary.wiley.com/doi/abs/10.1111/jiec.13452.

[301] C. Vaalma, D. Buchholz, M. Weil, and S. Passerini, "A cost and resource analysis of sodium-ion batteries," en, *Nat Rev Mater*, vol. 3, no. 4, p. 18 013, Mar. 2018, ISSN: 2058-8437. DOI: 10.1038/natrevmats.2018.13. [Online]. Available: https://www.nature.com/articles/natrevmats201813 (visited on 02/09/2026).

[302] B. Blakey-Milner *et al.*, "Metal additive manufacturing in aerospace: A review," *Materials & Design*, vol. 209, p. 110 008, 2021, ISSN: 0264-1275. DOI: https://doi.org/10.1016/j.matdes.2021.110008. [Online]. Available: https://www.sciencedirect.com/science/article/pii/S0264127521005633.

[303] R. Sacchi *et al.*, "Prospective environmental impact assement (premise): A streamlined approach to producing databases for prospective life cycle assessment using integrated assessment models," *Renewable and Sustainable Energy Reviews*, vol. 160, p. 112 311, 2022, ISSN: 1364-0321. DOI: https://doi.org/10.1016/j.rser.2022.112311. [Online]. Available: https://www.sciencedirect.com/science/article/pii/S136403212200226X.

[304] G. Luderer *et al.*, *REMIND - REgional Model of INvestments and Development*, version 3.5.2.dev464, Feb. 2026. [Online]. Available: https://github.com/remindmodel/remind.

[305] D. Wolff, L. Canals Casals, G. Benveniste, C. Corchero, and L. Trilla, "The effects of lithium sulfur battery ageing on second-life possibilities and environmental life cycle assessment studies," *Energies*, vol. 12, no. 12, 2019, ISSN: 1996-1073. DOI: 10.3390/en12122440. [Online]. Available: https://www.mdpi.com/1996-1073/12/12/2440.

[306] A. Colozza, "High altitude propeller design and analysis overview," *NASA/CR*, pp. 98–208 520, 1998.

[307] J. B. Delano, "The Effect of High Solidity on Propeller Characteristics at High Forward Speeds from Wind-Tunnel Tests of the NACA 4-(3)(06.3)-06 and NACA 4-(3)(06.4)-09 Two-Blade Propellers," NACA, Tech. Rep. NACA-RM-L6L19, Feb. 1947, NTRS Author Affiliations: National Advisory Committee for Aeronautics. Langley Aeronautical Lab. NTRS Document ID: 20050019462 NTRS Research Center: Langley Research Center (LaRC). [Online]. Available: https://ntrs.nasa.gov/citations/20050019462 (visited on 08/22/2022).

[308] P. Giannakakis, I. Goulos, P. Laskaridis, P. Pilidis, and A. I. Kalfas, "Novel propeller map scaling method," *Journal of Propulsion and Power*, vol. 32, no. 6, pp. 1325–1332, 2016. DOI: 10.2514/1.B35894.

[309] J. Brusse, A. E. Cronk, and C. F. Kettleborough, "Tests on propellers under static thrust conditions," NASA, Tech. Rep. NASA-CR-1501, Dec. 1969, NTRS Author Affiliations: Texas A&M Univ. NTRS Document ID: 19700004830 NTRS Research Center: Legacy CDMS (CDMS). [Online]. Available: https://ntrs.nasa.gov/citations/19700004830 (visited on 09/30/2022).

[310] N. Erroui, "High power conversion chain for hybrid aircraft propulsion," Ph.D. dissertation, Laplace Institute, 2019. [Online]. Available: https://theses.hal.science/tel-04169643/.

[311] A. Cassou, Q. Chuc Nguyen, P. Tounsi, J.-P. Fradin, M. Budinger, and I. Hazyuk, "Extraction of compact transient thermal models for a global optimization of a power system based on SiC MOSFETs switches," in *IEEE THERMINIC 2020*, ser. 2020 26th International Workshop on Thermal Investigations of ICs and Systems (THERMINIC), Berlin, Germany: IEEE, Sep. 2020. [Online]. Available: https://laas.hal.science/hal-03655834.

[312] M. S. Rognan, M. Margni, and G. Majeau-Bettez, "Sself: A specific semiautomated lifecycle footprinting framework to go beyond generic data in lca," *Journal of Industrial Ecology*, vol. 29, no. 4, pp. 1397–1413, 2025. DOI: https://doi.org/10.1111/jiec.70056. eprint: https://onlinelibrary.wiley.com/doi/pdf/10.1111/jiec.70056. [Online]. Available: https://onlinelibrary.wiley.com/doi/abs/10.1111/jiec.70056.

[313] E. Pierrat, L. Rupcic, M. Z. Hauschild, and A. Laurent, "Global environmental mapping of the aeronautics manufacturing sector," *Journal of Cleaner Production*, vol. 297, p. 126 603, 2021, ISSN: 0959-6526. DOI: https://doi.org/10.1016/j.jclepro.2021.126603. [Online]. Available: https://www.sciencedirect.com/science/article/pii/S0959652621008234.

[314] R. Kawamoto *et al.*, "Estimation of co2 emissions of internal combustion engine vehicle and battery electric vehicle using lca," *Sustainability*, vol. 11, no. 9, 2019, ISSN: 2071-1050. DOI: 10.3390/su11092690. [Online]. Available: https://www.mdpi.com/2071-1050/11/9/2690.

[315] M. A. J. Huijbregts *et al.*, "ReCiPe2016: A harmonised life cycle impact assessment method at midpoint and endpoint level," en, *Int J Life Cycle Assess*, vol. 22, no. 2, pp. 138–147, Feb. 2017, ISSN: 0948-3349, 1614-7502. DOI: 10.1007/s11367-016-1246-y. [Online]. Available: http://link.springer.com/10.1007/s11367-016-1246-y (visited on 09/22/2025).

[316] C. Bulle *et al.*, "IMPACT World+: A globally regionalized life cycle impact assessment method," en, *Int J Life Cycle Assess*, vol. 24, no. 9, pp. 1653–1674, Sep. 2019, ISSN: 0948-3349, 1614-7502. DOI: 10.1007/s11367-019-01583-0. [Online]. Available: http://link.springer.com/10.1007/s11367-019-01583-0 (visited on 09/22/2025).

[317] M. Damiani, N. Ferrara, and F. Ardente, "Understanding product environmental footprint and organisation environmental footprint methods," no. KJ-NA-31-236-EN-N (online), 2022, ISSN: 1831-9424 (online). DOI: 10.2760/11564(online).

[318] W. Kloepffer, "Life cycle sustainability assessment of products," en, *Int J Life Cycle Assess*, vol. 13, no. 2, pp. 89–95, Mar. 2008, ISSN: 0948-3349, 1614-7502. DOI: 10.1065/lca2008.02.376. [Online]. Available: http://link.springer.com/10.1065/lca2008.02.376 (visited on 09/22/2025).

[319] M. Pizzol, A. Laurent, S. Sala, B. Weidema, F. Verones, and C. Koffler, "Normalisation and weighting in life cycle assessment: Quo vadis?" en, *The International Journal of Life Cycle Assessment*, vol. 22, no. 6, pp. 853–866, Jun. 2017, ISSN: 0948-3349, 1614-7502. DOI: 10.1007/s11367-016-1199-1. [Online]. Available: http://link.springer.com/10.1007/s11367-016-1199-1 (visited on 11/13/2024).

Appendix A

Reproducibility and accessibility

This appendix aims to detail the organization of the repository where the data associated with this thesis are stored. Most of the work was undertaken in Python scripts that can be run on any computer after installing the requirements specified in the repository.

A.1 Organization of powertrain component model directories

Lessons learned from the literature review helped organize the code for clarity, ease of reuse, and traceability. Mainly:

1. The code base is open-source[1] and designed to be modular, enabling customization of the sizing process and facilitating extensions to higher-fidelity methods, additional physics, and new powertrain components. This choice stems from the necessity for quick, easy-to-use tools that are capable of capturing the multidisciplinary synergies to better perform trade-off studies on the design of the aircraft identified in Chapter 2. It also serves as a way to quickly assess multiple configurations by letting users adapt and customize the process for different needs. The simple format of the input files (.YML for the configuration and powertrain file, and .XML for the input file) also enables the sharing of information and allows reproducibility.

2. Given the number of degrees of freedom and constraints added to the design problem, the use of gradient-based solvers and optimizers was highlighted as a key enabler for the framework and the sizing of innovative configurations in general. As such, the question of the computation of partial derivatives was raised, and it was concluded that analytically differentiable models should be preferred. Therefore, unit tests to ensure the proper implementation of the models and their derivatives were coded using OpenMDAO's features.

3. In Chapter 3, it was highlighted that each component had a specific role to play in the propulsive architecture: from the propulsor that converts mechanical power into useful

[1] https://github.com/florentLutz/FAST-OAD-CS23-HE, Accessed 2025-12-09

thrust to on-board power sources and electrical networks. This observation has led to an organization of the code following these roles.

A.1.1 Model implementation directories

Component type organization

As discussed in Chapter 3 and recalled in the introductory part of that Appendix, in the code base, components were organized according to the function they fulfill.

i The folder `connectors` contains the models for all power electronics, gearboxes, fuel lines, and components of the electric network. As such, it contains the models for buses, splitters, breakers, cables, DC/DC converters, inverters, rectifiers, gearboxes, and fuel systems.

ii The folder `loads` contains the models for all the components that draw power from the electrical network. Currently, it only contains models for AFPMSM and SM-PMSM electric motors, but this category also suits other actuators or even other electric motor architectures.

iii The folder `propulsor` contains the models for all elements whose primary function is the generation of thrust. As for the `loads` folder, it currently contains only one item: the propeller. That folder would however be suited for other components like ducted fans.

iv The folder `source` contains the model for the components that provide power to the electrical network, which includes batteries, generators, turboshaft, and piston engines. Note that this category could also be applicable to other components like fuel cells.

v Finally, the folder `tanks` contains the model for the fuel reservoirs. Currently, as discussed in Chapter 3, it is fairly limited, but following the remark on fuel cells, it should be noted that this is were model for hydrogen tanks would be stored.

In addition to influencing the organization of the code, the role the components play is also used to categorize what type of output they are expected to provide. For instance, propulsors are expected to have as inputs to the model a value of thrust. Additionally, a value of shaft power is expected as an output of the model. Logically, loads, which transform electrical power into mechanical power, are expected to accept shaft power as input and then provide the required electrical power as an output. This also helps define interfaces between component which the code uses to ensure that each connection defined in the powertrain file is valid and thus solves one of the issues of the original implementation of the load flow analysis method. Indeed, from a user friendliness point of view, one of the difficulties the original implementation of the load flow analysis method had was consistently connecting the proper physical quantities of one component of the powertrain (voltage, current, torque,

...) to the corresponding quantity in a connected component's model. In addition to that, the problem is that what corresponds to the input/output of a physical component, defined as the side of the component closer to the power sources/power loads, respectively, does not necessarily correspond to input or output in the OpenMDAO sense of the term. To solve that problem and because only one orientation of the models exists, a list of the OpenMDAO inputs and outputs required for each side of the physical components has been implemented. It is used, in conjunction with the *component_connections* section of the powertrain file, to ensure that the correct connections are consistently made without requiring the user to do so. For instance, the model for the DC/DC converter defines that, at its physical input (the side connected to the battery), the voltage is an OpenMDAO input, and the current is an OpenMDAO output. As for the battery pack, at its output side, the voltage is defined as an OpenMDAO output while the current is defined as an OpenMDAO input. Voltage and currents can thus be connected from the battery to the converter, which ensures proper solving of state equations. While this organization can be seen as strenuous from a developer perspective, it ensures consistency in the code, and, given the fact that existing components can be reused as templates, the addition of new components is, in the end, easy.

Model type organization

The folder containing the models for individual physical components of the powertrain is located one step further down the folder hierarchy. As discussed in Chapter 2, for each component of the powertrain, multiple types of models were identified: estimation models, simulation models, and evaluation models. This categorization of the models was used to organize the models implemented for each component. More concretely, this led to the addition of prefixes to the script's names. More information on the type of models and the associated prefixes is given in Section 2.3.2.

Model implementation

FAST-OAD, which this work builds upon, is implemented using the OpenMDAO framework [2]. Therefore, it inherits certain requirements regarding the implementation of models. In particular, each model is implemented as a specific OpenMDAO class called a `Component`. Multiple types of components exist depending on the formulation adopted for the model (explicit equation, implicit equations, ...), but they all share three methods that must be implemented:

1. the `setup` method: this method defines the inputs and outputs of a model. This function is also used to define how the partials will be computed. In the vast majority of scripts, and because analytically differentiable models were explicitly chosen, the partials will be computed analytically. In a few rare cases, finite differences are used.

[2] https://openmdao.org/, Accessed 2025-12-09

2. the `compute` method: this method defines how the outputs are computed based on the inputs.

3. the `compute_partials` method: this method defines how the partial derivatives of the outputs with respect to the inputs are computed.

When models were not taken from literature, i.e., when they were developed from scratch for the needs of this framework, scripts detailing their creation were also included for reproducibility. In that case, those scripts are contained in the same component's folder under the `methodology` sub-folder.

A.2 Organization of test cases directories

The scripts associated with all the study and validation cases explored in Chapter 4 and 5 are located in the `integration_tests` folder of the FAST-OAD-CS23-HE repository. Tests are organized according to the reference aircraft they are based on. As such, there are folders for the Pipistrel aircraft, for the Cirrus SR22 test cases, for the DAHER TBM900 and the EcoPulse test cases, for the Quest Kodiak test cases, as well as a folder for the Cessna 208 test cases. Each folder then contains three similar elements: (1) a folder, called `data`, which contains all the input files necessary to run the test cases, (2) scripts using these input files to run the processes written with the `pytest` format and (3) a folder, named `results` containing the results of those case studies.

Regarding the input file necessary to conduct a sizing process using the framework developed here, three are mandatory and will be present for each test case:

1. the configuration file, using the .YML format, is meant to be, in the FAST-OAD process, the heart of the problem definition. It contains a list of the models to include in the OpenMDAO problem, the location of the temporary file that the code might need to write, the choice of the solvers and optimizers, as well as the definition of the optimization (design variables, objective function, constraints, ...)

2. the powertrain file, which also uses the .YML format and which has already been extensively described in the Section 2.3. This file contains a graph-based description of the powertrain, where the components and how they are connected are listed. Thanks to the automatic interfacing between components and OpenMDAO's ability to dynamically create the sizing process and connect variables, it is possible to evaluate virtually any propulsive architecture.

3. the input file, which uses the .XML format. As discussed in Chapter 2, this file contains all the values of the inputs required for the sizing process to start. Due to FAST-OAD's naming format, which categorizes variables based on the disciplines they are used in, and because of OpenMDAO's ability to easily change the design variables, the type of

these inputs is not clearly visible in that file. More information about the different types of inputs can be found in Table 2.2.

Thanks to the lightweight, human-readable format adopted for those input files, they can easily be shared. Therefore, replication of the results on any machine with the same version of the framework is possible, thus helping reproducibility and accessibility.

Appendix B

Appendix to the Part I

B.1 Establishment of the propeller performances surrogate model

B.1.1 Identification of dimensionless parameters

The surrogate for the computation of the propeller performances was made using the Variable Power Law Meta-model (VPLM) methodology. The first part of the methodology usually starts with the identification of key dimensionless parameters computed based on the relevant parameters of the design problem using the Buckingham theorem. Because propellers have been extensively used, a lot of literature on the subject exists, and so the key dimensionless parameters are already known. They are:

- C_T, C_P, J: which have been presented in Section 3.4.1.
- M_{tip}: the propeller tip Mach number, which serves as a measure of the importance of compressibility effects on the blade. It is usually limited by design to avoid the formation of shock waves on the blades [306]. It is computed using the following formula:

$$M_{\text{tip}} = \frac{\sqrt{V_\infty^2 + \left(\omega \times \frac{D}{2}\right)^2}}{a} \tag{B.1}$$

  where a is the speed of sound.

- Re_D: the propeller blade Reynolds number, computed as

$$Re_D = \frac{V_\infty \times D}{\nu} \tag{B.2}$$

  where ν is the kinematic viscosity.

- σ: the propeller's solidity [307], a measure of how much area the propeller's blade occupies when compared to the total area swept by the blades, is computed as follows:

$$\sigma = \frac{N_b}{\pi \times D^2/4} \int_{R_{\text{hub}}}^{R_{\text{tip}}} c(r)dr \tag{B.3}$$

where R_{hub} and R_{tip} are the hub radius and tip radius respectively.

- AF**:** the propeller's activity factor [306, 308, 309] which is a measure of the location of the propeller's section with the greatest chord. It is computed as follows:

$$AF = \frac{10^5}{16} \int_{R_{\text{hub}}}^{R_{\text{tip}}} \frac{c(r)}{D} \left(\frac{r}{R}\right)^3 d\left(\frac{r}{R}\right) \tag{B.4}$$

- $\theta_{\textbf{blade}}$**:** the propeller's blade twist, a measure of how twisted the propeller is between the hub and the tip.

B.1.2 Training and validation dataset generation

Data to establish the surrogate model were then generated by running an improved version of the original BEMT-ADT methodology on a wide sample of virtual propellers working in a wide range of scenarios. For the description of the propellers, their diameters, chord laws, blade twist, and number of blades were varied. As for the operating conditions, the revolution speed, freestream velocity, and working altitude were changed. Before running the code, a first filter was applied to ensure that the combination of propeller characteristics and working conditions would not lead to an unfeasible scenario, which was determined as a limit M_{tip} of 0.95 and a blade angle of attack at 75% of the chord between -12° and 17°. Results of the run for the feasible points were then filtered again to rule out convergence issues or points at which the propeller won't be working during the mission. Mostly, it was ensured that thrust and power had the same sign and that the efficiency was between 0.5 and 1.0. This led to a database of over 7600 points, covering a wide range of values for each similarity parameter as listed in Table B.1.

Table B.1 Range of values for the similarity parameters covered in the surrogate.

Similarity parameter Π_i	C_P	C_T	J	M_{tip}	Re_D	σ	AF	θ_{blade}
Minimal value	0.1	0.004	0.31	0.076	5.7e5	0.03	51	1°
Maximum value	2.41	0.75	3.27	0.9	2.8e7	0.55	290	45°

Out of these 7600 points, 267 were randomly selected as a training set for the creation of the methodology, while the rest served as a validation set.

B.1.3 Creation of the surrogate

To perform the regression, the pyVPLM package [130] was used. As the final objective of this model was to be able to compute the shaft power for a given propeller geometry and flight conditions, it was decided to generate the surrogate in such a manner to obtain a formula like the one described in Equation 3.5.

The choice for the order and number of terms in the surrogate was made to ensure that the mean error and standard deviation were both below 5%, which led to the results in Figure B.1.

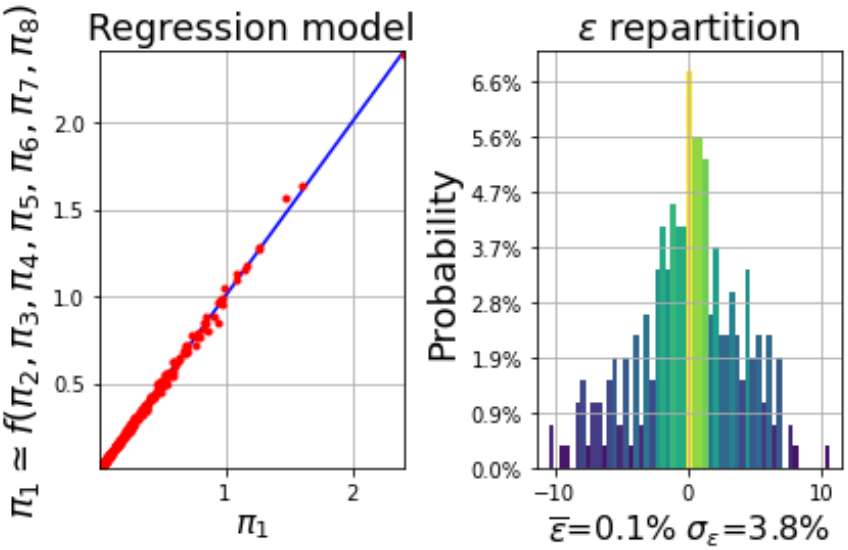

Figure B.1 Results of the surrogate modeling for the propeller performances.

The final expression yields:

$$
\begin{aligned}
log_{10}(C_P) = 2.43553 + log_{10}(J) \times [0.61554 + 0.06980 \times log_{10}(J) \times log_{10}(C_T) \times log_{10}(\theta_{\text{blade}}) \\
-0.01794 \times log_{10}(Re_D) \times log_{10}(C_T) \times log_{10}(AF) + 0.02595 \times log_{10}(M_{\text{tip}}) \times log_{10}(\sigma) \times log_{10}(C_T) \\
+ 0.00430 \times log_{10}(J) \times log_{10}(Re_D)^2 + 0.09827 \times log_{10}(C_T) \times log_{10}(\theta_{\text{blade}}) \\
+ 0.03663 \times log_{10}(\sigma) \times log_{10}(AF)] + log_{10}(M_{\text{tip}}) \times [-0.00097 \times log_{10}(Re_D)^2 \times log_{10}(M_{\text{tip}})] \\
+ log_{10}(Re_D) \times [-0.35804 + 0.00018 \times log_{10}(Re_D)^3 - 0.01879 \times log_{10}(C_T)^3 \\
+ 0.00119 \times log_{10}(Re_D) \times log_{10}(\sigma) \times log_{10}(AF) - 0.00886 \times log_{10}(C_T)^2 \times log_{10}(\theta_{\text{blade}})] \\
+ log_{10}(\sigma) \times [0.08015 \times log_{10}(C_T)^2 \times log_{10}(AF) + 0.04562 \times log_{10}(\sigma) \times log_{10}(AF)^2 \\
- 0.04121 \times log_{10}(\sigma) \times log_{10}(C_T) \times log_{10}(\theta_{\text{blade}})] + log_{10}(C_T) \times [1.33164 \\
+ 0.06989 \times log_{10}(C_T) \times log_{10}(AF) + 0.00206 \times log_{10}(C_T) \times log_{10}(\theta_{\text{blade}})^2 \\
+ 0.03617 \times log_{10}(C_T)^2 \times log_{10}(AF)] \quad \text{(B.5)}
\end{aligned}
$$

The obtained surrogate was then compared to the validation set to ensure the validity of the results, which led to the results displayed in Figure B.2

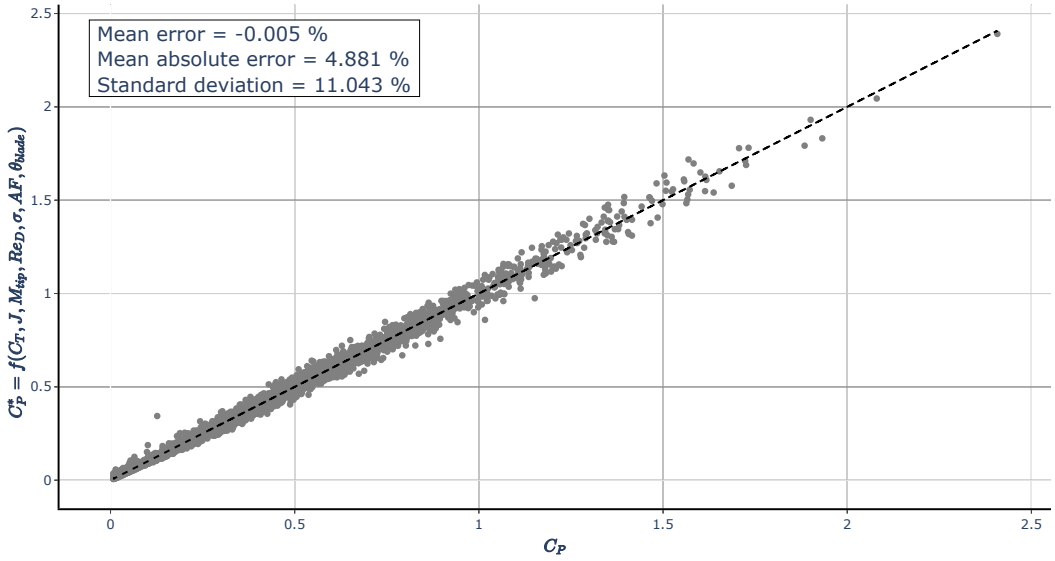

Figure B.2 Comparison, on the validation set, of the values computed by the surrogate (gray dots) and the ones computed with the original method (dashed line).

B.2 Establishment of the turboshaft performances surrogate model

To define realistic bounds for the data to be used to construct the surrogate, a preliminary analysis on the engine of the PT6 turboshaft family was performed. Simplifying assumptions were made to reduce the complexity of the surrogate models, namely: the component efficiencies and pressure drop were assumed constant across all engines, the ratio of offtake bleed to engine mass flow is constant, and the design point will always be static at sea level. Based on the original model as well as a preliminary correlation analysis, the following inputs were selected: the engine design parameters (design Overall Pressure Ratio (OPR) OPR_{des}, design turbine entry temperature TET_{des} and design power P_{des}); the engine operating conditions (Mach number M, air density ratio σ and power required P_{req}) as well as its components limits (limit OPR OPR_{limit}, limit inter turbine temperature ITT_{limit} and shaft power limit P_{limit}). Those input parameters will be used for all the equations presented in 3.19.

A dataset of 5000 points was generated with values for the input parameters covering the range of values presented in Table B.2. It will be used for all the regressions.

Table B.2 Range of values for the input parameters covered in the dataset.

Input	σ	M	P_{des}	OPR_{des}	TET_{des}	P_{req}	OPR_{lim}	ITT_{lim}
Min.	0.31	0.04	864 kW	7	990 °K	100 kW	8.37	958 °K
Max.	1.0	0.6	2890 kW	19.5	1420 °K	1280 kW	22.5	1273 °K

To perform the regressions, the pyVPLM package [130] was used. The choice for the order and number of terms in the surrogates was made to ensure that the mean error and standard deviation were both below 5%, which led to the results in Figure B.3 for the fuel consumption.

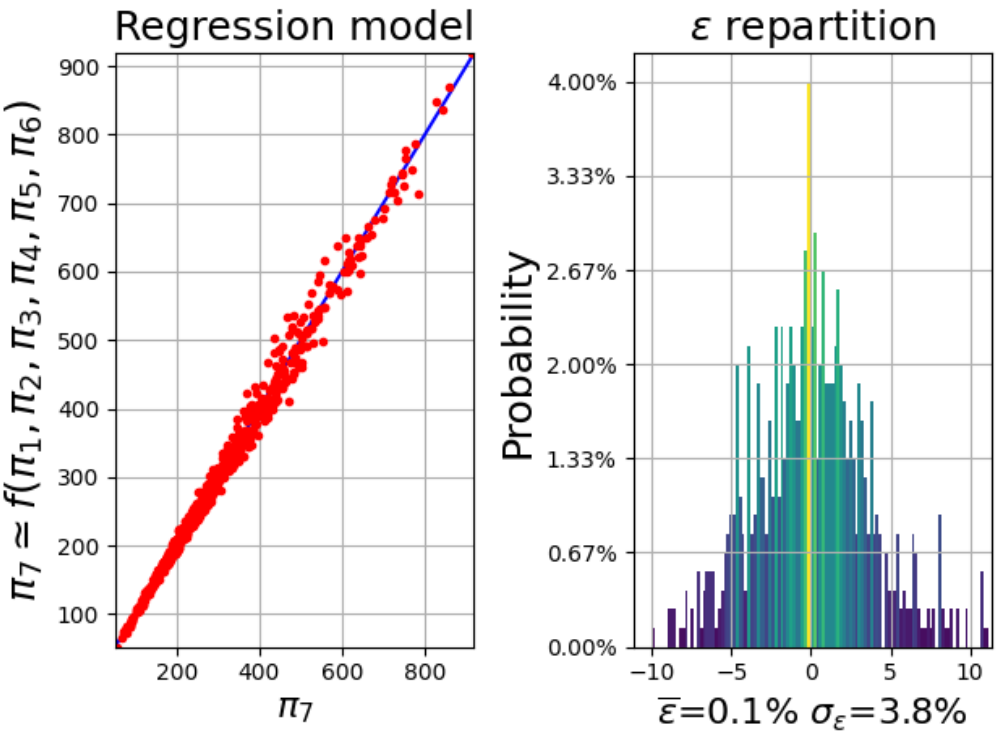

Figure B.3 Results of the surrogate modeling for the turboshaft fuel consumption.

Similarly, surrogates were built to allow the expression of the maximum power imposed by the limits on the Overall Pressure Ratio (OPR) and the Inter Turbine Temperature (ITT). However, to ease their use for identifying the maximum power, they were expressed in a different way from the original model [91]. Instead, they will be expressed as: "What would be the rated power which would make it so that the current power requirement would be limited by the ITT or the OPR ?"

Finally, surrogates were built to estimate what is the residual thrust produced by the ejection of hot gases through the exhaust. While the exhaust thrust was part of the database of results from the original model, a proper fit with a reasonable number of terms could not be achieved. Nonetheless, good agreement with the data could be obtained for the air velocity at the exhaust and the air mass flow through the engine. This then allows to compute the residual thrust using Equation B.6.

$$T_9 = \dot{m}_0 \times (V_9 - V_0) \tag{B.6}$$

B.3 Inverters and Rectifiers losses model

The losses in PWM converters are primarily associated with conduction and switching losses occurring in the six arms of the converter [125]. Consequently, losses in inverters and rectifiers can be written as:

$$P_{losses} = 6 \times (P_{cond,IGBT} + P_{cond,diode}) + 6 \times (P_{sw,IGBT} + P_{sw,diode}) \tag{B.7}$$

For the computation of each term, existing formulas taken from literature were used [93, 125, 130, 201, 310, 311]. Most of these formulas, however, depend on the technical characteristics of the semiconductors. For those scaling laws, a module using the IGBT technology will be retained. New inverters using Silicon Carbide MOFSET have been shown to have higher efficiency and increased power density with respect to classical Silicon IGBT [291]. Due to high prices, low market availability, and an abundance of literature on Silicon-based IGBT, however, Silicon Carbide MOFSET will not be used. Switching losses depend on turn-on, turn-off, and recovery energy, which itself depends on the current flowing through the semiconductor. This leads to the expression of switching and conduction losses presented in Equations B.8.

$$P_{cond,IGBT} = V_{CE,0}\frac{I}{2\pi}\left(1 + \frac{\pi}{4}\beta cos\phi\right) + R_{d,IGBT}\frac{I^2}{8}\left(1 + \frac{8}{3\pi}\beta cos\phi\right) \tag{B.8a}$$

$$P_{cond,diode} = V_{D,0}\frac{I}{2\pi}\left(1 - \frac{\pi}{4}\beta cos\phi\right) + R_{d,D}\frac{I^2}{8}\left(1 - \frac{8}{3\pi}\beta cos\phi\right) \tag{B.8b}$$

$$P_{sw,IGBT} = f_{sw}\left(E_{on} + E_{off}\right) \tag{B.8c}$$

$$P_{sw,IGBT} = f_{sw}E_{rr} \tag{B.8d}$$

Where $V_{CE,0}$ is the gate voltage of the IGBT module in V, $V_{D,0}$ is the gate voltage of the diode in V, I is the current in one arm of the inverter in A, β is the modulation index, $cos\phi$ is the power factor, $R_{d,IGBT}$ is the on-state resistance of the IGBT module in Ω, $R_{d,D}$ is the on-state resistance of the diode in Ω, f_{sw} is the switching frequency in Hz and E_{on}, E_{off}, E_{rr} are the turn-on, turn-off and recovery energy, in J. The amplitude of these energies, contrary to most of the parameters mentioned above, depends on the current flowing through the arm of the inverter, as can be seen in Figure B.4.

To solve that issue, an approximation of these curves with a polynomial fit was proposed along with a scaling law on the fitting coefficients [125]. Because this approach allows to infer how these curves will change between components and because using scaling laws allows for the analytical differentiation of the model, this is the approach that will be retained.

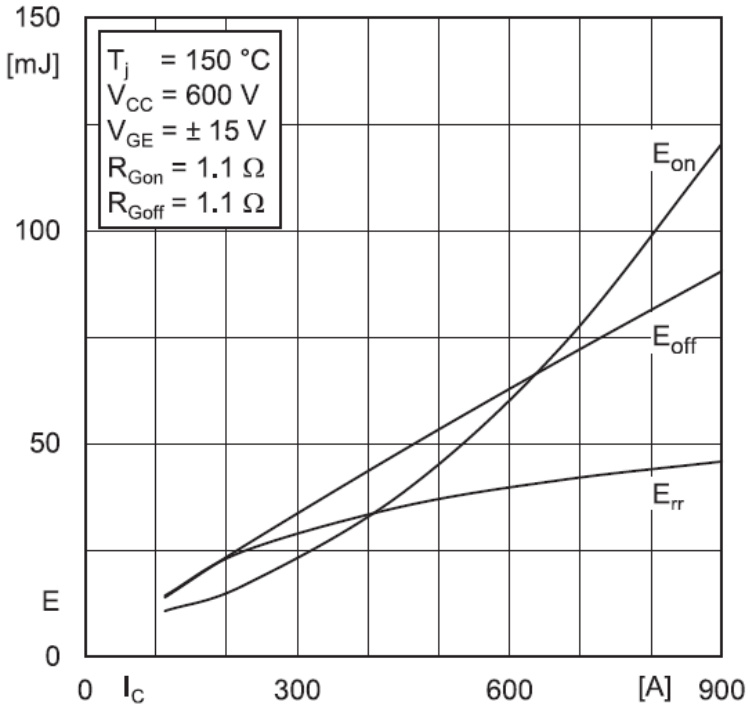

Figure B.4 Typical turn-on/-off energy for the SEMiX453GB12M7p semi-conductor from *the manufacturer's website*.

Appendix C

Appendix to the Part II

C.1 Virus SW 121

The first validation case for the newly developed tool is the thermal version of the Pipistrel SW 121 aircraft. This two-seater, high-wing, single-engine aircraft is made of composite material. It has fixed landing gear and is primarily used for training. Although it can be fitted with different engines from the Rotax catalog, the version used for this study was the one equipped with a Rotax 912 engine. The validation process will consist of feeding the TLARs and main geometric parameters of the aircraft to the code and performing an MDA, the results of which will then be compared to data on the reference aircraft. As already discussed in Chapter 2, the FAST-OAD process can require hundreds of variables as problem inputs, some of which are not worth detailing. Therefore, only specifications, architectural choices, and main model assumptions will be discussed and presented in Table C.1. The full list of inputs, however, can be found online as discussed in Appendix A. The powertrain architecture, which, as discussed in Chapter 2, is now an input of the sizing process, will be modeled as two tanks feeding fuel into an ICE. The Virus SW 121 has a composite airframe, so a multiplicative factor of 0.85 for the mass of airframe components was considered [60].

Table C.1 Main input parameters for the validation study on the Pipistrel Virus SW 121.

TLAR	Design payload:	188 kg
	Design range:	513 nm
	Design mission speed:	119 KTAS
	Design mission altitude:	2000 ft
	Approach speed:	58.5 KTAS
Geometry	Wing aspect ratio:	12.04
Propulsion	Rotax 912 SFC:	256 g/kW/h
	Propeller diameter:	1.7 m
	Propeller rpm:	From 2263 to 2099 depending on flight phase

Similar to the inputs, FAST-OAD computes and writes the outputs of all intermediate steps in the output file. Consequently, only the main outputs and those used for the discussion will be presented in Table C.2. Additionally, the computed performance of the simulated aircraft during the flights is plotted in Figure C.1 along with reference data points extracted from the POH. Regarding the geometry, the initial runs of MDA showed significant differences between the VTP area computed by the code and that estimated using a three-view drawing of the aircraft. This issue concerning the estimation of the VTP area in FAST-OAD has already been raised in the literature [226] and is linked with sizing criteria that were not adapted for small, single-engine aircraft. Therefore, the sizing process was adjusted so that the VTP area would be used as an input. This was done by leveraging the modularity of the FAST-OAD framework to remove the component responsible for computing that area, thereby turning it into an aircraft specification. For other parameters, very good agreement between the data and the estimated area of the other lifting surface of the aircraft can be seen. Similarly, the difference between the estimated masses and the reference data is less than 5%.

Table C.2 Main outputs for the FAST-OAD sizing process of the Pipistrel Virus SW 121.

	FAST-OAD sizing	**Reference**	**Diff. wrt ref. (%)**
MTOM (kg)	589	600	-1.8
OME (kg)	335	349	-4
Wing area (m^2)	9.68	9.51	+1.8
HTP area (m^2)	1.03	1.02	<1
Mission fuel burn (kg)	65.5	63	+4
Motor max. continuous power (kW)	68	69	-1.4

While the aforementioned results demonstrate the convergence of the multidisciplinary sizing process to a point close to the real aircraft in terms of overall design, it should be noted that these results are mostly a consequence of the original FAST-OAD-CS23 modules. The performances shown in Figure C.1 and whose main results are listed in the final lines of Table C.2, on the other hand, mostly stem from the newly implemented model. As opposed to other versions of FAST-OAD, in FAST-OAD-CS23 and -HE, the performances of the aircraft are TLARs, and the required power at each step of each phase of the flight is then computed as a result. Good agreement can be found in the estimated cruise power, around 4.3% difference, which, along with the specific fuel consumption being an input, leads to a very accurate estimate of the fuel required during the mission. And while the difference in shaft power is much more pronounced in reserve and climb, their contribution to the sizing fuel is negligible. Finally, the shaft power requirement, along with the incorporation of the loss in available power due to lower air density, leads to a required rated power of 69kW for the ICE that is acceptably close to the Maximum Continuous Power (MCP) specified in the TCDS. Overall, the order of magnitude of the difference between the reference and computed data remains

within an acceptable margin for the preliminary design phase, thereby increasing confidence in the methodology and providing a basis for comparison with the electric version of the airframe presented in Section 4.3.1.

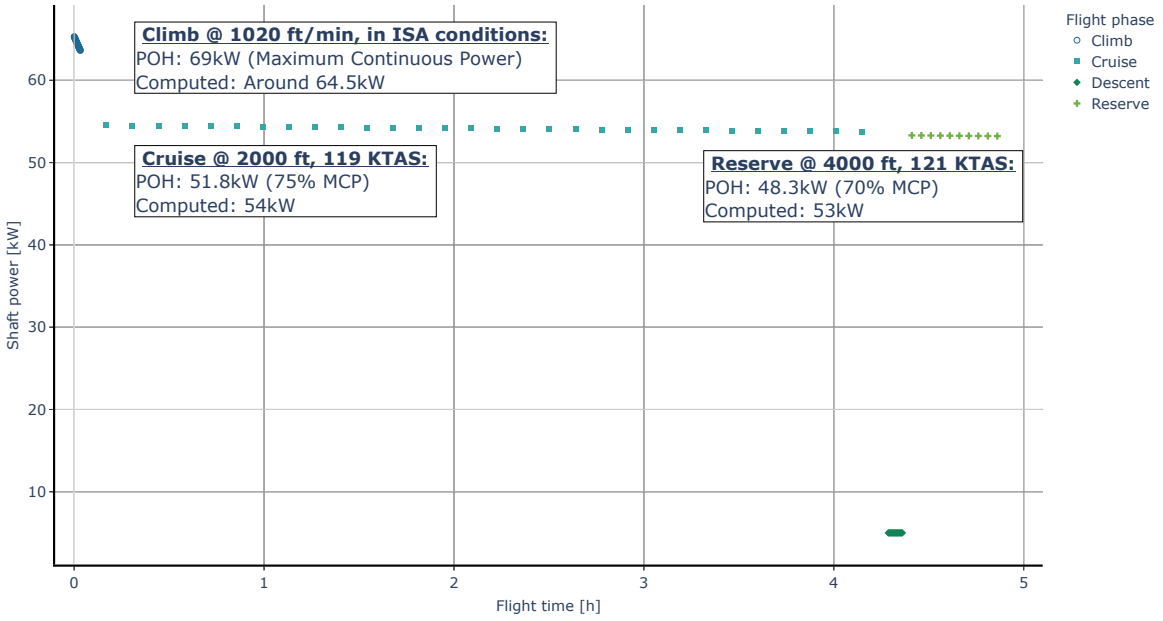

Figure C.1 Comparison of the flight performances computed by the code with those published in the POH for the Virus SW121.

C.2 Reference Cirrus SR22

As discussed in the main part of this work, the Cirrus SR22, in addition to being a suitable candidate for electrification, is already a reference case of the original FAST-OAD-GA framework. This framework, on which this work builds, however uses different models. Consequently, and to ensure the consistency of results after the change in modeling paradigm described in 2, it was reevaluated. The powertrain will be modeled in the same way as the Pipistrel Virus SW 121, although here, the engine, a Continental IO-550-N rated at 310hp, can be modeled with the approach inherited from the FAST-OAD-GA framework. Consequently, the SFC will be computed based on operating conditions rather than being treated as an input. It was also decided to set the maximum sea level power as an input and ensure that the constraint is satisfied rather than enforce it. The main specifications, architectural choices, and model assumptions are presented in Table C.3

The results of the sizing run are shown in Table C.4 and compared to reference values from literature, technical documentation, and also to the output values of the legacy framework.

Table C.3 Main input parameters for the validation study on the Cirrus SR22.

TLAR	Design payload:	375 kg
	Design range:	971 nm
	Design mission speed:	160 KTAS
	Design mission altitude:	8000 ft
	Approach speed:	79 KTAS
Geometry	Wing aspect ratio:	10.12
Propulsion	IO-550-N rated power:	231 kW
	Propeller diameter:	1.98 m
	Propeller rpm:	2500

Table C.4 Main outputs for the FAST-OAD sizing process of the Cirrus SR22.

	FAST-OAD sizing	**Sizing legacy**	**Reference**	**Diff. wrt ref. (%)**
MTOM (kg)	1600	1656	1633	-2
OME (kg)	990	1028	1029	-3.7
Fuel mission (kg)	233	252	250	-6.8
Wing area (m^2)	13.3	13.7	13.5	-1.5
HTP area (m^2)	3.4	3.6	3.5	-2.8
VTP area (m^2)	1.4	1.4	1.4	<1
Aircraft length (m)	7.65	7.7	7.9	-3.1

The main difference lies in the estimation of the fuel consumption and empty mass of the aircraft. Upon further analysis, the reasons for the difference in fuel consumption are twofold. First, the efficiency of the propeller and SFC during cruise is computed to slightly more advantageous values in the FAST-OAD-CS23-HE framework. This difference exists because of the transformation of the models to allow analytical differentiation. The second reason is that more points of the mission were computed in the original framework (about 300 vs 100 in the FAST-OAD-CS23-HE framework). With the same amount of points, the difference is reduced to 4%. For the maximum power of the engine, the input value was found to be slightly more than the maximum value required in the mission (around 3%), which validates the engine. For the difference in empty mass, and while a detailed mass breakdown is not available in literature, the results were compared to those of the original framework, for which the total mass showed good agreement. The difference seems to arise mostly from the mass of the fuel lines for which a different empirical relation was used in the present work. Overall, however, results remain within an acceptable range for the preliminary phase. Additionally, since most of the inputs and models will be reused for the hybrid and electric versions that we will study, the same offsets should be found.

C.3 Reference DAHER TBM 900

The TBM 900 is a high-performance single-engine turboprop business aircraft with a low-wing and conventional tail configuration. Just like for the previous reference cases, the powertrain of the DAHER TBM 900 is known. It is powered by a PT6A-66D turboprop engine coupled to a five-bladed propeller that allows it to reach cruising speeds of up to 330 knots, making it a good representative of the high-performance part of the CS-23. Similarly to the Cirrus SR22, it is also a reference case in the original FAST-OAD-GA framework. For brevity, the specifications and architectural choices are not presented here but can be found in literature describing the legacy models [91]. A brief comparison of the results obtained with the legacy powertrain models and the new paradigm is presented in Table C.5.

Table C.5 Main outputs for the Daher TBM 900 run compared with original results [91].

	FAST-OAD sizing	**Sizing legacy**	**Reference**	**Diff. with ref. (%)**
MTOM (kg)	3375	3358	3370	<1
OME (kg)	2087	2114	2109	1
Fuel mission (kg)	801	763	774	3.5
Wing area (m^2)	18.05	18.07	18.0	<1
HTP area (m^2)	4.52	4.94	4.76	5
VTP area (m^2)	2.88	2.85	$\approx$ 3.00	4

The difference with the reference data mostly lies in the estimation of the fuel consumption, although, as opposed to the Level 2 case, here the fuel is slightly overestimated. The results remain within an acceptable range for preliminary design.

C.4 Reference Quest/DAHER Kodiak

The Kodiak 100 is a single-engine turboprop utility aircraft with a high-wing and conventional tail configuration. It is a versatile aircraft powered by a PT6A-34 engine. Combined with a four-bladed propeller, the aircraft has Short Take Off and Landing capabilities and can carry a payload of more than 1100 kg. For the powertrain file, a simple chain consisting of a propeller, turboshaft, fuel system, and tanks was considered. The mass of the aircraft's systems was also directly used as a specification because they were readily available in the POH. The same problem inputs as presented in the literature [226] will be used. The outputs of the sizing process are presented in Table C.6. Most of the results show very good agreement for the preliminary design phase. The results of the fuel consumption models were compared outside the sizing loop to known data. This resulted in the addition of a 1.05 correction factor. Even so, there is only a slight difference in the fuel consumed.

The post-processing tools available in the FAST-OAD-CS23-HE framework, as well as performance data available in the POH, were used to further investigate that difference. The

Table C.6 Main outputs for the FAST-OAD sizing process of the Kodiak 100.

Parameter	FAST-OAD sizing	Reference	Diff. with ref. (%)
MTOM (kg)	3280	3290	0.3
OME (kg)	1727	1712	0.8
Fuel mission (kg)	933	960	3.1
Wing area (m^2)	23.04	22.3	3.1
HTP area (m^2)	6.43	6.21	3.5

main source of error comes from the estimation of the fuel consumed during the reserve and cruise phases. The former is mainly because the target height and speed set for the reserve phase were taken equal to that of a cruise at 10000 ft in the maximum range profile. These, however, correspond to the performances of a fully loaded aircraft, while the framework considers that the aircraft has already consumed fuel for the climb, cruise, and descent phases. This led to an error of around 7 kg, which equates to around 10% of reserve fuel. For the cruise, while the relative error is much smaller (around 2%), it still accounts for 15 kg on the overall mission. As the hourly fuel consumption gave a good match, this difference was not looked into further.

The post-processing tools were also used to analyse the evolution of the power that the turboshaft is required to provide in order to better guide the choice for hybridising the aircraft. A required cruise power of 200kW was computed which showed good agreement with cruise performances indicated in the POH. Surprisingly, however, the power required to reach target descent performances was found to be greater than the power required for cruise. While the aircraft thrust is indeed lower, the fact that the descent airspeed was set at 160 KEAS results in a greater power required. This yields descent power decreasing from 230 to 200 kW. Results were still considered valid as the fuel consumed during descent seemed to closely match the data from the POH. The choice was however made to consider a descent speed of 140 KEAS for further computation.

The performances of the Kodiak 100 were also evaluated on a shorter operational mission with a range corresponding to the range selected in section 4.5.2. For that mission, a payload corresponding to the Kodiak 100 max payload was selected. The conditions for climb, reserve, and cruise were selected equal to those of the design mission. The corresponding flight profile is presented in Figure C.2.

C.5 Reference Cessna 208B

Similar to the Kodiak 100 that has already been discussed, the Cessna Caravan 208B is a single-engine, high-wing aircraft with a conventional tail. The version we selected is powered by a 675 hp PT6-114A turboprop coupled with a three-bladed propeller and has

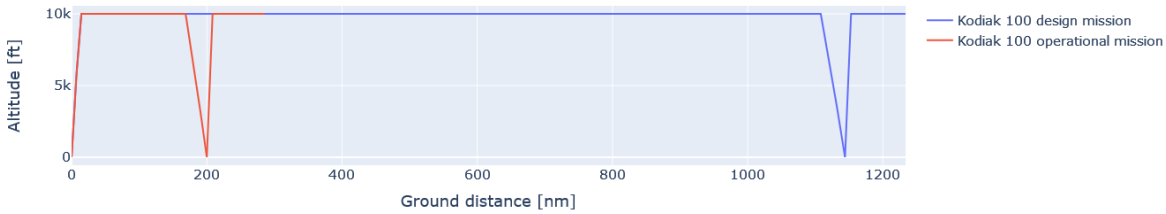

Figure C.2 Comparison of Kodiak 100 design mission and operational mission.

STOL capabilities with maximum ranges of around 1000 nm. The mass of the furniture was set as an input and estimated at around 100kg based on the difference between the published standard empty mass and the basic empty mass. For the sizing mission, we considered a long-range/low-power profile as it is predicted to be more suitable for hybridizing. A final remark to be made on the Cessna 208B is the possibility of including a belly fairing in which a battery pack could be installed. A synthesis of the specifications, architectural choices, and model assumptions considered is presented in Table C.7.

Table C.7 Main input parameters for the validation study on the Cessna 208B.

TLAR	Design payload:	840 kg
	Design range:	1030 nm
	Design mission speed:	155 KTAS
	Design mission altitude:	12000 ft
	Approach speed:	79 KTAS
Geometry	Wing aspect ratio:	9.7
Propulsion	PT6A-114A rated power:	675 hp
	Propeller diameter:	2.64 m
	Propeller rpm:	1750 to 1900 depending on flight phase

Results for the sizing process on the reference Cessna 208B are presented in Table C.8, and are compared to the value extracted from the POH. Good agreement can be found between the reported data and the data at the output of the multi-disciplinary sizing process. An exact result was even found for the aircraft MTOM, which, upon further investigation, is the result of the compensation of a fuel mass overestimation with an OME underestimation. Results were also compared with outputs of another OAD software called JPAD, whose results are reported in literature [244]. While different sizing missions were selected in both cases, good agreement on the MTOM and the standard empty mass could be observed. A detailed analysis of the aircraft's performances was also conducted to identify avenues of improvement for the hybrid design. Doing so, significant differences between the input rated power and the maximum power required on the shaft of the turboprop were found. Part of that underestimation was found to be linked with a slight underestimation of the climb rate, but was mainly attributed to a lack of modeling of the takeoff phase, which is also known to be power-intensive. Finally, the power required in cruise was found to be, on average, equal

to 285 kW. This seems to be consistent with the choice made for the Eco-Caravan concept, as, after consideration of the derating due to air density decrease at altitude, the power output of the piston engine retained should be between 270 and 290 kW.

Table C.8 Main outputs for the FAST-OAD sizing process of the Cessna 208B.

Parameter	**FAST-OAD sizing**	**Reference**	**Diff. with ref. (%)**
MTOM (kg)	3968	3968	<1
OME (kg)	2130	2146	<1
Fuel mission (kg)	998	982	1.6
Wing area (m^2)	24.95	25.96	3.9

C.6 Summary of battery cells used for prospective electrification scenarios

The battery pack model implemented in this framework, discussed in Section 3.6.1, relies on the performances of individual cells to estimate those of the pack. As opposed to top-down Wh/kg models, this approach allows to take more of the cells' constraints into consideration. Indeed, studies conducted in this chapter showed that changing the performances of the cells could have major impacts on the pack design and thus on the aircraft. In particular, it showed that depending on the case, cells designed for power output or designed for energy demand, two competing objectives, could lead to significantly different results. Table C.9 summarizes the cells used in each case along with their main characteristics. They are also represented on a Ragone plot in Figure C.3. It is interesting to note that the cell from Amprius stands out as opposed to the two Samsung cells, which show a clear exchange between power and energy. It is also worth noting that, as opposed to all the other cells, which are prismatic, the cell used for the prospective study on the electric Cirrus, the Ampirius 1.34Ah Balanced Power+Energy, is a pouch cell.

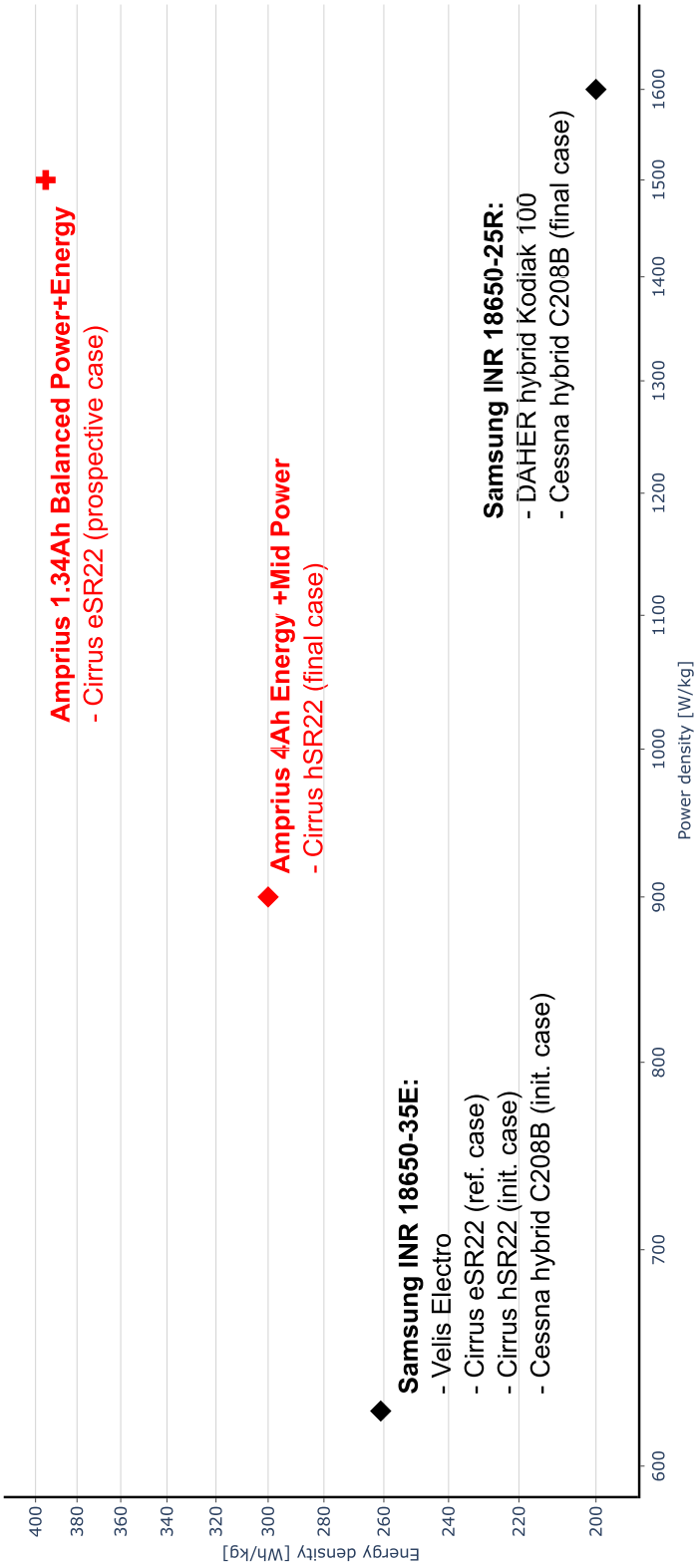

Figure C.3 Position of the cells used for the case studies on a Ragone plot.

Table C.9 Summary of cells used for the case studies and their characteristics.

	Study case	Cell name	Energy density	Power density	Lifespan
Level 1	Virus SW121		N/A		
	Velis Electro	Samsung INR18650-35E (ref.)	261 Wh/kg	624 W/kg	700 c. [227]
Level 2	Cirrus SR22		N/A		
	eSR22 (ref.)	Samsung INR18650-35E[a] (ref.)	261 Wh/kg	624 W/kg	700 c. [227]
	eSR22 (prosp.)	Amprius 1.34Ah Balanced Power+Energy[b]	395 Wh/kg	1.5 kW/kg	150 c.
	hSR22 (init.)	Samsung INR18650-35E (ref.)	261 Wh/kg	624 W/kg	700 c. [227]
	hSR22 (final)	Amprius 4Ah Energy+Mid Power[b]	300 Wh/kg	900 W/kg	600 c.
Level 3	DAHER TBM900		N/A		
	EcoPulse (retrofit)		N/A		
	EcoPulse (scratch)		N/A		
	DAHER Kodiak 100		N/A		
	Hybrid Kodiak 100	Samsung INR18650-25R	200 Wh/kg	1.6 kW/kg	700 c.
Level 4	Cessna 208B		N/A		
	Hybrid C208B (init.)	Samsung INR18650-35E (ref.)	261 Wh/kg	624 W/kg	700 c. [227]
	Hybrid C208B (final)	Samsung INR18650-25R[c]	200 Wh/kg	1.6 kW/kg	700

[a]: https://www.orbtronic.com/content/samsung-35e-datasheet-inr18650-35e.pdf, Accessed: 2024-01-26

[b]: https://amprius.com/solutions/simaxx/, Accessed: 2025-10-23

[c]: https://www.dnkpower.com/wp-content/uploads/2018/04/Samsung-INR18650-25R-Datasheet.pdf, Accessed: 2025-10-23

Appendix D

Appendix to the Part III

D.1 LCA in the context of the aeronautics sector

An LCA is performed in four steps [246, 248, 259]: (1) the definition of the system, scope, and goals for the analysis, (2) the inventory of emissions and extractions, (3) the analysis of the impacts, (4) the interpretation.

D.1.1 Goal and Scope definition

The first step of an LCA is the definition of the goals of the study and the scope of the system to be considered. This step is of high importance because it is at this point that crucial decisions that will impact the rest of the analysis must be made [246]. The first question to be answered is that of the public to whom the LCA will be presented, and for what it will be used. In the literature reviewed, LCA was seen to be used to assess the impacts of an existing aircraft, the A320, for instance, being a surprisingly common choice of case study [110, 124, 259–261]. LCA can also be used as a tool to guide the design process and study the impacts of alternative design choices, like the use of a hybrid or all-electric powertrain [227], or the impacts of a change in airframe material [253]. In such cases, the LCA is used as a tool to enable eco-design approaches, as exemplified in Figure D.1.

The function of the system, based on which it will be evaluated, is then defined, as well as the reference flow necessary to perform that function. It is also a paramount step of the analysis, as it will then be used to identify all the sub-processes required for the system to function. The goal is to provide a reference to which inventory data can be applied to ensure that different systems are comparable on a common basis [259]. A distinction is made between the *functional unit*, which refers to the qualification of the function and/or service provided by the system being evaluated, and the *reference flow*, which describes the amount of product required to fulfill the defined function. In the aeronautics sector, one of the functional units that is most commonly used is "the transportation of one revenue passenger in a safe way over one kilometer" [110, 247, 250, 253]. Derivatives have also been used in literature

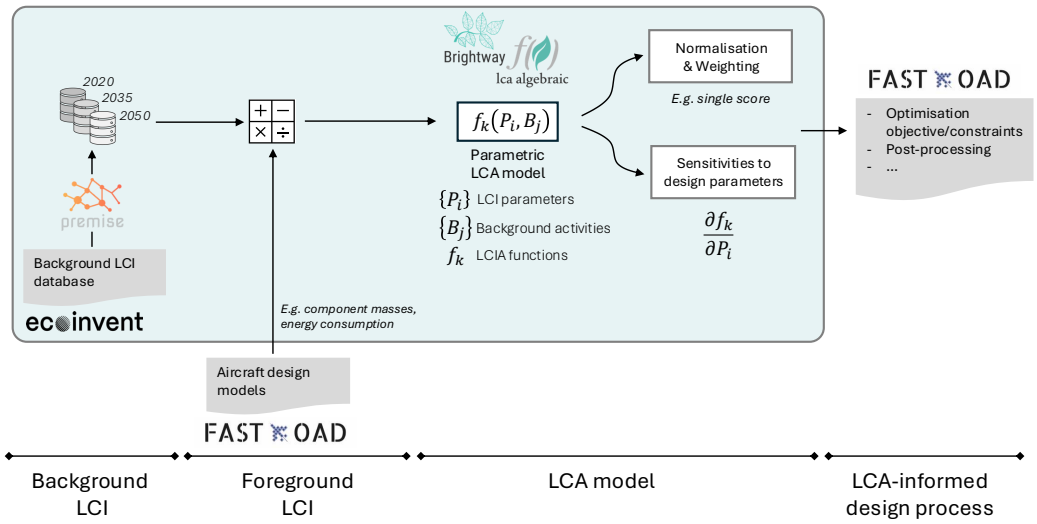

Figure D.1 Schematic view of the integration of an environmental module in an aircraft design framework in support of eco-design [276].

to account for both luggage and also in the case where the aircraft also carries freight [253, 259, 262, 266]. In this case, "the transportation of a given mass over one kilometer" is used. This way, the distinction between freight and paying passengers does not have to be made. It is worth noting that using this functional unit implies the main function of the aircraft is to transport passengers from point A to point B. In the context of General Aviation, while this might be suited for small commuters and tourism aircraft, other functional units have been proposed, especially for trainer aircraft. For such aircraft, literature proposes the use of "flying one hour" [227]. Finally, a review of the application of LCA in the aviation sector also revealed that, when particular focus was set on a specific subpart of the aircraft, "one kg of OWE" could also be used [259]. Regardless of what unit is used, correlation can then be used to assess what fraction of the system, i.e., the reference flow, is required to perform the function, which allows to distribute the cost of producing the system over its whole lifespan [248].

Finally, the boundaries of the system under study shall be defined to identify which unit processes are included in the LCA and which are not. The reference flow is usually the starting point for that part because it directly defines "how much" of the system is required to fulfill the functional unit. Based on that reference flow, contributing sub-processes can then be identified, they are then used to identify sub-sub-processes, etc ... In the first step of the LCA, that recursive search is usually stopped after a few steps. That rough granularity allows to assess what processes are relevant and which ones can be cut off either because their contribution is minor or because they are out of the scope. A typical example of such flow charts is shown in Figure 5.1 for a two-seater electric aircraft. For aircraft, the PEFCR recommends considering raw material extraction and pre-processing, final assembly,

distribution, operation, and end-of-life. It however advises excluding from the scope activities such as the commuting of employees and administrative services. Theoretically, this would include research and development activities, although literature does not seem to have found a clear consensus on that topic [248].

D.1.2 Extraction and Emissions inventory

The second step of an LCA consists in cataloging all the elementary emissions and extractions from the biosphere necessary to perform the function. While there are multiple approaches to listing elementary interactions with the biosphere, the process-based approach is the most common. This approach usually starts from sub-processes contributing to the reference flow which were identified during the definition of the boundaries of the system. Processes contributing to these sub-processes are then identified, making them sub-sub-processes, and so on, recursively until elementary exchanges with the biosphere can be identified. Additionally, at each step, the processes are weighted by how much they contribute to the functional unit or parent processes. The airframe, for instance, is produced once but can fulfill the functional unit multiple times during its lifespan. As such, its impact will be weighed by the number of times the functional unit is performed during its whole life. Similarly, for all processes contributing to the production and assembly of the airframe. The case in which a component must be replaced during the life of the system can also be accounted for. If, for instance, the engine(s) of the aircraft must be replaced once during the lifetime of the aircraft, then the contribution of the engine production to the airframe assembly will be "paid" twice. The same goes for the use phase, as the aircraft typically transport more than one passenger over more than one kilometer, the impacts of the use phase will be distributed proportionally to the number of PAX.km for the flight. This entails that it is particularly important to consider the product's lifetime, explaining why extending lifespan is such an important part of product design and product usage. More specifically, in the case of aviation, the number of passengers and the distance of the flights can widely vary based on demand. Consequently, assessing the off-design performances of the aircraft either through a payload-range [276] or a discrete event simulation [259], and especially the load factor [247], is paramount for the proper assessment of the impacts. As only processes contributing to the functional unit shall be included, in particular, it means that the reserve phase will not be considered. Indeed, while a reserve must be planned for, meaning reserve fuel will be loaded for the mission, it is rarely used, and thus, only the fact that it will make the aircraft heavier will be accounted for.

This list of elementary flows is then compiled into the so-called Life Cycle Inventory (LCI), which is the output of the second step of an LCA. While in principle, this approach sounds easy, there are some showstoppers. First, the sheer quantity of data required to develop the process tree back to elementary flow is phenomenal. Additionally, the question of the accessibility of data can be raised. While for industrials and sector experts, it can be easy

to assess first or second-order contributors to the reference flow, quantifying elementary exchanges is challenging because it relies on supplier knowledge. These difficulties are exemplified in Figure D.2.

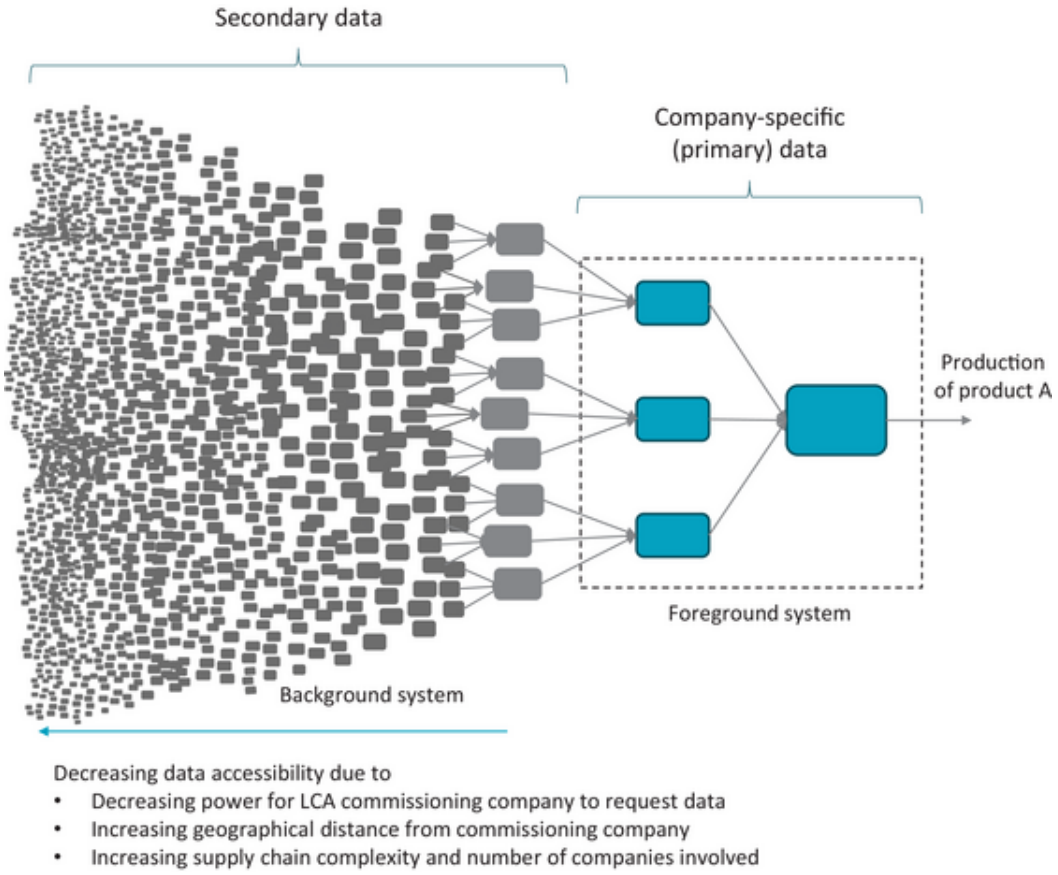

Figure D.2 Data collection challenges in a typical process tree in life cycle assessment (LCA) [312].

Figure D.2 also illustrates the fundamental difference between foreground and background parameters. While foreground parameters, which represent the parameters computed during the design process, can be influenced, background parameters cannot. They represent processes that are required, like energy for the assembly or transport of the subsystem to the final assembly line, but can't be directly influenced by the designer [275]. In the realms of aeronautics, and although processes controlled by primary manufacturers at Tier 0 account for a significant part of energy demands and emissions, the impacts of suppliers' activity are at least the same order of magnitude [313]. In practice, huge databases aggregating results for existing processes exist. From there, the inventory is, in theory, simplified as the flowchart exploration can be stopped as soon as a known process is found. Nonetheless, multiple issues arise, among which is the question of the quality and availability of data [250, 252]. Indeed, to enable replicable and trustworthy results, all practitioners should use the same sets of data.

The accuracy of those datasets, however, is closely linked to both the geography and the time, as the issue of the carbon intensity of the electric mix, already raised in the main part of the manuscript, clearly illustrates. While it is not specific to the aeronautics sector, the issue of data sharing between major actors, like OEMs and suppliers, also contributes to the relative scarcity of a common database for LCA in aviation. While solutions to address this particular issue have been proposed in literature, like the use of blockchain [250], it still remains an open problem. Using proxies, i.e. process that are acceptably representative (e.g., assuming that the ESC for a drone is equivalent to an ESC for a scooter [109]), can be a partial solution to the problem of availability. In conjunction with the fact that for other sectors accessible databases exist, like in the automotive sector [255, 314], this provides resources to simplify the emissions and extractions inventory. While, as previously mentioned, the PEFCR for aircraft is still at the status of a draft, insights can also be gained by looking into similar products. In particular, EASA has established a standardized PEFCR for eVTOL and delivery drones [1] to enable manufacturers and operators to quantify their aircraft's environmental impact. Literature reveals that, for LCA in the realms of aircraft, the ecoinvent database [212] is frequently used [110, 227, 251, 253, 262]. This database, however, is not freely accessible. Despite that, there have been calls to expand it and even create aviation-specific datasets, as it represents an inevitable step for the assessments of future configuration [259].

D.1.3 Impact assessment

Relying on all the elementary emissions and extractions cataloged at the output of the second step of the LCA, the third step consists in quantifying the ability of these species to cause potential impacts on the environment. This is done using the Life Cycle Impact Assessment (LCIA) method that allows linking the inventory to the raw environmental impacts of the species. Regardless of which method is used, they all consist of modeling and quantifying how a given amount of each species damages the environment, which is called the characterization factor. In practice, for each category or type of impacts, the potential of a species can be expressed as a ratio of the impact of a reference species. For the impact on climate change, for instance, and as we have done in Chapter 4, CO_2 is used as a reference, hence why the units $gCO_{2,eq}$ was used. A species can have impacts in multiple categories, just as it can have impacts only in one. This, in addition to depending on the species, depends on the categories of impacts considered, the list of which is specific to each LCIA method. While there are many categories of impacts, they can be classified into two categories: midpoint impacts and endpoint impacts. Endpoint impacts represent quantifiable and explicit damages to areas of the environment that need protection, such as damage to ecosystems or the effects on human health. They represent the end of the causality chain of emissions, extractions, and

[1] https://www.easa.europa.eu/en/en/domains/drones-air-mobility/drones-air-mobility-landscape/noise-sustainability/sustainability-environmental-footprint, Accessed 2025-09-24

their impacts. Depending on the methods, intermediate impacts, called midpoint impacts, can also be computed as a step of the cause-and-effect chain. It is worth noting that the characterization factor that represents pathways to damage can only be modeled, which introduces uncertainties, especially at the end of the chain [246, 262].

LCIA methods like the ReCiPe2016 method [315], with 18 midpoint indicators and three endpoint indicators, the ImpactWorld+ method [316], and the Environmental Footprint (EF) method [317], proposed by the European Union, are among the most popular. While there are many others available in literature, particular focus will be put on the ReCiPe2016 method and the EF method. For the former, the choice was made as it was frequently used by papers in the literature reviewed [110, 227, 262]. A list of the impact categories it encompasses is presented in Figure D.3. For the latter and because it was developed by the European Commission, the PEFCR for aircraft strongly recommends its use in an effort to ease product comparison. This, in addition to its use in recent studies on the environmental impact of aviation [259], makes it particularly interesting.

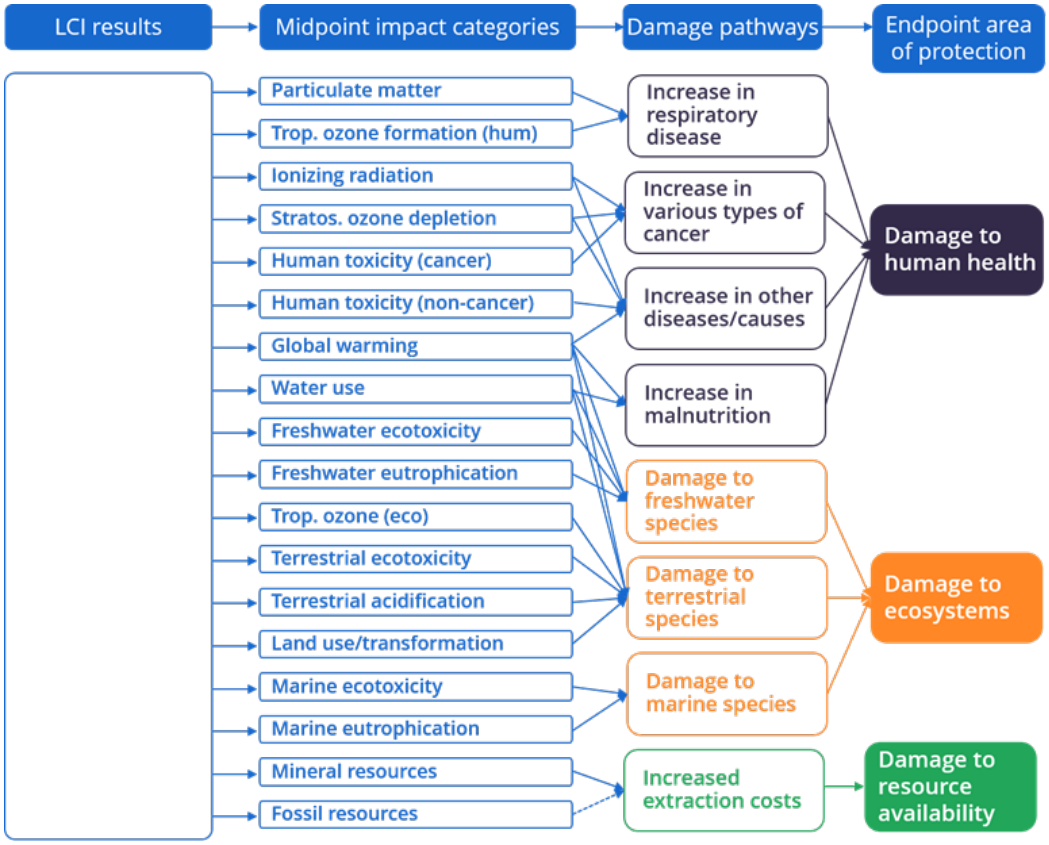

Figure D.3 Framework of the ReCiPe method: Relationship between LCI results, midpoint impact category, and endpoint impact categories. Source: https://pre-sustainability.com/articles/recipe/, Accessed 2025-09-22.

In addition to these mandatory steps, additional optional steps can be performed to facilitate the interpretation of results. Indeed, because each category expresses impacts in different reference units, it is not easy to compare their relative significance. A first step to improving the interpretability of results and their communication is the normalization step. It consists in comparing the impacts in each category to the impacts of a reference system. Usually, this system consists of the total effects of human activities averaged at the level of a region or even globally. This step, however, can introduce additional uncertainties because its outputs highly depend on the choice of reference system. For instance, if a system where one impact category, like global warming, is over-represented, is considered. Then, for future study where that system is used as a reference, the impact on the over-represented category would be way smaller. The same thing can happen if one particular extraction or emission is missing from the reference. Additionally, because the reference is often a system representing impacts stemming from current consumption, there is no consideration of the planet's capability of sustaining those damages. This gave rise to a specific branch of the LCA called the Life Cycle Sustainability Assessment [318].

An additional optional step that can be performed is the weighting of normalized impacts. Indeed, while the normalization step enables easier comparison with a reference, there is no notion of the relative importance of each category. Multiple approaches exist for the definition of those weighting factors, but they are generally based on either monetary considerations (a willingness to pay for damages), on expert knowledge, or on a distance to a target [246]. With the impacts weighed, it is also possible to sum the results in all categories to form a single metric quantifying all environmental damage, often called the single score. This is particularly interesting in the case of an optimization framework because it allows to regroup all impacts in one objective function. However, just like for the normalization step, it can introduce severe biases in the analysis. Even though the normalization and weighting steps are seen in the LCA community as useful for decision making, they still need to be improved in terms of robustness [319]. They introduce uncertainties that are not science-based but rather based on value choices. Therefore, their adoption by the community is not unanimous [234].

D.1.4 Interpretation

The final step of an LCA is the interpretation of the previously obtained results. During this phase, and based on the results obtained during the first three steps, analysis of hotspots in the life cycle of the system can be performed. It allows the identification of the most damaging processes and phases of the system and the identification of where the search for alternatives should be prioritized. Conclusions can then be formulated to best inform decision-makers on how to proceed to reduce the impacts of the system. However, this step relies on the quality of the results obtained in prior steps, which, as was discussed, depending

on the models and reliability of the data, can introduce uncertainties. As such, studies on the assumptions made should also be performed in that last step. The scope of the study is then reviewed, the uncertainties are quantified, and key assumptions are challenged. Overall, due to the role of this step as an insurance of the quality and transparency of the results, it is highly coupled with all the other steps as illustrated in Figure 5.2.

D.2 Background processes used for the LCI of General Aviation aircraft

The processes described in Table D.1 and taken from the version 3.9.1 of the ecoinvent database [212] were used as the background processes. When multiple specific geographies were used for the needs of a study, multiple entries in the Table D.1 were added.

Table D.1 Ecoinvent 3.9.1 processes for the LCI of the GA aircraft.

Component	**Unit**	**Ecoinvent processes**
Carbon Fibre Reinforced Plastic	kg	Market for carbon fibre reinforced plastic, injection moulded [GLO]
Aluminium	kg	Market for aluminium, cast alloy [GLO]
Steel	kg	Market for steel, unalloyed [GLO]
Titanium	kg	Titanium production [GLO]
Magnesium	kg	Market for magnesium-alloy, AZ91 [GLO]
Nickel	kg	Market for iron-nickel-chromium alloy [GLO]
Metal-matrix composite	kg	Market for aluminium alloy, metal matrix composite [GLO]
Electric machines	kg	Electric motor production, vehicle (electric powertrain) [GLO]
Power electronics	kg	Inverter production, for electric passenger car [GLO]
Electric bus	kg	Power distribution unit production, for electric passenger car [GLO]
Battery pack	kg	Battery production, Li-ion, NMC111, rechargeable, prismatic [RoW]
Internal Combustion Engine	kg	Internal combustion engine production, passenger car [GLO]
Electricity consumption US	kWh	market for electricity, high voltage [US-WECC]
Electricity consumption Europe	kWh	market group for electricity, high voltage [RER]
Kerosene	kg	Market for kerosene [RoW]
Unleaded AvGas	kg	Market for petrol, unleaded [RoW]
Tetraethyllead	kg	Market for lead [GLO]

Résumé

Dans le cadre de la transition écologique du secteur aéronautique, des objectifs ambitieux pour réduire l'impact environnemental de l'aviation sont visés. Si le CO2 est souvent mentionné, les avions rejettent d'autres polluants qui contribuent également à l'impact du secteur. Malgré leur faible contribution aux émissions du secteur, les avions de l'aviation générale ont un rôle majeur dans cette transition. Bien qu'ils ne représentent qu'une infime partie de la consommation de carburant du secteur, ils sont responsables de 10% des émissions d'imbrûlés, de 40% des émissions de CO et de la totalité des émissions de plomb. En outre, ils sont utilisés différemment et moins intensément que leurs homologues commerciaux, indiquant une voie différente vers la soutenabilité. Par ailleurs, en raison de leur faible puissance et de leur faible autonomie, ils constituent des candidats idéaux pour dérisquer les nouvelles technologies avant leur adoption sur les avions commerciaux. Une solution potentielle pour répondre à la question de la transition est l'introduction de la propulsion électrifiée. Bien que cette technologie en soit encore à ses débuts, soulevant des questions de certifiabilité, elle offre des avantages allant d'une réduction à une élimination des émissions pendant le vol. Elle offre également la perspective de synergies multidisciplinaires et de permettre d'alléger les contraintes de conception. Parmi les nombreux projets proposés pour explorer cette solution, diverses approches, allant de la conception "feuille blanche" à la réutilisation de cellules existantes, ont été explorées. Il est donc nécessaire de créer des méthodologies de dimensionnement capables de tirer parti de ces synergies et d'évaluer les impacts, au niveau de l'avion, des groupes propulseurs électrifiés. Compte tenu de la diversité des architectures et de la nécessité de pouvoir modéliser différentes approches de conception, une formulation dynamique est nécessaire.

Cette thèse répond à ce besoin en présentant de nouvelles méthodes et modèles permettant d'évaluer, au niveau de l'avion, les effets de la chaîne de propulsion électrifiée. Tout d'abord, une revue des méthodes de dimensionnement existantes est proposée, soulignant la nécessité d'un cadre capable de saisir les synergies multidisciplinaires introduites par la propulsion électrique. Cette thèse contribue en proposant l'intégration, dans le code FAST-OAD, d'un nouveau module capable de modéliser n'importe quelle architecture de propulsion. L'intégration de modèles capables de capturer les gains issus de plusieurs disciplines ainsi que les degrés de liberté supplémentaires dans la conception est ensuite abordée. Des modèles de fidélité moyenne sont choisis comme compromis idéal entre les méthodes de densités et

rendements constants et les simulations coûteuses de haute fidélité. L'application de cette méthode à divers scénarios d'hybridation pour les avions dans la catégorie de certification CS-23 est ensuite discutée. Les résultats montrent que, même si une électrification permettant d'atteindre les mêmes niveaux de performances que les avions conventionnels n'est pas réalisable, elle peut être mise en œuvre et s'avérer avantageuse pour les missions plus courtes et pour de petits aéronefs, même avec les technologies actuelles. Un point de bascule en termes de maturité technologique est également mis en évidence, montrant que certaines chaînes hybrides ne seront compétitives que temporairement. Enfin, il est montré que, pour certaines configurations, la réduction des émissions ne peut être obtenue qu'en tirant parti du soulagement des contraintes de conception, et non grâce à la faible intensité carbone de l'électricité. Ces comparaisons sont ensuite approfondies en utilisant une ACV dans le processus de conception. Cela permet d'obtenir des pistes cruciales sur les impacts de la propulsion électrique et de nuancer les gains découlant des nouvelles compositions chimiques des cellules de batterie.

RÉPUBLIQUE FRANÇAISE
Liberté
Égalité
Fraternité

Université de Toulouse

Titre : Optimisation d'un problème de conception d'avion pour des configurations hybride-électriques sous contraintes de fabrication et de certification

Mots clés : avion, électrique, hybride, multidisciplinaire, conception avion

Résumé : Dans le cadre de la transition écologique du secteur aéronautique, des objectifs ambitieux pour réduire l'impact environnemental de l'aviation sont visés. Si le CO2 est souvent mentionné, les avions rejettent d'autres polluants qui contribuent également à l'impact du secteur. Malgré leur faible contribution aux émissions du secteur, les avions de l'aviation générale ont un rôle majeur dans cette transition. Bien qu'ils ne représentent qu'une infime partie de la consommation de carburant du secteur, ils sont responsables de 10% des émissions d'imbrûlés, de 40% des émissions de CO et de la totalité des émissions de plomb. En outre, ils sont utilisés différemment et moins intensément que leurs homologues commerciaux, indiquant une voie différente vers la soutenabilité. Par ailleurs, en raison de leur faible puissance et de leur faible autonomie, ils constituent des candidats idéaux pour dérisquer les nouvelles technologies avant leur adoption sur les avions commerciaux. Une solution potentielle pour répondre à la question de la transition est l'introduction de la propulsion électrifiée. Bien que cette technologie en soit encore à ses débuts, soulevant des questions de certifiabilité, elle offre des avantages allant d'une réduction à une élimination des émissions pendant le vol. Elle offre également la perspective de synergies multidisciplinaires et de permettre d'alléger les contraintes de conception. Parmi les nombreux projets proposés pour explorer cette solution, diverses approches, allant de la conception "feuille blanche" à la réutilisation de cellules existantes, ont été explorées. Il est donc nécessaire de créer des méthodologies de dimensionnement capables de tirer parti de ces synergies et d'évaluer les impacts, au niveau de l'avion, des groupes propulseurs électrifiés. Compte tenu de la diversité des architectures et de la nécessité de pouvoir modéliser différentes approches de conception, une formulation dynamique est nécessaire. Cette thèse répond à ce besoin en présentant de nouvelles méthodes et modèles permettant d'évaluer, au niveau de l'avion, les effets de la chaîne de propulsion électrifiée. Tout d'abord, une revue des méthodes de dimensionnement existantes est proposée, soulignant la nécessité d'un cadre capable de saisir les synergies multidisciplinaires introduites par la propulsion électrique. Cette thèse contribue en proposant l'intégration, dans le code FAST-OAD, d'un nouveau module capable de modéliser n'importe quelle architecture de propulsion. L'intégration de modèles capables de capturer les gains issus de plusieurs disciplines ainsi que les degrés de liberté supplémentaires dans la conception est ensuite abordée. Des modèles
de fidélité moyenne sont choisis comme compromis idéal entre les méthodes de densités et rendements constants et les simulations coûteuses de haute fidélité. L'application de cette méthode à divers scénarios d'hybridation pour les avions dans la catégorie de certification CS-23 est ensuite discutée. Les résultats montrent que, même si une électrification permettant d'atteindre les mêmes niveaux de performances que les avions conventionnels n'est pas réalisable, elle peut être mise en œuvre et s'avérer avantageuse pour les missions plus courtes et pour de petits aéronefs, même avec les technologies actuelles. Un point de bascule en termes de maturité technologique est également mis en évidence, montrant que certaines chaînes hybrides ne seront compétitives que temporairement. Enfin, il est montré que, pour certaines configurations, la réduction des émissions ne peut être obtenue qu'en tirant parti du soulagement des contraintes de conception, et non grâce à la faible intensité carbone de l'électricité. Ces comparaisons sont ensuite approfondies en utilisant une ACV dans le processus de conception. Cela permet d'obtenir des pistes cruciales sur les impacts de la propulsion électrique et de nuancer les gains découlant des nouvelles compositions chimiques des cellules de batterie.

Title: Optimization of an aircraft design problem for hybrid-electric configurations under manufacturing and certification constraints

Key words: aircraft, electric, hybrid, multidisciplinary, Overall Aircraft Design

Abstract: As part of the ecological transition of the aeronautics sector, many national and international agencies have set very ambitious targets to reduce the environmental footprint of aviation. While scrutiny is usually on CO2, aircraft release a wider range of pollutants that also contribute to sector's impact on the environment. Although they contribute only marginally to the emissions of the sector as a whole, General Aviation aircraft pose themselves as an essential step of this transition. Firstly, although they represent only a minute fraction of the total fuel burn in the sector, they account for 10% of unburnt hydrocarbons, 40% of CO emissions, and the entirety of lead emissions. Additionally, they are used in different ways and with a different intensity when compared to their commercial counterpart thereby indicating a different path to sustainability. Secondly, on account of their lower required power and lower ranges, they are ideal candidates to de-risk and gain knowledge about newer technologies before adoption on commercial aircraft. A popular potential solution to the question of the sustainability of the aeronautics sector is the introduction of electrified propulsion. Although the technology is still in its infancy, raising questions about its certifiability, it offers gains ranging from reduced to zero emissions during flight. It also offers the prospect of multidisciplinary synergies and relieving design constraints on the aircraft. Out of the numerous projects proposed to explore this solution, numerous approaches, ranging from blank sheet design to retrofit, have been adopted to address those novel designs. This thus creates a need for new sizing methodologies capable of capturing those synergies and capable of assessing the impacts, at aircraft level, of electrified powertrains. Given the variety of propulsive architectures and the need to be able to model both retrofit aircraft and new designs from scratch, dynamic formulation is necessary. This thesis addresses the need for such a methodology by presenting new methods and models enabling the assessment, at aircraft level, of the effects of electrified propulsion chain. First, a review of existing methods for the sizing of aircraft is proposed, highlighting the need for integrated framework capable of capturing multidisciplinary synergies introduced by electric propulsion. This thesis contributes by proposing the integration, into the existing modular framework FAST-OAD, of a new module capable of dynamic reconfiguration of the MDAO problem to model any propulsive architecture. The integration of models capable of capturing gains stemming from multiple disciplines as well as the added degrees of freedom in the design is then discussed. Medium fidelity models are chosen as an ideal compromise between top-down kW/kg and efficiency methods and expensive high fidelity simulations. The application of this method to various hybridization scenarios for CS-23 certification category aircraft is then discussed. This reveals that while electrification achieving same levels of performances as conventional design is unfeasible, it can be achieved and beneficial for shorter mission and small aircraft, even with current technologies. A tipping point in terms of electric technology maturity is also highlighted showing that, for some aircraft, hybrid designs will only be competitive temporarily. Finally, it is shown that, for certain configuration, reductions of emissions can only be achieved by leveraging the relief of aircraft design constraints enabled by electric propulsion and not thanks to its low carbon intensity. Lastly, the comparison between conventional and electrified designs is further investigated by using Life Cycle Assessment inside the aircraft design process. It enables critical insights into the impacts of electric propulsion and nuances the gains stemming from new battery cell chemistries.